SAPIENZA
UNIVERSITÀ DI ROMA

Sapienza University of Rome

Doctoral School in Astronomical, Chemical, Physical, Mathematical and Earth Sciences "Vito Volterra"
Ph.D. in Physics

Thesis For The Degree Of Doctor Of Philosophy

Quasinormal Modes of Black Holes in Einstein-dilaton Gauss-Bonnet Gravity

Thesis Advisor
Prof. Leonardo Gualtieri
Prof. Paolo Pani

Candidate
Lorenzo Pierini
1654514

Academic Year MMXIX-MMXXII (XXXV cycle)

Abstract

The detection of the first gravitational wave marked the beginning of gravitational wave astronomy, which opened up new avenues to test Einstein's General Relativity in the previously unreachable strong-field regime of gravity. Even though the gravitational waves detected so far have not shown any sign of departure from General Relativity, it is widely acknowledged that the theory is not an ultimate and complete description of gravity, highlighting the need to continue testing and developing viable extensions. One promising strategy to pursue this goal is Gravitational Spectroscopy, which involves measuring black hole quasinormal modes from the ringdown gravitational wave signal emitted in the aftermath of a compact binary coalescence. The quasinormal modes, which are the characteristic oscillation frequencies of the perturbed remnant black hole, are inherently linked to the underlying theory of gravity and as such are perfect tools to perform tests of General Relativity.

As the ringdown signal is expected to be observed with more and more accuracy thanks to design-sensitivity interferometers and next-generation detectors, the possibility of performing theory-specific ringdown tests relies on theoretical predictions of quasinormal modes in alternative theories of gravity.

In this Thesis, we present the first computation of the gravitational quasinormal modes of rotating black holes up to second order in spin in Einstein-dilaton Gauss-Bonnet gravity, arguably one of the simplest theories that modify the large-curvature regime of gravity and that can be tested with black hole observations. To enhance the domain of validity of the spin expansion, we perform a Padé resummation of the quasinormal modes and, from a comparison with the general relativistic case, we find that this approach should be accurate up to the astrophysically relevant spins ~ 0.7. Our findings indicate that neglecting the second order in the spin could result in a serious underestimation of the effect of gravity modifications.

Finally, we outline two possible strategies to perform tests of General Relativity by using a parametrized ringdown template called ParSpec. From a null test with the future detectors Cosmic Explorer and Einstein Telescope, we find that with at least $\mathcal{O}(10^3)$ ringdown observations of realistic sources we will be able to put stringent bounds on three beyond-GR parameters with both detectors; performing a theory-specific test of Einstein-dilaton Gauss-Bonnet gravity with the LIGO-Virgo data of GW150914 we were not able to put meaningful constraints on the theory, which are expected to improve with a higher signal-to-noise ratio and by stacking multiple events.

Keywords: General Relativity, Black Holes, Quasinormal Modes, Black Hole Spectroscopy, Einstein-dilaton Gauss-Bonnet, Tests of General Relativity, Black Hole Perturbation Theory.

Contents

List of Figures

List of Tables

Nomenclature

α_{GB}	Einstein-dilaton Gauss-Bonnet coupling constant
$\bar{a}$	dimensionless spin parameter
ϕ	angular coordinate
φ	dilaton field
ζ	Einstein-dilaton Gauss-Bonnet dimensionless coupling constant

Acronyms

BBHs Binary Black Holes

BHs Black Holes

CE Cosmic Explorer

DBHs Dilatonic Black Holes

ECO Exotic Compact Object

EdGB Einstein-dilaton Gauss-Bonnet

EFTs Effective Field Theories

ESGB Einstein-Scalar Gauss-Bonnet

ET Einstein Telescope

GR General Relativity

GW Gravitational Wave

IMR Inspiral-Merger-Ringdown

LVK LIGO-Virgo-KAGRA

MCMC Markov Chain Monte Carlo

NR Numerical Relativity

ODE Ordinary Differential Equation

QNMs Quasinormal Modes

SNR Signal-to-Noise Ratio

Chapter 1

Introduction

Almost one century after the birth of Einstein's General Relativity (GR), the first Gravitational Wave (GW) detection in 2015 [5], describing the coalescence of a binary system of Black Holes (BHs) 1.4 billion lightyears away, marked the origin of GW astronomy.

With three catalogs of events [6–9], the Advanced LIGO detectors at Hanford, Washington and Livingston, Louisiana [10], and the Advanced Virgo detector in Cascina, Italy [11], have now detected about 90 GW events from the merger of compact objects identified as neutron stars and/or BHs. This result represents an incredible effort in engineering and experimental physics that unlocked an astounding new opportunity to explore the Universe. Thanks to this milestone in scientific discovery, we were able to get new astrophysical and cosmological information [12, 13] on the population of compact objects in our local universe and, crucially, to test GR in a highly dynamical, non-linear and strong-field regime of gravity, previously unreachable [14–18].

Einstein's theory of gravity remains remarkably successful to this day, having been validated by recent observations of a BH shadow image in the electromagnetic spectrum captured by the Event Horizon Telescope [19, 20] and by numerous GW detections made by the LIGO/Virgo interferometers. These recent findings complement earlier experiments conducted within the Solar System [21] (which correspond to weak and approximately static gravity), binary-pulsar [22–24] (strong-field, static regime of gravity) and galactic-center observations [25, 26], as well as cosmological measurements [27–30].

The currently available GW observations, probing a regime characterized by strong gravitational fields and large spacetime curvature, have ruled out large deviations of GR within this range [14, 15, 31–33]. However, with the next generation of GW detectors, such as Cosmic Explorer [34], Einstein Telescope [35, 36], and the space-based observatory LISA [37], we will reach sensitivieties able to capture even tiny GR modifications [38–41].

Regardless of the success of General Relativity, it is crucial to keep testing and developing viable extensions of the theory [42]. This is primarily because we anticipate the theory to break down at some length scale, as it cannot provide a consistent description of the gravitational interaction at the quantum level. However, the reasons to explore theories beyond GR are multiple and of different natures. Several fundamental open questions in physics could potentially be answered by introducing modifications to the gravitational sector: the accelerated expansion of the universe caused by the dark energy [28, 43], the elusive dark matter needed to explain the observed galactic rotation curves [27, 44, 45], the matter/antimatter asymmetry in the universe [27, 45], the inflationary period of

the early universe [27–29, 45], and the aforementioned unification of GR with Quantum Mechanics [27, 46]. As a matter of fact, introducing a scalar field in the gravity action [47, 48] or making the graviton massive [49–51] could explain the late-time acceleration of the Universe [52, 53] without the need of a cosmological constant or of the dark energy.

Even though it is now accepted that General Relativity is not the ultimate theory of gravity, it can be viewed as the leading-order manifestation of a more fundamental theory. String theory and other ultraviolet completions of the Standard Model usually introduce higher-order curvature corrections to GR's Einstein-Hilbert action; it has been shown that considering quadratic curvature terms, such as in low-energy realizations of string theory [54], already makes the theory renormalizable [55], although such terms are not sufficient to make it viable.

Even without evoking observational concerns, a straightforward yet critical motivation to rigorously test GR is that there is no a-priori reason for the assumptions underlying the theory to be true: it is only logical to scrutinize each one of them and to consider the available alternatives [17, 18], since a new regime – that of *strong gravity* – is now observable.

The Binary Black Holes (BBHs) detected by LIGO and Virgo, providing insights into the strong-field regime of gravity, could potentially offer enlightening clues about the true description of the gravitational interaction.

Testing any modified theory of gravity with high accuracy relies on having (at least part of the) waveform models in such theories, which is only possible with an accompanying significant theoretical development. Despite recent advancements both on the analytical [56–69] and numerical [70–86] sides, so far the LIGO-Virgo collaboration has mainly focused on *null tests* of GR, being the best-understood theory currently available. These tests assume that this is the correct prescription of gravity, and then look for generic departures from it [14, 15, 32, 33, 87, 88]. Without precise waveform templates in modified theories of gravity, it is still unclear how well null tests can actually detect and constrain any specific GR violation [89].

The goal of this Thesis, already explored in our works [67, 68], is to provide new theoretical predictions on the late part of the gravitational waveform of a BH in a paradigmatic extension of GR, called Einstein-dilaton Gauss-Bonnet (EdGB), and outline some example of tests of GR. We will show how these results will help to further develop theory-specific tests of GR, in order to ultimately advance our knowledge on beyond-GR physics.

1.1 Gravitational Wave Tests of General Relativity

In General Relativity, the evolution of a BBH comprises of three different stages: during the *inspiral* [90] the two objects get adiabatically closer and closer to each other losing energy through GW emission until, in the *merger* phase [91–93], a common horizon is formed and a perturbed remnant object remains, settling down to the final equilibrium configuration, namely a Kerr BH, during the *ringdown* [94–98]. In particular, the ringdown stage can be well described as a superposition of damped sinusoids with characteristic frequencies and damping times: the Quasinormal Modes (QNMs), labeled by the overtone number n, with $n = 0$ being the least damped mode, and by the harmonic indices (l, m) [1].

Modifications of GR can manifest in the GW signal primarily in its generation, propagation, or polarization. The generation of the gravitational wave carries information on how the source's

properties are related to the radiation it emits and on the dynamics that characterize the underlying theory of gravity. In the case of BH sources, a deviation from GR may show up if the black holes have different characteristics from the Schwarzschild or Kerr solutions. The propagation of the wave can be affected by different dispersion relations [99], birefringence [100] and amplitude damping [101, 102]. Finally, while in GR the gravitational wave is fully described by two tensor polarizations (referred to as *plus*"+" and *cross*"×") [103], a general metric theory of gravity can have up to six modes of polarization: two tensor, two vector, and two scalar [104]; detections of additional polarizations (which requires more than two GW detectors to be significant) would be a clear indication of GR violation.

Tests of GR can follow mainly two strategies: a *theory-agnostic test* assumes that the GW signal is well described by GR and includes additional parameters to account for any generic deviation, while *theory-specific tests* directly compare the data with the prescriptions of a proposed modified gravity theory. So far, the former method, which uses the GW data to check for consistency with GR predictions and ultimately put constraints on the non-GR parameters [15, 31, 33, 87, 105–108], has been predominantly adopted, due to our greater understanding of GR with respect to its possible extensions. However, recent developments, such as Numerical Relativity (NR) simulations [72–74] and QNM computations beyond-GR [3, 4, 66, 109–117] – including our works [67, 68] – have allowed the first theory specific-tests to be performed with current GW data [84, 118].

Focusing on the first category, null tests of the GW generation [87, 88, 119–121], propagation [122], polarization [21, 123, 124] have not reported any deviation from GR.

While the inspiral part of the GW signal provides useful insights on possible extra radiation channels [14, 31, 125, 126], the ringdown allows remarkable tests of GR and of the remnant object's nature [118, 127–132] through measurements of the QNMs [1], which are closely linked to the underlying theory of gravity.

Testing GR with quasinormal modes requires high Signal-to-Noise Ratio (SNR) in the ringdown part of the gravitational waveform. Currently available ground-based detectors are limited in the achievable SNR [15, 32, 33], which inevitably affects the precision of the QNM measurement. However, next-generation detectors will be capable of reaching high enough values of the SNR for this purpose [36–41, 133–137].

1.2 No-hair Theorems and Black Hole Spectroscopy

In GR, according to well-established *no-hair theorems* [138–142], a BH is expected to be completely characterized by its mass and spin – an electric charge is believed to be irrelevant for astrophysical BHs [143]. Consequently, BH QNMs in GR are determined solely by the mass and spin of the black hole

This unique relationship between the black hole's properties and its QNM spectrum makes analyzing the gravitational waves emitted by perturbed remnant black holes after the merger of compact objects an effective and compelling way to test General Relativity. If the measured frequencies and damping times of the QNMs differ from the predictions of General Relativity, it would indicate a clear deviation from Einstein's theory or from the black hole nature of the final object. In such cases, the remnant may instead be an Exotic Compact Object (ECO) [143–152].

The analytical computation of QNMs involves using BH perturbation theory, which was first

developed by Regge and Wheeler [153] and later by Zerilli [154] and Teukolsky [155]. This theory takes advantage of the symmetry of spacetime and tensor fields to separate the radial and angular components of gravitational or scalar perturbations, similar to what is done in quantum mechanics. Vishveshwara [95] was the first to apply this approach to numerically study GW scattering by Schwarzschild black holes, discovering that the late-time waveform consists of damped sinusoids. Press [96] identified these signals as the free oscillation modes of the black hole, later connected by Goebel to perturbations of the "light ring" [156]. Significant progress was made by Chandrasekhar and Detweiler [97, 98, 157], while Leaver [158] devised an accurate method for calculating QNMs.

The characteristic modes of rotating BHs in GR are usually obtained by solving the Teukolsky master equation [155, 159] under the assumption that the remnant BH in a BBH coalescence relaxes to a Kerr configuration, which is referred to as *Kerr hypothesis* [160, 161].
If BH solutions in modified theories of gravity do exist [18, 162], they can either be characterized by different dynamics or a different metric from Kerr (or Kerr-Newman) [18, 163], generally exhibiting additional hairs. In both cases, the resulting QNM spectrum will differ from the corresponding GR values and it will carry the imprint of the underlying theory of gravity.

This is why, starting from the 1970s, the idea of treating compact objects such as BHs as "gravitational atoms" and viewing their QNM spectrum as a unique fingerprint of the spacetime dynamics, in analogy with atomic spectra, started to grow [164]. Now, this fully established idea, referred to as *gravitational spectroscopy* – or BH spectroscopy in the case it is applied to BHs – is used to perform tests of GR [1]. It can be employed for example as a test of the area law [165, 166], which states that the total area of a classical BH horizon does not decrease over time, or to probe the nature of the remnant object, examining BH thermodynamics [167–169] and the BH area quantization [151, 152].

One of the main applications of BH spectroscopy is to test the GR no-hair conjecture – in the case that multiple modes are observed for the same event [164, 170–172]: the values of the mass and spin inferred from one mode [173], assuming a Kerr BH, would determine the whole spectrum, then the measurement of a second mode should be consistent with the predictions of the first one (model-independent, null test) [127–131, 133, 164, 172, 174–176]. Inconsistency in the results would be the manifestation of a non-BH nature of the remnant object or an actual deviation from GR.

Other tests that take advantage of a spectroscopic analysis of the ringdown of GR are Inspiral-Merger-Ringdown (IMR) consistency tests [31, 177], which check that independent measurements of the remnant BH mass and spin from the inspiral and merger-ringdown phases of the signal are consistent, assuming GR is correct [106, 107, 178]. This test, which requires only the measurement of one mode unlike the no-hair theorem test, can be also generalized to modified theories of gravity [179–181].

BH spectroscopy has been applied to currently available GW data: while there is consensus on the measurement of the least damped (*fundamental*) mode in the first GW detected, GW150914 [31, 129–131, 150], which agrees with the GR prediction within 16% uncertainty [15, 31–33, 106, 178], many studies, with different positions, focused on understanding if additional modes are present in the signal in order to test the no-hair theorem; with this goal, a possible detection of the first overtone $n = 1, l = m = 2$ in GW150914 has been reported [131, 182, 182–184]. The same motivation led to a thorough spectroscopic ringdown analysis for other GW events [15, 33, 130, 178, 185], possibly finding the $l = m = 3$ fundamental mode in GW190521 [186]. So far, none of these model-

independent analyses have found proof of GR violations.

However, BH spectroscopy can also be used to perform theory-specific tests of GR: if QNM values in modified theories of gravity were available, it would be possible to determine which description of gravity is favored based on the data [118, 187, 188]. This kind of test relies on the theoretical computation, using BH perturbation theory, of the QNM spectrum in such theories. Since realistic black holes are expected to be rapidly rotating, especially the end products of coalescences, it is important to include the effects of rotation in the computation, which has been done only for a handful of cases [4, 66, 69]. The difficulty arises since, while for the Kerr BHs [161, 189] the master equation for perturbations is separable [155, 190], the differential operators governing the QNM perturbations in rotating black hole backgrounds in theories of gravity are, in general, non-separable.

In this Thesis, we compute the QNMs of *rotating* BHs in a specific theory of gravity, EdGB, using the formalism first developed by Hartle [191, 192] and later by Kojima [193], and we lay down some basic examples of both theory-agnostic and theory-specific tests using QNMs, as first steps towards a more comprehensive analysis currently in development [194, 195].

1.3 Quadratic Gravity: the Case of Einstein-dilaton Gauss-Bonnet

Theoretical predictions in modified theories of gravity, such as the knowledge of the QNM spectrum, would allow us to move past null tests of GR and, using already available data or future observation, constrain specific alternatives to unprecedented levels. This could provide extremely valuable insights on the ultimate description of the gravitational interaction.

Many theories of gravity have been proposed to address the unresolved issues within GR and offer alternatives to its underlying assumptions, generally expressed through Lovelock's theorem [18]: the gravitational interaction in GR is only mediated by a massless metric tensor, the spacetime is four-dimensional, the theory must be position- and Lorentz- invariant, and the gravitational action is invariant under parity transformations.

From a phenomenological point of view, among all the various potential manifestations of new physics, one obvious instance would be the presence of a new field, effectively evading the first assumption of Lovelock's theorem. The simplest field we could consider is a massless scalar field (note that the no-hair theorems imply that in GR scalarized states are not supported by stationary BHs [139, 196–200]). If we try to build a viable theory of gravity that includes an additional scalar interaction, we could introduce the scalar field in the gravitational action together with polynomial terms in the curvature, while also requiring second-order and shift symmetric (with respect to the scalar field) field equations. In this case, only a term consisting of a scalar field coupled to the so-called *Gauss-Bonnet* invariant, which is quadratic in the curvature, could originate a scalar hair in stationary, asymptotically flat configurations [200][1].

From a theoretical perspective, effective actions deriving from string theory [201, 202] fix the coupling of the scalar field with the Gauss-Bonnet invariant to be of an exponential form. The resulting theory, called Einstein-dilaton Gauss-Bonnet (EdGB) [17, 201–209], where the "dilaton" refers to the aforementioned scalar field, is known to lead to BHs with scalar hairs [18, 201, 210–217].

[1] More generally, if we do not require shift symmetry, the coupling with the Gauss-Bonnet invariant would still be the simplest way to evade the no-hair theorem [18].

Since the effects of the EdGB modification appear in the GW signal of BBH mergers, it is possible to directly test or constrain the theory. On one hand, BBHs in EdGB can source scalar-dipole radiation [65, 203, 218, 219] (which appears at -1 PN order in the GW phase with respect to the dominant quadrupolar term in GR); on the other hand the dilaton field, introducing a new kind of interaction coupled to gravity, affects the response of the compact objects to linear perturbations and consequently the QNMs. Specifically, when separating such perturbations in *polar* and *axial* according to their parity-transformation properties, the scalar field couples only to the polar sector, creating a new radiation channel and breaking the equivalence between polar and axial QNMs, that is a well-known property of Schwarzschild BHs in GR [220–224].

While GR can be considered as a well-posed initial value problem, the same cannot be said with certainty for EdGB [225, 226]. However, if one considers the dilaton field and metric perturbatively around the GR solution, then the equations at each perturbative order are well-posed [73, 76, 225, 227, 228]. If the EdGB modification of an isolated BH is not stable, meaning that it pathologically grows in time, then it has the potential to gradually accumulate over a full BBH system evolution and affect both the inspiral, merger, and ringdown stages. As a result, this instability can also manifest in QNMs in the form of exponentially growing modes. The stability of static, nonrotating EdGB BHs has been proved in detail [3, 109, 229, 230], however the full stability of rotating BHs has not been established yet.

The existence of EdGB black holes is subject to a theoretical constraint on the coupling constant of the theory $0 < \alpha_{GB} \lesssim 0.691 M^2$ [229], which gives an indication of the scale at which EdGB effects could appear. Since it is a universal constant, such a bound automatically translates to a physical constraint when M is chosen to be the mass of the lightest BH observed: J1655-40, with $M \simeq 5.4 M_\odot$, implies $\sqrt{\alpha_{GB}} < 6.6\,km$; if the secondary object in GW190814, with mass $M \simeq 2.6 M_\odot$ turns out to be a BH, then $\sqrt{\alpha_{GB}} < 3.3\,km$ [2].

Combining multiple GW observations can lead to an increased accuracy when constraining the theory, as the bounds tend to become progressively tighter with each additional stacked detection [128, 130, 174, 180, 231]. In this way, considering BBHs from the GWTC-1 and GTWC-2 catalogs [6, 7], it was possible to put the bound $\sqrt{\alpha_{GB}} < 9.1\,km$ [232, 233]. Instead, using the Neutron Star-Black Hole binaries GW200105 and GW200115 [234], led to $\sqrt{\alpha_{GB}} < 7.1\,km$ [235].

While the spacetime properties of EdGB black holes are well understood [201, 208, 229, 230], the computation of the QNM spectrum of rotating BHs in this paradigmatic case of quadratic gravity [18] presents a new and remarkable opportunity to perform theory-specific tests of GR and gain new information about the kinds of deviations we should expect and at which scale.

1.4 Structure of the Thesis

The Thesis is structured as follows. In Chapter 2 we review some basic knowledge about BH perturbation theory and QNMs, including applications to nonrotating and slowly rotating BHs. We discuss in detail the direct integration method we employ for the QNM computation, highlighting its limits and its strengths, as well as its potential for beyond-GR applications.

In Chapter 3 we define the spacetime of a slowly rotating BH in EdGB gravity, which serves as

[2] When comparing with other bounds in the literature, one needs to be careful of the convention used, see e.g. [73, 118].

the background for studying its linear perturbations.

Chapter 4 focuses on testing our framework by comparing our QNM computations for a test scalar field on a slowly rotating EdGB BH with literature results.

In Chapter 5 we continue this comparison by investigating the more involved case of gravitational perturbations, but restricting the analysis to the static, nonrotating case.

Chapter 6 expands on the concepts and techniques presented in the previous chapters to analyze gravitational QNMs of slowly-rotating BHs in EdGB gravity at first and second order in the spin. We show that, with the Padé Resummation method, we can extend the results up to astrophysically relevant spins.

In Chapter 7, we present some initial tests of GR using both theory-independent and theory-specific frameworks, based on the results of the previous chapter. Additionally, we discuss the next steps required to perform more comprehensive tests of the theory.

Finally, in Chapter 8 we summarize our findings and we outline possible extensions of this work.

Chapter 2

Quasinormal Modes

In this chapter, we introduce the concept of *quasinormal modes* (QNMs), which is fundamental for the scope of the thesis, and then we will lay out some examples of QNM computation, providing the basis for more complicated cases explored in the next chapters.

2.1 General Definition

Quasinormal modes are eigenfrequencies of the eigenvalue problem associated with a perturbed dissipative system and describe the response to the perturbation (after a transient time) [1, 236, 237]. In this thesis we shall focus on perturbed black holes, which are intrinsically dissipative systems: energy is lost at the event horizon, which acts as a one-way membrane, and at infinity, where it is radiated away in the form of gravitational waves. Dissipative systems are ubiquitous in nature and the study of their characteristic oscillation frequencies in physics has been proven to be an outstanding tool, e.g. in atmospheric science and leaky resonant cavities, to get information about the properties of the oscillating system itself, such as its structure and composition. Although the properties of QNMs have long been investigated, their study in astrophysical applications can have still a lot to uncover and provide extremely valuable information.

In more idealized physical examples without dissipation, such as the one of a vibrating string, one has a conservative system and perturbations of the system can be described through normal modes, that have a real frequency. In presence of dissipation, it is not possible to expand the solutions of the perturbed equations governing the system in normal modes [237–239], but instead the related eigenfrequencies are *quasi*normal modes [1], described by *complex* frequencies, with the imaginary part associated with the decay time-scale of the perturbation. In fact, dissipative systems are not time-symmetric and hence they will have specific timescales associated with the characteristic oscillations. For black holes, there is a unique timescale that is fully determined, in geometric units, by the mass of the object [170]. The presence of the horizon is the main feature that makes the boundary value problem non-Hermitian and the associated eigenvalues complex [236, 237, 240, 241]. The eigenfunctions corresponding to the QNMs, which have intrinsically a transient nature, are usually not normalizable and, in general, do not form a complete set [236, 242].
From a more rigorous mathematical point of view, further detailed in Sec. 2.4, QNMs can be defined as the poles in the complex plane of the Green Function associated with an inhomogeneous wave equation [238, 243–246].

In this thesis, we shall see how quasinormal modes can provide exceptional information about the theory of gravity that describes perturbed compact objects.
In GR (but not exclusively), the perturbations of a given background spacetime, such as the Schwarzschild or Kerr BH solutions [189, 247], obey linear second-order differential equations, characterized by symmetry properties closely related to the ones of that particular background [248]. These symmetries usually allow, with a suitable choice of coordinates, the separation of the equations' variables between the time-radial part and the angular one. As a result, we obtain either a set of linear ordinary differential equations (ODEs) or a single ODE. Once we impose the proper boundary conditions at the black-hole horizon and at infinity, we automatically single out an *infinite*, *discrete* set of eigenmodes of this system of equations: the QNMs.
The possible methods to simplify the perturbation equations to one (or more) ODEs depend on the specific metric considered [159, 220] and can become quite challenging, especially in modified theories of gravity.

We shall start by focusing on QNMs in General Relativity (GR) – reviewed for example in Refs. [1, 159, 249] – in some easier cases, such as scalar field perturbations, with the ultimate goal to expand the results to linear perturbations of BHs in a modified theory of gravity, in Chapters 4, 5, 6. Throughout this work, we will use geometric units ($G = c = 1$), in which the mass has the units of length.

2.2 Scalar Field Perturbations

We shall start with a paradigmatic and simple application of black hole perturbation theory, and consider perturbations induced by a probe scalar field Φ propagating in a background spacetime. Assuming that Φ contributes very little to the energy density (no quadratic terms of the field), we can fix the background metric to be a solution of Einstein equations. For simplicity, we shall consider the spherically symmetric line element

$$ds^2 = -A(r)dt^2 + \frac{1}{B(r)}dr^2 + r^2\left(d\theta^2 + \sin^2\theta\, d\phi^2\right) , \tag{2.1}$$

which we can identify with the Schwarzschild solution when $A(r) = B(r) = 1 - 2M/r$.

The evolution of the scalar field on this background is governed by the Klein-Gordon equation

$$\left(\Box - \mu^2\right)\Phi = 0\,, \tag{2.2}$$

with μ being the mass of the scalar field. This equation can be recast as

$$\frac{1}{\sqrt{-g}}\partial_\mu\left(\sqrt{-g}g^{\mu\nu}\partial_\nu\Phi\right) - \mu^2\Phi = 0\,, \tag{2.3}$$

with $g_{\mu\nu}$ being the metric tensor in coordinates $x^\mu = (t, r, \theta, \phi)$, such that $ds^2 = g_{\mu\nu}dx^\mu dx^\nu$ in Eq. (2.1), and g its determinant.

Given the spherical symmetry of the background spacetime, which is nonrotating, the scalar field evolution will inherit the same characteristics and will not be affected by any rotation. This allows a separation of the field equations between the time-radial dependence (t, r) and the angular

dependence (θ, ϕ), which can be achieved with the use of scalar spherical harmonics, forming a complete orthonormal set of functions for the angular part. Since we are looking for solutions that are damped in time (corresponding to the QNMs), and thus described by complex frequencies $\omega = \omega_R + i\omega_I$, we assume a time dependence of the perturbation $e^{-i\omega t}$. Hence, the scalar field shall be described by

$$\Phi(t, r, \theta, \phi) = \sum_{l=0}^{\infty} \sum_{m=-l}^{l} \frac{\Psi_{lm}(r)}{r} Y_{lm}(\theta, \phi) e^{-i\omega t}\,, \tag{2.4}$$

where we have introduced the radial function $\Psi_{lm}(r)$, and the spherical harmonics $Y_{lm}(\theta, \phi) = P_{lm}(\theta)e^{im\phi}$ are the spherical harmonics and $P_{lm}(\theta)$ the associated Legendre functions, which satisfy

$$\frac{1}{\sin\theta}\partial_\theta(\sin\theta\partial_\theta P_{lm}) - \frac{m^2}{\sin^2\theta}P_{lm} = -l(l+1)P_{lm}\,. \tag{2.5}$$

Using the expansion in Eq. (2.4) in the field equation (2.3), simplifying with Eq. (2.5), we obtain a radial wave equation for the function $\Psi_{lm}(r)$

$$AB\frac{d^2}{dr^2}\Psi_l + \frac{1}{2}(AB)'\frac{d}{dr}\Psi_l + \left[\omega^2 - (\mu^2 A + \frac{l(l+1)}{r^2}A + \frac{(AB)'}{2r}\right]\Psi_l = 0\,. \tag{2.6}$$

We note that there is no dependence on the azimuthal number m, since the background metric is spherically symmetric, so we shall remove this index from Ψ_l.

In order to recast Eq. (2.6) in a more familiar, Schroedinger-like wave equation, we introduce a generalized tortoise coordinate r_* to remove the first-order derivative, such that

$$\frac{dr}{dr_*} \equiv \sqrt{AB}\,. \tag{2.7}$$

In this way, we obtain

$$\frac{d^2}{dr_*^2}\Psi_l + \left[\omega^2 - V_{scalar}(\mu)\right]\Psi_l = 0\,, \tag{2.8}$$

with the potential

$$V_{scalar}(\mu) \equiv A\mu^2 + A\frac{l(l+1)}{r^2} + \frac{(AB)'}{2r}\,, \tag{2.9}$$

which becomes, in the Schwarzschild case ($A(r) = B(r) = 1 - 2M/r$),

$$V^S_{scalar}(\mu) = \left(1 - \frac{2M}{r}\right)\left(\mu^2 + \frac{l(l+1)}{r^2} + \frac{2M}{r^3}\right)\,. \tag{2.10}$$

2.3 Gravitational Perturbations

We shall now turn to gravitational perturbation of the same spherically symmetric spacetime as in Eq. (2.1). Now, instead of a scalar perturbation, the gravitational case will be identified by a

perturbation tensor $h_{\mu\nu}$, such that the full metric is

$$g_{\mu\nu} = g^0_{\mu\nu} + \epsilon h_{\mu\nu}\,, \tag{2.11}$$

with $g^0_{\mu\nu}$ the unperturbed background metric of Eq. (2.1), and ϵ a small bookkeeping parameter, $\epsilon \ll 1$.

In order to find the differential equations that describe the perturbation, we need to solve Einstein equations (in vacuum) for the metric in Eq. (2.11)

$$G_{\mu\nu}[g_{\mu\nu}] = G^0_{\mu\nu}[g^0_{\mu\nu}] + \epsilon\delta G_{\mu\nu}[h_{\mu\nu}] + \mathcal{O}(\epsilon^2) = 0\,, \tag{2.12}$$

where we are considering the vacuum case since the QNMs correspond to the proper oscillation modes of an isolated perturbed black hole. The information about the excitation of each mode is instead closely related to the nature of the perturbation, for example to the progenitors in a coalescence event producing the perturbed BH in question, and thus it requires solving a full inhomogeneous equation (see Section 2.4 for details).

The term $G^0_{\mu\nu}[g^0_{\mu\nu}]$, which corresponds to the Einstein tensor computed for the nonperturbed metric, will be zero in the cases in which $g^0_{\mu\nu}$ is an exact solution of the unperturbed Einstein equation, such as the Swarzschild metric. When instead the form of the metric is unknown, solving the $\mathcal{O}(\epsilon^0)$ equation $G^0_{\mu\nu}[g^0_{\mu\nu}] = 0$ will determine the unknown metric components, such as A and B in Eq. (2.1).

We can find the explicit expression of $\delta G_{\mu\nu}$ in Eq. (2.12), which controls the dynamics of the perturbations, in terms of $g^0_{\mu\nu}$ and $h^0_{\mu\nu}$ by recalling that

$$G_{\mu\nu} \equiv R_{\mu\nu} - \frac{1}{2} g_{\mu\nu} R \tag{2.13}$$

and that the Ricci tensor is given by

$$R_{\mu\nu} = \partial_\alpha \Gamma^\alpha{}_{\mu\nu} - \partial_\nu \Gamma^\alpha{}_{\mu\alpha} + \Gamma^\alpha{}_{\sigma\alpha}\Gamma^\sigma{}_{\mu\nu} - \Gamma^\alpha{}_{\sigma\nu}\Gamma^\sigma{}_{\mu\alpha}\,, \tag{2.14}$$

with the affine connections $\Gamma^\rho_{\mu\nu}$ computed for the perturbed metric (we now include ϵ in $h_{\mu\nu}$ for simplicity of notation)

$$\Gamma^\rho{}_{\mu\nu}(g) = \Gamma^\rho{}_{\mu\nu}(g^0) + \delta\Gamma^\rho_{\mu\nu}(h) + \mathcal{O}(h^2)\,. \tag{2.15}$$

The two terms are given by

$$\Gamma^\rho_{\mu\nu}(g^0) = \frac{1}{2} g^{0\rho\alpha}[g^0_{\alpha\nu,\mu} + g^0_{\mu\alpha,\nu} - g^0_{\mu\nu,\alpha}]\,, \tag{2.16}$$

$$\delta\Gamma^\rho_{\mu\nu}(h) = \frac{1}{2} g^{0\rho\alpha}(\nabla_\nu h_{\alpha\mu} + \nabla_\mu h_{\alpha\nu} - \nabla_\alpha h_{\mu\nu})\,. \tag{2.17}$$

By substituting Eq. (2.15) in the Ricci tensor (Eq. (2.14)), we get $R_{\mu\nu} \equiv R^0_{\mu\nu}(g^0) + \delta R^0_{\mu\nu}$ with

$$\delta R_{\mu\nu} = \nabla_\rho \delta\Gamma^\rho_{\mu\nu} - \nabla_\nu \delta\Gamma^\rho_{\mu\rho} = \frac{1}{2}\left(\nabla_\alpha\nabla_\nu h^\alpha{}_\mu + \nabla_\alpha\nabla_\mu h^\alpha{}_\nu - \nabla_\alpha\nabla^\alpha h_{\mu\nu} - \nabla_\nu\nabla_\mu h^\alpha{}_\alpha\right)\,, \tag{2.18}$$

while the perturbation of the Ricci scalar is given by

$$\delta R = g^{0\mu\nu}\delta R_{\mu\nu} - h^{\mu\nu}R^0_{\mu\nu}\,. \tag{2.19}$$

By comparing Eq. (2.13) with (2.12) we finally find

$$\delta G_{\mu\nu} = \delta R_{\mu\nu} - \frac{1}{2}g^0_{\mu\nu}(g^{0\alpha\beta}\delta R_{\alpha\beta} - h^{\alpha\beta}R^0_{\alpha\beta}) - \frac{1}{2}h_{\mu\nu}R^0\,, \tag{2.20}$$

with $\delta R_{\mu\nu}$ given by Eq. (2.18).

We are interested in the linear order perturbations, so we shall neglect every $\mathcal{O}(\epsilon^2)$ term in Eq. (2.12). However, there has been an increasing interest in studying also nonlinear effects induced by the perturbation that can produce visible effects in the QNM spectrum [250–253].

Starting from the set of perturbation equations $\delta G_{\mu\nu}[h_{\mu\nu}] = 0$, analogous to Eq. (2.3) for the scalar field case, we want to follow the same logical steps as Section 2.2 and try to expand the perturbation tensor $h_{\mu\nu}$ in a suitable basis to separate the time and radial variables (t, r) from the angular ones (θ, ϕ). Once again we can exploit the spherical symmetry of the background metric and define a generalized set of spherical harmonics being able to capture the tensor nature of the perturbation [153, 249, 254, 255]. See Appendix A for details on the scalar, vector, and tensor spherical harmonics decomposition used.

In the Regge-Wheeler gauge [153] and assuming, due to stationarity, a time dependence $e^{-i\omega t}$ of the perturbations, the components of $g_{\mu\nu}$ can be written as

$$g^0_{\mu\nu} = \begin{pmatrix} -A(r) & 0 & 0 & 0 \\ 0 & 1/B(r) & 0 & 0 \\ 0 & 0 & r^2 & 0 \\ 0 & 0 & 0 & r^2\sin^2\theta \end{pmatrix}, \tag{2.21}$$

$$h^{pol}_{\mu\nu} = \begin{pmatrix} A(r)H_{0,lm}(r) & H_{1,lm}(r) & 0 & 0 \\ H_{1,lm}(r) & 1/B(r)H_{2,lm}(r) & 0 & 0 \\ 0 & 0 & r^2K_{lm}(r) & 0 \\ 0 & 0 & 0 & r^2\sin^2\theta K_{lm}(r) \end{pmatrix} Y^{lm}e^{-i\omega t}\,, \tag{2.22}$$

$$h^{ax}_{\mu\nu} = \begin{pmatrix} 0 & 0 & -\frac{h_{0,lm}(r)}{\sin\theta}Y^{lm}_{,\phi} & h_{0,lm}(r)\sin\theta Y^{lm}_{,\theta} \\ 0 & 0 & -\frac{h_{1,lm}(r)}{\sin\theta}Y^{lm}_{,\phi} & h_{1,lm}(r)\sin\theta Y^{lm}_{,\theta} \\ -\frac{h_{0,lm}(r)}{\sin\theta}Y^{lm}_{,\phi} & -\frac{h_{1,lm}(r)}{\sin\theta}Y^{lm}_{,\phi} & 0 & 0 \\ h_{0,lm}(r)\sin\theta Y^{lm}_{,\theta} & h_{1,lm}(r)\sin\theta Y^{lm}_{,\theta} & 0 & 0 \end{pmatrix} e^{-i\omega t}\,, \tag{2.23}$$

where we have separated the polar and axial parts of the perturbation tensor $h_{\mu\nu} = h^{ax}_{\mu\nu} + h^{pol}_{\mu\nu}$ depending on the nature of the perturbation functions they contain (see Appendix A), we have left implicit the sum over the harmonic indexes l, m and the dependence $Y^{lm} = Y^{lm}(\theta, \phi)$.

Eqs. (2.22)-(2.23) provide an expansion for tensor quantities analogous to the scalar case in Eq. (2.4). With the same procedure, one can obtain a similar result for electromagnetic perturbations.

The next step is to insert these expansions into the field equations (2.12). Assuming $g^0_{\mu\nu}$ is the Swarzschild metric, then $G^0_{\mu\nu}[g^0] = 0$, and we have to solve $\delta G_{\mu\nu}[h] = 0$, with the expression given in Eq.(2.20). Given the separation in h^{ax} and h^{pol}, we find that each component of the perturbation

equations describes independently either the polar quantities or the axial quantities. We will see that this is not always the case: in presence of rotation or in modified theories of gravity there can be couplings between the different sectors, making the resulting QNM spectrum richer.

Let us now focus on the *polar* set of equations, as it will also be the one considered in the rest of the thesis. We select the components δG_{tt}, δG_{tr}, δG_{rr}, $\delta G_{t\phi}$,$\delta G_{r\theta}$, $\delta G_{\theta\theta}/\sin^2\theta - \delta G_{\phi\phi}$,$\delta G_{\theta\theta}/\sin^2\theta + \delta G_{\phi\phi}$, where the last two combinations have been chosen to separate the angular part.

When considering an axisymmetric, not spherically symmetric spacetime, if we adopt the spherical harmonics decomposition approach, the situation becomes more involved, as the spherical harmonics cannot separate the variables as we did in the spherically symmetric case [256]; however, the problem has been solved for a Kerr BH by Teukolsky in 1973 [155, 190, 241] adopting spheroidal harmonics instead of the spherical ones. As we will see in the next chapters, the situation for modified theories of gravity is even more intricate, and there is not a known procedure to obtain decoupled radial and angular equations, although there have recently been some developments in that sense [4, 257, 258].

In Appendix B we review briefly the procedure to obtain a single second-order perturbation equation describing polar gravitational perturbations of a Schwarzschild black hole [153, 154, 254, 259]. Here we report the final equation in the Schroedinger-like form, which, for polar perturbations, takes the name of *Zerilli equation*

$$\frac{d^2 Z_l}{dr_*^2} + \left(\omega^2 - V_{polar}\right) Z_l = 0\,, \tag{2.24}$$

with

$$V_{polar} = \left(1 - \frac{2M}{r}\right) \frac{2\Lambda^2(\Lambda+1)r^3 + 6\Lambda^2 M r^2 + 18\Lambda M^2 r + 18M^3}{r^3(\Lambda r + 3M)^2} \tag{2.25}$$

and $\Lambda = (l-1)(l+2)/2$. Analogously, for the axial sector, we find the *Regge-Wheeler* equation

$$\frac{d^2 \Psi_l}{dr_*^2} + \left(\omega^2 - V_{axial}\right) \Psi_l = 0\,, \tag{2.26}$$

$$V_{axial} = -\left(1 - \frac{2M}{r}\right) \frac{2}{r^3} \left[3M - (\Lambda+1)r\right]\,. \tag{2.27}$$

The fact that we are able to describe the gravitational perturbations with a single Schroedinger-like ordinary wave equation, just as we did for the scalar case in Eq. (2.8), is very remarkable. Furthermore, the potentials of the polar and axial sectors can be related by a simple relation [97, 157, 220]: calling $V^{(+)} = V_{polar}$ and $V^{(-)} = V_{axial}$, it can be verified that

$$V^{(\pm)} = \pm(6M)\frac{dW}{dr_*} + (6M)^2 W^2 + 4\Lambda(\Lambda+1)W\,, \tag{2.28}$$

with

$$W \equiv \frac{r(r-2M)}{2r^3(\Lambda r + 3M)}\,. \tag{2.29}$$

This has some important consequences, such as the *isospectrality* between the two sectors of perturbations, meaning that they both yield the same QNM spectrum. Note that, even if the QNMs for polar and axial perturbations are the same, as we will see, the amplitudes with which they are excited are different, and they need to be found solving Eqs. (2.24)-(2.26) with the source term describing the physics responsible of the perturbation, e.g. infall into the black hole, binary merger, etc. [246]. Another interesting property of the perturbation equations, as already anticipated, is that there is a similarity between the scalar, electromagnetic, and gravitational cases. For electromagnetic perturbations of a Schwarzschild black hole the equation has the effective potential [1, 249]

$$V_{EM} = \left(1 - \frac{2M}{r}\right)\left[\frac{2(\Lambda+1)}{r^2}\right] . \tag{2.30}$$

Comparing the potential in Eq. (2.10) for $\mu = 0$ and Eqs. (2.27), (2.30), we see that we can enclose all these cases in

$$\frac{d^2\Psi_s}{dr_*^2} + \left(\omega^2 - V_s\right)\Psi_s = 0 \tag{2.31}$$

$$V_s = \left(1 - \frac{2M}{r}\right)\left[\frac{l(l+1)}{r^2} + (1-s^2)\frac{2M}{r^3}\right] , \tag{2.32}$$

with $s = 0$ for massless scalar perturbations, $s = \pm 1$ for electromagnetic perturbations and $s = 2$ for Regge-Wheeler gravitational perturbations. Zerilli and half-integer perturbations have different forms from Eq. (2.32), but, as we mentioned, the spectrum of Zerilli perturbations is isospectral to Regge-Wheeler one, and the two perturbation functions are connected by analytic relations [1].

These properties are just other examples that show how special General Relativity is, as other theories of gravity do not necessarily carry these features that make the task of describing perturbations of compact objects easier.

Even though some characteristics of the equations are peculiar to GR, the methods we will discuss to compute the perturbation equations and then the QNMs can be generalized to more complicated cases in modified theories of gravity.

2.4 Quasinormal Modes as Poles of the Green's Function

In this section, we define and compute QNMs starting from the perturbation equations discussed in the previous sections.

Let us consider a generic perturbation, either scalar, vectorial or tensorial of the form in Eq.(2.31), characterized by the perturbation function $\Psi(r)$ (we drop the spin s label)

$$\frac{d^2\Psi}{dr_*^2} + \left(\omega^2 - V\right)\Psi = 0\,, \tag{2.33}$$

where the tortoise coordinate r_* is a radial coordinate such that the horizon is located at $r_* \to -\infty$ and radial infinity is $r_* \to +\infty$.

Finding the characteristic oscillation frequencies of the perturbed black hole, i.e. the QNMs, means finding the ωs that satisfy Eq. (2.33) together with physically appropriate boundary condi-

tions at the horizon and at infinity.

For a Schwarzschild background and for most spacetimes of interest $V \to 0$ for $r_* \to -\infty$, thus, in this limit, the solutions of Eq. (2.33) behave as $\Psi \sim e^{-i\omega(t \pm r_*)}$. Furthermore, considering that classically nothing leaves the horizon, we need to select the plus sign in order to get a purely ingoing wave

$$\Psi \sim e^{-i\omega(t+r_*)} \qquad (r_* \to -\infty)\,. \tag{2.34}$$

This also follows from regularity requirements that would not be satisfied by the outgoing waves [1].

On the other hand, considering asymptotically flat spacetimes such as Schwarzschild, the metric at spatial infinity becomes the Minkowski metric and the potential goes to zero. Discarding unphysical waves coming from infinity and not from the source, we can identify the boundary condition at infinity as

$$\Psi \sim e^{-i\omega(t-r_*)} \qquad (r_* \to +\infty)\,. \tag{2.35}$$

Requiring that the solution of Eq. (2.33) satisfies these conditions automatically identifies the QNMs, as they represent the radiation emitted by the perturbed dissipative system, with waves either going into the BH or escaping to infinity. Only a discrete (and infinite) set of complex eigenfunctions, the QNMs $\omega_{QNM} = \omega_R + i\omega_I$, will satisfy the boundary conditions (2.34)-(2.35).

It should be noted that QNMs are not a complete set of wavefunctions [237, 240]; physically speaking, this means that they are quasistationary states, manifesting for a limited amount of time, being excited only at a particular instant and decaying exponentially with time.

This infinite set of complex eigenfunctions is usually sorted according to the magnitude of the imaginary part ω_I (whose inverse represents the damping time $\tau = 1/|\omega_I|$). The least damped mode is the *fundamental mode*, labeled with $n = 0$, then the more damped ones will have an increasing value of $n \in \mathbb{N}$ and are called *overtones*.

In order to find the actual response of the black hole to a specific kind of perturbation, including the magnitude of the excitation of each QNM, we need to consider the presence of the source that induced the perturbation. This means that we need to solve Eq. (2.33) with a specific source term, that can represent, for example, another small compact object merging with the primary black hole

$$\frac{d^2\Psi}{dr_*^2} + \left(\omega^2 - V\right)\Psi = I(\omega, r)\,. \tag{2.36}$$

The QNM contribution to the BH response to the perturbation can be formally isolated from other features of the signal, such as the late-time tail, considering the Green's function solution to the inhomogeneous wave equation (2.36) [238, 243–245].

Let us consider an asymptotically flat spacetime and two linearly independent solutions of the homogeneous equation, that we call Ψ_H and Ψ_∞, the former satisfying the proper boundary condition (only) at the horizon, Eq. (2.34), the latter satisfying the boundary condition (only) at infinity,

Eq. (2.35). This means that the two solutions will behave as

$$\lim_{r\to r_H} \Psi_H = e^{-i\omega r_*} \tag{2.37}$$

$$\lim_{r\to +\infty} \Psi_H = A_{in}(\omega)e^{-i\omega r_*} + A_{out}(\omega)e^{+i\omega r_*} \tag{2.38}$$

$$\lim_{r\to r_H} \Psi_\infty = B_{in}(\omega)e^{-i\omega r_*} + B_{out}(\omega)e^{+i\omega r_*} \tag{2.39}$$

$$\lim_{r\to +\infty} \Psi_\infty = e^{+i\omega r_*} \tag{2.40}$$

where we have introduced the coefficients $A_{in}, A_{out}, B_{in}, B_{out}$ to take into account that where the QNM boundary conditions are not satisfied, the generic solution of the homogeneous equation will be a mixture of ingoing and outgoing modes.

The Wronskian associated with the homogeneous equation is

$$W(\omega) \equiv \Psi_H {\Psi'}_\infty - {\Psi'}_H \Psi_\infty \,, \tag{2.41}$$

which, given the structure of the differential equation, is constant with respect to the radial coordinate r_*. Thus, we can compute it for simplicity at spatial infinity

$$W(\omega) = 2i\omega A_{in}(\omega) \,. \tag{2.42}$$

The general solution to the inhomogeneous equation will be [238]

$$\Psi(\omega, r) = \Psi_\infty \int_{-\infty}^{r_*} \frac{I(\omega, r)\Psi_H}{2i\omega A_{in}} {dr'}_* + \Psi_H \int_{r_*}^{+\infty} \frac{I(\omega, r)\Psi_\infty}{2i\omega A_{in}} {dr'}_* \,. \tag{2.43}$$

When we perform an inverse Laplace transform to get the time-domain solution

$$\Psi(t, r) = \frac{1}{2\pi} \int_{-\infty+ic}^{\infty+ic} \Psi(\omega, r) e^{-i\omega t} d\omega \,, \tag{2.44}$$

where c a small real constant that will be sent to zero for the computation of the integral, we follow the integration contour in the complex plane shown in Fig. 2.1, obtaining three different contributions:

- *Prompt response* (in flat-space), i.e. waves propagating directly from the source to the observer at the speed of light. It arises from the integral over the quarter circles at infinite frequency and represents the early time response of the black hole to the perturbation.

- *Late-time tails*, due to backscattering off the background curvature and characteristic of the specific asymptotic behavior of the spacetime [260–263]. They arise because of the branch cut we perform along the negative imaginary ω axis to avoid the branch point at $\omega = 0$ (depending on the structure of the potential V). In this way, we obtain two-quarter circles for $|\omega| \to \infty$ instead of a single half circle.

- *Quasi-normal modes*. This contribution is associated with the sum over the residuals at the poles in the complex plane, namely the zeros of $A_{in}(\omega)$ at the denominator. As it can be seen from Eq. (2.38) when $A_{in} = 0$, the poles correspond to perturbations satisfying both the

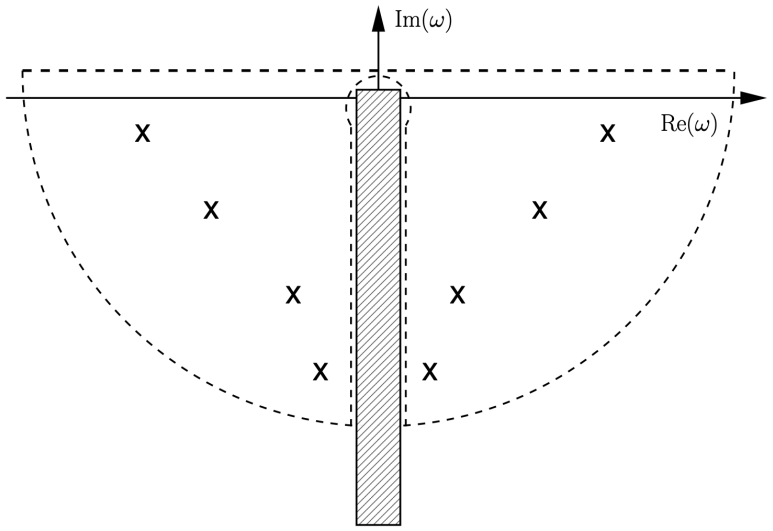

Figure 2.1: *Integration path for Eq.* (2.36) *[1]. The crosses are the zeros of the Wronskian and the shaded area is the branch cut to avoid the essential singularity at* $\omega = 0$.

ingoing wave condition at the horizon and the outgoing wave condition at infinity and thus, by definition, they are associated to the QNMs.

Although we worked assuming the asymptotic behavior of the solutions of the wave equation, the procedure can be generalized to any not-asymptotically-flat spacetime. We also note that, since QNMs have a negative imaginary part and $\Psi(t,r) \sim e^{-i\omega t}$, there are no exponentially growing modes, meaning that the BH is stable.

Focusing on the QNM contribution of the integral in Eq. (2.44), far away from the source we get

$$\Psi(t,r) = -Re\left[\sum_n B_n e^{-i\omega_n(t-r_*)} \int_{-\infty}^{+\infty} \frac{I(\omega,r)\Psi_H}{A_{out}} dr'_*\right], \tag{2.45}$$

where the sum is over all the poles in the complex plane, labeled by n, and the B_n, defined as

$$B_n \equiv \frac{A_{out}}{2\omega}\left(\frac{dA_{in}}{d\omega}\right)\Bigg|_{\omega=\omega_n}, \tag{2.46}$$

are the *quasinormal excitation factors* (QNEFs). The QNEFs depend only on the background geometry and thus can be computed independently from the specific kind of perturbation. They have been computed for Schwarzschild and Kerr BHs [238, 244–246, 264].

Equation (2.45) can be recast in the form

$$\Psi(t,r) = -Re\left[\sum_n C_n e^{-i\omega_n(t-r_*)}\right], \tag{2.47}$$

where the

$$C_n \equiv B_n \int_{-\infty}^{+\infty} \frac{I(\omega, r)\Psi_H}{A_{out}} dr'_* \tag{2.48}$$

are called *quasinormal excitation coefficients*. Since they depend explicitly on the initial conditions of the perturbation through $I(\omega, r)$, they encapsulate the features of the specific source of the QNMs and quantify the QNM content of the gravitational waveform. Being complex numbers, they characterize both the amplitudes and the phases of the QNMs. Although we have left it implicit in the previous derivations, the QNM frequencies ω_n, the B_n and C_n will all depend on the harmonic indexes l, m, which identify the angular shape in space of the radiation, and on the spin of the perturbing field s. By investigating the excitation coefficients for each QNM in different astrophysical scenarios, one could understand which mode is more excited, for example between overtones and higher l, m fundamental modes [265]. However, computing the C_n in perturbation theory for a variety of initial data can be quite a challenging task, therefore one usually finds the C_n by requiring the matching and continuity of the waveform in the ringdown part of the signal with the results of Numerical Relativity (NR) simulations.

In General Relativity, gravitational radiation is quadrupolar, thus GWs have $l \geq 2$ [103, 248]. Typically, for realistic astrophysical sources, the fundamental modes ($n = 0$) with $l = 2$ are the most excited. For example, for perturbed BHs that are the remnants of a binary black hole system, one finds that the gravitational radiation is dominated by the fundamental $l = |m| = 2$ component, while the contribution of higher multipoles is subdominant [266, 266, 267]; this is indeed verified in real gravitational wave events like GW150914 [33, 129].

In this work, our main interest is to find the quasinormal mode frequencies, not the excitation factors, therefore we can simply ignore the specific source of the perturbation for the computation. However, the information on the most excited modes is important when choosing which QNMs to include in the model of the gravitational waveform (see e.g. [268–272]).

In Fig. 2.2 we can see a typical gravitational waveform describing all the stages of a binary BH coalescence: the *inspiral*, where the two objects get progressively closer to each other until they merge in the *merger* phase and produce a remnant BH that relaxes to the equilibrium configuration in the *ringdown* part of the signal. When the QNM contribution to the ringdown is dominant, i.e. for $t > t_0$, with t_0 to be determined by the analysis of the signal, the most generic ringdown template based on Kerr perturbation theory for the complex-valued ringdown strain, $h \equiv h_+ - ih_\times$, takes the form of a superposition of damped sinusoids [1]

$$h = \frac{M}{r} \sum_{n=0}^{\infty} \sum_{l=2}^{\infty} \sum_{m=-l}^{l} \left[\mathcal{C}_{nlm} e^{-i\omega_{nlm}(t-t_0)} {}_{-2}S_{nlm}(\iota, \beta) + \mathcal{C}'_{nlm} e^{-i\omega'_{nlm}(t-t_0)} {}_{-2}S'_{nlm}(\iota, \beta) \right] , \tag{2.49}$$

where ${}_{-2}S_{nlm}$ are the spin-weighted spheroidal harmonics and $\mathcal{C}_{nlm}, \mathcal{C}'_{nlm}$ complex amplitudes. Furthermore, we have taken into account that the QNMs always come "in pairs" [158, 170, 269]: for Kerr, for a given (l, m) and a given value of $\bar{a} = J/M^2$, the eigenvalue problem admits two solutions:

[1] We have seen that QNMs are not a complete set, since they are not related to a self-adjoint operator and thus the expansion in QNMs is not well defined mathematically; however, from numerical simulations and real events, the approximation given by the linear superposition of damped sinusoids has been found to be reliable at intermediate times.

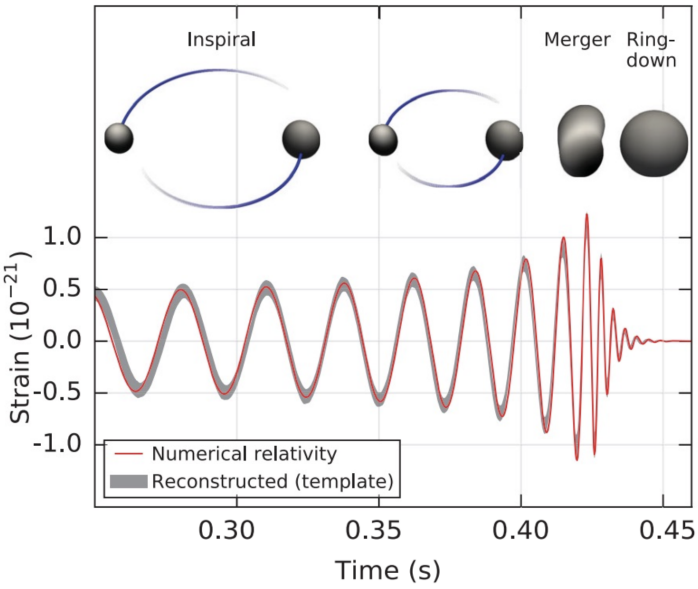

Figure 2.2: *Waveform of the gravitational wave event GW150914 describing a binary BH merger [2]. In the first part, the "inspiral", the two BHs orbit around each other, getting closer and closer until they reach the "merger" phase, in which a common horizon starts to form and a single remnant BH is originated. The final perturbed object reaches the equilibrium state by emitting the "ringdown" radiation, which in the late part is characterized by the quasinormal modes and takes the form of Eq.* (2.49).

one with positive frequency f_{nlm}, $\omega_{nlm} \equiv 2\pi f_{nlm} - i/\tau_{nlm}$, the other with negative frequency f'_{nlm} and different damping time τ'_{nlm}, $\omega'_{nlm} \equiv 2\pi f'_{nlm} - i/\tau'_{nlm}$. The former is usually referred to as "prograde" or "corotating" mode, while the latter is usually labeled as "retrograde", "counterrotating", or "mirror" mode (with possible slight changes in the notation). Due to the symmetry properties of the Kerr (and Schwarzschild) spacetime, specifically the parity-time symmetry, one can see from the perturbation equations that the following relations are valid

$$f'_{nlm} = -f_{nl-m}, \quad \tau'_{nlm} = \tau_{nl-m} \implies \omega'_{nlm} \equiv -\omega^*_{nl-m}\,. \tag{2.50}$$

For $m = 0$ and Schwarzschild QNMs, which are degenerate in m, the two "mirror" solutions are degenerate in modulus of the frequency and damping time. However, in general, for any given (l, m) we will always have a superposition of two different damped exponentials since the damping times and excitation amplitudes are different. Usually one neglects the retrograde modes in the ringdown analysis since their excitation amplitudes have been found to be orders of magnitude smaller than the corresponding prograde mode in the case of binaries in which the BHs rotate in the same sense as the orbit [273–276].

In this Thesis we shall focus on modes with positive frequency, however, we will always consider spacetimes for which the relation to find the retrograde modes (2.50) is valid.

2.5 Direct Integration Method

As described in the previous section, in order to find the QNM frequencies, we need linearly independent solutions of the homogeneous wave equation (2.33). However, exact solutions are generally hard to find analytically, and this is why usually one employs numerical methods, each one coming

with its own strengths and shortcomings (see Ref. [159] for a review of the most notable ones). In this section, we will focus on one method in particular, the *direct integration* method (see e.g. Refs. [277, 278] for some applications), which has the advantage of being easily extendable to modified theories of gravity, where it is not always possible to obtain a single master equation of the form (2.33). Its strength relies on the fact that it can be applied directly to a set of coupled ODE, such as Eqs. (B.8)-(B.9) for the Schwarzschild perturbation case, without the need to find a function, such as the Zerilli or Regge-Wheeler function, that would cast the system into a single second-order differential equation.

Let us assume we have a system of N first-order ODEs for N perturbation functions, which we can collect together in a N-dimensional vector $\mathbf{\Psi}$, with N an even integer. Let us also assume that, working in the frequency domain, we can write the system in the following way

$$\frac{d}{dr}\mathbf{\Psi} + \hat{V}\mathbf{\Psi} = \mathbf{0}\,, \tag{2.51}$$

with $\hat{V}$ an $N \times N$ matrix that depends on ω and r. Since we are interested in computing the QNMs, we look for solutions of Eq. (2.51) that satisfy the correct boundary conditions at the horizon and at infinity, namely

$$\mathbf{\Psi}(r_* \to -\infty) = \boldsymbol{A}_{in} e^{-i\omega r_*} \sim e^{-i\omega r_*} \quad (ingoing) \tag{2.52}$$

$$\mathbf{\Psi}(r_* \to +\infty) = \boldsymbol{A}_{out} e^{i\omega r_*} \sim e^{i\omega r_*} \quad (outgoing)\,, \tag{2.53}$$

where we have introduced the tortoise coordinate r_* and the vectors $\boldsymbol{A}_{in}, \boldsymbol{A}_{out}$.

The vector space given by the set of solutions has dimension N, with N the order of the matrix $\hat{V}$. To construct a basis for this space we can consider $N/2$ solutions $\mathbf{\Psi}^{(i)}_H,\ (i = 1, ..., N/2)$ obtained integrating from the horizon outwards and satisfying the ingoing boundary condition (2.52), and other $N/2$ solutions $\mathbf{\Psi}^{(i)}_\infty,\ (i = 1, ..., N/2)$, obtained integrating from the infinity inwards and satisfying the outgoing boundary condition (2.53).
If we require the vectors $\boldsymbol{A}_{in}, \boldsymbol{A}_{out}$ to be proportional to linearly independent vectors, such as $\{(1, 0, 0, ...), (0, 1, 0, ...), ...\}$, corresponding to switching off some perturbation functions at the boundaries, the corresponding solutions $\{\mathbf{\Psi}^{(i)}_H, \mathbf{\Psi}^{(i)}_\infty\}$ will also be linearly independent and can be used as a basis for the solution space.

We then build a matrix $\hat{X}$ that has the same dimensions of $\hat{V}$ and has the j-th vector of the solutions basis as the j-th column

$$\hat{X}(\omega, r) = \begin{pmatrix} \mathbf{\Psi}^{(1)}_H & ... & \mathbf{\Psi}^{(N/2)}_H & \mathbf{\Psi}^{(1)}_\infty & ... & \mathbf{\Psi}^{(N/2)}_\infty \end{pmatrix}. \tag{2.54}$$

By construction, this matrix itself will satisfy

$$\frac{d}{dr}\hat{X} + \hat{V}\hat{X} = 0\,. \tag{2.55}$$

By definition, the QNMs are the eigenfrequencies of the system of Eqs.(2.51) that satisfy simultaneously *both* the ingoing boundary condition at the horizon and outgoing boundary condition at infinity. This means that for $\omega = \omega_{QNM}$ the corresponding ingoing and outgoing solutions $\mathbf{\Psi}^{(i)}_{r_H}, \mathbf{\Psi}^{(i)}_\infty$ will describe the same eigenfunction of the system (2.51), hence no longer being linearly

independent.

Thanks to the properties of the determinant of a matrix, which becomes null when rows or columns of the matrix are linearly dependent, finding the QNMs is equivalent to requiring

$$det\hat{X}(\omega, r)\Big|_{\omega=\omega_{QNM}} = 0\,. \tag{2.56}$$

This condition is true regardless of the choice of r; in practice, we evaluate the matrix $\hat{X}$ at a matching point $r = r_m$ located between the horizon and the numerical infinity, i.e. the number chosen to represent infinity in the numerical implementation. We also note that the exact values of the constants of proportionaly appearing in $\boldsymbol{A}_{in}, \boldsymbol{A}_{out}$, as long as they are linearly independent, do not matter, since the determinant would be zero in any case.

We have seen that the task of finding the eigenfrequencies is reduced to computing the complex roots of $det\hat{X}(\omega)$, which can be done, for example, through a one-parameter shooting method, providing a tentative guess ω_{guess} as the starting point.

The main disadvantage of this method is that it can be affected by some numerical errors due to the intrinsic divergence occurring at the boundaries in this prescription. Considering that the QNMs $\omega = \omega_R + i\omega_I$ have $\omega_R > 0$ and $\omega_I < 0$, they are, on one hand, stable in time, meaning that $e^{-i\omega t} = e^{-i\omega_R t}e^{\omega_I t} \to 0$ for $t \to \infty$, on the other hand, focusing only on spatial behavior, we obtain an exponential divergence $e^{i\omega r_*} = e^{i\omega_R r_*}e^{-\omega_I r_*} \to \infty$ for $r_* \to +\infty$. This divergence is not physical, since when we integrate in the radial coordinate we are keeping the time fixed. In reality, a physical radial trajectory would be also described by a changing time coordinate, thus, in the time domain, $e^{-i\omega(t-r_*)}$ would not generate a divergence. As it often happens, to have the correct physical picture we must look at the time domain, not the frequency domain.
Nonetheless, adding subleading terms in powers of r to $\boldsymbol{A}_{in}, \boldsymbol{A}_{out}$, we can move away from the "proper" boundaries (r_H, ∞) and restrict the integration to a smaller numerical value of infinity R_∞, ultimately avoiding the divergence. Furthermore, since the exponential $e^{|\omega_I| r_*}$ diverges earlier the larger the absolute value of the imaginary part is, we can also understand why this method is not particularly suited for the computation of overtones [97].

As shown in Ref. [159], an alternative method is to find the QNMs by requiring any ingoing component at infinity and outgoing component at the horizon to vanish. However, this relies on identifying the subleading contributions at the boundaries, which can present some numerical precision problems. After trying both methods, we found the results of the method presented here to be more reliable, especially when including modifications of GR. An analogous procedure to the one described in this section for first-order ODEs can be implemented for second-order differential equations.

2.5.1 Schwarzschild Quasinormal Modes

As a first example of the direct integration method, we shall consider the Schwarzschild case. In Appendix B we showed how gravitational polar perturbations of the Schwarzschild spacetime can be fully described by the set of two coupled first-order differential equations (B.8)-(B.9) for the

functions $K_l(r), H_{1l}(r)$. Written in a symbolic way, these equations are

$$H_{1l}{}'(r) + a_l(\omega, r)K_l(r) + b_l(\omega, r)H_{1l}(r) = 0\,, \tag{2.57}$$

$$K_l{}'(r) + c_l(\omega, r)K_l(r) + d_l(\omega, r)H_{1l}(r) = 0\,, \tag{2.58}$$

with

$$a_l(\omega, r) \equiv -\frac{2ir\omega\left(9M^2 + 2Mr\left(l^2+l-4\right) + r^4\omega^2 - r^2\left(l^2+l-2\right)\right)}{(r-2M)^2\left(6M + r\left(l^2+l-2\right)\right)} \tag{2.59}$$

$$b_l(\omega, r) \equiv \frac{12M^2 + Mr(3l(l+1)-4) - 2r^4\omega^2}{r(r-2M)\left(6M + r\left(l^2+l-2\right)\right)} \tag{2.60}$$

$$c_l(\omega, r) \equiv \frac{12M^2 + Mr\left(l^2+l-6\right) - 2r^4\omega^2}{r(2M-r)\left(6M + r\left(l^2+l-2\right)\right)} \tag{2.61}$$

$$d_l(\omega, r) \equiv -i\frac{4Ml(l+1) + r\left(4r^2\omega^2 + l^4 + 2l^3 - l^2 - 2l\right)}{2r^2\omega\left(6M + r\left(l^2+l-2\right)\right)}\,. \tag{2.62}$$

We can then recast this system in the form of Eq. (2.51) as

$$\frac{d}{dr}\mathbf{\Psi}_l + \hat{V}_l(\omega, r)\mathbf{\Psi}_l = \mathbf{0}\,, \tag{2.63}$$

where

$$\mathbf{\Psi}_l \equiv \begin{pmatrix} H_{1l} \\ K_l \end{pmatrix} \tag{2.64}$$

is a $N = 2$ vector and

$$\hat{V}_l(\omega, r) = \begin{pmatrix} a_l & b_l \\ c_l & d_l \end{pmatrix} \tag{2.65}$$

a 2×2 matrix. To build a basis of solutions of the vector equation, we shall consider *two* solutions, one *ingoing* $\mathbf{\Psi}_{l\,H}$, i.e. that behaves $\sim e^{-i\omega r_*}$ near the horizon ($r_* \to -\infty$), and one *outgoing* $\mathbf{\Psi}_{l\,\infty}$, i.e. that behaves like $\sim e^{+i\omega r_*}$ at infinity ($r \to \infty$)[2], in which we the tortoise coordinate r_* for Schwarzschild is given, as usual, by

$$\frac{dr}{dr_*} = 1 - \frac{2M}{r} \Rightarrow r_* = r + 2Mlog\left(\frac{r}{2M} - 1\right)\,. \tag{2.66}$$

The matrix $\hat{X}_l$ containing the basis of solutions will be the 2×2 matrix

$$\hat{X}_l = \begin{pmatrix} \mathbf{\Psi}_{l\,H} & \mathbf{\Psi}_{l\,\infty} \end{pmatrix} = \begin{pmatrix} H_{1l\,H} & H_{1l\,\infty} \\ K_{l\,H} & K_{l\,\infty} \end{pmatrix}\,. \tag{2.67}$$

[2]The perturbation functions may have different asymptotic behaviors. For example $H_1 \sim re^{i\omega r_*}$ for $r \to \infty$, so one has to take it into account when imposing the boundary conditions. Alternatively, since there is some freedom when choosing the functions describing the perturbations, one could for example define a perturbation function H_1/r such that at infinity its behavior is $\sim e^{i\omega r_*}$

The QNMs ω_{nl} are the infinite set of complex frequencies that make the two solutions linearly dependent, i.e.

$$det\hat{X}_l\Big|_{\omega=\omega_{nl}} = 0\,, \tag{2.68}$$

where, in this case, the QNMs are only labeled by the overtone number n and the harmonic index l, as there is a degeneracy in the azimuthal number m due to the spherical symmetry of the Schwarzschild background. This degeneracy will be broken as soon as we introduce rotation to the black hole spacetime.

The first fundamental Schwarzschild QNMs we find are [3]

$$M\omega_{02} = 0.373672 - i\,0.088962 \tag{2.69}$$

$$M\omega_{03} = 0.599443 - i\,0.092703\,, \tag{2.70}$$

in agreement with the literature (see e.g. [279]).

Boundary Conditions Implementation

Now we shall discuss in more detail the implementation of the ingoing and outgoing boundary conditions, as it will be useful for the rest of the thesis. For practical purposes, as mentioned in Section 2.4, in order to avoid numerical divergences, we choose to fix the boundaries condition for the horizon at a position $R_H = r_H(1+\epsilon)$ that is an $\epsilon \ll 1$ away from the physical horizon r_H ($r_H = 2M$ for a Schwarzschild BH), and for spatial infinity at an arbitrary numerical value R_∞, which must not be too large. Schematically, these numerical boundaries as shown in Fig. 2.3. For our computations, we choose $\epsilon \sim 10^{-3}$ and $R_\infty \sim 40M$. As explained in the last part of the section, we can verify that these are suitable choices by checking a posteriori that the results are stable for small variations around these values.

Since we are not actually at the physical boundaries, but a bit far away from them, the vectors $\boldsymbol{A}_{in}, \boldsymbol{A}_{out}$ in Eqs. (2.52)-(2.53) shall become functions of r, namely $\boldsymbol{A}_{in}(r) = \{k_l^H(\omega,r), h_{1l}^H(\omega,r)\}$, $\boldsymbol{A}_{out}(r) = \{k_l^\infty(\omega,r), h_{1l}^\infty(\omega,r)\}$. Explicitly the perturbation functions will be

$$K_l(\omega, r\sim r_H) = k_l^H(\omega,r)e^{-i\omega r_*} \tag{2.71}$$

$$H_{1l}(\omega, r\sim r_H) = h_{1l}^H(\omega,r)e^{-i\omega r_*} \tag{2.72}$$

$$K_l(\omega, r\sim \infty) = k_l^\infty(\omega,r)e^{i\omega r_*} \tag{2.73}$$

$$H_{1l}(\omega, r\sim \infty) = h_{1l}^\infty(\omega,r)e^{i\omega r_*}\,. \tag{2.74}$$

Since we are assuming to be sufficiently close to the boundaries, the functions $\{k_l^H, h_{1l}^H\}, \{k_l^\infty, h_{1l}^\infty\}$ can be Taylor expanded around the physical horizon in powers of $r - r_H$, and near infinity in powers of $1/r$. The precise power of the leading order term can be verified a posteriori from the differential

[3] To convert these values in Hz, they must be multiplied by $2\pi\, 5142\, Hz\, M_\odot/M$ [239].

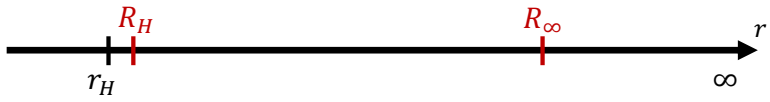

Figure 2.3: *The boundary conditions are imposed at the numerical values for the horizon R_H and for infinity R_∞ to avoid numerical divergences.*

equations (2.63), also Taylor-expanded. Near the horizon we have

$$k_l^H(\omega, r \sim r_H) = \sum_{i=0}^{N_H} k_{l,i}^H(\omega)(r-2M)^i \tag{2.75}$$

$$h_{1l}^H(\omega, r \sim r_H) = \sum_{i=0}^{N_H} h_{1l,i}^H(\omega)(r-2M)^{i-1}\,. \tag{2.76}$$

At infinity

$$k_l^\infty(\omega, r \sim \infty) = \sum_{i=0}^{N_\infty} \frac{k_{l,i}^\infty(\omega)}{r^i} \tag{2.77}$$

$$h_{1l}^\infty(\omega, r \sim \infty) = \sum_{i=0}^{N_\infty} \frac{h_{1l,i}^\infty(\omega)}{r^{i-1}}\,, \tag{2.78}$$

with N_H, N_∞ the orders of the series expansions, that must be chosen such that the resulting quasinormal modes are stable under small variations around those numbers. In particular, since the divergence at infinity is the main limitation to the integration method, it is essential to have a large value of N_∞ to balance the smaller choice of R_∞. We have verified, trying different options, that $N_H = 11, N_\infty = 13$ ensure stable results, as going to higher order does not affect them in a significant way.

We note that in the case of GR, it is possible to check the results with other integration methods, especially with the continued fraction method [158, 280, 281], which does not suffer as much from these numerical artifacts.

The coefficients in the expansions (2.75)-(2.78) are found by inserting Eqs. (2.71)-(2.74) in the differential equations (2.57)-(2.58), which are then expanded around the horizon and infinity and solved order by order in $r-2M$ or $1/r$ respectively.

All the coefficients will be proportional to one or more constants, corresponding to the leading order term of one of the perturbation functions. In fact, fixing these constants corresponds to choosing different solutions of the basis used to build the matrix $\hat{X}$ in Eq. (2.54). In the Schwarzschild case considered here, we only have one constant (one for the horizon expansion and one for the infinity expansion) since the leading order term of the other perturbation function can be expressed in terms of the one chosen. To show this concretely, we write the leading order terms of (2.71)-(2.74),

having selected the leading order term of K_l to be the arbitrary constant

$$K_l(\omega, r \sim r_H) = \left[k_{0l}^H + \mathcal{O}(r-2M)\right] e^{-i\omega r_*} \tag{2.79}$$

$$H_{1l}(\omega, r \sim r_H) = \left[-\frac{4M^2\omega(4M\omega - i)}{l^2 + l - 4iM\omega}\frac{k_{0l}^H}{r-2M} + \mathcal{O}(1)\right] e^{-i\omega r_*}\,, \tag{2.80}$$

$$K_l(\omega, r \sim \infty) = \left[k_{0l}^\infty + \mathcal{O}(1/r)\right] e^{+i\omega r_*} \tag{2.81}$$

$$H_{1l}(\omega, r \sim \infty) = \left[-i\omega r k_{0l}^\infty + \mathcal{O}(1)\right] e^{+i\omega r_*}\,. \tag{2.82}$$

The constants k_{0l}^H, k_{0l}^∞ are the free parameters described above, which we can fix $k_{0l}^H = 1, k_{0l}^\infty = 1$ to build $\hat{X}$ – any other value would not impact the computation of the determinant.

When finding the coefficients of the expansion at infinity, we need to be careful in solving the equations to get them. Let us assume that, having substituted Eqs. (2.73)-(2.74), we expand the differential equations (2.57)-(2.58) in $1/r$ up to $1/r^{M_{L.O.}+M_\infty}$, with $M_{L.O.}$ the leading order power of the expansion of each equation (e.g. $M_{L.O} = 0$ for K_l, $M_{L.O} = -1$ for H_{1l}).

As an obvious choice, one could think of taking M_∞ to be the same as the order of the expansions of the functions, namely $M_\infty = N_\infty$, as this would in general provide enough equations for the number of variables to find. However, one eventually discovers that, once the first coefficients are found, these equations become degenerate, thus not allowing one to determine the remaining coefficients. Nevertheless, we are not forced to stop at $M_\infty = N_\infty$, since we require the expansions (2.75)-(2.78) to satisfy the differential equations, without assuming a specific M_∞. The additional conditions to find the coefficients are then found by going at orders $\mathcal{O}(M_\infty = N_\infty + 1)$ or $\mathcal{O}(M_\infty = N_\infty + 2)$ and neglecting, for example, one of the equations at leading order. In this way, we find that $k_{l,1}^\infty = 0$.

The discussion above, however, is only relevant in the case of perturbation equations in the form of first-order ODEs. If we do the same procedure recasting the system as a second-order differential equation, e.g. working with just K_l or the Zerilli or Regge-Wheeler functions used to obtain Eq. (2.24), then this problem is not present and finding the asymptotic coefficients is straightforward. Since, as we mentioned, one usually needs a high-order expansion at infinity to avoid the exponential divergence, sometimes it is convenient to recast the set of equations in the second-order form just to compute the boundary conditions [4], otherwise one would need to consider equations at even higher orders in $1/r$. Switching to the second-order formalism is possible also in modified gravity theories, although typically in such theories there is no equivalent of a Zerilli or Regge-Wheeler function, so there will still be the problem of having coupled differential equations (with half of the degrees of freedom of the first order system).

Stability

We checked the stability of the results under variations of the numerical parameters R_H,R_∞, N_H, N_∞,r_m. We tried different values of the expansion order coefficients N_H, N_∞ and we found that for the computation of the fundamental modes, $N_H = 11$ and $N_\infty = 13$ are sufficient to obtain stable

[4] For example, expressing H_1 in terms of K, K' we get the second order ODE in K; then we can find the boundary conditions for K from this equation and obtain the one for H_1 from the relation between the two perturbation functions.

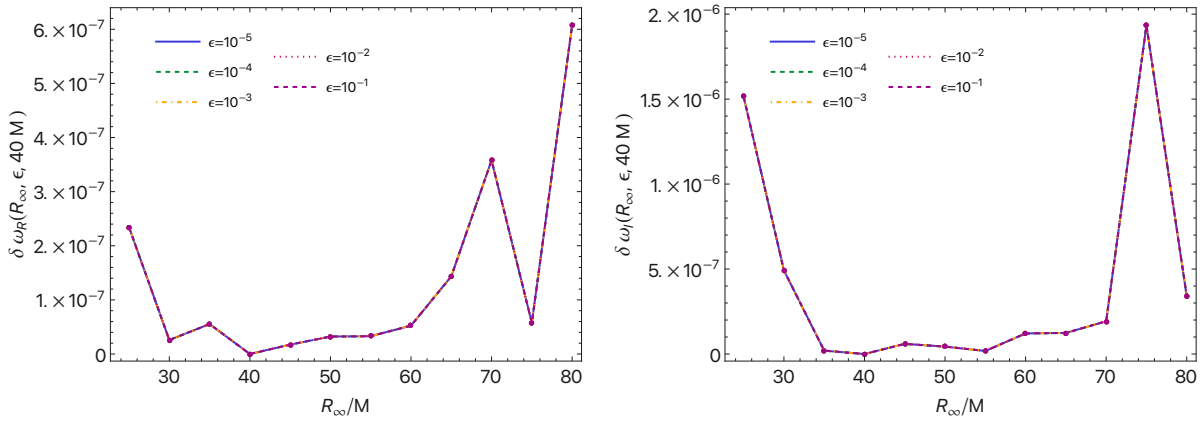

Figure 2.4: *Stability of Schwarzschild QNM for $n = 0, l = 2$ evaluated with the direct integration method with different values of numerical infinity and horizon. Choosing as a reference $R_\infty = 40M$, we plot the relative difference $\delta\omega(R_\infty, \epsilon, 40M) \equiv |\omega(R_\infty, \epsilon) - \omega(40M, \epsilon)|/|\omega(40M, \epsilon)|$. We see that, while the choice of the horizon deviation ϵ in $R_H = r_H(1+\epsilon)$ does not impact the results of integration, we can find a range of $R_\infty \in [35, 60]M$ for which we obtain stability of the results, which differ for less than $2 \cdot 10^{-7}$.*

results. The expansion order at infinity is more sensitive since, in order to avoid the numerical divergence, we actually need to select a not too-large finite value of infinity R_∞, thus requiring a high-order expansion. However, increasing up to $N_\infty = 17$, we verified that the difference in the fundamental modes is negligible for the scope of our work, while it has an important impact when trying the computation of the overtones, for which it affects the third decimal position. We note that the computation of the overtones is not treated in this work, as the direct integration method is not suited for the task, given the intrinsic problems when trying to compute modes with large imaginary parts [97]. Even though one manages to compute the first overtone for $l = 2$ with precision 10^{-3}, the high order expansion needed and, consequently, the high computational cost, together with the small values of the EdGB modification expected, indicate that an alternative method is needed for reliable estimates of the EdGB overtones.

We verified that the value of the matching point r_m at which the determinant (2.56) is computed does not affect almost at all the QNM values obtained, as expected. We have found that the most significant parameter to choose carefully is R_∞, since it may produce noticeably unstable results. In Fig. 2.4 we plot the relative difference $\delta\omega_{R,I}$ of the $l = 2$ Schwarzschild fundamental mode computed for different choices of R_∞ and horizon parameters ϵ, in $R_H = r_H(1+\epsilon)$, with respect to the mode computed with a specific value of $\bar{R}_\infty$, that we fixed to be $40M$, which reproduces well the results in Ref. [279]

$$\delta\omega_{R,I}(R_\infty, \epsilon, \bar{R}_\infty) \equiv \frac{|\omega_{R,I}(R_\infty, \epsilon) - \omega_{R,I}(\bar{R}_\infty, \epsilon)|}{|\omega_{R,I}(\bar{R}_\infty, \epsilon)|}\,. \tag{2.83}$$

We see that there is a range of R_∞, namely $[35, 60]M$, for which the results can be considered stable, since the relative deviation of the mode is $\delta\omega_{R,I}(R_\infty, \epsilon, 40M) \lesssim 2 \cdot 10^{-7}$. We find that the results are only very weakly affected by the choice of ϵ.

2.6 Quasinormal Modes of Slowly Rotating Black Holes

As we mentioned in the previous sections, in GR it is possible to describe gravitational perturbations of rotating black holes with a single master equation, i.e. the Teukolsky master equation [155, 190], after separating the angular variables from the radial one. However, this is not usually possible in modified theories of gravity, where there might be additional dynamical fields and degrees of freedom that introduce nontrivial couplings between the perturbations. Nonetheless, it is still of utmost importance to find QNMs of rotating compact objects in modified theories of gravity in order to perform theory-specific tests of general relativity, as all astrophysically relevant objects, especially the results of BH mergers, are expected to be rotating.

One possible approach to tackle this problem that can be generalized to allow GR modifications without many theoretical issues is to start from the nonrotating case and then perform a slow rotation expansion, i.e. a perturbative expansion in the spin of the object. Since we are sufficiently close to the spherically symmetric case, it is still possible to adopt the spherical harmonics decomposition.

In this section, we will schematically explain how to describe perturbations of slowly rotating black holes in GR; the same logic will be applied to more complicated theories in the next chapters. We shall follow the formalism introduced by Hartle and Thorne [191, 192], who applied it to stars, and later employed by Kojima [193, 282, 283] to explicitly compute the perturbation equations of neutron stars at first order in the spin. This framework was summarized and extended in Ref. [159] in the context of BH perturbations, after being applied in different scenarios [278, 284, 285].

2.6.1 Background Metric

The metric of a generic stationary, axially symmetric object, such as a neutron star or black hole, can be written as

$$ds^2 = -H^2(r,\theta)dt^2 + Q^2(r,\theta)dr^2 + r^2K^2(r,\theta)\left[d\theta^2 + \sin^2\theta(d\phi - L(r,\theta)dt)^2\right] . \tag{2.84}$$

$L(r,\theta)$ is the angular velocity, $d\phi/dt$, acquired by an observer falling freely from infinity to the point (r,θ) and represents the rate of rotation of the inertial frame at (r,θ) relative to the distant stars. Consequently, the non-vanishing $g_{t\phi}$ component implies the presence of dragging of the inertial frames.

If the object in question, which we shall consider to be a BH, is slowly rotating, we can perform a perturbative expansion in the angular momentum J around the nonrotating case

$$\begin{aligned} ds^2 = -A(r)\left[1+2h(r,\theta)\right]dt^2 + \frac{1}{B(r)}\left[1+2p(r,\theta)\right]dr^2 \\ + r^2\left[1+2k(r,\theta)\right]\left\{d\theta^2 + \sin^2\theta\left[d\phi - \varpi(r,\theta)dt\right]^2\right\} , \end{aligned} \tag{2.85}$$

where $A(r), B(r)$ are the functions describing the nonrotating spherically symmetric spacetime, as in Eq. (2.1) and $h(r,\theta), p(r,\theta), k(r,\theta), \varpi(r,\theta)$ describe the deformations due to rotation.

The metric of a stationary, axially symmetric system, such as the one described by the metric (2.84), is invariant under an inversion of the direction of rotation as well as under time reversal. For this reason, the expansions of H, Q, K in powers of J can only contain even powers, while the expansion of L will have only odd powers. Calling $\bar{a} \equiv J/M^2$ the dimensionless angular momentum,

with M mass of the black hole, we can expand the functions ϖ, h, p, k in Eq. (2.85) according to their symmetry properties in a complete basis of orthogonal functions given by

$$\varpi = \sum_{n=1,3,5...}^{N_{\bar{a}}-q} \sum_{l=1,3,5...}^{n} \bar{a}^n \omega_l^{(n)}(r) \left[-\frac{1}{\sin\theta} \frac{dP_l(\cos\theta)}{d\theta} \right] \tag{2.86}$$

$$h = \sum_{n=2,4,...}^{N_{\bar{a}}-v} \sum_{l=0,2,4...}^{n} \bar{a}^n h_l^{(n)}(r) P_l(\cos\theta) \tag{2.87}$$

$$p = \sum_{n=2,4,...}^{N_{\bar{a}}-v} \sum_{l=0,2,4...}^{n} \bar{a}^n p_l^{(n)}(r) P_l(\cos\theta) \tag{2.88}$$

$$k = \sum_{n=2,4,...}^{N_{\bar{a}}-v} \sum_{l=0,2,4...}^{n} \bar{a}^n k_l^{(n)}(r) P_l(\cos\theta)\,, \tag{2.89}$$

where $P_l(\cos\theta)$ are the Legendre polynomials. $v = 0$ ($q = 0$) when the order of the spin expansion $N_{\bar{a}}$ is even (odd), whereas $v = 1$ ($q = 1$) otherwise. We also note that we can set the functions $k_0^{(n)}(r) = 0$ without loss of generality thanks to the invariance of the metric (2.85) under a generic radial rescaling $r \to f(r)$ [191, 192].

In the following chapters of the Thesis, we will focus on the first and second-order spin corrections, therefore the maximum value of $N_{\bar{a}}$ we will consider is $N_{\bar{a}} = 2$. At second order we will have, explicitly

$$\varpi(r,\theta) = \bar{a}\,\omega_1^{(1)}(r) + \mathcal{O}(\bar{a}^3) \tag{2.90}$$

$$h(r,\theta) = \bar{a}^2 \left[h_0^{(2)}(r) + h_2^{(2)}(r) \frac{1}{2} \left(3\cos^2\theta - 1 \right) \right] + \mathcal{O}(\bar{a}^4) \tag{2.91}$$

$$k(r,\theta) = \bar{a}^2 \left[k_0^{(2)}(r) + k_2^{(2)}(r) \frac{1}{2} \left(3\cos^2\theta - 1 \right) \right] + \mathcal{O}(\bar{a}^4) \tag{2.92}$$

$$p(r,\theta) = \bar{a}^2 \left[p_0^{(2)}(r) + p_2^{(2)}(r) \frac{1}{2} \left(3\cos^2\theta - 1 \right) \right] + \mathcal{O}(\bar{a}^4)\,. \tag{2.93}$$

First-order Corrections

At first order in the spin, the metric (2.85) corresponds to a static spherically symmetric BH with a deformation in the $g_{t\phi}$ component due to the nonvanishing gravitomagnetic term $\varpi(r,\theta) = \bar{a}\,\omega_1^{(1)}(r) \equiv \omega(r)$

$$ds^2 = -A(r)dt^2 + \frac{1}{B(r)}dr^2 + r^2(d\theta^2 + \sin^2\theta d\phi^2) - 2r^2\omega(r)\sin^2\theta dt d\phi\,. \tag{2.94}$$

After computing Einstein equations for this metric, from the differential equation given by $G_{t\phi} = 0$, which is of order $\mathcal{O}(\bar{a})$, we find

$$\omega(r) = \frac{2J}{r^3}\,. \tag{2.95}$$

Where we have defined J to include any possible extra integration constants, so that it represents the physical angular momentum of the BH, as read off the asymptotic behavior of $g_{t\phi}$ (see Appendix C for more details). In general, we will use the same procedure to define the BH angular momentum

also in modified theories of gravity, where additional terms proportional to the coupling constants of the theory will enter the definition.

Second-order Corrections

The main corrections to a static metric due to rotation arise at $\mathcal{O}(\bar{a}^2)$, as the functions h, p, k in Eq. (2.85) become non-vanishing. As in the previous case, the coefficients of the expansions in Eqs. (2.87)-(2.89) are found integrating Einstein equations. In particular, we consider the radial equations obtained from $E_1 \equiv G_{tt} = 0$, $E_2 \equiv G_{rr} = 0$, $E_3 \equiv G_{\theta\theta} + \theta G_{\phi\phi}/\sin^2\theta = 0$, contracted with a Legendre polynomial

$$\int_0^\pi d\theta \sin\theta P_l(\cos\theta) E_i(r,\theta) = 0 \quad (i = 1,2,3;\, l = 0,2)\,, \tag{2.96}$$

in which we exploit the property

$$\int_0^\pi d\theta \sin\theta P_l(\cos\theta) P_{l'}(\cos\theta) = \frac{2}{2l+1}\delta_{ll'}\,. \tag{2.97}$$

In this way, we obtain a set of purely radial ordinary differential equations for $h_l^{(2)}(r), p_l^{(2)}(r), k_l^{(2)}(r)$ with $l = 0, 2$, after having set $k_0^{(2)}(r) = 0$ (corresponding to simply rescaling of the metric). When performing the integration, we require asymptotic flatness of the metric in order to fix some of the integration constants. As a result, we get

$$p_0^{(2)}(r) = -\frac{M^4}{(r-2M)r^3} - \frac{\delta m}{r-2M} \tag{2.98}$$

$$h_0^{(2)}(r) = \frac{M^4}{(r-2M)r^3} + \frac{\delta m}{r-2M} \tag{2.99}$$

$$h_2^{(2)}(r) = \frac{M^3(M+r)}{r^4} \tag{2.100}$$

$$k_2^{(2)}(r) = -\frac{M^3(2M+r)}{r^4} \tag{2.101}$$

$$p_2^{(2)}(r) = -\frac{M^3(r-5M)}{r^4}\,, \tag{2.102}$$

where δm is a constant representing the shift in the mass of the rotating BH with respect to the static case.

Similarly to what we have done at first order in the spin to define the angular momentum J, the Arnowitt-Deser-Misner mass $\mathcal{M}$ can be read off from the asymptotic behavior of the g_{tt} component of the metric (2.85). Assuming $A(r) = 1 - 2M/r$ as in Schwarzschild, we obtain

$$g_{tt} \to -1 + \frac{2}{r}\left(M - \bar{a}^2\delta m\right) + \mathcal{O}\left(\frac{1}{r^2}\right) \equiv -1 + \frac{2\mathcal{M}}{r} + \mathcal{O}\left(\frac{1}{r^2}\right)\,. \tag{2.103}$$

$\mathcal{M}$ is the only meaningful physical mass that describes the rotating BH and we will always refer to this quantity. Since the static black hole from which we built our rotating solution is no longer relevant, in the rest of the text, unless specified, we shall switch back to the notation $\mathcal{M} \to M$, with M physical mass of the BH.

The metric (2.85) can be recast in physical quantities M and J, obtaining

$$\begin{aligned} ds^2 =& -\left(1-\frac{2M}{r}+2\frac{J^2}{r^4}\right)\left[1+2\frac{J^2}{Mr^3}\left(1+\frac{M}{r}\right)P_2(\cos\theta)\right]dt^2 \\ &+\left(1-\frac{2M}{r}+2\frac{J^2}{r^4}\right)^{-1}\left[1-2\frac{J^2}{Mr^3}\left(1-\frac{5M}{r}\right)P_2(\cos\theta)\right]dr^2 \\ &+r^2\left[1-2\frac{J^2}{Mr^3}\left(1+\frac{2M}{r}\right)P_2(\cos\theta)\right]\left[d\theta^2+\sin^2\theta\left(d\phi-\frac{2J}{r^3}dt\right)^2\right], \end{aligned} \tag{2.104}$$

which is valid up to order J^2. We note that, as expected, when expressing the metric in physical quantities, the integration constant δm does not appear anywhere.

It is natural to compare the line element in Eq. (2.104), describing the geometry outside a slowly rotating configuration, with the exact solution of Einstein equations describing a rotating black hole – the Kerr metric [189], which in Boyer-Lindquist coordinates is

$$ds^2 = -\left(1-\frac{2Mr}{\Sigma}\right)dt^2+\frac{\Sigma}{\Delta}dr^2+\Sigma d\theta^2+\left(r^2+a^2+\frac{2Mra^2}{\Sigma}\sin^2\theta\right)\sin^2\theta d\phi^2-\frac{4Mra\sin^2\theta}{\Sigma}dtd\phi \tag{2.105}$$

with $a=J/M$, $\Sigma=r^2+a^2\cos^2\theta$, $\Delta=r^2-2Mr+a^2$. If we expanded it to the second order in J, we can obtain the Hartle-Thorne metric (2.104) using the simultaneous coordinate transformation

$$r\to r\left\{1-\frac{a^2}{2r^2}\left[\left(1+\frac{2M}{r}\right)\left(1-\frac{M}{r}\right)+\cos^2\theta\left(1-\frac{2M}{r}\right)\left(1+\frac{3M}{r}\right)\right]\right\} \tag{2.106}$$

$$\theta\to\theta-a^2\cos\theta\sin\theta\frac{1}{2r^2}\left(1+\frac{2M}{r}\right). \tag{2.107}$$

2.6.2 Perturbations

Now that we have the metric describing a slowly rotating BH up to second order in the angular momentum, as seen in Eq. (2.104), we want to perturb this background, which we refer to as $g^0_{\mu\nu}$, with the ultimate goal of finding the QNM spectrum and the shifts induced by the rotation with respect to the nonrotating case. In this section, we will write schematically the steps needed to compute the QNMs on the slowly rotating background, but we leave the details of the computations to the next chapters, where the same steps will be implemented in EdGB gravity.

A generic perturbation δX (either scalar, vector, or tensor) applied to this background can be expanded in a complete basis of spherical harmonics in the same way we discussed for the nonrotating case (see Appendix A). In the frequency domain, this expansion takes the form

$$\delta X_{\mu_1\dots}(t,r,\theta,\phi)=\delta X^{(i)}_{lm}(r)\mathcal{Y}^{lm\,(i)}_{\mu_1\dots}(\theta,\phi)e^{-i\omega t}, \tag{2.108}$$

where $\mathcal{Y}^{lm\,(i)}_{\mu_1\dots}(\theta,\phi)$ is a suitable basis of scalar, vector, or tensor spherical harmonics, depending on the nature of the perturbation δX. $\delta X^{(i)}_{lm}(r)$ are radial functions that can be classified either as *polar*, if they have the same behavior of the scalar spherical harmonics under parity transformations, or *axial*, if they have the opposite behavior.

After substituting this expansion in the field equations and integrating the angular part using

the properties of spherical harmonics, the linear response of the system to the perturbation is fully described by a set of coupled ODEs in the perturbation functions $\delta X^{(i)}_{lm}(r)$. However, in contrast with the spherically symmetric case discussed earlier in the chapter, in the rotating, axially symmetric background, perturbations with different harmonic index l become coupled, while the ones with different values of m remain decoupled.

Schematically, the general structure of the perturbation equations can be written as

$$\begin{aligned} 0 =& \mathcal{P}_{l\,m} + \bar{a}\, m\, \bar{\mathcal{P}}_{l\,m} + \bar{a}^2 \hat{\mathcal{P}}_{l\,m} + m^2\, \bar{a}^2 \bar{\bar{\mathcal{P}}}_{l\,m} \\ &+ \bar{a} \left(Q_{l\,m} \tilde{\mathcal{A}}_{l-1\,m} + Q_{l+1\,m} \tilde{\mathcal{A}}_{l+1\,m} \right) \\ &+ \bar{a}^2 \left(Q_{l-1\,m} Q_{l\,m} \breve{\mathcal{P}}_{l-2\,m} + Q_{l+1\,m} Q_{l+2\,m} \breve{\mathcal{P}}_{l+2\,m} \right) \\ &+ m\, \bar{a}^2 \left(Q_{l\,m} \check{\mathcal{A}}_{l-1\,m} + Q_{l+1\,m} \check{\mathcal{A}}_{l+1\,m} \right) , \end{aligned} \tag{2.109}$$

$$\begin{aligned} 0 =& \mathcal{A}_{l\,m} + \bar{a}\, m\, \bar{\mathcal{A}}_{l\,m} + \bar{a}^2 \hat{\mathcal{A}}_{l\,m} + m^2\, \bar{a}^2 \bar{\bar{\mathcal{A}}}_{l\,m} \\ &+ \bar{a} \left(Q_{l\,m} \tilde{\mathcal{P}}_{l-1\,m} + Q_{l+1\,m} \tilde{\mathcal{P}}_{l+1\,m} \right) \\ &+ \bar{a}^2 \left(Q_{l-1\,m} Q_{l\,m} \breve{\mathcal{A}}_{l-2\,m} + Q_{l+1\,m} Q_{l+2} \breve{\mathcal{A}}_{l+2\,m} \right) \\ &+ m\, \bar{a}^2 \left(Q_{l\,m} \check{\mathcal{P}}_{l-1\,m} + Q_{l+1\,m} \check{\mathcal{P}}_{l+1\,m} \right) , \end{aligned} \tag{2.110}$$

where $\bar{a} = J/M^2$,

$$Q_{lm} = \sqrt{\frac{(l-m)(l+m)}{(2l-1)(2l+1)}}\,, \tag{2.111}$$

and $\mathcal{P}_{l\,m}, \bar{\mathcal{P}}_{l\,m}, \hat{\mathcal{P}}_{l\,m}, \bar{\bar{\mathcal{P}}}_{l\,m}, \tilde{\mathcal{P}}_{l\,m}, \breve{\mathcal{P}}_{l\,m}, \check{\mathcal{P}}_{l\,m}$ ($\mathcal{A}_{l\,m}, \bar{\mathcal{A}}_{l\,m}, \hat{\mathcal{A}}_{l\,m}, \bar{\bar{\mathcal{A}}}_{l\,m}, \tilde{\mathcal{A}}_{l\,m}, \breve{\mathcal{A}}_{l\,m}, \check{\mathcal{A}}_{l\,m}$) are linear combinations, which do not depend explicitly on m, of the polar (axial) perturbation functions. At zeroth order in the spin we get, as expected, no couplings between different ls, i.e. $\mathcal{P}_{l\,m} = 0$, $\mathcal{A}_{l\,m} = 0$, corresponding for example to Eqs. (2.57)-(2.58).

The structure of Eqs. (2.109)-(2.110) is similar to many results in Quantum Mechanics, where the slow rotation technique is often used, and it interestingly resembles a Laporte-like selection rule [286]:

- at *first order* in $\bar{a}$, perturbations with a given value of l are only coupled to perturbations with $l \pm 1$ and opposite parity;
- at *second order* in $\bar{a}$, perturbations with a given value of l are also coupled to same parity perturbations with $l \pm 2$ and, when $m \neq 0$, to opposite parity perturbations with $l \pm 1$.

The symmetries of the harmonic expansion guarantee that this scheme is preserved at any order in $\bar{a}$. We note that in the case $|m| = l$ we have $Q_{lm} = 0$, thus the couplings of perturbations with index l to perturbations with indices $l-1$ and $l-2$ are suppressed, leaving only couplings to $l+1$ and $l+2$, in analogy to the "propensity rule" in atomic theory, stating that $l \to l+1$ transitions are strongly favored over $l \to l-2$.

The boundary conditions defining the QNM are

$$\delta X^{(i)}_{lm}(r \sim r_H) \sim e^{-ik_H r_*} \tag{2.112}$$

$$\delta X^{(i)}_{lm}(r \to \infty) \sim e^{i\omega r_*}\,, \tag{2.113}$$

where we have included the frame-dragging effect on the frequency near the horizon through $k_H = \omega - m\Omega_H$, with $\Omega_H = -\lim_{r\to r_H} g^{(0)}_{t\phi}/g^{(0)}_{\phi\phi}$ the angular velocity of the BH.

2.6.3 Quasinormal Mode Spectrum

Due to the aforementioned couplings between different multipolar indices and different parities, the computation of the QNM spectrum of a rotating black hole in the slow rotation expansion can become very intricate. Luckily, when our focus is only to compute the spectrum at a specific spin order and not to find the exact form of the perturbation functions, the equations (2.109)-(2.110) can be further simplified.

We remark that both the equations (2.109)-(2.110) and the boundary conditions (2.112)-(2.113) are invariant under the transformation $(\bar{a}, m) \to (-\bar{a}, -m)$, as long as axial perturbations change sign and polar perturbations remain the same. Therefore, the quasi-normal modes are also invariant under this transformation, and consequently, the $\mathcal{O}(\bar{a})$ corrections to the spectrum are odd in m, while the $\mathcal{O}(\bar{a}^2)$ corrections are even [159, 278, 285]. Hence, since the equations are at most quadratic in m, a reasonable ansatz satisfying these properties is

$$\omega^{nlm}(\bar{a}) = \omega^{nl}_0 + \bar{a} m \omega^{nl}_1 + \bar{a}^2(\omega^{nl}_{2a} + m^2\omega^{nl}_{2b}) + \mathcal{O}(\bar{a}^3)\,, \tag{2.114}$$

where the coefficients ω_r $(r = 0, 1, 2a, 2b)$ do not depend on m and ω_0 are the frequencies for the nonrotating case – see e.g. Eqs. (2.69)-(2.70).

We note that the QNM spectrum of BHs in GR, according to no-hair theorems [18, 287], depends only on the mass M, which is implicit in Eq. (2.114), and the spin $\bar{a}$. In modified theories of gravity, the no-hair theorems can be violated and this translates to additional parameter dependences in the QNM spectrum, which provides an important tool to perform tests of GR.

First Order

At first order in the spin Eqs. (2.109)-(2.110) become

$$0 = \mathcal{P}_{l\,m} + \bar{a}\, m\, \bar{\mathcal{P}}_{l\,m} + \bar{a}\left(Q_{l\,m}\tilde{\mathcal{A}}_{l-1\,m} + Q_{l+1\,m}\tilde{\mathcal{A}}_{l+1\,m}\right) \tag{2.115}$$

$$0 = \mathcal{A}_{l\,m} + \bar{a}\, m\, \bar{\mathcal{A}}_{l\,m} + \bar{a}\left(Q_{l\,m}\tilde{\mathcal{P}}_{l-1\,m} + Q_{l+1\,m}\tilde{\mathcal{P}}_{l+1\,m}\right)\,. \tag{2.116}$$

An example of the explicit form of these equations for neutron stars can be found in Ref. [193].
We now want to determine which terms actually contribute to the first order QNM coefficient ω_1 in Eq.(2.114). Since $\tilde{\mathcal{A}}_{l\pm1\,m}, \tilde{\mathcal{P}}_{l\pm1\,m}$ are not multiplied by m and do not depend explicitly on it, the only terms that could give rise to the m dependence in the expansion (2.114) are the ones containing $\bar{\mathcal{A}}_{l\pm1\,m}, \bar{\mathcal{P}}_{l\pm1\,m}$.

Therefore, as long as we are interested in computing the *first-order correction* to the QNM

spectrum, the eigenvalue problem is equivalent to the set of equations

$$0 = \mathcal{P}_{l\,m} + \bar{a}\, m\, \bar{\mathcal{P}}_{l\,m} \tag{2.117}$$

$$0 = \mathcal{A}_{l\,m} + \bar{a}\, m\, \bar{\mathcal{A}}_{l\,m}\,, \tag{2.118}$$

which are *decoupled*. The spectrum at first order is then

$$\omega^{nlm}(\bar{a}) = \omega_0^{nl} + \bar{a}\, m\, \omega_1^{nl}\,, \tag{2.119}$$

where we see that the degeneracy in m that was present in the spherically symmetric case is now broken, similarly to what happens in the quantum mechanics with the Zeeman-like splitting of the energy levels of an atom in a static external magnetic field [1].

Second Order

In order to understand which terms of the Eqs. (2.109)-(2.110) actually contribute to the QNM spectrum at the second order in the spin, it is useful to consider the expansions of a generic polar perturbation P_{lm} and axial perturbation A_{lm}

$$P_{lm} = P_{lm}^{(0)} + \bar{a} P_{lm}^{(1)} + \bar{a}^2 P_{lm}^{(2)} \tag{2.120}$$

$$A_{lm} = A_{lm}^{(0)} + \bar{a} A_{lm}^{(1)} + \bar{a}^2 A_{lm}^{(2)}\,. \tag{2.121}$$

Since perturbations with index $l \pm 1$ are always multiplied by at least $\bar{a}$ in the equations (2.109)-(2.110), their second-order terms, $P_{l\pm1m}^{(2)}, A_{l\pm1m}^{(2)}$, will not contribute to the equations at this order; moreover, when they are multiplied by $\bar{a}^2$, their first-order terms $P_{l\pm1m}^{(1)}, A_{l\pm1m}^{(1)}$, do not contribute as well.
Similarly, perturbations with index $l \pm 2$ contribute to the equations (2.109)-(2.110) only with their 0-order part $P_{l\pm2m}^{(0)}, A_{l\pm2m}^{(0)}$.

Let us now assume that a source only excites a polar perturbation with a given harmonic index l. The rotation-induced couplings in the field equations will source perturbations with both axial and polar parity, and with harmonic index $l' \neq l$. However, since this only occurs in presence of rotation, the axial perturbations with l, l' and polar perturbations with l' will not be present in the nonrotating limit, meaning

$$A_{lm}^{(0)} = A_{l'm}^{(0)} = P_{l'm}^{(0)} = 0\,, \tag{2.122}$$

so that the only perturbations present at this order are $P_{lm}^{(0)}$. Axial parity perturbations with index $l \pm 1$ are excited through the rotation-induced couplings at first order in the spin, thus

$$A_{l\pm1m} = \bar{a} A_{l\pm1m}^{(1)} + \bar{a}^2 A_{l\pm1m}^{(2)}\,. \tag{2.123}$$

Similarly, polar parity perturbations with index $l \pm 2$ are excited through the rotation-induced couplings at second order in the spin, and are

$$P_{l\pm2m} = \bar{a}^2 P_{l\pm2m}^{(2)}\,. \tag{2.124}$$

Calling the *polar-led* sector the one in which only a polar perturbation is nonvanishing in the nonrotating limit [288], applying the considerations above to Eqs. (2.109)-(2.110), we get the polar-led set of equations

$$\begin{aligned}
&\mathcal{P}_{l\,m} + \bar{a}\, m\, \bar{\mathcal{P}}_{l\,m} + \bar{a}^2 \hat{\mathcal{P}}_{l\,m} + \; m^2\, \bar{a}^2 \bar{\bar{\mathcal{P}}}_{l\,m} + \bar{a}\left(Q_{l\,m}\tilde{\mathcal{A}}_{l-1\,m} + Q_{l+1\,m}\tilde{\mathcal{A}}_{l+1\,m}\right) = 0 \\
&\mathcal{A}_{l+1\,m} + \bar{a}\, m\, \bar{\mathcal{A}}_{l+1\,m} + \bar{a}\, Q_{l+1\,m}\tilde{\mathcal{P}}_{l\,m} + m\, \bar{a}^2\, Q_{l+1\,m}\check{\mathcal{P}}_{l\,m} = 0 \\
&\mathcal{A}_{l-1\,m} + \bar{a}\, m\, \bar{\mathcal{A}}_{l-1\,m} + \bar{a}\, Q_{l\,m}\tilde{\mathcal{P}}_{l\,m} + m\, \bar{a}^2\, Q_{l\,m}\check{\mathcal{P}}_{l\,m} = 0\,.
\end{aligned} \tag{2.125}$$

from which we can compute the polar-led subset of QNMs up to the second order in the spin $\bar{a}$.

Through completely analogous considerations when in the nonrotating case only an axial perturbation is excited, we can find the *axial-led* set of equations

$$\begin{aligned}
&\mathcal{A}_{l\,m} + \bar{a}\, m\, \bar{\mathcal{A}}_{l\,m} + \bar{a}^2 \hat{\mathcal{A}}_{l\,m} + \; m^2\, \bar{a}^2 \bar{\bar{\mathcal{A}}}_{l\,m} + \bar{a}\left(Q_{l\,m}\tilde{\mathcal{P}}_{l-1\,m} + Q_{l+1\,m}\tilde{\mathcal{P}}_{l+1\,m}\right) = 0 \\
&\mathcal{P}_{l+1\,m} + \bar{a}\, m\, \bar{\mathcal{P}}_{l+1\,m} + \bar{a}\, Q_{l+1\,m}\tilde{\mathcal{A}}_{l\,m} + m\, \bar{a}^2\, Q_{l+1\,m}\check{\mathcal{A}}_{l\,m} = 0 \\
&\mathcal{P}_{l-1\,m} + \bar{a}\, m\, \bar{\mathcal{P}}_{l-1\,m} + \bar{a}\, Q_{l\,m}\tilde{\mathcal{A}}_{l\,m} + m\, \bar{a}^2\, Q_{l\,m}\check{\mathcal{A}}_{l\,m} = 0\,.
\end{aligned} \tag{2.126}$$

which gives the axial-let subset of QNMs.

As we can see from Eqs. (2.125)-(2.126), to compute the QNM spectrum at second order in the spin, it is not necessary to include couplings with index $l \pm 2$, which would contribute only to the next order of spin corrections. Even though, for a given l, rotation couples terms with opposite parity and different multipolar index, the subsystems (2.125)-(2.126) are closed, meaning that they contain a finite number of equations that fully describe the dynamics to second order in the spin. Without these considerations, we would have an infinite number of equations and a truncation at a specific l_{max} would have been necessary.

It is important to remark that the "polar-led" ("axial-led") class is a subset of the whole set of solutions to Eqs. (2.109)-(2.110), since it has been obtained under the main assumption that only polar (axial) perturbations with harmonic index l are activated at zeroth order in the rotation (which is reasonable when a specific multipolar contribution l is dominant) [285][5]. Nonetheless, all solutions belonging to one of the two classes which fulfill the appropriate QNM boundary conditions, are also solutions of the full system (2.109)-(2.110) and hence belong to the eigenspectrum [278] .

We have computed the QNMs at second order in the spin

$$\omega^{nlm}(\bar{a}) = \omega_0^{nl} + \bar{a} m \omega_1^{nl} + \bar{a}^2(\omega_{2a}^{nl} + m^2 \omega_{2b}^{nl})\,, \tag{2.127}$$

for slowly rotating BHs in GR, for $n = 0, l = 2, l = 3$ with a direct integration method (for further details see the implementation in the following chapters). The coefficients $\omega_{r\,R,I}^{nl} \;\; r = 0, 1, 2a, 2b$ are shown in Tab. 2.1.

The $n = 0, l = 2$ case has also been computed by Hatsuda et al. [289] using the Chandrasekhar-Detweiler and Sasaki-Nakamura equations; our results are in very good agreement with their find-

[5]This is usually the case for realistic scenarios of BBH mergers, where the $l = 2$ is usually dominant, while other modes like $l = 3$ are only mildly (or not at all) excited [31, 33, 128, 266, 267]. Nevertheless, since we are considering linear perturbations we can study each l-index perturbation at zeroth order independently and find the related rotating frequencies. In case more perturbations are excited at zeroth order in the spin, we can then take into account all the contributions separately.

ings.

Table 2.1: *Values of the coefficients for the slow rotation expansion for fundamental modes with $l = m = 2$ and $l = m = 3$ for perturbations of a slowly rotating BHs in GR.*

spin order r	$\omega^{02}_{r\,R}$	$\omega^{02}_{r\,I}$	$\omega^{03}_{r\,R}$	$\omega^{03}_{r\,I}$
0	0.37367	−0.08896	0.59944	−0.09270
1	0.06289	0.00010	0.06737	0.00065
2a	0.03591	0.00638	0.04758	0.00659
2b	0.00896	−0.00031	0.00661	0.00006

Padé Resummation

The expansion of the QNM frequencies in Eq.(2.127) is a Taylor expansion and as such is valid in the proximity of $\bar{a} = 0$; the more terms in the expansion the better the agreement with the Kerr QNMs, especially for larger spins. Once the modes $\omega^{nlm}(\bar{a})$ are computed, taking the derivatives with respect to $\bar{a}$ yield the expansion coefficients ω^{nl}_r $(r = 0, 1, 2a, 2b)$ – where the separation between ω_{2a} and ω_{2b} can be obtained by repeating the computation for different values of m and linearly combining them.

The Taylor expansions (2.127) can be resummed using *Padé approximants* [290, 291]. The Padé resummation, which consists in replacing polynomials with rational functions, often improves the convergence of an expansion, as it has been seen in applications, for instance, to post-Newtonian expansions [290] and, more recently, to the computation of BH sensitivities in EdGB gravity [218, 219]. Padé resummation also improves the convergence of the spin expansion of BH QNMs [289], and we will exploit this feature to extend the validity of our slow-rotation approximation.

Given a Taylor expansion $T_K(x)$ of order K around $x = 0$, we can construct a Padé approximant $P[M, N]$, with M, N integer numbers such thar $M + N = K$, given by

$$P[M,N](x) = \frac{A_0 + A_1 x + A_2 x^2 + ... + A_M x^M}{B_0 + B_1 x + B_2 x^2 + ... + B_N x^N} \tag{2.128}$$

such that $P[M, N](x) = T_K(x)$ up to order K. Solving order by order in x, the coefficients $A_0, ...A_M$, $B_0, ..., B_N$ can be determined as combinations of the Taylor expansion coefficients.

Since the Taylor expansion to second order is not accurate for QNMs of rotating BHs with large spins (we note that a BH in the aftermath of a binary coalescence has typically $\bar{a} \sim 0.7$), we shall perform a Padé resummation of the second-order expansion (2.127). In this case the Taylor approximant of $\omega^{nlm}(\bar{a})$ is of second order, and, for each $(n, l, m \neq 0)$, the possible choices of Padé approximants are:

$$P[1,1](\bar{a}) = \frac{m\,\omega_0^{nl}\omega_1^{nl} + \left[m^2\,{\omega_1^{nl}}^2 - \omega_0^{nl}\omega_2^{nlm}\right]\bar{a}}{m\,\omega_1^{nl} - \omega_2^{nlm}\bar{a}} \tag{2.129}$$

and

$$P[0,2](\bar{a}) = \frac{{\omega_0^{nl}}^3}{{\omega_0^{nl}}^2 + \bar{a}^2 m^2 {\omega_1^{nl}}^2 - \bar{a}\omega_0^{nl}\left[m\omega_1^{nl} + \bar{a}\omega_2^{nlm}\right]}\,, \tag{2.130}$$

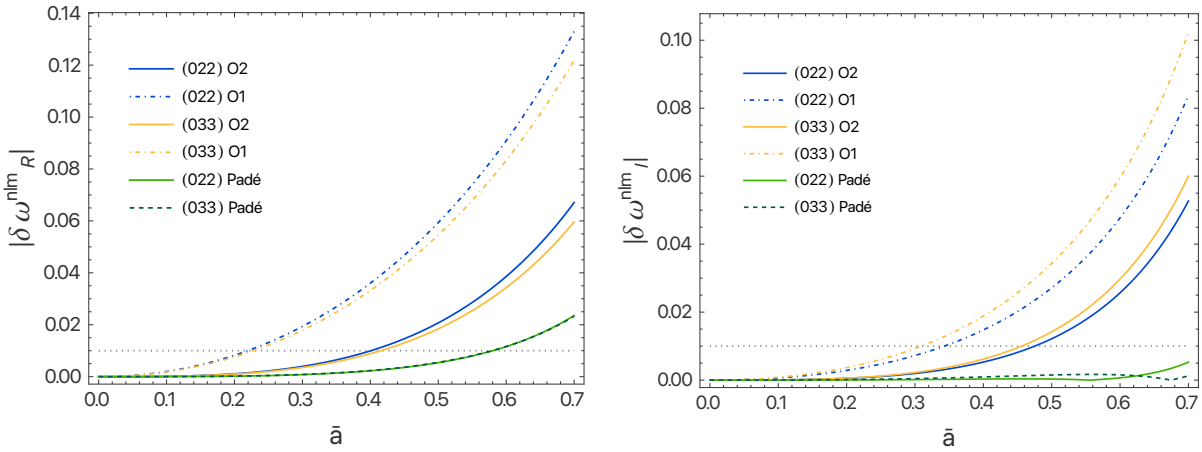

Figure 2.5: Real (upper panel) and imaginary (lower panel) parts of the relative difference between the QNMs of Kerr BHs and those of rotating BHs computed within the slow-rotation approximation, for the $(nlm) = (022)$, (033) modes. The slow-rotation expansion is performed to first order ($O1$), to second order ($O2$), to second order with Padé resummation (*Padé*). The horizontal dotted line represents a 1% error.

where we recall that $\omega_2^{nlm} = \omega_{2a}^{nl} + m^2\omega_{2b}^{nl}$. Note that since the QNMs are complex, the coefficients of the Taylor and Padé approximants are complex as well.

As suggested in Ref. [290], we shall use the "diagonal" Padé, $P[1,1]$, unless it is not accurate due to the presence of a pole or a reduction of order in the polynomials, in which case we instead use $P[0,2]$. In practice, for the QNMs with $n = 0$, $l = 2, 3$ we shall always use $P[1,1]$ except for $m = 0$ (since Eq. (2.129) reduces to a constant) and for the imaginary parts of the modes with $m = \pm 1$, for which $P[1,1]$ has a pole close to the spin interval which we have considered. A similar computation has been done in Ref. [289], where instead $P[1,1]$ was used for all values of m.

We have computed the QNMs of a slowly rotating BH in GR, using the direct integration method, to first order in the spin (neglecting $\mathcal{O}(\bar{a}^2)$ terms in the background and in the perturbation equations), and then to second order, with the QNMs Taylor-expended to the same order, as Eqs. (2.119) or (2.127) respectively. Moreover, the QNMs at second order in the spin have been resummed using Padé approximants. Finally, we have compared the frequencies of these modes with those of Kerr BHs (see e.g. [279]), by computing the discrepancies

$$\delta\omega^{nlm}(\bar{a}) = \frac{\omega^{nlm}_{\rm T,P} - \omega^{nlm}_{\rm Kerr}}{\omega^{nlm}_{\rm Kerr}} \,, \tag{2.131}$$

where the subscripts 'T' and 'P' refer to the modes (computed in slow-rotation expansion) Taylor-expanded and Padé resummed, respectively, while the subscript "Kerr" refers to the modes of Kerr BHs.

In Fig. 2.5 we show real and imaginary parts of the discrepancies (2.131) as functions of $\bar{a}$, for the QNMs with $(nlm) = (022)$ and $(nlm) = (033)$, which are expected to be the most excited in typical binary BH coalescences [133, 178, 292, 293]. The curves labeled $O1$, $O2$ show the discrepancies between the modes of Kerr BHs and those computed within the slow-rotation approximation, to $\mathcal{O}(\bar{a})$ and to $\mathcal{O}(\bar{a}^2)$, respectively. Instead, the curves labeled *Padé* show the discrepancies with the $\mathcal{O}(\bar{a}^2)$ modes resummed using Padé approximants.

At first order, the discrepancy of the Taylor expansion is smaller than 1% as long as $\bar{a} \lesssim 0.22$;

when we include the second order correction, the discrepancy is smaller than 1% for $\bar{a} \lesssim 0.4$. Applying the Padé resummation improves the accuracy of the expansion, which is accurate to $\sim 1\%$ for $\bar{a} \lesssim 0.6$ and to $\sim 2\%$ for $\bar{a} \lesssim 0.7$.

Repeating the analysis for modes with different values of m, we obtain the same (or better) accuracy for the Padé-resummed modes. However, we need to employ the approximant $P[0,2]$ instead of $P[1,1]$ in two cases: when $m = 0$, for which Eq. (2.129) reduces to a constant, and for the imaginary parts of the modes when $m = \pm 1$. In the latter case, the Padé approximant $P[1,1]$ leads to a larger error, compared with that of the Taylor approximant, for $\bar{a} \sim 0.7$ [6]; if, instead, we use $P[0,2]$ for the imaginary parts of the modes with $n = 0$, $l = 2, 3$, $m = \pm 1$, the error is smaller than 1% for $\bar{a} \lesssim 0.7$.

We will apply this Padé Resummation analysis also to a modified theory of gravity in Chapter 6, where the results obtained here for the GR case will be used as a reference of the extent to which we can consider our slow-rotation approximation to be reliable.

2.7 Going Beyond General Relativity

In this section we are going to summarize schematically some of the main differences we expect from the framework described in this chapter, when going to a modified theory of gravity, such as EdGB, introduced in the next chapter:

- The separability of the radial and angular parts of the perturbation equations without the introduction of couplings is not guaranteed to be possible when there are modifications of the GR and it is a characteristic that reflects how special the Schwarzschild and Kerr solutions are;

- There is not a single master equation like the Zerilli/Regge-Wheeler equations or the Teukolsky equation describing BH perturbations. Some methods to compute the QNMs – including Leaver, WKB and Pöschl-Teller [1] – rely on having an effective potential such as the ones in (2.25)-(2.27). In modified theories of gravity, however, it is not always possible to find an effective potential and consequently use these methods. However, for some cases, it was possible to apply them even if the equations are coupled (see e.g. Refs. [294, 295]);

- If we introduce an additional dynamical field that couples to the curvature in the theory's action, we expect isospectrality to be broken, due to the coupling of the new field with either the axial or polar sector [18];

- The null geodesic correspondence [296–298], which assumes that QNMs, for $l \gg 1$, correspond to waves trapped near the peak of the potential barrier for null particles (the photon sphere) and slowly leaking out, is a method useful to compute QNMs in GR, but it is not necessarily valid beyond-GR, especially when there are additional degrees of freedom and isospectrality is broken;

- The no-hair conjecture valid in GR [287] might no longer hold, and the QNM spectrum can depend on additional hairs.

[6] we believe this is due to the presence of a pole close to the considered range of values for the spin.

- The physical quantities, such as the mass and angular momentum, will take into account the GR modifications;
- When the background spacetime is no longer a solution of Einstein GR equations, one needs to find a new suitable definition of the tortoise coordinate that reproduces specific properties.

Chapter 3

Black Holes in Einstein-dilaton Gauss-Bonnet Gravity

In the previous chapter, we reviewed some applications of BH perturbation theory in the context of General Relativity that will be useful when including modifications of the theory.

We introduced some of the needs and the reasons to go beyond Einstein's theory of General Relativity in Ch. 1. Alternative theories have been proposed, which make specific and, thanks to present and future technology, potentially testable predictions of how exactly GR would be modified [136]. To do that, we should be able to predict the structure and dynamics of compact objects and the gravitational radiation they emit, whether isolated or in binary systems. Of course, even if we add additional degrees of freedom, we still must have a theory that is cosmologically viable and consistent with GR in the intermediate energy regime, where we know that GR works astonishingly well.

The possible ways to modify GR are countless, but we can divide them into groups depending on which fundamental assumption of the theory is put aside [18]. Lovelock's theorem states that [299, 300]:
In four spacetime dimensions the only divergence-free symmetric rank-2 tensor constructed solely from the metric $g_{\mu\nu}$ and its derivatives up to second differential order, and preserving diffeomorphism invariance, is the Einstein tensor plus a cosmological term.
This leads naturally to the Einstein equations:

$$G_{\mu\nu} + \Lambda g_{\mu\nu} = \chi T_{\mu\nu} \,. \tag{3.1}$$

The divergence-free condition on Einstein tensor implies $\nabla_\mu T^{\mu\nu} = 0$, that is necessary for geodetic motion, and it guarantees the validity of the weak equivalence principle, i.e. the universality of free fall (the curves followed by test particles do not depend on their mass or composition) [301]. The equations of motion (3.1) can be obtained from the variation of the Einstein-Hilbert action:

$$S = \frac{c^3}{16\pi G} \int d^4x \sqrt{-g} R + S_M \,, \tag{3.2}$$

with S_M the Standard Model action.

There are at least four nonequivalent ways to circumvent Lovelock's theorem:

- **Additional fields**: we can add extra degrees of freedom in the form of fundamental (scalar, vector, tensor) dynamical fields coupled with the metric tensor, leaving more options to construct the left-hand side of (3.1). Alternatively, we drop the assumption that $T_{\mu\nu}$ enters linearly in the Einstein equations, so that the right-hand side is a nonlinear combination of the stress-energy tensor such that $\nabla_\mu T^{\mu\nu} = 0$ still holds. The coupling to matter shall then be different.

- **Violations of diffeomorphism invariance**: we can introduce violations of Lorentz invariance (a particular case of diffeomorphism) at high energies or we can attribute mass to the mediator of gravity, which is required to be, according to the diffeomorphism invariance, a massless spin-2 field.

- **Higher dimensions**: Einstein-Hilbert action (3.2) is not unique in higher dimensions and the theories of gravity in dimensions other than four have a strong theoretical interest (string theories, dependence on spacetime dimension).

- **WEP violation**: giving up the divergence-free request means sacrificing the condition $\nabla_\mu T^{\mu\nu} = 0$ and thus the weak equivalence principle (WEP). However, this principle has been tested with excellent precision, so this case is less appealing.

The theory we shall focus on is *Einstein-dilaton Gauss-Bonnet (EdGB)* gravity, which fits in the first case and it is one of the simplest modifications of gravity that features the addition of a scalar dynamical field (the dilaton field) coupled to a scalar combination of the metric. It is natural to couple this scalar field to a *quadratic* term in the curvature tensor so that in the weak-field regime this contribution would be negligible and GR would be recovered, in line with the current observational constraints.

If we consider Einstein-Hilbert action (3.2) as the first term in an expansion containing all possible curvature invariants (the *Ricci* scalar is the simplest), as suggested by low-energy effective string theories [54], quadratic curvature terms already make the theory renormalizable [55]. In general, this carries the cost of having higher-derivative terms in the field equations, thus being subject to Ostrogradsky's instability [302], which may lead to ghosts or other pathologies.
Therefore, if we consider a theory with only linear and quadratic terms in the action, we should consider it as effective, i.e. a truncation of a theory with additional terms that are neglected in the perturbative regime.

At the second order in the curvature, the only possible independent curvature invariants are

$$R^2,\ R^2_{\mu\nu},\ R^2_{\mu\nu\rho\sigma}\ {}^*RR \tag{3.3}$$

where $R^2_{\mu\nu} \equiv R_{\mu\nu}R^{\mu\nu}$, $R^2_{\mu\nu\rho\sigma} \equiv R_{\mu\nu\rho\sigma}R^{\mu\nu\rho\sigma}$, ${}^*RR = \frac{1}{2}R_{\mu\nu\rho\sigma}\epsilon^{\nu\mu\lambda\kappa}R^{\rho\sigma}_{\lambda\kappa}$ (Pontryagin or Chern-Simons scalar). Of particular interest are the Pontryagin scalar and the *Gauss-Bonnet (GB) scalar*,

$$\mathcal{R}^2_{GB} \equiv R^2 - 4R^2_{\mu\nu} + R^2_{\mu\nu\rho\sigma}\,, \tag{3.4}$$

because they emerge in low-energy realizations of string theory. One of the main candidates for a theory of quantum gravity is in fact string theory [303]. Since geometrical studies are still difficult in superstring theories, it is useful to work with effective theories that are a low-energy truncation of

string theory. One paradigmatic example is the one-loop corrected four-dimensional effective theory of the heterotic superstrings at low energies known as *Einstein-dilaton-Gauss-Bonnet (EdGB) theory* [304]. If we consider the GB scalar (3.4) alone in the action, it does not yield modifications to Einstein's equations in four spacetime dimensions because it would appear in an integral that is a topological invariant and only accounts for boundary terms. Thus, in the EdGB theory, this quadratic term in the curvature is coupled to a scalar dynamical field, the *dilaton* field φ, in an exponential form e^{φ}. The more general theory in which the coupling with the dilaton field can appear in other functional forms is referred to as Einstein-Scalar Gauss-Bonnet (ESGB).

Quadratic terms in the action are responsible for changing the behavior of stationary BHs. If we were to include in the linear gravitational action one or more scalar fields, we would still obtain vacuum BH solutions that are the same as in GR [197, 198, 305], since this theory would still satisfy the no-hair theorems (see e.g. [306–308] for cases in which these theorems can be violated). Instead, including quadratic terms in the action, besides modifying the strong-field regime, guarantees that stationary BH solutions are different from GR.

EdGB gravity is considered one of the simplest and most consistent high-energy extensions of GR because the GB term is such that it avoids some pathological features, like ghosts [302]. Indeed, it avoids Ostrogradsky instability thanks to the field equations being of second order in time (this also allows the use of the Regge-Wheeler gauge) for *any* coupling, not only in the weak-coupling limit as we would have for Effective Field Theories (EFTs) [18, 208]. Furthermore, the post-Newtonian expansion of this theory (i.e. in powers of v/c, with v the velocity and c the speed of light) is identical, to the lowest order, to that of GR, which means that it passes all Solar system experimental tests of gravity at intermediate scales [309], where the deviations from Newton's theory of gravity are small. The differences arise only at higher orders, i.e. large curvature; thus, ideal places to look for these modifications are in the strong-field regime, near compact objects such as BHs.

In classical Einstein-Maxwell theory, the no-hair theorem states that BHs are characterized only by three parameters [142, 287]: mass M, electric charge Q (~ 0 for astrophysical BHs) and angular momentum $J \equiv \bar{a}M^2 \leq M^2$. EdGB gravity admits BH solutions, which are scalarized, i.e. endowed with a non-trivial scalar field profile outside the horizon [210, 212, 213, 215–217, 310], thus they possess an additional scalar hair and they are usually called Dilatonic Black Holes (DBHs) [201, 230]. One possibility of ruling out these alternative theories is therefore given by testing the no-hair theorem for example through gravitational wave observations [211, 311]. The dilaton field introduces an additional force interaction coupled with the gravitational interaction. Given this additional interaction, two DBHs in a binary orbit would decay faster than what is predicted by GR, due to the additional radiation channel associated with the scalar emission [180].

The stability under different perturbations of stationary EdGB BHs, studied in Refs. [3, 229, 230, 312], makes the BH solutions in this theory proper alternative spacetimes to the Schwarzschild and Kerr metrics found in GR, which are not solutions of EdGB. We remark that the general well-posedness of ESGB, necessary to perform numerical relativity simulations of merger events, is still under investigation [226, 313, 314].

One of the most important imprints left by the modification of GR on observable quantities is given by the shift in the QNM spectrum with respect to the GR values. In fact, BH QNMs are intrinsically linked to the underlying theory of gravity, as they depend on the same quantities that

can either support or confute the no-hair conjectures: QNMs in GR depend only on the mass and spin of the BH, while in EdGB they would depend also on the additional scalar charge connected to the presence of the dilaton field [3, 180].
Therefore, if we had the QNM spectrum in EdGB gravity, we would be able to compare the theoretical predictions with present and future GW observations to look for GR deviations [118, 137, 178, 311]; this approach is called *gravitational spectroscopy* [1].

In this Chapter, we define the Black Hole solution in EdGB gravity, which we will use as background to apply BH perturbation theory in the following chapters and ultimately find the corresponding QNM spectrum.

3.1 Action and Field Equations

EdGB gravity is obtained from the Einstein-Hilbert action (3.2) describing GR, by introducing an additional quadratic term in the curvature in the following way

$$S = \int d^4x \frac{\sqrt{-g}}{16\pi} \left(R - \frac{1}{2}\partial_\mu\varphi\partial^\mu\varphi + \frac{\alpha_{GB}}{4} e^{\varphi} \mathcal{R}^2_{GB} \right) + S_m \,, \tag{3.5}$$

where we adopt geometric units $G = c = 1$,

$$\mathcal{R}^2_{GB} = R_{\mu\nu\rho\sigma}R^{\mu\nu\rho\sigma} - 4R_{\mu\nu}R^{\mu\nu} + R^2 \tag{3.6}$$

is the *Gauss-Bonnet* term, and S_m is the matter action, which we neglect since we are assuming that the matter is not coupled with the dilaton field φ, and because we are interested in studying the ringdown emission of isolated black holes.
As already mentioned, since the Gauss-Bonnet term is topological, it is coupled with the scalar field φ, the *dilaton*, in an exponential form through a coupling constant α_{GB}. Because we are introducing a scalar field, we also have the corresponding kinetic term in the action.

EdGB gravity belongs to the wider class of theories, called *Einstein-Scalar Gauss-Bonnet* (ESGB), in which, instead of the exponential coupling e^{φ}, there is a generic function of the scalar field $f(\varphi)$. When $f'(\varphi) = df/d\varphi \neq 0$, as for EdGB, BHs always support scalar hair. When instead $f'(\varphi) = 0$ for some constant φ_0, as for the Gaussian $f(\varphi) \propto exp(-\varphi^2)$ and quadratic $f(\varphi) \propto \varphi^2$ couplings, the theory admits the same stationary, asymptotically flat BH solutions as GR [315], together with additional scalarized BH solutions [316–319].

The coupling between the curvature and a scalar field implies that the gravitational interaction is no longer mediated by the curvature only, but also by the dilaton field. Of course, this is expected to be a small effect since the Gauss-Bonnet term is quadratic in the curvature and thus negligible in the weak-field regions of spacetime, where we know that the predictions of GR are correct.

By extremizing the action (3.5) with respect to the metric and to the scalar field, we get the equations

$$\Box\varphi = \frac{1}{\sqrt{-g}}\partial_\mu(\sqrt{-g}g^{\mu\nu}\partial_\nu\varphi) = \frac{\alpha_{GB}}{4} e^{\varphi}\mathcal{R}^2_{GB} \,, \tag{3.7}$$

$$G_{\mu\nu} = \frac{1}{2}\partial_\mu\varphi\partial_\nu\varphi - \frac{1}{4}g_{\mu\nu}(\partial_\rho\varphi)(\partial^\rho\varphi) - \alpha_{GB}\mathcal{K}_{\mu\nu} \equiv T_{\mu\nu} \,, \tag{3.8}$$

where

$$\mathcal{K}_{\mu\nu} = \frac{1}{8}(g_{\mu\rho}g_{\nu\sigma} + g_{\mu\sigma}g_{\nu\rho})\epsilon^{\delta\sigma\gamma\xi}\nabla_\epsilon\left(\tilde{R}^{\rho\epsilon}{}_{\gamma\xi}\partial_\delta e^{\varphi}\right) \tag{3.9}$$

and

$$\tilde{R}^{\mu\nu}_{\rho\sigma} = \epsilon^{\mu\nu\delta\gamma}R_{\delta\gamma\rho\sigma}\,. \tag{3.10}$$

The tt component of the effective stress-energy tensor $T_{\mu\nu}$ in Eq. (3.8) can be seen as the local energy density $\mathcal{E} = -T_{tt}$, which can become negative [201]. Since this is a main hypothesis of the no-hair theorem [197], in EdGB this theorem is in fact evaded [229] and black holes are endowed with an additional scalar hair, the *dilaton charge*.

From the scalar field equation (3.7) we see that, at the leading order, the correction to the scalar field is of the order α_{GB}. From Eq. (3.8) we see that the corrections to the metric quantities are instead of the order α^2_{GB}, since there is either a scalar field multiplied for α_{GB} or two scalar fields. The same holds true for the QNMs, which will get corrections at $\mathcal{O}(\alpha^2_{GB})$ in the gravitational sector of the spectrum, and at $\mathcal{O}(\alpha_{GB})$ in the scalar sector [3, 4].

3.2 Black Hole Solutions in Einstein-dilaton Gauss-Bonnet: Perturbative Approach

Before being able to compute the QNMs in EdGB gravity, we have to define BHs solutions in EdGB. We proceed gradually, first considering the static case and then introducing the rotation, following the approach of Ref. [208].

3.2.1 Static Case

To compute the metric of a static, nonrotating DBH, we adopt a perturbative approach with respect to the EdGB coupling constant $\zeta \equiv \alpha_{GB}/M^2$, meaning that we start from the GR solution and then, considering the small coupling limit $\zeta \ll 1$, we add perturbative corrections that we determine analytically solving the field equations (3.7)-(3.8). Assuming spherical symmetry, a dilatonic BH will be described by the spacetime

$$ds^2 = -A(r)dt^2 + \frac{1}{B(r)}dr^2 + r^2 d\Omega^2 = -A(r)dt^2 + \frac{1}{B(r)}dr^2 + r^2\left(d\theta^2 + \sin^2\theta d\varphi^2\right) \tag{3.11}$$

and by the dilatonic field profile $\varphi(r)$, with $A(r), B(r), \varphi(r)$ functions to be determined – their dependence on α_{GB} is left implicit. These functions must be such that they satisfy regular boundary conditions, allowing the presence of a horizon and describing asymptotically flat spacetimes.

Far away from the BH, the unknown functions can be expanded in a power series $1/r$. Substituting them into the field equations, we can express these expansions in terms of three parameters, namely the asymptotic value of the dilaton field φ_∞, the Arnowitt-Deser-Misner mass M, and the dilaton charge D, defined as [320]

$$D = -\frac{1}{4\pi}\int d^2\Sigma^\mu \nabla_\mu \varphi\,, \tag{3.12}$$

where the integral is over a two-sphere at spatial infinity. Asymptotically, we shall have [230]

$$A(r) = 1 - \frac{2M}{r} + \mathcal{O}\left(\frac{1}{r^3}\right) \tag{3.13}$$

$$B(r) = 1 - \frac{2M}{r} + \frac{D^2}{4r^2} + \mathcal{O}\left(\frac{1}{r^3}\right) \tag{3.14}$$

$$\varphi(r) = \varphi_\infty + \frac{D}{r} + \frac{MD}{r^2} + \mathcal{O}\left(\frac{1}{r^3}\right) , \tag{3.15}$$

where we can fix $\varphi_\infty = 0$ if we require that the scalar field vanishes at infinity. Thus, at infinity, we can fully characterize the black hole with the parameters (M, D). It can be shown that for each value of M (and for a given value of α_{GB}) there is only one solution describing a nonrotating dilatonic BH, meaning that D is a *secondary hair*, as it can be determined in terms of the mass M.

At the horizon, the behavior of the functions can be described by the ansatz [201]

$$A(r) = a_1(r - r_H) + a_2(r - r_H)^2 + \mathcal{O}((r - r_H)^3) \tag{3.16}$$

$$B(r) = b_1(r - r_H) + b_2(r - r_H)^2 + \mathcal{O}((r - r_H)^3) \tag{3.17}$$

$$\varphi(r) = \varphi_H + {\varphi'}_H(r - r_H) + {\varphi''}_H(r - r_H)^2 + \mathcal{O}((r - r_H)^3) , \tag{3.18}$$

which can be verified a posteriori from the field equations (3.7)-(3.8), along with the values of the coefficients in the expansion. When solving the field equations evaluated near the horizon, one finds a solution for the derivative of the dilaton field

$$\varphi'_H = \frac{r_H}{\alpha_{GB}} e^{-\varphi_H} \left(-1 \pm \sqrt{1 - 6\alpha_{GB}^2 \frac{e^{2\varphi_H}}{r_H^4}} \right) , \tag{3.19}$$

with the sign + corresponding to the solution that guarantees asymptotic flatness. It can be verified that a_1 is also a function of φ'_H, while b_1 is a constant that can be fixed requiring asymptotic flatness.

The condition to have real solutions for the scalar field in (3.19)

$$e^{\varphi_H} \leq \frac{1}{\sqrt{6}\alpha_{GB}} r_H^2 \tag{3.20}$$

translates to the fact that black hole solutions for a fixed horizon radius can exist only if the GB coupling constant α_{GB} is smaller than a critical value, given by the magnitude of the horizon scale.

These black hole solutions are uniquely characterized by two parameters (φ_H, r_H), which correspond to a unique choice of (M, D).

We now note that the field equations are invariant under the simultaneous transformation

$$\varphi \to \varphi + \hat{\varphi} \tag{3.21}$$

$$r \to r e^{\hat{\varphi}/2} \tag{3.22}$$

with $\hat{\varphi}$ a constant. As a consequence of the radial rescaling, the two other asymptotic parameters

(M, D), found expanding in $1/r$, are then rescaled in the following way

$$M \to M e^{\hat{\varphi}/2} \tag{3.23}$$

$$D \to D e^{\hat{\varphi}/2} \,. \tag{3.24}$$

Using this invariance, we can rescale the scalar field and require that its asymptotic value is finite [1]. In order to describe different BH solutions, it is then sufficient to vary only one parameter between r_H and φ_H. Following Ref. [201], we keep r_H fixed while varying φ_H. As found numerically in Ref. [229], after the rescaling, Eq. (3.20) can be expressed in terms of the coupling constant of the theory as

$$0 < \frac{\alpha_{GB}}{M^2} \lesssim 0.691 \,, \tag{3.25}$$

which correspond to $D/M \lesssim 0.572$. For larger values of $\zeta \equiv \alpha_{GB}/M^2$, it is not possible to impose physical boundary conditions for the field equations and thus no dilatonic BH solution can exist, as it would present a naked singularity [213].

Since the value of the coupling constant of the theory α_{GB} is universal, meaning it has the same value for every black hole, the existence of the lightest BH observed, J1655-40, with mass $M \simeq 5.4 M_\odot$ implies $\sqrt{\alpha_{GB}} \lesssim 6.6\, km$; if the secondary object in GW190814, which has a mass $M \simeq 2.6 M_\odot$, turns out to be a BH, then $\sqrt{\alpha_{GB}} \lesssim 3.3\, km$ [132] [2]. For a summary of the most recent constraints from gravitational wave events, see e.g. Ref. [235]. $\sqrt{\alpha_{GB}}$ provides an indication of the scale at which we expect the EdGB corrections to manifest.

Perturbative Approach

Defining the dimensionless coupling constant

$$\zeta \equiv \frac{\alpha_{GB}}{M^2} \,, \tag{3.26}$$

we must have $0 < \zeta < \zeta_{max} \simeq 0.691$ to guarantee the existence of a dilatonic black hole, as stated by Eq. (3.20) [229]. Since ζ_{max} is strictly less than unity, we are motivated to adopt a perturbative approach to find analytically the functions $A(r,\zeta), B(r,\zeta), \varphi(r,\zeta)$ that describe the spherically symmetric spacetime. This means assuming that they deviate only perturbatively from the GR values of a Schwarzschild BH, $A(r) = B(r) = 1 - 2M/r$, $\varphi(r) = 0$, which are recovered in the limit $\zeta \to 0$.
Explicitly, we shall write

$$A(r,\zeta) = 1 - \frac{2M}{r} + \sum_{j=2}^{N_\zeta} \zeta^j A^{(j)}(r) \tag{3.27}$$

$$B(r,\zeta) = 1 - \frac{2M}{r} + \sum_{j=2}^{N_\zeta} \zeta^j B^{(j)}(r) \tag{3.28}$$

[1] We shall then take this constant to be zero at infinity. A non-zero value, which would translate to a cosmological constant, hence the same for every BH, could be reabsorbed by a redefinition of α_{GB}.

[2] For a comparison with other bounds in the literature arising from astrophysical observations [204, 321], taking into account differences in notations and conventions, see Ref. [73].

$$\varphi(r,\zeta) = \sum_{j=1}^{N_\zeta} \zeta^j \varphi^{(j)}(r)\,, \tag{3.29}$$

where N_ζ is the chosen order of the perturbative expansion – in our case $N_\zeta = 6$. As mentioned in Sec. 3.1, in agreement with the equations (3.7)-(3.8), the leading order corrections to the metric functions must be $\mathcal{O}(\zeta^2)$, while for the dilaton field $\mathcal{O}(\zeta)$.
By substituting these expansions in the field equations, integrating them order by order in ζ, and requiring regularity conditions at the boundaries, we are able to determine the expansion coefficients. In particular, the integration constants are fixed by requiring the right behavior of the functions at the horizon r_H, e.g. $A(r \to r_H) = 0$, and at infinity, where we assume $\varphi(r \to \infty) = 0$. In this way we obtain $A^{(j)}(r)$, $B^{(j)}(r)$, $\varphi^{(j)}(r)$; their expressions can be found in the Supplemental Material [322].

Another possibility explored in the literature is not to adopt the small coupling limit and instead to solve the Einstein equations numerically to find $A(r), B(r), \varphi(r)$ in the whole domain of ζ, as done in Refs. [3, 201]. Throughout the thesis, however, we will always use the perturbative framework.

Since we have found the metric and dilaton field for a nonrotating configuration starting from the Schwarzschild BH solution, physical quantities such as the mass M, scalar charge D, the horizon r_H must be suitably defined, as shown in Appendix C.

3.2.2 Rotating Case

In order to find the expression of the metric and dilaton field of a rotating black hole in EdGB gravity, we start from the nonrotating configuration of the previous section and then apply the slow rotation formalism, originally developed by Hartle [191], and summarized in Section 2.6 for GR.

The solution describing a stationary, rotating BH in EdGB gravity has been found numerically [209, 323], by solving non-perturbatively the field equations, and analytically [208, 229] in terms of a perturbative expansion in the spin $\bar{a} = J/M^2$, where J is the angular momentum of the black hole. We will follow the latter approach.

A slowly rotating DBH can be described by the axially symmetric metric

$$\begin{aligned} ds^2 = &-A(r,\zeta)[1+2h(r,\theta,\zeta)]dt^2 + \frac{1}{B(r,\zeta)}[1+2p(r,\theta,\zeta)]dr^2 \\ &+ r^2[1+2k(r,\theta,\zeta)]\left[d\theta^2 + \sin^2\theta(d\varphi - \varpi(r,\theta,\zeta)dt)^2\right] \end{aligned} \tag{3.30}$$

that has the same form of (2.85), but with the additional dependence on ζ, and by the dilaton field profile $\varphi(r,\zeta)$. $A(r,\zeta)$, $B(r,\zeta)$ are the functions of the nonrotating case described in Section 3.2.1, while the functions $h(r,\theta,\zeta)$, $p(r,\theta,\zeta)$, $k(r,\theta,\zeta)$, $\varpi(r,\theta,\zeta)$, to be determined, define the deformation of the spherically symmetric case induced by the rotation. Following the same strategy of Section 2.6, we further expand the metric and dilaton field by exploiting the symmetries of the problem and

using the complete orthogonal basis given by the Legendre polynomials

$$\varpi(r,\theta,\zeta,\bar{a}) = \sum_{j=0}^{N_\zeta} \sum_{n=1,3,5...}^{N_{\bar{a}}-q} \sum_{l=1,3,5...}^{n} \zeta^j \bar{a}^n \omega_l^{(nj)}(r) \left[-\frac{1}{\sin\theta} \frac{dP_l(\cos\theta)}{d\theta} \right] \tag{3.31}$$

$$h(r,\theta,\zeta,\bar{a}) = \sum_{j=0}^{N_\zeta} \sum_{n=2,4,...}^{N_{\bar{a}}-p} \sum_{l=0,2,4...}^{n} \zeta^j \bar{a}^n h_l^{(nj)}(r) P_l(\cos\theta) \tag{3.32}$$

$$p(r,\theta,\zeta,\bar{a}) = \sum_{j=0}^{N_\zeta} \sum_{n=2,4,...}^{N_{\bar{a}}-p} \sum_{l=0,2,4...}^{n} \zeta^j \bar{a}^n p_l^{(nj)}(r) P_l(\cos\theta) \tag{3.33}$$

$$k(r,\theta,\zeta,\bar{a}) = \sum_{j=0}^{N_\zeta} \sum_{n=2,4,...}^{N_{\bar{a}}-p} \sum_{l=0,2,4...}^{n} \zeta^j \bar{a}^n k_l^{(nj)}(r) P_l(\cos\theta) \tag{3.34}$$

and

$$\varphi(r,\theta,\zeta,\bar{a}) = \sum_{j=1}^{N_\zeta} \sum_{n=0,2,4,...}^{N_{\bar{a}}-p} \sum_{l=0,2,4...}^{n} \zeta^j \bar{a}^n \varphi_l^{(nj)}(r) P_l(\cos\theta)\,, \tag{3.35}$$

where $P_l(\theta)$ are the Legendre polynomials, N_ζ, $N_{\bar{a}}$ are the orders of the expansions in the coupling and in the spin, respectively. As usual, $v = 0$ ($q = 0$) when the order of the spin expansion $N_{\bar{a}}$ is even (odd), whereas $v = 1$ ($q = 1$) otherwise.

Using the expansions in Eqs. (3.31)-(3.35), our goal is to integrate order by order in ζ the field equations (3.7), (3.8), also expanded in the coupling constant, with suitable boundary conditions, to find the functions $\omega_l^{(nj)}(r)$, $h_l^{(nj)}(r)$, $p_l^{(nj)}(r)$, $k_l^{(nj)}(r)$, $\phi_l^{(nj)}(r)$.

Separating in two steps the slow rotation and the small coupling approximation of Eq. (3.31), at first order in the spin, we only have a modification in the $g_{t\phi}$ term due to $\varpi(r,\theta,\bar{a},\zeta) \equiv \bar{a}\,\omega(r,\zeta)$. From the component $G_{t\phi}$ of the Einstein equations (that is of order $\bar{a}$) we get

$$\omega'' + \frac{\omega'}{rB\left(r - e^{\varphi}\alpha_{GB}B\varphi'\right)}\Big\{ -\frac{A'}{A} + \Big[r^2B' - rB\left(3e^{\varphi}\alpha_{GB}B'\varphi' - 8\right) - 2e^{\varphi}\alpha_{GB}B^2\left(3\varphi' + r\varphi'^2\right)\Big]\Big\} = 0\,, \tag{3.36}$$

where the prime denotes the radial derivative and $\alpha_{GB} = \zeta M^2$. For $\alpha_{GB} = 0$ we recover the GR result of Eq. (2.95). In order to get the EdGB corrections to the gravitomagnetic term, we now perform the small coupling expansion $\omega(r,\zeta) = \sum_j \zeta^j \omega_1^{(1j)}(r)$ and substitute Eqs. (3.27)-(3.29) in the field equation (3.36), and solving them at each order j requiring asymptotic flatness.

At the leading order of the EdGB correction to the gravitomagnetic term, we find

$$\varpi(r,J,\zeta) = \left\{ \frac{2J}{r^3} - \zeta^2 J \frac{3M^2}{80r^5} + \mathcal{O}\left(\frac{J\zeta^3}{r^6}\right) \right\} + \mathcal{O}(J^3)\,, \tag{3.37}$$

where we have included any remaining integration constants (see Appendix C) in the definition of the angular momentum J, as read-off from the asymptotic behavior of the gravitomagnetic term

$$\omega \to \frac{2J}{r^3} \tag{3.38}$$

similarly to what we did for the ADM mass and scalar charge.

At the second order in the spin, the procedure is analogous to the one described in Section 2.6.1, with the difference that now there is also the small coupling expansion in ζ: each equation, after integrating the angular part exploiting the Legendre polynomials property (2.97), is then solved at each order j.

As already mentioned, the integration process at each order in $\bar{a}, \zeta$ yields some integration constants that can be either uniquely fixed or reabsorbed in the physical definitions, requiring that

- the metric is asymptotically flat, and the scalar field vanishes at spatial infinity;
- the condition for the existence of the horizon is satisfied, and perturbations are regular there;
- the physical mass M and angular momentum J of the DBH are the ones measured by an observer at spatial infinity

The functions $\omega_l^{(nj)}(r)$, $h_l^{(nj)}(r)$, $p_l^{(nj)}(r)$, $k_l^{(nj)}(r)$, $\varphi_l^{(nj)}(r)$ and the final expression of the metric and dilaton field can be found, up to order $\mathcal{O}(\bar{a}^2, \zeta^6)$, in the Supplemental Material [322]. Our results are in agreement with Maselli et al. [208], who made the computation up to order $\mathcal{O}(\bar{a}^5, \zeta^7)$.

In the following we will consider as a background solution to perform BH perturbation theory the expansion (3.30), together with (3.31)-(3.35) up to $N_\zeta = 6$ and $N_{\bar{a}} = 2$. An estimate based on the subsequent terms in the perturbation expansion shows that the truncation error on quantities characterizing the background (such as the location of the horizon and the innermost stable circular orbit) is $\lesssim 2\%$ for $\bar{a} \leq 0.7$ and $\zeta \leq 0.6$ [208].

The scalar charge D and horizon radius r_H, found from the largest root of $g_{\phi\phi} g_{tt} - g_{t\phi}^2 = 0$ (see e.g. [324]), acquire corrections at the second order in the spin that can be expressed in terms of the dimensionless coupling constant ζ and dimensionless spin $\bar{a} = J/M^2$

$$\frac{r_H}{M} = \sum_{j=0}^{6} \zeta^i (a_j + b_j \bar{a}^2) \tag{3.39}$$

$$\frac{D}{M} = \sum_{j=0}^{6} \zeta^j (c_j + d_j \bar{a}^2)\,, \tag{3.40}$$

with the coefficients, in agreement with Ref. [208], reported in Tab. 3.1. The two quantities are shown, as functions of ζ and $\bar{a}$, in Fig. 3.1. We note that the scalar charge is not greatly affected by the spin, while the horizon is more sensitive to it. We also see how DBHs are more compact with respect to a GR black hole with the same mass and angular momentum [229]. It is also evident the secondary hair nature of the scalar charge D, which is not an independent parameter, as it is a function of the primary hair M (and of course of the coupling constant ζ).

In Ref. [229], where a slow-rotation approach together with a non-perturbative numerical method for the EdGB correction has been employed, Pani et al. show how the angular velocity $\omega(r, \zeta)$ of a DBH can be up to $\sim 40\%$ higher than the one of a slowly rotating Kerr BH. Since we are considering a rotating spacetime, ergoregions can develop and can be found by looking at the surface where g_{tt} vanishes. The width of the ergoregion for a DBH can be up to $\sim 50\%$ larger than for a slowly rotating Kerr BH [208]. This implies that, when we introduce perturbations to the DBH, superradiance in EdGB is expected to be stronger than GR [229]. To the purpose of

this thesis, which is the computation of QNMs of slowly rotating DBHs, it can be seen that the superradiant regime is not relevant. Given the angular velocity at the horizon

$$\Omega_H = -\lim_{r\to r_H} \frac{g_{t\phi}}{g_{\phi\phi}} \tag{3.41}$$

and the frequency ω of a perturbation ψ, near the horizon we would have $\psi \sim exp\,[-i(\omega - m\Omega_H)r_*]$ so that, when $\omega < m\Omega_H$, an observer at infinity would see wave outgoing from the horizon. It can be verified that the range of frequencies for which the condition $\omega < m\Omega_H$ is satisfied corresponds to the superradiant regime [325, 326]. Nonetheless, for the perturbations and values of spin and coupling constant considered in the next chapters, the condition is never verified.

Finally, we note that the bound in Eq. (3.20) has been found non-perturbatively for stationary nonrotating black holes. The maximum value ζ_{max} for which we still have DBHs can be modified for large rotation values [209]. In fact, the same bound can still be taken into account remembering that the physical mass M has now corrections in spin included in its definition (see Appendix C). Nonetheless, the bound on ζ does not actually appear in the small-coupling approach, which already assumes $\zeta \ll 1$.

Rotating DBHs for finite values of coupling constant and spin have been studied numerically in Ref. [209, 323], which is extremely useful if one wants to investigate their properties for large values of these parameters – e.g. DBHs can exceed the Kerr bound and have $\bar{a} > 1$. However, to study perturbations and QNMs of DBHs we found more practical working with the analytical, perturbative framework, which is also motivated by the fact that we expect small deviations from GR, especially in the ringdown GW signal.

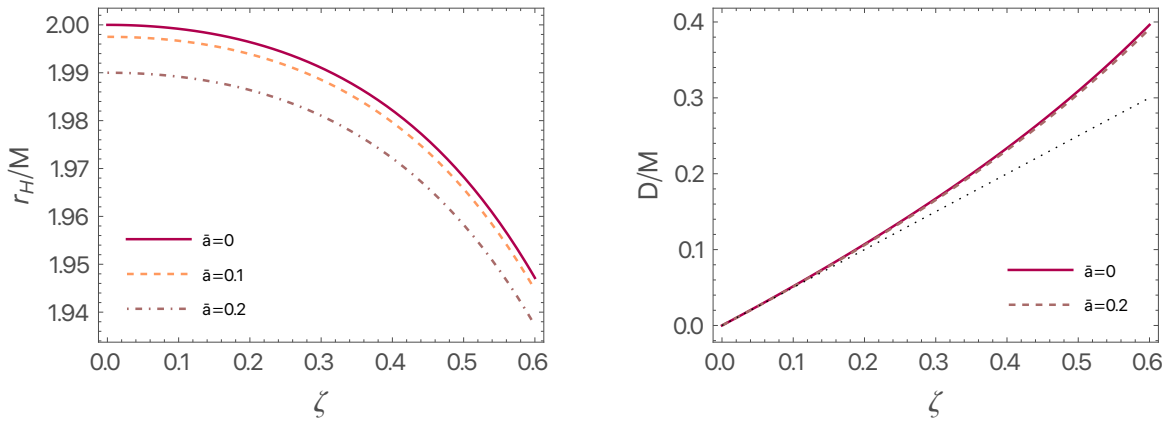

Figure 3.1: *The horizon radius (left panel) and dilaton charge (right panel) as a function of ζ for fixed values of spin $\bar{a}$. The dotted black line on the right panel represent the asymptotic behavior $D \sim \zeta/2$ as $\zeta \to 0$.*

Table 3.1: *Values of the coefficients for the slow rotation and small coupling expansion of the horizon and dilaton charge as written in Eqs.* (3.39)-(3.40). (a_j, c_j) *are the zeroth order in the spin coefficients,* (b_j, d_j) *the second order.*

EdGB expansion order	r_H/M		D/M	
j	a_j	b_j	c_j	d_j
0	2	−0.25	0	0
1	0	0	0.5	−0.125
2	−0.0766	−0.0053	0.1521	−0.0656
3	−0.0548	0.0034	0.0966	−0.0650
4	−0.0514	0.0074	0.0818	−0.0672
5	−0.0527	0.0122	0.0789	−0.0751
6	−0.0575	0.0181	0.0825	−0.0879

Chapter 4

Quasinormal Modes of a Scalar Field on a Slowly Rotating Dilatonic Black Hole

Before venturing into the analysis of gravitational and scalar perturbations together and the corresponding QNMs, it is easier to first consider only scalar perturbations as an intermediate step.

In this chapter, we generalize the procedure described in Sec. 2.2 to the case of QNMs of a test scalar field on a slowly rotating BH background in EdGB gravity. In particular, we want to compare our results with those of *Cano et al.* [4], which are based on a different approach. While we work with a perturbative expansion in the spin $\bar{a} = J/M^2$, they consider a test scalar field on a rapidly rotating BH background. In fact, they were able to extend Teukolsky formalism [155, 190] for the scalar field to the EdGB case, finding a radial master equation and using a high-order spin expansion. So far, this result has been achieved only for the scalar field case, while our approach can be straightforwardly generalized to the gravitational case. Nonetheless, the different hypotheses behind the two frameworks will require care when comparing the results.

The procedure we follow is the one used in [67], which implements and extends the approach of [159] to slowly rotating EdGB black holes.

4.1 Perturbation Equations

Let us consider a slowly rotating DBH, which is described by the metric given by Eqs.(3.30)-(3.34) and dilaton field φ in Eq. (3.35). We introduce perturbations of a *massless* test scalar field Φ (not to be confused with the dilaton scalar field), which satisfies the Klein-Gordon equation

$$\nabla_\mu \nabla^\mu \Phi = 0 \tag{4.1}$$

in the slowly rotating DBH background up to second order in the spin. The metric enters explicitly in (4.1) through the covariant derivatives

$$\frac{1}{\sqrt{-g}} \partial_\mu \left[\sqrt{-g} g^{\mu\nu} \partial_\nu \Phi(t, r, \theta, \phi) \right] = 0 \,. \tag{4.2}$$

Since the perturbation is a scalar, we can expand it using the usual scalar spherical harmonics

$$\Phi(t,r,\theta,\phi) = \frac{1}{r}\sum_{lm}\Phi^{lm}(t,r)Y^{lm}(\theta,\phi)\,, \tag{4.3}$$

where the radial factor $1/r$ has been arbitrarily factored out just for practical reasons. We look for solutions with the time dependence $\Phi^{lm}(t,r) = \Phi^{lm}(r)e^{-i\omega t}$.
Using $\chi \equiv \cos\theta$ to simplify the notation and substituting the expansion above, Eq. (4.2) can be symbolically rewritten to make the angular dependence explicit, as

$$\left(c_1^{lm}\ \chi^2 + c_2^{lm}\right) Y_{lm} + c_3^{lm}\ \chi(\chi^2-1)\partial_\chi Y_{lm} = 0\,, \tag{4.4}$$

where the sum over lm is left implicit. The coefficients c_1^{lm}, c_2^{lm}, c_3^{lm} are radial functions which contain the scalar field perturbation $\Phi^{lm}(r)$ (see the Supplemental material for the explicit expression [322]).

From the definition and properties of the spherical harmonics one finds the relations

$$\chi^2 Y_{lm} = \left(Q^2_{l+1\,m} + Q^2_{lm}\right) Y_{lm} + Q_{l+1\,m}Q_{l+2\,m}Y_{l+2\,m} + Q_{lm}Q_{l-1\,m}Y_{l-2\,m} \tag{4.5}$$

$$\chi(\chi^2-1)\partial_\chi Y_{lm} = \left[lQ^2_{l+1\,m} - (l+1)Q^2_{lm}\right] Y_{lm} + lQ_{l+1\,m}Q_{l+2\,m}Y_{l+2\,m} - Q_{lm}Q_{l-1\,m}(l+1)Y_{l-2\,m} \tag{4.6}$$

with

$$Q_{lm} \equiv \sqrt{\frac{l^2-m^2}{4l^2-1}}\,. \tag{4.7}$$

Using these relations, we can remove the angular derivative from Eq. (4.4), at the cost of introducing couplings with different harmonic indices $l \pm 2$, while the index m remains unaffected

$$\begin{aligned} &c_2^{lm}Y_{lm} + c_1^{lm}\left[Q^2_{l+1\,m} + Q^2_{lm}\right] Y_{lm} + c_3^{lm}\left[lQ^2_{l+1\,m} - (l+1)Q^2_{lm}\right] Y_{lm} + c_1^{lm}\ Q_{l+1\,m}Q_{l+2\,m}Y_{l+2\,m} \\ &\quad + c_3^{lm}\ lQ_{l+1\,m}Q_{l+2\,m}Y_{l+2\,m} + c_1^{lm}\ Q_{lm}Q_{l-1\,m}Y_{l-2\,m} - c_3^{lm}\ (l+1)Q_{lm}Q_{l-1\,m}Y_{l-2\,m} = 0\,. \end{aligned} \tag{4.8}$$

Taking advantage of the orthogonality of the spherical harmonics $\int d\Omega\, Y^*_{l'm'}Y_{lm} = \delta_{l'l}\delta_{mm'}$, we can remove the implicit sum over all the harmonic indices and focus on a single lm mode by multiplying Eq. (4.8) by $Y^*_{l'm'}$ and by integrating over the solid angle (for more details see App. F). Finally, we find the radial differential equation

$$\begin{aligned} &c_2^{lm} + c_1^{lm}\left(Q^2_{l+1\,m} + Q^2_{lm}\right) + c_3^{lm}\left[lQ^2_{l+1\,m} - (l+1)Q^2_{lm}\right] + c_1^{l-2\,m}\ Q_{lm}Q_{l-1\,m} \\ &\quad + c_3^{l-2\,m}\ (l-2)Q_{lm}Q_{l-1\,m} + c_1^{l+2\,m}\ Q_{l+1\,m}Q_{l+2\,m} - c_3^{l+2\,m}\ (l+3)Q_{l+1\,m}Q_{l+2} = 0\,. \end{aligned} \tag{4.9}$$

Substituting the definitions of the coefficients c_j^{lm} $(j=1,2,3)$ and expanding in $\bar{a} = J/M^2$ up to second order, the previous equation takes the form

$$\begin{aligned} &\Phi''_{lm} + \frac{1}{2}\left(\frac{A'}{A} + \frac{B'}{B}\right)\Phi'_{lm} + V_{lm}\Phi_{lm} + \bar{a}^2\Big[C_{1,l-2\,m}\Phi'_{l-2\,m} + C_{2,l+2\,m}\Phi'_{l+2\,m} + C_{3,lm}\Phi'_{lm} \\ &\quad + C_{4,l-2\,m}\Phi_{l-2\,m} + C_{5,l+2\,m}\Phi_{l+2\,m} + C_{6,lm}\Phi_{lm}\Big] = 0\,, \end{aligned} \tag{4.10}$$

where we have introduced new radial coefficients $C_{i,lm}$ $(i=1,...,6)$ and A, B are the radial functions

appearing in g_{tt}, g_{rr} – see Eq.(3.30). In the limit $\bar{a} = 0$ we recover the expression (2.6) (with $\mu = 0$, being Φ a massless scalar field). Denoting with the superscript $^{(0)}$ the quantities appearing for $\bar{a} = 0$, we define the potential V_{lm} as

$$V_{lm} \equiv V_l^{(0)} + \bar{a}\, T_{lm}\,, \tag{4.11}$$

with

$$V_l^{(0)} \equiv \frac{1}{AB}\left[\omega^2 - \frac{A'B + B'A}{2r} - A\frac{l(1+l)}{r^2}\right] \tag{4.12}$$

$$T_l \equiv -\frac{2m\,\omega\,\omega_1^{(1)}(r)}{AB} \tag{4.13}$$

where $\omega_1^{(1)} \equiv \sum_j^{N_\zeta} \zeta^j \omega_1^{1j}$ is the first-order spin coefficient of the background expansion (3.31), describing the gravitomagnetic term. In GR $\omega_1^{(1)} = 2J/r^3$.

Let us suppose we wanted to solve Eq. (4.10) as it is, for $l = 2$, to find the perturbation function Φ_2. Then, we would also need the solutions for $l = 0$ and $l = 4$, which, in return, would depend on the $l = 6$ solution, and so on; this means that we would have to solve an infinite set of coupled differential equations. In this case we could choose a maximum value for the harmonic index L_{max} and truncate the set of equations to include only up to $l = L_{max}$.

However, if the goal is the computation of QNMs up to order $\mathcal{O}(\bar{a}^2)$, the problem can be simplified with some considerations about the spin orders of the different perturbation functions that enter into the equation. First, keeping the spin expansion only up to the second order, the functions Φ_{lm}, Φ'_{lm} appearing in square brackets in Eq. (4.10), can be taken to be as the corresponding nonrotating functions, meaning that they satisfy

$$\Phi''_{lm}{}^{(0)} + \frac{1}{2}\left(\frac{A'}{A} + \frac{B'}{B}\right)\Phi'_{lm}{}^{(0)} + V_l^{(0)}\Phi_{lm}^{(0)} = 0 \tag{4.14}$$

because, due to the factor $\bar{a}^2$ in front, the higher-order terms would contribute at $\mathcal{O}(\bar{a}^3)$.

Secondly, let us consider the case in which a scalar field perturbation with index l is excited. At zeroth order in the spin no other $l' \neq l$ is present, while the $l \pm 2$ perturbations are excited only at $\mathcal{O}(\bar{a}^2)$, since they appear at that order in (4.10). This translates into the fact that the l perturbation can be expanded as

$$\Phi_{lm} = \Phi_{lm}^{(0)} + \bar{a}\Phi_{lm}^{(1)} + \bar{a}^2\Phi_{lm}^{(2)}\,, \tag{4.15}$$

while the $l \pm 2$ will be of order $\mathcal{O}(\bar{a}^2)$

$$\Phi_{l\pm2\,m} = \bar{a}^2\Phi_{l\pm2\,m}^{(2)}\,. \tag{4.16}$$

Hence, we see that the terms with $l \pm 2$ would contribute to the QNM spectrum only at $\mathcal{O}(\bar{a}^4)$, so that, to compute the modes at second order in rotation, we can simply solve the equation without

couplings

$$\Phi''_{lm} + \frac{1}{2}\left(\frac{A'}{A} + \frac{B'}{B}\right)\Phi'_{lm} + V_{lm}\Phi_{lm} + \bar{a}^2\Big[C_{3,lm}\Phi'_{lm} + C_{6,lm}\Phi_{lm}\Big] = 0\,. \tag{4.17}$$

To confirm these simplifications, in the perspective to apply them also in the gravitational case, as described in Sec 2.6.3, we decided to compute the fundamental $l = 2$ mode in both ways: keeping the $l \pm 2$ couplings and truncating at $L_{max} = 4$, and neglecting the couplings, i.e. solving Eq. (4.17).

We can recast the second order differential equation (4.10) in a set of first order differential equations in the form

$$\frac{d}{dr}\mathbf{\Psi}_{lm} + \hat{V}_{lm}\mathbf{\Psi}_{lm} = \hat{S}_{l-2\,m}\mathbf{\Psi}_{l-2\,m} + \hat{S}_{l+2\,m}\mathbf{\Psi}_{l+2\,m}\,, \tag{4.18}$$

where we have defined

$$\mathbf{\Psi}_{lm} \equiv \begin{pmatrix}\Phi_{lm}\\ \Phi'_{lm}\end{pmatrix}\,, \tag{4.19}$$

with the prime denoting differentiation with respect to r. The matrices $\hat{V}_{lm} = \hat{V}_l^{(0)} + \bar{a}m\hat{V}_l^{(1)} + \bar{a}^2\hat{V}_{lm}^{(2)}$, $\hat{S}_{lm} = \bar{a}^2\hat{S}_{lm}^{(2)}$ are two-dimensional square matrices. The expansions in the coupling parameter ζ up to $O(\zeta^4)$ of the components of these matrices are given in the supplemental MATHEMATICA notebook [322].

The first approach consists of computing the $n = 0, l = 2$ mode truncating the harmonic expansion up to $L_{max} = 4$, so we solve the three coupled equations (4.18) with $l = 0, 2, 4$ (the equations with odd values of l are decoupled from those with even values, and correspond to different modes). We can further recast this system as

$$\frac{d}{dr}\boldsymbol{Z} + \hat{W}\boldsymbol{Z} = 0\,, \tag{4.20}$$

where $\boldsymbol{Z}$ is the six-dimensional vector

$$\boldsymbol{Z} \equiv \begin{pmatrix}\mathbf{\Psi}_{0m}\\ \mathbf{\Psi}_{2m}\\ \mathbf{\Psi}_{4m}\end{pmatrix} \tag{4.21}$$

with $-2 < m < 2$, and $\hat{W}$ is the six-dimensional matrix

$$\hat{W} \equiv \begin{pmatrix}-\hat{V}_0 & \hat{S}_2 & \hat{0}\\ \hat{S}_0 & -\hat{V}_2 & \hat{S}_4\\ \hat{0} & \hat{S}_2 & -\hat{V}_4\end{pmatrix}\,, \tag{4.22}$$

where $\hat{0}$ is the null 2×2 matrix.

In the second approach, where the couplings $\mathbf{\Psi}^{l\pm2}$ are neglected, we will simply solve

$$\frac{d}{dr}\mathbf{\Psi}_{lm} + \left[\hat{V}_l^{(0)} + \bar{a}m\hat{V}_l^{(1)} + \bar{a}^2\hat{V}_{lm}^{(2)}\right]\mathbf{\Psi}_{lm} = 0\,, \tag{4.23}$$

corresponding to Eq.(4.17).

After verifying that the two approaches actually produce the same results, we compare them with the computation from [4]. Since in [4] the EdGB corrections are included up to $O(\zeta^2)$, we also

compute the scalar field QNMs up to $N_\zeta = 2$.

4.2 Quasinormal Mode Spectrum

The quasinormal modes are the solutions of the perturbation equation with Sommerfeld boundary conditions, i.e. outgoing waves at infinity and ingoing waves at the horizon. With an appropriate definition of the tortoise coordinate r_* (see Appendix E), the scalar perturbation function Φ_{lm} behave at the horizon and at infinity as

$$\begin{aligned} &A^{lm}_{in} e^{-ik_H r_*} + A^{lm}_{out} e^{ik_H r_*} \quad (r \to r_H) \\ &A^{lm}_{in} e^{-i\omega r_*} + A^{lm}_{out} e^{i\omega r_*} \quad (r \to \infty)\,, \end{aligned} \tag{4.24}$$

where

$$k_H \equiv \omega - m\Omega_H \tag{4.25}$$

takes into account the frame-dragging effect due to the presence of rotation, being

$$\Omega_H = -\lim_{r\to r_H} \frac{g^{(0)}_{t\phi}}{g^{(0)}_{\phi\phi}} \tag{4.26}$$

the angular velocity at the horizon of locally nonrotating observers, calculated with respect to the non-perturbed metric $g^{(0)}_{\mu\nu}$, and expanded at order $\mathcal{O}(\bar{a}^2)$. Explicitly, at the second order in the coupling constant and in the spin,

$$k_H = \omega - m\Omega_H = \omega - \bar{a}\frac{m}{r_H}\left[\frac{1}{2} + \zeta^2 \frac{7}{512}\right] + \mathcal{O}\left(\zeta^3\right) + \mathcal{O}\left(\bar{a}^3\right)\,. \tag{4.27}$$

At the horizon and at infinity, the couplings with $l \pm 2$ in Eq.(4.10) are subleading, so that the perturbation equation can be written in the familiar second-order differential equation form

$$\Phi^{lm}_{,r_*r_*} + k_H^2 \Phi^{lm}_{,r_*r_*} = \mathcal{O}(r - r_H) \quad (r \to r_H) \tag{4.28}$$

$$\Phi^{lm}_{,r_*r_*} + \omega^2 \Phi^{lm}_{,r_*r_*} = \mathcal{O}\left(\frac{1}{r^2}\right) \quad (r \to \infty)\,. \tag{4.29}$$

The Sommerfeld boundary conditions are then

$$\Phi^{lm} \sim e^{-ik_H r_*} \quad (r \to r_H) \tag{4.30}$$

$$\Phi^{lm} \sim e^{i\omega r_*} \quad (r \to \infty)\,, \tag{4.31}$$

which are satisfied only by a discrete set of frequencies, the BH QNMs $\omega = \omega_R + i\omega_I$.

The tortoise coordinate $r_*(r)$ maps the region outside the BH horzion $r \in [r_H, \infty]$ into $r_* \in [-\infty, +\infty]$. Calling $F(r)$ the function

$$F(r) \equiv \frac{dr}{dr_*}\,, \tag{4.32}$$

we shall have

$$F(r) \sim r - r_H \quad (r \to r_H)$$
$$F(r) \to 1 \quad (r \to \infty)\,. \tag{4.33}$$

Since the intrinsic geometry of the slowly rotating metric in the Hartle form is nonspherical [208], it is not straightforward to define a tortoise coordinate that maps null geodesics into straight lines, as one can do for Schwarzschild and Kerr. Thus, in this case, we can find the explicit expression of $F(r)$ requiring the property that, using the tortoise coordinate, the perturbation equation reduces, at the boundaries, to Eqs. (4.28)-(4.29). These conditions allow some arbitrariness and can lead to different choices; however, we verified that different options, which still satisfy Eqs. (4.28)-(4.29), yield negligible differences in the QNMs, compatible with numerical intrinsic uncertainty. Imposing the stronger requirement at infinity

$$\Phi^{lm}_{,r_*r_*} + \omega^2 \Phi^{lm}_{,r_*r_*} = \frac{l(l+1)}{r^2}\Phi^{lm} + \mathcal{O}\left(\frac{1}{r^3}\right) \quad (r \to \infty)\,, \tag{4.34}$$

the function $F(r)$ is uniquely determined and, up to $\mathcal{O}(\zeta^2)$ and $\mathcal{O}(\bar{a}^2)$ is

$$F(r) = \left(1 - \frac{r_H}{r}\right)\left\{1 - \bar{a}^2\frac{r_H(r^2 + rr_H + r_H^2)}{8r^3} - \zeta^2\Big[\frac{r_H}{3840r^4}(147r^3 + 117r^2 r_H - 526rr_H^2 + 263r_H^3)\right.$$
$$\left. + \bar{a}^2\frac{r_H}{30720r^3}(375r^2 + 435rr_H + 343r_H^2)\Big]\right\}. \tag{4.35}$$

Proceeding as in Sec. 2.5 and working with the full vectorial form of Eq. (4.18), we find (by direct integration from the horizon) three independent solutions $\boldsymbol{Z}_i^H$ $(i = a, b, c)$ satisfying the boundary conditions at the horizon (4.30), and (by direct integration from infinity) three independent solutions $\boldsymbol{Z}_i^\infty$ satisfying the boundary conditions at infinity (4.31). Thus, we define the six-dimensional square matrix containing these solutions

$$\hat{X} = \begin{pmatrix} \boldsymbol{\Psi}_a^{0H} & \boldsymbol{\Psi}_b^{0H} & \boldsymbol{\Psi}_c^{0H} & \boldsymbol{\Psi}_a^{0\infty} & \boldsymbol{\Psi}_b^{0\infty} & \boldsymbol{\Psi}_c^{0\infty} \\ \boldsymbol{\Psi}_a^{2H} & \boldsymbol{\Psi}_b^{2H} & \boldsymbol{\Psi}_c^{2H} & \boldsymbol{\Psi}_a^{2\infty} & \boldsymbol{\Psi}_b^{2\infty} & \boldsymbol{\Psi}_c^{2\infty} \\ \boldsymbol{\Psi}_a^{4H} & \boldsymbol{\Psi}_b^{4H} & \boldsymbol{\Psi}_c^{4H} & \boldsymbol{\Psi}_a^{4\infty} & \boldsymbol{\Psi}_b^{3\infty} & \boldsymbol{\Psi}_c^{4\infty} \end{pmatrix}. \tag{4.36}$$

The QNMs ω^{nlm} are found by requiring

$$\det\hat{X}(\omega^{nlm}) = 0\,. \tag{4.37}$$

4.2.1 Boundary Conditions

The procedure of the numerical integration is analogous to the one for GR described in Sec 2.5.1, but now we must take into account the perturbative expansions in ζ and $\bar{a}$. In particular, to accommodate the fact that the numerical integration boundaries lie in a smaller range $[R_H = r_H(1+\epsilon), R_\infty]$ with respect to the physical boundaries $[r_H, \infty)$ (see Fig. 2.3), we shall perform an expansion of the perturbation functions in powers of $r - r_H$ near the horizon and $1/r$ near infinity. Calling $N_{\bar{a}}, N_{H/\infty}$ the expansion orders in the spin and in the radius, respectively, at the numerical

horizon $r = R_H \sim r_H$ we shall have

$$\Phi_l(\omega, r \sim r_H, \zeta) = e^{-ik_H r_*} \sum_{j=0}^{N_{\bar{a}}} \sum_{i=0}^{N_H} \bar{a}^j \phi^H_{l,ij}(\omega, \zeta)(r - r_H)^i \tag{4.38}$$

$$\Phi'_l(\omega, r \sim r_H, \zeta) = e^{-ik_H r_*} \sum_{j=0}^{N_{\bar{a}}} \sum_{i=0}^{N_H} \bar{a}^j \xi^H_{l,ij}(\omega, \zeta)(r - r_H)^{i-1} , \tag{4.39}$$

while at the numerical infinity $r = R_\infty$

$$\Phi_l(\omega, r \to \infty, \zeta) = e^{i\omega r_*} \sum_{j=0}^{N_{\bar{a}}} \sum_{i=0}^{N_\infty} \bar{a}^j \frac{\phi^\infty_{l,ij}(\omega, \zeta)}{r^i} \tag{4.40}$$

$$\Phi'_l(\omega, r \to \infty, \zeta) = e^{i\omega r_*} \sum_{j=0}^{N_{\bar{a}}} \sum_{i=0}^{N_\infty} \bar{a}^j \frac{\xi^\infty_{l,ij}(\omega, \zeta)}{r^i} , \tag{4.41}$$

where the asymptotic behavior can be verified a posteriori from the perturbation equations. In our computation we have set $N_{\bar{a}} = 2$, $N_H = 11$, $N_\infty = 13$. The coefficients $\phi^H_{l,ij}, \xi^H_{l,ij}, \phi^\infty_{l,ij}, \xi^\infty_{l,ij}$ are found solving the perturbation equations at each order in $r - r_H$ or $1/r$ after substituting the expansions (4.38)-(4.41), and are then expanded in ζ.
Following this procedure, we find that there is a couple of free parameters (one for the horizon and one for infinity) not constrained by the equations, for example $\phi^H_{l,00}, \phi^\infty_{l,00}$. Fixing arbitrarily these parameters is equivalent to choosing different vectors of the solution basis that constitutes the matrix $\hat{X}$ in Eq. (4.36): $(\phi^H_{0,00}, \phi^H_{2,00}, \phi^H_{4,00})$ identify the outgoing solutions $\boldsymbol{Z}^H_i$ satisfying the horizon boundary condition (4.38)-(4.39), while $(\phi^\infty_{0,00}, \phi^\infty_{2,00}, \phi^\infty_{4,00})$ identify the ingoing solutions $\boldsymbol{Z}^\infty_i$ satisfying the infinity boundary conditions (4.40)-(4.41).

4.2.2 Results

Since we are working at order $\mathcal{O}(\zeta^2)$ and $\mathcal{O}(\bar{a}^2)$ in the perturbative framework, we compute the QNMs for different values of $\zeta, \bar{a}$ in the range $\zeta \lesssim 0.15$ and $\bar{a} \lesssim 0.1$, and then we fit the data, obtaining the following analytical expressions for the $(n, l, m) = (0, 2, 2)$ mode [1]

$$M\omega^{022}_R = 0.48365 + 0.15049\bar{a} + 0.07309\bar{a}^2 + \zeta^2 \left(0.00653 + 0.00945\bar{a} + 0.00523\bar{a}^2\right) \tag{4.42}$$

$$M\omega^{022}_I = -0.09676 + 0.00014\bar{a} + 0.00553\bar{a}^2 + \zeta^2 \left(0.00048 + 0.00006\bar{a} + 0.00081\bar{a}^2\right) . \tag{4.43}$$

We find that the shift due to EdGB with respect to GR is the same in the two approaches described in the previous section, one including the $l \pm 2$ couplings and truncating at $L_{max} = 4$, and one without couplings, up to a relative difference $\sim 10^{-6}$ for $\bar{a} = 0.1$. This being a subleading and negligible difference, we think it is entirely due to the numerical precision, thus we can consider the approach that neglects the $l \pm 2$ couplings to be validated confidently.

[1] In this case, since there is no coupling between the test scalar field Φ and the curvature, the leading order correction to the QNMs is of $\mathcal{O}(\zeta^2)$. Instead, when we will consider perturbations of the dilaton field φ, which is coupled to the Gauss-Bonnet term in the Klein-Gordon equation, the EdGB correction to the QNMs will be of $\mathcal{O}(\zeta)$.

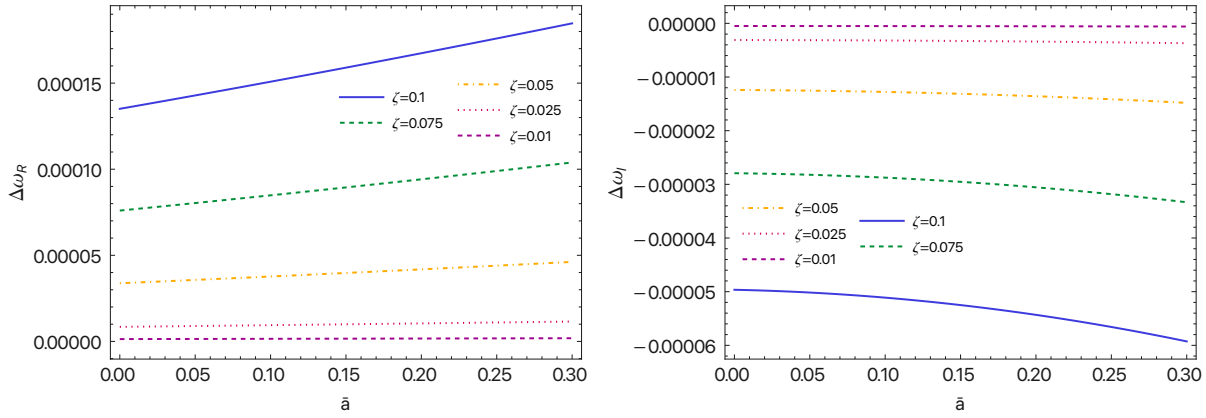

Figure 4.1: *Relative difference with respect to GR of the* $(nlm) = (022)$ *scalar quasinormal mode, for fixed values of* ζ *and as a function of the spin* $\bar{a}$*.*

In Fig. 4.1 we plot the relative difference with respect to GR

$$\Delta\omega^{nlm}_{R,I}(\bar{a},\zeta) \equiv \frac{\omega^{nlm}_{R,I}(\bar{a},\zeta) - \omega^{nlm}_{R,I}(\bar{a},0)}{\omega^{nlm}_{R,I}(\bar{a},0)} \tag{4.44}$$

for the $(nlm) = (022)$ mode for different values of ζ as a function of the spin $\bar{a}$, using the spectrum given in Eqs. (4.42)-(4.43).

We finally compare our results with those of [4] in the limit of small spins. In order to estimate the contribution of the $O(\bar{a}^2)$ terms, we repeat the computation by neglecting the quadratic terms in the spin; in this case, the matrices $\hat{V}^{(2)}$ and $\hat{S}$ vanish in Eq. (4.18). We define the shifts

$$f^{A}_{R,I}(\zeta,\bar{a}) \equiv \lim_{\zeta\to 0} \frac{\omega^{A}_{R,I}(\zeta,\bar{a}) - \omega^{A}_{R,I}(\zeta=0,\bar{a})}{\zeta^2\,\omega^{A}_{R,I}(\zeta=0,\bar{a})} \tag{4.45}$$

describing the leading-order $\mathcal{O}(\zeta^2)$ EdGB corrections to the real and imaginary parts of the QNMs; $A = 1$ ($A = 2$) refers to the computation of the QNMs up to $\mathcal{O}(\bar{a})$ (up to $\mathcal{O}(\bar{a}^2)$). We denote with $f^{\rm C}_{R,I}$ the corresponding shifts obtained by the numerical fits in [4]. In Table 4.1 we show that our results are in good agreement with those of [4] for $\bar{a} \leq 0.1$ if the quadratic terms in the spin are included; the agreement is much worse with the computation to $\mathcal{O}(\bar{a})$, in particular for the imaginary part [2].

With our two-parameter perturbation framework, consisting of a perturbative expansion for small values of the coupling constant ζ and of the spin $\bar{a}$, we verified our computation of the QNM spectrum of a test scalar field in an EdGB BH spacetime against the results in the literature [4]. Furthermore, we were also able to check our considerations about which terms in the perturbation equations actually contribute to the spectrum at a certain order in the spin, and this result will be used as a basis for the gravitational case explored in the next chapters.

[2] This is not true for the smallest value of the spin in Table 4.1, $\bar{a} = 0.01$. We think this is due to the fact – also remarked by the authors of [4] – that their fit is optimized to describe the entire range $0 \leq \bar{a} \leq 0.7$, and thus it may not coincide with a perturbative expansion for $\bar{a} \ll 1$.

Table 4.1: *Leading-order EdGB corrections to the $n = 0$, $l = m = 2$ QNM, defined in Eq.* (4.45)*, up to first and to second order in the spin, and as computed in [4].*

$\bar{a}$	f_R^{C}	f_R^1	f_R^2
0.01	0.013653	0.013667	0.013660
0.05	0.014273	0.014576	0.014274
0.1	0.015065	0.016565	0.015004
$\bar{a}$	f_I^{C}	f_I^1	f_I^2
0.01	-0.005178	-0.005092	-0.005035
0.05	-0.005287	-0.006337	-0.005089
0.1	-0.005410	-0.007087	-0.005272

Chapter 5

Quasinormal Modes of Nonrotating Dilatonic Black Holes

In order to compute the QNMs of rotating BHs in EdGB, we analyze increasingly difficult scenarios, following our work in Refs. [67, 68]. In the previous chapter, we explored the computation of QNMs of a test scalar field in a slowly rotating EdGB spacetime; now we shall consider the more involved case of gravitational perturbations.

We first focus on gravitational perturbations of *nonrotating* EdGB black holes. In Sec. 2.5 we explained how to use the direct integration method to compute the QNMs of a Schwarzschild BH; in this chapter, we will generalize the same method to EdGB gravity, in the small coupling limit.

While we know that Schwarzschild BHs are stable against linear perturbations [94], the stability in the EdGB case has been explored in Refs. [3, 109, 229, 230, 312]. A way to have linearized mode stability for a certain spacetime is to check that all the QNMs have a negative imaginary part, in order to avoid exponential divergences in time due to the $e^{-i\omega t}$ dependence of the eigenfunction [1]. The analysis of Blázquez-Salced et al. [3, 109] was performed for nonrotating DBHs by spanning all of the parameter space of $\zeta = \alpha_{GB}/M^2 \lesssim 0.691$ using a numerical approach. Nonetheless, working in the small coupling limit $\zeta \ll 1$, we naturally find QNMs that only slightly differ from the GR values of a Schwarzschild, which we know to be stable, and thus remaining stable themselves for sufficiently small couplings[1].

In this chapter, we compute the QNMs of static, nonrotating, EdGB black holes, and check the agreement with the results of Ref. [3]. Once verified that our Wolfram Mathematica code is able to reproduce the results present in the literature, as already confirmed for the test scalar field, we will introduce the effects of rotation on gravitational perturbations in the following chapter.

5.1 Metric and Scalar Perturbations

The static solution of the EdGB field equations is the one described in Section 3.2.1, calculated in the small-coupling approximation up to order $\mathcal{O}(\zeta^6)$. The static DBH is characterized by the metric $g^{(0)}_{\mu\nu}$ in Eq. (3.11), with the functions $A(r,\zeta), B(r,\zeta)$ given by Eqs. (3.27)-(3.28), and by the dilaton field, here referred to as $\varphi^{(0)}(r,\zeta)$, given by (3.29). We use the symbol "(0)" to indicate that

[1] We expect this to hold also in the slow rotation case explored in the following chapter, where the spins are assumed to be small and the QNMs are sufficiently close to the values of GR.

the BH corresponds to the nonperturbed, equilibrium solution of Einstein and scalar field equations (3.7)-(3.8).

In order to find the characteristic oscillation modes, i.e. the quasinormal modes, of the background DBH we introduce a small metric perturbation $h_{\mu\nu}$ and scalar field perturbation $\delta\varphi$ to $g^{(0)}_{\mu\nu}$, $\varphi^{(0)}$

$$g_{\mu\nu} = g^{(0)}_{\mu\nu} + h_{\mu\nu} \tag{5.1}$$
$$\varphi = \varphi^{(0)} + \delta\varphi\,, \tag{5.2}$$

where now $g_{\mu\nu}$ and φ are the full perturbed metric and dilaton field and $|h_{\mu\nu}| \ll 1, |\delta\varphi| \ll 1$.

As explained in Appendix A, any function of (t, r, θ, ϕ) can be expanded in a combination of functions of t and r (that does not change the properties of transformation under rotation) multiplied by suitable spherical harmonics (scalar, vector, tensor) of given parities. The same rule holds true for the perturbation components, which can be written in a multipole expansion as Eq. (A.7).

Analogously to the GR case summarized in Sec. 2.3, the gravitational perturbation is described by 10 functions of t and r that we call $H_0^{lm}(t,r)$, $H_1^{lm}(t,r)$, $H_2^{lm}(t,r)$, $q_0^{lm}(t,r)$, $q_1^{lm}(t,r)$, $K^{lm}(t,r)$ and $G^{lm}(t,r)$ for the *even parity* (or *polar*) *modes*, and $h_0^{lm}(t,r)$, $h_1^{lm}(t,r)$, $h_2^{lm}(t,r)$ for the *odd parity* (or *axial*) *modes*.

In the Regge Wheeler (RW) gauge[2] we set $q_0^{lm}(t,r) = q_1^{lm}(t,r) = G^{lm}(t,r) = 0$ and $h_2^{lm}(t,r) = 0$, so that

$$g^0_{\mu\nu} = \begin{pmatrix} -A(r) & 0 & 0 & 0 \\ 0 & 1/B(r) & 0 & 0 \\ 0 & 0 & r^2 & 0 \\ 0 & 0 & 0 & r^2\sin^2\theta \end{pmatrix} \tag{5.3}$$

$$h^{pol}_{\mu\nu} = \begin{pmatrix} A(r)H_0^{lm} & H_1^{lm} & 0 & 0 \\ H_1^{lm} & 1/B(r)H_2^{lm} & 0 & 0 \\ 0 & 0 & r^2K^{lm} & 0 \\ 0 & 0 & 0 & r^2\sin^2\theta K^{lm} \end{pmatrix} Y^{lm} \tag{5.4}$$

$$h^{ax}_{\mu\nu} = \begin{pmatrix} 0 & 0 & -\frac{h_0^{lm}}{\sin\theta}Y_{,\phi}^{lm} & h_0^{lm}\sin\theta Y_{,\theta}^{lm} \\ 0 & 0 & -\frac{h_1^{lm}}{\sin\theta}Y_{,\phi}^{lm} & h_1^{lm}\sin\theta Y_{,\theta}^{lm} \\ -\frac{h_0^{lm}}{\sin\theta}Y_{,\phi}^{lm} & -\frac{h_1^{lm}}{\sin\theta}Y_{,\phi}^{lm} & 0 & 0 \\ h_0^{lm}\sin\theta Y_{,\theta}^{lm} & h_1^{lm}\sin\theta Y_{,\theta}^{lm} & 0 & 0 \end{pmatrix}, \tag{5.5}$$

where the sum over the l, m indices is left implicit. Focusing on a Fourier mode with complex frequency ω, we can summarise the gravitational perturbation as $h_{\mu\nu} = h^{\rm pol}_{\mu\nu} + h^{\rm ax}_{\mu\nu}$, with

$$h^{\rm pol}_{\mu\nu}(t,r,\theta,\phi)dx^\mu dx^\nu = \\ \left[A(r)H_0^{lm}(r)dt^2 + 2H_1^{lm}(r)dtdr + B^{-1}(r)H_2^{lm}(r)dr^2 + K^{lm}(r)(dr^2 + \sin^2\theta d\varphi^2)\right] Y^{lm}(\theta,\phi)e^{-i\omega t} \tag{5.6}$$

[2] We can use this gauge since the equations of motions in EdGB still contain only up to second order derivatives of the metric (see Ref. [229])

$$h^{\rm ax}_{\mu\nu}dx^\mu dx^\nu = 2(h_0^{lm}(r)dt + h_1^{lm}(r)dr) \times (S_\theta(\theta,\phi)d\theta + S_\phi(\theta,\phi)d\phi)e^{-i\omega t}\,, \tag{5.7}$$

where $(S_\theta^{lm}, S_\phi^{lm}) = (-(\sin\theta)^{-1}Y^{lm}_{,\phi}, \sin\theta Y^{lm}_{,\theta})$.

Differently from GR, we also have the dilaton field perturbation

$$\delta\varphi(t,r,\theta,\varphi) = \frac{1}{r}\Phi^{lm}(r)Y^{lm}(\theta,\phi)e^{-i\omega t} \tag{5.8}$$

in which the factor $1/r$ is introduced for practical convenience. Being a scalar perturbation, Φ^{lm} belongs to the polar sector, and it will appear coupled to the other polar gravitational perturbations in the field equations, introducing nontrivial effects on the polar QNM spectrum. The axial gravitational sector is decoupled from the scalar field perturbations [229], but it is still inherently different from the GR case due to the different background solution considered.

5.2 Perturbation Equations

Replacing the perturbed metric and dilaton field in Eqs. (5.1)-(5.2), properly expanded in spherical harmonics according to the prescriptions (5.6)-(5.8), into the field equations (3.7) - (3.8), we obtain a set of partial differential equations in r and θ. The coordinates t and ϕ can be factored out as $\sim e^{i(m\phi-\omega t)}$, due to the stationarity and axial symmetry of the background, and therefore the equations with different values of m, ω are decoupled.
Separating the ϕ-dependent part of the spherical harmonics by defining $Y^{lm}(\theta)$ such that $Y^{lm}(\theta,\phi) \equiv Y^{lm}(\theta)e^{i\,m\phi}$, we can integrate easily the angular dependence in the equations by exploiting the orthonormality properties of the spherical harmonics $\int\int d\phi d\theta \sin\theta Y_l^*(\theta)Y_{l'}(\theta)e^{i(m-m')\phi} = \delta_{ll'}\delta_{mm'}$ and the integrals (F.2)-(F.3); since the only dependence on m is coming from the spherical harmonics and give rise to the $\delta_{mm'}$, the azimuthal number m plays no active role in the final equations, as expected in a spherically symmetric spacetime, so we shall drop this index. On the other hand, the resulting radial equations will describe each mode l individually.

Focusing on the *polar sector*, we are left with six radial differential equations and an algebraic relation in H_0^l, H_1^l, H_2^l, K^l, Φ^l, $\Phi^{l\prime}$. However, not all the perturbation functions are necessary to fully describe the perturbation; indeed these equations can be further manipulated in order to obtain a first-order Ordinary Differential Equation (ODE) system in H_1^l, K^l, $\Phi^l, \Phi^{l\prime}$:

$$\frac{d}{dr}\mathbf{\Psi}_l + \hat{V}_l\mathbf{\Psi}_l = \mathbf{0} \tag{5.9}$$

where

$$\mathbf{\Psi}_l \equiv \begin{pmatrix} H_{1l} \\ K_l \\ \Phi_l \\ \Phi_l' \end{pmatrix} \tag{5.10}$$

and $\hat{V}_l$ is a four-dimensional square matrix, whose components $V_{l,ij}(r)\,(i,j=1,...,4)$ are linear in H_{1l}, K_l, Φ_l, Φ_l'. The expression of $\hat{V}_l$ is given in Appendix D up to $\mathcal{O}(\zeta^2)$, while the full equations and the matrix components are given in the Supplemental Material [322] up to sixth order in the coupling parameter ζ. We note that in this case, the equations are *not* coupled between different

values of the harmonic index l, meaning that every mode can be computed independently from the others. We will see that this is not true in the presence of rotation.

Eq. (5.9) shows explicitly that the scalar perturbations and gravitational perturbations are coupled through the effect of the matrix $\hat{V}$. This does not happen in the axial sector because the scalar field is of polar parity and it would not enter in the axial perturbation equation, which has the same form of (5.9) but two-dimensional, with the perturbation functions given by the vector composed of two axial functions, e.g. $\mathbf{\Psi}^{ax} = \{h_0, h_1\}$.

5.3 Quasinormal Mode Computation

To compute the QNM spectrum of a static DBH, we use the direct integration method described in Section 2.5 for GR, where now the dimension of the problem, controlled by the order of the matrix $\hat{V}$ in Eq. (5.9), is $N = 4$.

We construct a basis of four solutions of Eq. (5.9), two of them, $\{\mathbf{\Psi}^{(1)}_{l,H}(r), \mathbf{\Psi}^{(2)}_{l,H}(r)\}$, found integrating two times from the horizon r_H outwards to a point r, and the other two, $\{\mathbf{\Psi}^{(1)}_{l,\infty}(r), \mathbf{\Psi}^{(2)}_{l,\infty}(r)\}$, found integrating from infinity inwards up to r, satisfying the boundary conditions

$$\begin{aligned} \mathbf{\Psi}_l &\sim e^{-i\omega r_*} \quad (r \to r_H) \\ \mathbf{\Psi}_l &\sim e^{i\omega r_*} \quad (r \to \infty)\,, \end{aligned} \tag{5.11}$$

with the tortoise coordinate r_* such that

$$\frac{dr_*}{dr} = \frac{1}{\sqrt{A(r)B(r)}}\,. \tag{5.12}$$

For more details on the tortoise coordinate, see Appendix E.

We then build the 4×4 matrix $\hat{X}_l$ that contains the four vectors of the basis

$$\hat{X}_l(\omega, r, \zeta) = \begin{pmatrix} \mathbf{\Psi}^{(1)}_{l,H} & \mathbf{\Psi}^{(2)}_{l,H} & \mathbf{\Psi}^{(1)}_{l,\infty} & \mathbf{\Psi}^{(2)}_{l,\infty} \end{pmatrix}\,. \tag{5.13}$$

The solutions will be in general linearly independent unless the frequency is the QNM frequency or, in other terms, the eigenvectors satisfy *both* the ingoing boundary condition at the horizon and outgoing boundary condition at infinity (5.11).

Thanks to the properties of the determinant of a matrix, which is null when two or more components are linearly dependent, we can find the quasinormal mode $\omega_{nl}(\zeta)$ from the root of

$$det\hat{X}_l(\omega, r, \zeta)\Big|_{\omega=\omega_{nl}} = 0\,. \tag{5.14}$$

Since this condition is true regardless of the choice of r, for our calculation the matrix $\hat{X}$ will be evaluated at a matching point $r = r_m$ of the other of the horizon radius r_H.

5.3.1 Boundary Conditions

Implementing the boundary conditions (5.11) in the numerical integration process requires some care, as explained in Sec. 2.5.1. In particular, we need to pay attention to the choice of numerical

values for

- the *horizon radius* R_H, as we cannot impose the boundary condition exactly at $r = r_H$, where some perturbation functions diverge; The solution is to consider a position which is an $\epsilon \ll 1$ away from the physical horizon: $R_H \equiv r_H(1+\epsilon)$, with $\epsilon \sim 10^{-4} - 10^{-2}$;
- *infinity*, which will assume a finite value R_∞. The choice of R_∞ is influenced by the fact that for values of the radial coordinate that are too large, the exponential behavior at infinity $\exp(i\omega r_*) = \exp(i\omega_R r_*)\exp(-\omega_I r_*)$ would explode, as $\omega_I < 0$ – being the mode stable. Hence, it is necessary to choose R_∞ large enough to still be considered "infinity", but not too large to create instabilities. We found that a good range to consider is $R_\infty \in [15, 40] r_H$.

To avoid these numerical artifacts, when we integrate Eq. (5.14) to build the matrix $\hat{X}$ in Eq. (5.13), we impose the boundary conditions at $r = R_H$ and at $r = R_\infty$, as shown in Fig. 2.3

In order to compensate for this workaround, the perturbation $\mathbf{\Psi}$ is expanded perturbatively around the horizon in powers of $r - r_H$ and around infinity in powers of $1/r$. The larger the expansion order, namely N_H for the horizon and N_∞ for infinity, the smaller will be the error induced by imposing the "numerical" boundary conditions, instead of the physical ones.

Explicitly, at $r = R_H \sim r_H$ we will use

$$K_l(\omega, r \sim r_H, \zeta) = e^{-i\omega r_*} \sum_{i=0}^{N_H} k^H_{l,i}(\omega,\zeta)(r - r_H)^i \tag{5.15}$$

$$H_{1l}(\omega, r \sim r_H, \zeta) = e^{-i\omega r_*} \sum_{i=0}^{N_H} h^H_{1l,i}(\omega,\zeta)(r - r_H)^{i-1} \tag{5.16}$$

$$\Phi_l(\omega, r \sim r_H, \zeta) = e^{-i\omega r_*} \sum_{i=0}^{N_H} \phi^H_{l,i}(\omega,\zeta)(r - r_H)^i \tag{5.17}$$

$$\Phi'_l(\omega, r \sim r_H, \zeta) = e^{-i\omega r_*} \sum_{i=0}^{N_H} \xi^H_{l,i}(\omega,\zeta)(r - r_H)^{i-1}\,, \tag{5.18}$$

while at $r = R_\infty$,

$$K_l(\omega, r \to \infty, \zeta) = e^{i\omega r_*} \sum_{i=0}^{N_\infty} \frac{k^\infty_{l,i}(\omega,\zeta)}{r^i} \tag{5.19}$$

$$H_{1l}(\omega, r \to \infty, \zeta) = e^{i\omega r_*} \sum_{i=0}^{N_\infty} \frac{h^\infty_{1l,i}(\omega,\zeta)}{r^{i-1}} \tag{5.20}$$

$$\Phi_l(\omega, r \to \infty, \zeta) = e^{i\omega r_*} \sum_{i=0}^{N_\infty} \frac{\phi^\infty_{l,i}(\omega,\zeta)}{r^i} \tag{5.21}$$

$$\Phi'_l(\omega, r \to \infty, \zeta) = e^{i\omega r_*} \sum_{i=0}^{N_\infty} \frac{\xi^\infty_{l,i}(\omega,\zeta)}{r^i}\,. \tag{5.22}$$

At variance with the GR case, we also have to set the behavior at the boundaries of the dilaton field perturbation Φ_l and of its derivative Φ'_l. Our assumption for the scalar field perturbation Φ_l is that it is regular at the boundaries, meaning it tends asymptotically to a finite value.

The behavior of Φ_l' at the boundaries takes into account that for $r_* \to \pm\infty$, being $\Phi_l \sim \phi_l(\omega, r)e^{\pm i\omega r_*}$, the $dr_*/dr = 1/\sqrt{AB}$ factor that comes from the derivative $\Phi_l' = \partial_r \Phi_l$ diverges near the horizon.

Analogously to the procedure in Section 2.5.1, the set of coefficients $k_{l,i}^{H,\infty}, h_{1l,i}^{H,\infty}, \phi_{l,i}^{H,\infty}, \xi_{l,i}^{H,\infty}$ are found by substituting the expansions (5.15)-(5.18) and (5.19)-(5.22) into the field equations (5.9) and solving them, after expanding them near the horizon and infinity respectively, order by order in $r - r_H$ or $1/r$. These coefficients will depend on four free parameters, two for the horizon case and two for the infinity case, that we choose to be $k_{l,0}^{H,\infty}, \phi_{l,0}^{H,\infty}$, and that will allow selecting different independent solutions to construct the matrix $\hat{X}_l$. For example, two independent ingoing solutions can be found from $(k_{l,0}^H, \phi_{l,0}^H) = \{(1,0),(0,1)\}$, two independent outgoing solutions can be found from$(k_{l,0}^\infty, \phi_{l,0}^\infty) = \{(1,0),(0,1)\}$.

5.3.2 Quasinormal Mode Spectrum

The QNM spectrum is composed of a scalar sector and a gravitational sector. The scalar waves can be detected only if the dilaton field is coupled to matter in the action term S_m in Eq. (3.5). This coupling is expected to be small, but possible detection strategies have been recently investigated in Ref. [327].
The gravitational sector can be further divided according to the parity transformation properties of the perturbations, in *axial* and *polar* families. The axial sector is decoupled from the scalar field, thus it is easier to compute, as the only modifications appear in the background spacetime. The axial QNMs for nonrotating EdGB black holes have been computed in Refs. [3, 109] and are not studied here, since they were found to be closer to the GR values than the polar perturbations, at least in the static case. In the polar gravitational sector, since the metric perturbations are coupled to the dilaton-field perturbations, we can identify two sub-families of QNMs:

- *gravitational-led* modes, which reduce to the quasinormal modes of a Schwarzschild BH for $\zeta \to 0$;
- *scalar-led* modes, which reduce to the quasinormal modes of a test scalar field on a Schwarzschild spacetime for $\zeta \to 0$.

For the coalescence of two equal mass BHs the shift in the ringdown frequency due to EdGB gravity is expected to be dominated by the gravitational-led modes, since the scalar-led are only mildly excited [3]. We note that while in GR the geometric correspondence [296–298] can be used to compute the QNMs in the limit $l \gg 1$, in EdGB this procedure can be generalized only to find the axial QNMs. Instead in the polar sector, which is intrinsically different due to the coupling with the dilaton field and hence the two sub-families of modes, the geometric approach fails to capture all the features of the spectrum [3, 328]

Once we have determined the boundary conditions as described in the Sec. 5.3.1 and built the matrix $\hat{X}$ containing a basis of solutions of the system (5.9), we find the quasinormal modes from the condition (5.14) for specific values of harmonic index l and coupling constant ζ. Throughout this work, we shall always consider $\zeta < 0.4$, since this is the maximum value for which there is good agreement between a $\mathcal{O}(\zeta^6)$ small coupling expansion and the full numerical results, as stated in Ref. [3]. By repeating the integration for different values of ζ we can then find analytical fits for the EdGB spectrum in the range considered.

We focus on the fundamental $l = 2, 3$ gravitational-led polar modes and the $l = 2$ scalar-led mode. As mentioned in Sec. 5.2, due to the spherical symmetry of the nonrotating DBH, there is degeneracy in the azimuthal number m. The resulting spectrum ω^{nl} up to order $\mathcal{O}(\zeta^6)$ for the gravitational-led modes is

$$M\omega_R^{02}(\zeta) = 0.37367 - \left(1.406 \cdot 10^{-2}\right)\zeta^2 - \left(7.55 \cdot 10^{-3}\right)\zeta^3 + \left(1.53 \cdot 10^{-3}\right)\zeta^4 + \left(6.42 \cdot 10^{-3}\right)\zeta^5 - \left(9.9 \cdot 10^{-4}\right)\zeta^6 \tag{5.23}$$

$$M\omega_I^{02}(\zeta) = -0.08896 - \left(4.70 \cdot 10^{-3}\right)\zeta^2 - \left(6.10 \cdot 10^{-3}\right)\zeta^3 - \left(3.22 \cdot 10^{-3}\right)\zeta^4 - \left(1.65 \cdot 10^{-3}\right)\zeta^5 - \left(1.4 \cdot 10^{-4}\right)\zeta^6 \tag{5.24}$$

for $l = 2$, while for $l = 3$ is

$$M\omega_R^{03}(\zeta) = 0.59944 - \left(5.445 \cdot 10^{-2}\right)\zeta^2 - \left(3.235 \cdot 10^{-2}\right)\zeta^3 + \left(7.382 \cdot 10^{-2}\right)\zeta^4 - \left(3.49 \cdot 10^{-3}\right)\zeta^5 - \left(2.390 \cdot 10^{-5}\right)\zeta^6 \tag{5.25}$$

$$M\omega_I^{03}(\zeta) = -0.09270 - \left(7.19 \cdot 10^{-3}\right)\zeta^2 - \left(1.097 \cdot 10^{-2}\right)\zeta^3 + \left(9.98 \cdot 10^{-3}\right)\zeta^4 + \left(2.173 \cdot 10^{-2}\right)\zeta^5 - \left(3.380 \cdot 10^{-2}\right)\zeta^6 . \tag{5.26}$$

For the scalar-led fundamental $l = 2$ mode we find

$$M\omega_R^{s02}(\zeta) = 0.48364 - \left(5.27 \cdot 10^{-3}\right)\zeta + \left(2.588 \cdot 10^{-2}\right)\zeta^2 + \left(7.139 \cdot 10^{-2}\right)\zeta^3 - \left(2.448 \cdot 10^{-2}\right)\zeta^4 \tag{5.27}$$

$$M\omega_I^{s02}(\zeta) = -0.09676 - \left(3.7 \cdot 10^{-4}\right)\zeta + \left(2.88 \cdot 10^{-3}\right)\zeta^2 + \left(6.21 \cdot 10^{-3}\right)\zeta^3 + \left(1.018 \cdot 10^{-2}\right)\zeta^4 . \tag{5.28}$$

We stress that a fit is intrinsically different from a Taylor expansion, since the former describes the whole range of $\zeta \in [0, 0.4]$, while the latter is accurate for $\zeta \ll 1$. The choice of a polynomial fit comes naturally from the small coupling limit framework we adopted throughout this work, but, in principle, one could have different functional expressions. To decide which order of the polynomial better describes the data we estimated the error associated with the functional form of the fit δ_f by computing the mean over 100 attempts of the relative difference between the fit, performed on randomly selected 80% of the data points, and the remaining 20% of the data. Considering a sixth-order polynomial for the gravitational-led modes and a fourth-order polynomial for the scalar-led modes we find at most $\delta_f \sim 10^{-7}$, thus we believe the polynomial form of the fit to be sufficiently accurate.

In Fig. 5.1 (5.2) we plot the ratio between the EdGB gravitational-led (scalar-led) modes and the corresponding GR one $\omega_{R,I}^{nl}(\zeta)/\omega_{R,I}^{nl}(0)$, and we compare the results with the analytical fits given in Ref. [3]. Considering for example $\zeta = 0.3$, the fits for the gravitational-led modes agree up to 0.08% for the real part and up to 0.12% for the imaginary part. For the scalar-led mode these number become 0.15% for the real part and 0.02% for the imaginary part. However, from an approximate visual comparison, some of our results seem to better reproduce the numerical results in Fig.2 of Ref. [3] rather than their small-coupling fit [3].

[3] We do not make further considerations from the comparison since we did not have access to the original data that generated the fourth-order polynomial fits in Ref. [3] and the numerical values plotted in their Fig. 2.

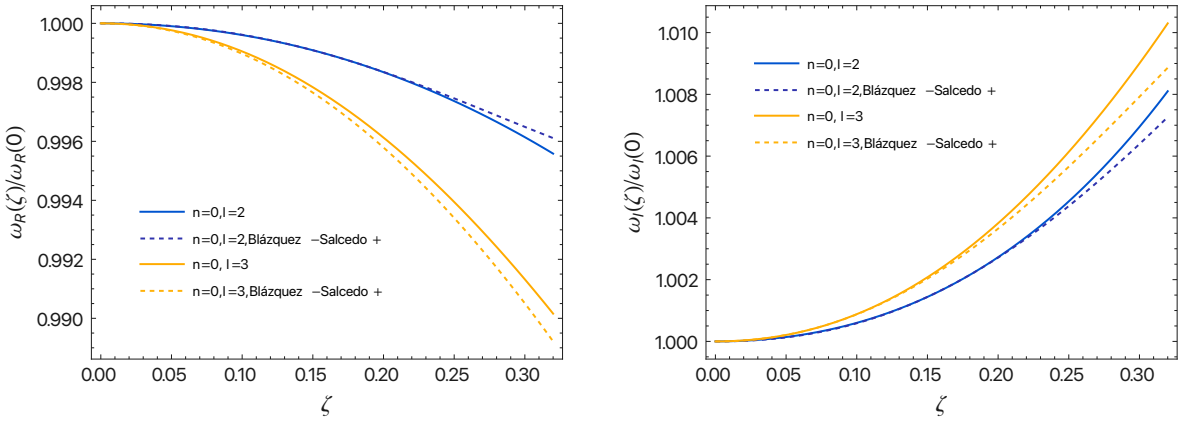

Figure 5.1: *Comparison of the ratio between the $n = 0, l = 2, 3$ polar gravitational EdGB mode and GR mode $\omega_{R,I}(\zeta)/\omega_{R,I}(\zeta = 0)$ with the analytical fits provided in Blázquez-Salcedo et al. [3], as a function of ζ.*

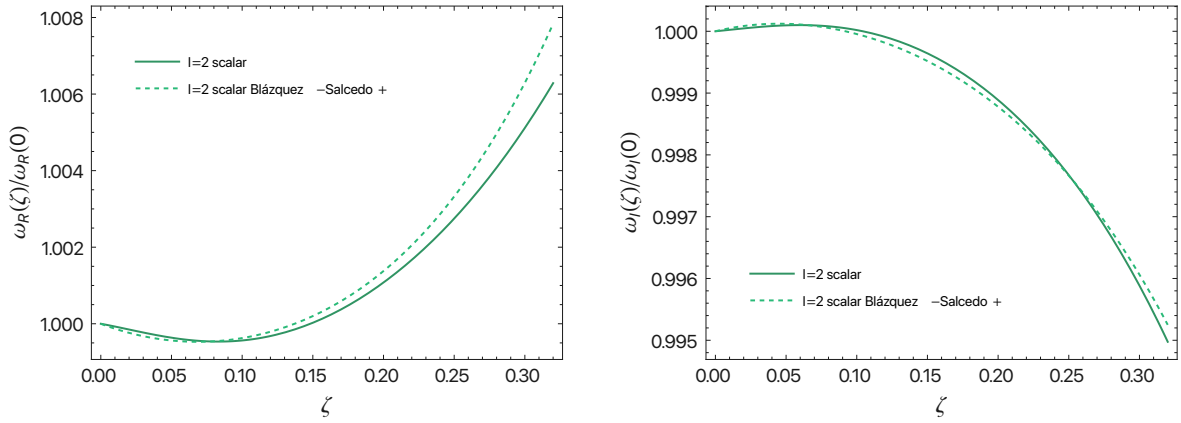

Figure 5.2: *Comparison of the ratio between the $n = 0, l = 2$ polar scalar EdGB mode and GR mode $\omega_{R,I}(\zeta)/\omega_{R,I}(\zeta = 0)$ with the analytical fits provided in Blázquez-Salcedo et al. [3], as a function of ζ.*

We see that the effect of the EdGB corrections, for the range of coupling constant considered here, is to decrease the real part of the gravitational-led mode – for $\zeta = 0.3$ of about 0.4% for $l = 2$ and 1% for $l = 3$ – and increase the imaginary part of the mode (thus decreasing the damping time $\tau = -1/\omega_I$) – of about 0.6% for $l = 2$ and 1% for $l = 3$.

For the $l = 2$ scalar-led mode we find a difference with respect to GR of about 0.6% for the real part of the mode, 0.5% for the imaginary part.

Numerical Stability

The results we have computed are evaluated in the small-coupling framework at order $\mathcal{O}(\zeta^6)$. In order to assess the error introduced by stopping at a certain expansion order $\mathcal{O}(\zeta^s)$ instead of going to the next order $s + 1$, we define the *truncation error*

$$\varepsilon^{nl(s)}_{r\,R,I}(\zeta) \equiv \frac{\left|\omega^{nl(s+1)}_{r\,R,I}(\zeta) - \omega^{nl(s)}_{r\,R,I}(\zeta)\right|}{\left|\omega^{nl(s)}_{r\,R,I}(\zeta)\right|}\,, \tag{5.29}$$

where r is the order in the spin expansion – here $r = 0$, the subscripts R, I refer, as usual, to the real and imaginary parts of the mode. The results are plotted in Fig. 5.3 for an expansion order in

ζ up to $s = 5$.
Since we did not compute the $s = 7$ order, we cannot know the truncation error at $s = 6$, but we can have an order of magnitude estimate, considering that $\varepsilon^{02(5)}_{0\,R,I} \lesssim 10^{-5}$ up to $\zeta \lesssim 0.4$.

Throughout the numerical integration, we have fixed some parameters, namely the orders of the series expansions near the horizon and infinity N_H, N_∞, the small deviation ϵ from the horizon $R_H = r_H(1 + \epsilon)$, the numerical value of infinity R_∞, and the matching point r_m at which the determinant of $\hat{X}$ is computed. Our goal is for the final spectrum to be dependent with good approximation only on the physically meaningful parameters characterizing the QNMs: the coupling constant ζ and the harmonic index l. In order to achieve this, we verify that by varying these numerical parameters we reach a range of values for which the results are stable, meaning that the difference is less than a certain arbitrary small value.
Similarly to what we have discussed in Sec. 2.5.1, we found that the effects of a specific choice of r_m can be considered negligible, whereas $N_H = 11$, $N_\infty = 13$ are good values for the expansion orders, while still requiring a reasonable computation time (for these values, their effects are of the order $\mathcal{O}(10^{-8})$ per QNM, which are subleading with respect to other systematics). The main parameter to calibrate is, also in this case, R_∞. In Fig. 5.4 we plot the $n = 0, l = 2$ polar gravitational mode for a fixed value of $\zeta = 0.3$ and different values of (R_∞, ϵ) and we see that, for $R_\infty \gtrsim 60M$, the results become clearly unstable, and only then the choice of ϵ affects greatly the outcome.
Choosing $\bar{R}_\infty = 40M$ as a reference, we plot in Fig. 5.5 the relative variation in the QNM between the choices of infinity and horizon

$$\delta\omega_{R,I}(R_\infty, \epsilon, \zeta, \bar{R}_\infty) \equiv \frac{|\omega_{R,I}(R_\infty, \epsilon, \zeta) - \omega_{R,I}(\bar{R}_\infty, \epsilon, \zeta)|}{|\omega_{R,I}(\bar{R}_\infty, \epsilon, \zeta)|} \tag{5.30}$$

and we see that in the range $R_\infty \in [25, 45]M$, the variation due to a different choice of R_∞ is at most of order $\sim 10^{-4}$, while the shift introduced by EdGB with respect to GR

$$\Delta\omega^{nl}_{R,I}(\zeta) \equiv \frac{|\omega_{R,I}(\zeta) - \omega_{R,I}(0)|}{|\omega_{R,I}(0)|} \tag{5.31}$$

is of the order $\sim 10^{-3}$, meaning that this deviation is still in principle measurable, regardless of the value of R_∞. These values are computed for $\zeta = 0.3$, which is almost at the limit of validity of the small coupling limit expansion $\zeta \sim 0.4$ [3]: for smaller values of the coupling constant the results are more stable. Our chosen values for the integrations are $\epsilon = 10^{-2}, R_\infty = 35M$.

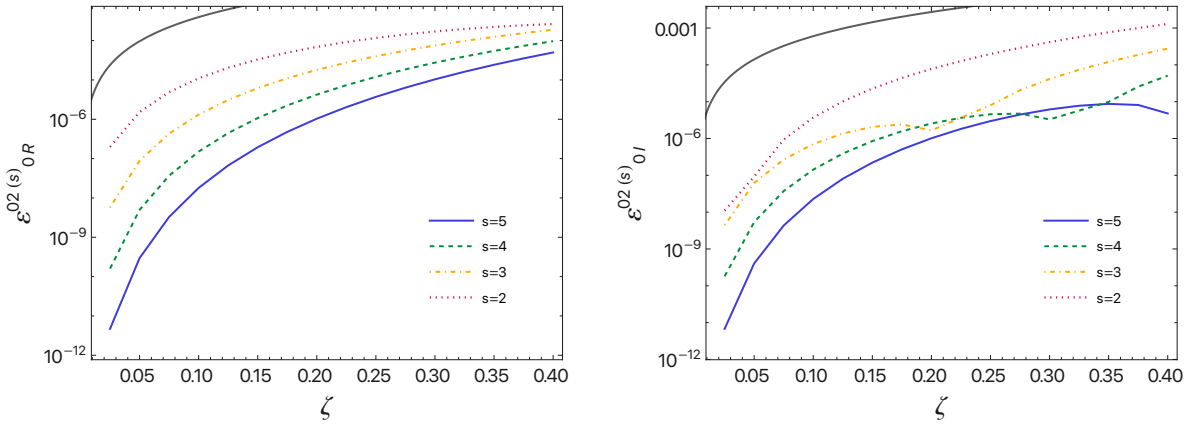

Figure 5.3: *Truncation error at order $s \leq 5$ for the $n = 0, l = 2$ QNM as a function of the dimensionless coupling constant ζ. The truncation error is always smaller than the relative correction due to the EdGB modification to GR (solid black curve).*

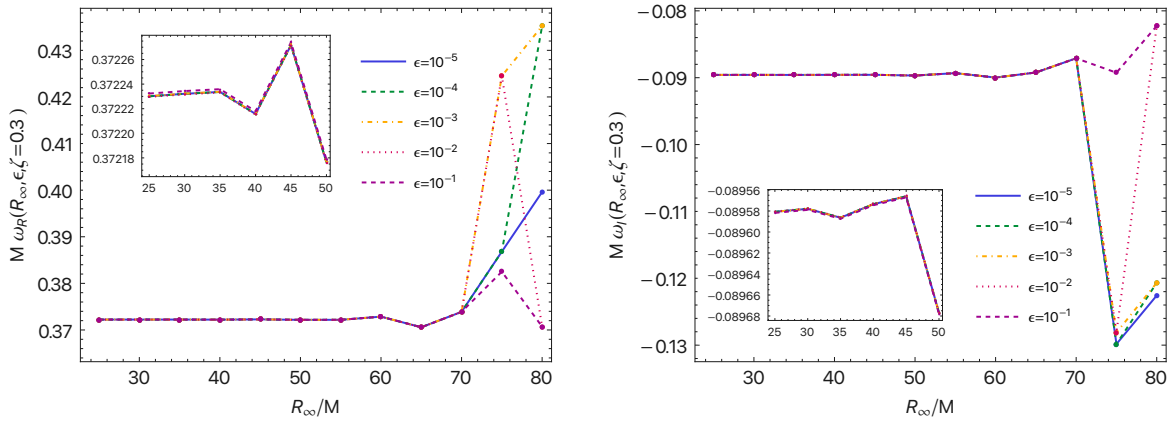

Figure 5.4: *Stability of the $n = 0, l = 2$ quasinormal mode evaluated at $\zeta = 0.3$, for different choices of ϵ and R_∞. We see that for values of $R_\infty > 60M$ the results start to get highly unstable.*

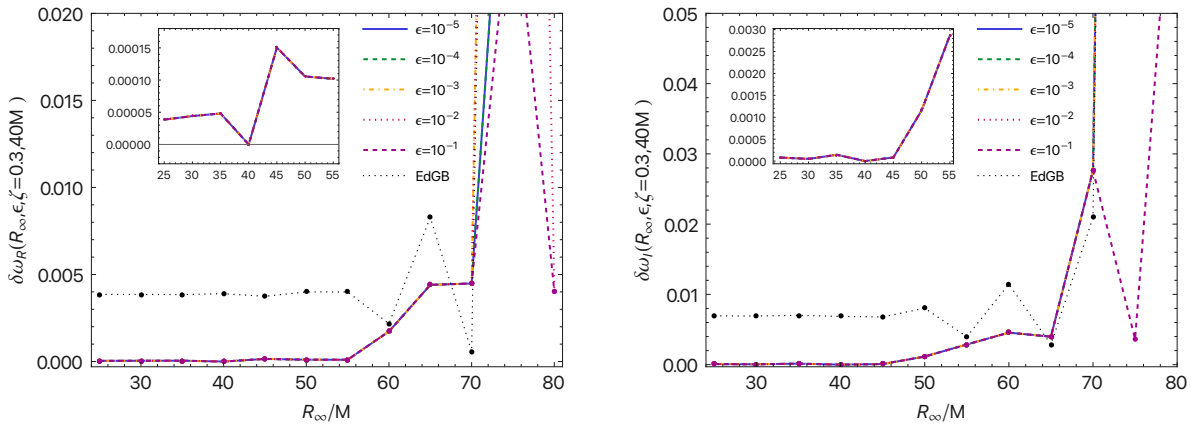

Figure 5.5: *Relative difference of the $n = 0, l = 2$ quasinormal mode, evaluated at $\zeta = 0.3$, with respect to a fixed value of infinity $\bar{R}_\infty = 40M$ and compared with the overall EdGB correction $|\omega_{R,I}(R_\infty, \zeta = 0.3) - \omega_{R,I}(R_\infty, \zeta = 0)|/|\omega_{R,I}(R_\infty, \zeta = 0)|$ to the GR mode (black dotted line).*

Chapter 6

Quasinormal Modes of Slowly Rotating Dilatonic Black Holes

In Chapter 4 we have introduced the effect of rotation to compute the QNMs of a test scalar field in EdGB gravity. In Chapter 5 we studied the problem of gravitational perturbations in EdGB gravity, but without including rotation. In this chapter, we put together the information gained from the previous cases and consider the QNMs of slowly rotating EdGB black holes, originating from perturbations of both the metric and of the dilaton field, as studied in our works [67, 68].

The main difference we expect in the following analysis is for the rotation to create couplings between the polar and axial sectors, and between different harmonic indices l, as described in Sec. 2.6.3 for General Relativity. In fact, while in the scalar field case we have verified that we can neglect the couplings to compute the QNM spectrum at second order in the spin, in this case, the couplings of perturbation functions with harmonic indexes $l \pm 1$ cannot be neglected, thus making the equations to solve more involved.

6.1 Perturbation Equations

We consider a perturbed, stationary, rotating DBH described by the spacetime metric $g_{\mu\nu}$ and dilaton field φ:

$$g_{\mu\nu} = g^{(0)}_{\mu\nu} + h^{pol}_{\mu\nu} + h^{ax}_{\mu\nu} \tag{6.1}$$

$$\varphi = \varphi^{(0)} + \delta\varphi\,, \tag{6.2}$$

where $g^{(0)}_{\mu\nu}$ is the non-perturbed metric in Eq. (3.30) and $\varphi^{(0)}$ is the background dilaton field, described by the expansion (3.35). Both the background quantities are computed analytically up to the second order in the spin $\bar{a} = J/M^2$ and to the sixth order in the dimensionless coupling constant $\zeta = \alpha_{GB}/M^2$. $h^{pol}_{\mu\nu}, h^{ax}_{\mu\nu}$ are small gravitational perturbations separated in *polar* and *axial* according to the transformation properties under rotation. As usual, we can expand the perturbations in a suitable basis of spherical harmonics – scalar, vector, tensor (see Appendix A). Assuming a time dependence $\sim e^{-i\omega t}$, in the Regge-Wheeler gauge [153], and leaving the sum over lm implicit, we

have

$$h^{\rm pol}_{\mu\nu}(t,r,\theta,\phi)dx^\mu dx^\nu = \\ \left[A(r)H_0^{lm}(r)dt^2 + 2H_1^{lm}(r)dtdr + B^{-1}(r)H_2^{lm}(r)dr^2 + K^{lm}(r)(dr^2+\sin^2\theta d\varphi^2)\right] Y^{lm}(\theta,\phi)e^{-i\omega t} \tag{6.3}$$

$$h^{\rm ax}_{\mu\nu}(t,r,\theta,\phi)dx^\mu dx^\nu = 2(h_0^{lm}(r)dt + h_1^{lm}(r)dr)\times(S_\theta(\theta,\phi)d\theta + S_\phi(\theta,\phi)d\phi)e^{-i\omega t} \tag{6.4}$$

$$\delta\varphi(t,r,\theta,\phi) = \frac{1}{r}\Phi^{lm}(r)Y^{lm}(\theta,\phi)e^{-i\omega t}\,, \tag{6.5}$$

with $(S^{lm}_\theta, S^{lm}_\phi) = (-(\sin\theta)^{-1}Y^{lm}_{,\phi}, \sin\theta Y^{lm}_{,\theta})$. When we replace these expansions in the linearized field equations (3.7)-(3.8), we find a set of partial differential equations in r,θ, since the t and ϕ terms can be factored out and possibly simplified.

The gravitational and scalar perturbations are fully identified by the radial functions $H_0^{lm}(r)$, $H_1^{lm}(r)$, $H_2^{lm}(r)$, $K^{lm}(r)$, $h_0^{lm}(r)$, $h_1^{lm}(r)$, $\Phi^{lm}(r)$. We note that we have defined the tt and rr components of the perturbation tensor, in Eqs. (6.3), with a factor $A(r)$ and $B(r)$ for convenience since, being a radial factor, it does not affect the properties under rotation of H_0 and H_1.

Following the formalism of Refs. [159, 193, 285], if we call $\mathcal{E}_{\mu\nu}$ the Einstein equations and $\mathcal{E}_\varphi$ the scalar field equation, the linearized equations (at second order in the spin) naturally separate into three groups, thanks to the transformation properties of the perturbation functions [159, 193]. Defining $Y_{lm}(\theta)\equiv Y_{lm}(\theta,\phi)e^{-im\phi}$, the first group has the form

$$\delta\mathcal{E}_{(I)} \equiv \left[A^{(I)}_{lm} + \tilde{A}^{(I)}_{lm}\cos\theta + \hat{A}^{(I)}_{lm}\cos^2\theta\right]Y_{lm}(\theta) + im\left[C^{(I)}_{lm} + \tilde{C}^{(I)}_{lm}\cos\theta\right]Y_{lm}(\theta) + m^2E^{(I)}_{lm}Y_{lm}(\theta) \\ + \left[B^{(I)}_{lm} + \tilde{B}^{(I)}_{lm}\cos\theta + imD^{(I)}_{lm}\right]\sin\theta\, Y'_{lm}(\theta) = 0\,, \tag{6.6}$$

where $I = 0,1,2,3,4$ correspond schematically to the components that behave as scalars under rotation, namely $tt,\ rr,\ rt,\ \theta\theta+\phi\phi/\sin^2\theta$ and the scalar field equation, respectively.
The second group, corresponding to the components of Einstein equations behaving as vectors under rotation, is given by

$$\delta\mathcal{E}_{(J\theta)} \equiv \left[\alpha^{(J)}_{lm} + \tilde{\alpha}^{(J)}_{lm}\cos\theta + \hat{\alpha}^{(J)}_{lm}\cos^2\theta\right]\sin\theta\, Y'_{lm}(\theta) - im\left[\beta^{(J)}_{lm} + \tilde{\beta}^{(J)}_{lm}\cos\theta + \hat{\beta}^{(J)}_{lm}\cos^2\theta\right]Y_{lm}(\theta) \\ + \left[\eta^{(J)}_{lm} + \tilde{\eta}^{(J)}_{lm}\cos\theta\right]\sin^2\theta Y_{lm}(\theta) + \left[\xi^{(J)}_{lm} + \tilde{\xi}^{(J)}_{lm}\cos\theta\right]\sin\theta X_{lm}(\theta) \\ + \left[\gamma^{(J)}_{lm} + \tilde{\gamma}^{(J)}_{lm}\cos\theta\right]\sin^2\theta W_{lm}(\theta) = 0\,, \tag{6.7}$$

$$\delta\mathcal{E}_{(J\phi)} \equiv -\left[\beta^{(J)}_{lm} + \tilde{\beta}^{(J)}_{lm}\cos\theta + \hat{\beta}^{(J)}_{lm}\cos^2\theta + \tilde{\Delta}^{(J)}_{lm}\sin^2\theta\right]\sin\theta\, Y'_{lm}(\theta) \\ - im\left[\alpha^{(J)}_{lm} + \tilde{\alpha}^{(J)}_{lm}\cos\theta + \hat{\alpha}^{(J)}_{lm}\cos^2\theta + \Delta^{(J)}_{lm}\sin^2\theta\right]Y_{lm}(\theta) - \left[\zeta^{(J)}_{lm} + \tilde{\zeta}^{(J)}_{lm}\cos\theta\right]\sin^2\theta\, Y_{lm}(\theta) \\ - \left[\gamma^{(J)}_{lm} + \tilde{\gamma}^{(J)}_{lm}\cos\theta\right]\sin\theta X_{lm}(\theta) + \left[\xi^{(J)}_{lm} + \tilde{\xi}^{(J)}_{lm}\cos\theta\right]\sin^2\theta W_{lm}(\theta) = 0\,, \tag{6.8}$$

with $J = 0,1$ corresponding to the components $t,\ r$.

The third group

$$\delta\mathcal{E}_{(\theta\phi)} \equiv \left[f_{lm} + \tilde{f}_{lm}\ \cos\theta\right]\sin\theta\ Y'_{lm}(\theta) + im\left[g_{lm} + \tilde{g}_{lm}\ \cos\theta\right]Y_{lm}(\theta) + k_{lm}\sin^2\theta\ Y_{lm}(\theta) + \left[s_{lm} + \hat{s}_{lm}\ \cos^2\theta\right]\frac{X_{lm}(\theta)}{\sin\theta} + \left[t_{lm} + \hat{t}_{lm}\ \cos^2\theta\right]W_{lm}(\theta) = 0 \tag{6.9}$$

$$\delta\mathcal{E}_{(-)} \equiv \left[g_{lm} + \tilde{g}_{lm}\ \cos\theta\right]\sin\theta\ Y'_{lm}(\theta) - im\left[f_{lm} + \tilde{f}_{lm}\ \cos\theta\right]Y_{lm}(\theta) + \hat{k}_{lm}\sin^2\theta\ Y_{lm}(\theta) - \left[t_{lm} + \hat{t}_{lm}\ \cos^2\theta\right]\frac{X_{lm}(\theta)}{\sin\theta} + \left[s_{lm} + \hat{s}_{lm}\ \cos^2\theta\right]W_{lm}(\theta) = 0 \tag{6.10}$$

corresponds to the components behaving as tensors, i.e. $\theta\phi$ and $\theta\theta - \phi\phi/\sin^2\theta$.
We have defined $X_{lm}(\theta), W_{lm}(\theta)$ as

$$X_{lm}(\theta) \equiv 2\,i\,m\left[Y'_{lm}(\theta) - \frac{\cos\theta}{\sin\theta}Y_{lm}(\theta)\right] \tag{6.11}$$

$$W_{lm}(\theta) \equiv -2\frac{\cos\theta}{\sin\theta}Y'_{lm}(\theta) - l(l+1)Y_{lm}(\theta) + 2m^2\frac{Y_{lm}(\theta)}{\sin^2\theta}\,. \tag{6.12}$$

The coefficients appearing in the equations above are linear combinations of the perturbation functions $h_0^{lm}(r)$, $h_1^{lm}(r)$, $H_0^{lm}(r)$, $H_1^{lm}(r)$, $H_2^{lm}(r)$, $K^{lm}(r)$, $\Phi^{lm}(r)$ and their derivatives, with coefficients that depend on l but not on m. In the same way as the perturbation functions, they can be divided into two sets according to their parity:

$$\text{Polar}: A_{lm}^{(I)},\ \hat{A}_{lm}^{(I)},\ C_{lm}^{(I)},\ E_{lm}^{(I)},\ \tilde{B}_{lm}^{(I)},\ \alpha_{lm}^{(J)},\ \hat{\alpha}_{lm}^{(J)},\ \tilde{\beta}_{lm}^{(J)},\ \tilde{\eta}_{lm}^{(J)},\ \xi_{lm}^{(J)},\ \tilde{\gamma}_{lm}^{(J)},\ \Delta_{lm}^{(J)},\ \zeta_{lm}^{(J)},\ f_{lm},\ \tilde{g}_{lm},\ \hat{k}_{lm},\ s_{lm},\ \hat{s}_{lm}$$

$$\text{Axial}: \tilde{A}_{lm}^{(I)},\ \tilde{C}_{lm}^{(I)},\ B_{lm}^{(I)},\ D_{lm}^{(I)},\ \tilde{\alpha}_{lm}^{(J)},\ \beta_{lm}^{(J)},\ \hat{\beta}_{lm}^{(J)},\ \eta_{lm}^{(J)},\ \tilde{\xi}_{lm}^{(J)},\ \gamma_{lm}^{(J)},\ \tilde{\Delta}_{lm}^{(J)},\ \tilde{\zeta}_{lm}^{(J)}, \tilde{f}_{lm},\ g_{lm},\ k_{lm},\ t_{lm},\ \hat{t}_{lm}\,.$$

The coefficients

- $A_{lm}^{(I)}$, $\alpha_{lm}^{(J)}$, $\beta_{lm}^{(J)}$, s_{lm}, t_{lm} contain both zeroth and second-order terms in the spin $\bar{a}$;
- $\tilde{A}_{lm}^{(I)}$, $C_{lm}^{(I)}$, $B_{lm}^{(I)}$, $\tilde{\alpha}_{lm}^{(J)}$, $\tilde{\beta}_{lm}^{(J)}$, $\eta_{lm}^{(J)}$, $\xi_{lm}^{(J)}$, $\gamma_{lm}^{(J)}$, $\zeta_{lm}^{(J)}$, f_{lm}, g_{lm} are of order $\mathcal{O}(\bar{a})$;
- $\hat{A}_{lm}^{(J)}$, $\tilde{C}_{lm}^{(J)}$, $E_{lm}^{(J)}$, $\tilde{B}_{lm}^{(J)}$, $D_{lm}^{(J)}$, $\hat{\alpha}_{lm}^{(J)}$, $\hat{\beta}_{lm}^{(J)}$, $\tilde{\eta}_{lm}^{(J)}$, $\tilde{\xi}_{lm}^{(J)}$, $\tilde{\gamma}_{lm}^{(J)}$,$\tilde{\zeta}_{lm}^{(J)}$, $\Delta_{lm}^{(J)}$, $\tilde{\Delta}_{lm}^{(J)}$, $\tilde{f}_{lm}^{(J)}$, $\tilde{g}_{lm}^{(J)}$, $k_{lm}^{(J)}$, $\hat{k}_{lm}^{(J)}$, $\hat{s}_{lm}^{(J)}$, $\hat{t}_{lm}^{(J)}$ are of second order in the spin.

Their explicit expansions in the coupling parameter ζ, up to $\mathcal{O}(\zeta^6)$, are given in the Supplemental Material [322].

We decouple the angular dependence from the equations by integrating on the solid angle and exploiting the properties of the spherical harmonics, as described in detail in Appendix F. In par-

ticular, we shall compute the following integrals:

$$0 = \sum_{l'm'} \int d\Omega Y^*_{lm} \delta\mathcal{E}^{l'm'}_{(I)} \tag{6.13}$$

$$0 = \sum_{l'm'} \int d\Omega \left[\frac{\partial_\theta Y^*_{lm} \delta\mathcal{E}^{l'm'}_{(J\theta)}}{\sin\theta} + im \frac{Y^*_{lm} \delta\mathcal{E}^{l'm'}_{(J\phi)}}{\sin^2\theta} \right] \tag{6.14}$$

$$0 = \sum_{l'm'} \int d\Omega \left[-\frac{\partial_\theta Y^*_{lm} \delta\mathcal{E}^{l'm'}_{(J\phi)}}{\sin\theta} + im \frac{Y^*_{lm} \delta\mathcal{E}^{l'm'}_{(J\theta)}}{\sin^2\theta} \right] \tag{6.15}$$

$$0 = \sum_{l'm'} \int d\Omega \left[W^*_{lm} \delta\mathcal{E}^{l'm'}_{(-)} + \frac{X^*_{lm}}{\sin\theta} \delta\mathcal{E}^{l'm'}_{(\theta\phi)} \right] \tag{6.16}$$

$$0 = \sum_{l'm'} \int d\Omega \left[W^*_{lm} \delta\mathcal{E}^{l'm'}_{(\theta\phi)} - \frac{X^*_{lm}}{\sin\theta} \delta\mathcal{E}^{l'm'}_{(-)} \right] , \tag{6.17}$$

where we have made the sum over the harmonic indexes explicit. The orthogonality of the harmonics removes the sum over all the indices $l'm'$ and isolates a single lm mode.
This procedure is valid for $l > 1$, while for $l = 0, l = 1$ some spherical harmonics previously defined vanish, so that the corresponding perturbation functions do not require to be fixed with the gauge as done in App. A. We can therefore use the residual gauge freedom to set to zero one or two additional degrees of freedom (see e.g. [3, 193, 254, 329]).

6.1.1 First Order Equations

We expect the form of the perturbations equations at first order in the spin to have a similar structure to the results of Ref. [193] for neutron stars. In the following sections, we shall factor out the spin dependence from the coefficients in Eqs. (6.6)-(6.10) (while leaving the name of the coefficient unchanged).

After the angular integration, from Eq. (6.13) we find

$$0 = A^{(I)}_{lm} + im\,\bar{a}\,C^{(I)}_{lm} + \bar{a}\,Q_{lm}\left[\tilde{A}^{(I)}_{l-1\,m} + (l-1)B^{(I)}_{l-1\,m}\right] + \bar{a}\,Q_{l+1\,m}\left[\tilde{A}^{(I)}_{l+1\,m} - (l+2)B^{(I)}_{l+1\,m}\right] . \tag{6.18}$$

From the integral (6.14) we get

$$\begin{aligned} 0 =& l(l+1)\alpha^{(J)}_{lm} - im\,\bar{a}\left[\tilde{\beta}^{(J)}_{lm} + \zeta^{(J)}_{lm} - (l-1)(l+2)\xi^{(J)}_{lm}\right] + \bar{a}\,Q_{lm}(l+1)\Big\{(l-1)\tilde{\alpha}^{(J)}_{l-1\,m} \\ & - \eta^{(J)}_{l-1\,m} + (l-2)(l-1)\gamma^{(J)}_{l-1\,m}\Big\} + \bar{a}\,Q_{l+1\,m}l\Big\{(l+2)\tilde{\alpha}^{(J)}_{l+1\,m} + \eta^{(J)}_{l+1\,m} - (l+2)(l+3)\gamma^{(J)}_{l+1\,m}\Big\} \end{aligned} \tag{6.19}$$

while from (6.15)

$$\begin{aligned} 0 =& l(l+1)\beta^{(J)}_{lm} + im\,\bar{a}\left[\tilde{\alpha}^{(J)}_{lm} + \eta^{(J)}_{lm} + (l-1)(l+2)\gamma^{(J)}_{lm}\right] + \bar{a}\,Q_{lm}(l+1)\Big\{(l-1)\tilde{\beta}^{(J)}_{l-1\,m} - \zeta^{(J)}_{l-1\,m} \\ & - (l-2)(l-1)\xi^{(J)}_{l-1\,m}\Big\} + \bar{a}\,Q_{l+1\,m}l\Big\{(l+2)\tilde{\beta}^{(J)}_{l+1\,m} + \zeta^{(J)}_{l+1\,m} + (l+2)(l+3)\xi^{(J)}_{l+1\,m}\Big\} . \end{aligned} \tag{6.20}$$

Finally, from Eqs. (6.16) and (6.17) we obtain

$$\begin{aligned}0 =& l(l-1)(l+1)(l+2)s_{lm} - im\,\bar{a}(l-1)(l+2)f_{lm} - \bar{a}\,Q_{lm}(l-1)(l+1)(l+2)g_{l-1\,m} \\ &+ \bar{a}\,Q_{l+1\,m}l(l-1)(l+2)g_{l+1\,m}\end{aligned} \tag{6.21}$$

$$\begin{aligned}0 =& l(l-1)(l+1)(l+2)t_{lm} + im\,\bar{a}(l-1)(l+2)g_{lm} - \bar{a}\,Q_{lm}(l-1)(l+1)(l+2)f_{l-1\,m} \\ &+ \bar{a}\,Q_{l+1\,m}l(l-1)(l+2)f_{l+1\,m}\end{aligned} \,, \tag{6.22}$$

where we have defined

$$Q_{lm} \equiv \sqrt{\frac{l^2-m^2}{4l^2-1}}\,. \tag{6.23}$$

We can see that decomposing the perturbations of an axisymmetric spacetime –as the one of a rotating DBH– on a sphere, using the spherical harmonics, comes with the cost of introducing additional terms in the perturbation equations with couplings between different harmonic indices.

The general layout of these equations can be highlighted using the schematic notation

$$\mathcal{P}_{lm} + \bar{a}m\bar{\mathcal{P}}_{lm} + \bar{a}\left(Q_{lm}\tilde{\mathcal{A}}_{l-1\,m} + Q_{l+1\,m}\tilde{\mathcal{A}}_{l+1\,m}\right) = 0 \tag{6.24}$$

$$\mathcal{A}_{lm} + \bar{a}m\bar{\mathcal{A}}_{lm} + \bar{a}\left(Q_{lm}\tilde{\mathcal{P}}_{l-1\,m} + Q_{l+1\,m}\tilde{\mathcal{P}}_{l+1\,m}\right) = 0\,, \tag{6.25}$$

with $\mathcal{P}_{lm}$, $\bar{\mathcal{P}}_{lm}$, $\hat{\mathcal{P}}_{lm}$, ($\mathcal{A}_{lm}$, $\bar{\mathcal{A}}_{lm}$, $\hat{\mathcal{A}}_{lm}$) are combinations of the polar perturbation functions H_0^{lm}, H_1^{lm}, H_2^{lm}, K^{lm}, Φ^{lm} (of the axial perturbation functions h_0^{lm}, h_1^{lm}); the coefficients of these functions in the combinations do not depend on the harmonic index m.

At zeroth order in the spin, the equations reduce to $\mathcal{P}_{lm} = 0$, $\mathcal{A}_{lm} = 0$, which can be recast in the form of Eq. (5.9), describing the perturbations of static, spherically symmetric DBHs discussed in Chapter 5. At first order in the spin, polar perturbations with l are coupled to axial perturbations with $l \pm 1$, and vice versa. Moreover, polar (axial) perturbations are coupled to perturbations having the same l and the same parity; the latter couplings are proportional to m. We note that the structure of these equations is in agreement with Kojima [193], as we expected.

6.1.2 Second Order Equations

In this section, factoring out the spin dependence, we call $A^{(I)}_{2,lm}, \alpha^{(I)}_{2,lm}, \beta^{(I)}_{2,lm}, s_{2,lm}, t_{2,lm}$ the second-order parts of the original coefficients $A^{(I)}_{lm}, \alpha^{(I)}_{lm}, \beta^{(I)}_{lm}, s_{lm}, t_{lm}$.
Performing the angular integration of the perturbation equations and keeping all the terms up to $\mathcal{O}(\bar{a}^2)$, we get, from the first group in Eq.(6.6)

$$\begin{aligned}&A^{(I)}_{lm} + \bar{a}^2 A^{(I)}_{2,lm} + \bar{a}^2\hat{A}^{(I)}_{lm}\left[Q^2_{lm} + Q^2_{l+1\,m}\right] + \bar{a}^2\tilde{B}^{(I)}_{lm}\left[lQ^2_{l+1\,m} - (l+1)Q^2_{lm}\right] + im\,\bar{a}\,C^{(I)}_{lm} + \bar{a}^2m^2E^{(I)}_{lm} \\ &+ Q_{lm}\Big\{\bar{a}\left[\tilde{A}^{(I)}_{l-1\,m} + (l-1)B^{(I)}_{l-1\,m}\right] + im\,\bar{a}^2\left[\tilde{C}^{(I)}_{l-1\,m} + (l-1)D^{(I)}_{l-1\,m}\right]\Big\} \\ &+ Q_{l+1\,m}\Big\{\left[\bar{a}\tilde{A}^{(I)}_{l+1\,m} - (l+2)B^{(I)}_{l+1\,m}\right] + im\,\bar{a}^2\left[\tilde{C}^{(I)}_{l+1\,m} - (l+2)D^{(I)}_{l+1\,m}\right]\Big\} \\ &+ \bar{a}^2Q_{lm}Q_{l-1\,m}\left[\hat{A}^{(I)}_{l-2\,m} + (l-2)\tilde{B}^{(I)}_{l-2\,m}\right] + \bar{a}^2Q_{l+1\,m}Q_{l+2\,m}\left[\hat{A}^{(I)}_{l+2\,m} - (l+3)\tilde{B}^{(I)}_{l+2\,m}\right] = 0\,.\end{aligned} \tag{6.26}$$

From the second group in Eqs. (6.7)-(6.8)

$$
\begin{aligned}
&l(l+1)\alpha^{(J)}_{lm} + \bar{a}^2 l(l+1)\alpha^{(J)}_{2,lm} - im\,\bar{a}\left[\tilde{\beta}^{(J)}_{lm} + \zeta^{(J)}_{lm} - (l-1)(l+2)\xi^{(J)}_{lm}\right] \\
&+ \bar{a}^2\left[(l+1)(l-2)Q^2_{lm} + l(l+3)Q^2_{l+1\,m}\right]\hat{\alpha}^{(J)}_{lm} + m^2\bar{a}^2\Delta^{(J)}_{lm} + \bar{a}^2\left[lQ^2_{l+1\,m} - (l+1)Q^2_{lm}\right]\tilde{\eta}^{(J)}_{lm} \\
&+ \bar{a}^2\left[2m^2 + Q^2_{lm}(l+1)(l^2-l+4) - Q^2_{l+1\,m}l(l^2+3l+6)\right]\tilde{\gamma}^{(J)}_{lm} \\
&+ Q_{lm}\Big\{\bar{a}\left[(l-1)(l+1)\tilde{\alpha}^{(J)}_{l-1\,m} - (l+1)\eta^{(J)}_{l-1\,m} + (l-2)(l-1)(l+1)\gamma^{(J)}_{l-1\,m}\right] \\
&\quad - im\,\bar{a}^2\left[2\hat{\beta}^{(J)}_{l-1\,m} + (l-1)\tilde{\Delta}^{(J)}_{l-1\,m} + \tilde{\zeta}^{(J)}_{l-1\,m} - (l-2)(l+3)\tilde{\xi}^{(J)}_{l-1\,m}\right]\Big\} \\
&+ Q_{l+1\,m}\Big\{\bar{a}\left[l(l+2)\tilde{\alpha}^{(J)}_{l+1\,m} + l\eta^{(J)}_{l+1\,m} - l(l+2)(l+3)\gamma^{(J)}_{l+1\,m}\right] \\
&\quad - im\,\bar{a}^2\left[2\hat{\beta}^{(J)}_{l+1\,m} - (l+2)\tilde{\Delta}^{(J)}_{l+1\,m} + \tilde{\zeta}^{(J)}_{l+1\,m} - (l-2)(l+3)\tilde{\xi}^{(J)}_{l+1\,m}\right]\Big\} \\
&+ \bar{a}^2 Q_{l-1\,m}Q_{lm}\Big\{(l-2)(l+1)\hat{\alpha}^{(J)}_{l-2\,m} - (l+1)\tilde{\eta}^{(J)}_{l-2\,m} + (l-2)(l+1)(l-3)\tilde{\gamma}^{(J)}_{l-2\,m}\Big\} \\
&+ \bar{a}^2 Q_{l+1\,m}Q_{l+2\,m}\Big\{l(l+3)\hat{\alpha}^{(J)}_{l+2} + l\tilde{\eta}^{(J)}_{l+2\,m} - l(l+3)(l+4)\;\tilde{\gamma}^{(J)}_{l+2\,m}\Big\} = 0\,,
\end{aligned}
\tag{6.27}
$$

$$
\begin{aligned}
&l(l+1)\beta^{(J)}_{lm} + \bar{a}^2 l(l+1)\beta^{(J)}_{2,lm} + im\,\bar{a}\left[\tilde{\alpha}^{(J)}_{lm} + \eta^{(J)}_{lm} + (l-1)(l+2)\gamma^{(J)}_{lm}\right] \\
&+ \bar{a}^2\left[(l+1)(l-2)Q^2_{lm} + l(l+3)Q^2_{l+1\,m}\right]\hat{\beta}^{(J)}_{lm} + \bar{a}^2\left[l^2Q^2_{l+1\,m} + (l+1)^2Q^2_{lm}\right]\tilde{\Delta}^{(J)}_{lm} \\
&+ \bar{a}^2\left[lQ^2_{l+1\,m} - (l+1)Q^2_{lm}\right]\tilde{\zeta}^{(J)}_{lm} - \bar{a}^2\left[2m^2 + Q^2_{lm}(l+1)(l^2-l+4) - Q^2_{l+1\,m}l(l^2+3l+6)\right]\tilde{\xi}^{(J)}_{lm} \\
&+ Q_{lm}\Big\{\bar{a}\left[(l-1)(l+1)\tilde{\beta}^{(J)}_{l-1\,m} - (l+1)\zeta^{(J)}_{l-1\,m} - (l-2)(l-1)(l+1)\xi^{(J)}_{l-1\,m}\right] \\
&\quad + im\,\bar{a}^2\left[2\hat{\alpha}^{(J)}_{l-1\,m} - (l+1)\Delta^{(J)}_{l-1\,m} + \tilde{\eta}^{(J)}_{l-1\,m} + (l-2)(l+3)\tilde{\gamma}^{(J)}_{l-1\,m}\right]\Big\} \\
&+ Q_{l+1\,m}\Big\{\bar{a}\left[l(l+2)\tilde{\beta}^{(J)}_{l+1\,m} + l\zeta^{(J)}_{l+1\,m} + l(l+2)(l+3)\xi^{(J)}_{l+1\,m}\right] \\
&\quad + im\,\bar{a}^2\left[2\hat{\alpha}^{(J)}_{l+1\,m} + l\Delta^{(J)}_{l+1\,m} + \tilde{\eta}^{(J)}_{l+1\,m} + (l-2)(l+3)\tilde{\gamma}^{(J)}_{l+1\,m}\right]\Big\} \\
&+ \bar{a}^2 Q_{l-1\,m}Q_{lm}\Big\{(l-2)(l+1)\hat{\beta}^{(J)}_{l-2\,m} - (l+1)\tilde{\zeta}^{(J)}_{l-2\,m} \\
&\quad - (l-2)(l+1)(l-3)\tilde{\xi}^{(J)}_{l-2\,m} - (l-2)(l+1)\tilde{\Delta}^{(J)}_{l-2\,m}\Big\} \\
&+ \bar{a}^2 Q_{l+1\,m}Q_{l+2\,m}\Big\{l(l+3)\hat{\beta}^{(J)}_{l+2\,m} + l\tilde{\zeta}^{(J)}_{l+2\,m} + l(l+3)(l+4)\tilde{\xi}^{(J)}_{l+2\,m} - l(l+3)\tilde{\Delta}^{(J)}_{l+2\,m}\Big\} = 0\,.
\end{aligned}
\tag{6.28}
$$

From the third group, according to Eqs. (6.9)-(6.10),

$$
\begin{aligned}
&l(l-1)(l+1)(l+2)\left[s_{lm}+\bar{a}^2 s_{2,lm}\right]-im\,\bar{a}(l-1)(l+2)f_{lm}\\
&+\bar{a}^2\left[2m^2+Q_{lm}^2(l+1)(l^2-l+4)-Q_{l+1\,m}^2 l(l^2+3l+6)\right]\tilde{g}_{lm}+\bar{a}^2\left[2m^2-l(l+1)\right.\\
&\quad\left.+(l+1)(l+2)Q_{lm}^2+l(l-1)Q_{l+1\,m}^2\right]\hat{k}_{lm}+\bar{a}^2\Big\{8m^2-2l(l+1)\\
&-Q_{lm}^2(l+1)\left[4(l-2)-l(l+1)(l+4)\right]-Q_{l+1\,m}^2 l\left[4(l+3)-l(l+1)(l-3)\right]\Big\}\hat{s}_{lm}\\
&-Q_{lm}\Big\{\bar{a}(l-1)(l+1)(l+2)g_{l-1\,m}+im\,\bar{a}^2\Big[(l-3)(l+2)\tilde{f}_{l-1\,m}-2(l+2)k_{l-1\,m}\\
&\quad+4(l-2)(l+2)\hat{t}_{l-1\,m}\Big]\Big\}+Q_{l+1\,m}\Big\{\bar{a}\,l(l-1)(l+2)g_{l+1\,m}-im\,\bar{a}^2\Big[(l-1)(l+4)\tilde{f}_{l+1\,m}\\
&\quad+2(l-1)k_{l+1\,m}+4(l-1)(l+3)\hat{t}_{l+1\,m}\Big]\Big\}\\
&+\bar{a}^2 Q_{l-1\,m}Q_{lm}(l+1)(l+2)\Big\{-(l-2)\tilde{g}_{l-2\,m}+\hat{k}_{l-2\,m}+(l-3)(l-2)\hat{s}_{l-2\,m}\Big\}\\
&+\bar{a}^2 Q_{l+1\,m}Q_{l+2\,m}l(l-1)\Big\{(l+3)\tilde{g}_{l+2\,m}+\hat{k}_{l+2\,m}+(l+3)(l+4)\hat{s}_{l+2\,m}\Big\}=0\,,
\end{aligned}
\tag{6.29}
$$

$$
\begin{aligned}
0=&\,l(l-1)(l+1)(l+2)\left[t_{lm}+\bar{a}^2 t_{2,lm}\right]+im\,\bar{a}(l-1)(l+2)g_{lm}\\
&+\bar{a}^2\left[2m^2+Q_{lm}^2(l+1)(l^2-l+4)-Q_{l+1\,m}^2 l(l^2+3l+6)\right]\tilde{f}_{lm}+\bar{a}^2\left[2m^2-l(l+1)\right.\\
&\quad\left.+(l+1)(l+2)Q_{lm}^2+l(l-1)Q_{l+1\,m}^2\right]k_{lm}+\bar{a}^2\Big\{8m^2-2l(l+1)\\
&-Q_{lm}^2(l+1)\left[4(l-2)-l(l+1)(l+4)\right]-Q_{l+1\,m}^2 l\left[4(l+3)-l(l+1)(l-3)\right]\Big\}\hat{t}_{lm}\\
&-Q_{lm}\Big\{\bar{a}(l-1)(l+1)(l+2)f_{l-1\,m}-im\,\bar{a}^2\Big[(l-3)(l+2)\tilde{g}_{l-1\,m}-2(l+2)\hat{k}_{l-1\,m}\\
&\quad+4(l-2)(l+2)\hat{s}_{l-1\,m}\Big]\Big\}+Q_{l+1\,m}\Big\{\bar{a}\,l(l-1)(l+2)f_{l+1\,m}+im\,\bar{a}^2\left[(l-1)(l+4)\tilde{g}_{l+1\,m}\right.\\
&\quad\left.+2(l-1)\hat{k}_{l+1\,m}+4(l-1)(l+3)\hat{s}_{l+1\,m}\right]\Big\}\\
&+\bar{a}^2 Q_{l-1\,m}Q_{lm}(l+1)(l+2)\Big\{-(l-2)\tilde{f}_{l-2\,m}+k_{l-2\,m}+(l-3)(l-2)\hat{t}_{l-2\,m}\Big\}\\
&+\bar{a}^2 Q_{l+1\,m}Q_{l+2\,m}l(l-1)\Big\{(l+3)\tilde{f}_{l+2\,m}+k_{l+2\,m}+(l+3)(l+4)\hat{t}_{l+2\,m}\Big\}\,,
\end{aligned}
\tag{6.30}
$$

These extremely involved equations can be schematically written as

$$
\begin{aligned}
0=&\mathcal{P}_{l\,m}+\bar{a}\,m\,\bar{\mathcal{P}}_{l\,m}+\bar{a}^2\hat{\mathcal{P}}_{l\,m}+\,m^2\,\bar{a}^2\bar{\bar{\mathcal{P}}}_{l\,m}+\bar{a}\left(Q_{l\,m}\tilde{\mathcal{A}}_{l-1\,m}+Q_{l+1\,m}\tilde{\mathcal{A}}_{l+1\,m}\right)\\
&+\bar{a}^2\left(Q_{l-1\,m}Q_{l\,m}\breve{\mathcal{P}}_{l-2\,m}+Q_{l+1\,m}Q_{l+2\,m}\breve{\mathcal{P}}_{l+2\,m}\right)\\
&+m\,\bar{a}^2\left(Q_{l\,m}\breve{\mathcal{A}}_{l-1\,m}+Q_{l+1\,m}\breve{\mathcal{A}}_{l+1\,m}\right)
\end{aligned}
\tag{6.31}
$$

$$
\begin{aligned}
0=&\mathcal{A}_{l\,m}+\bar{a}\,m\,\bar{\mathcal{A}}_{l\,m}+\bar{a}^2\hat{\mathcal{A}}_{lm}+\,m^2\,\bar{a}^2\bar{\bar{\mathcal{A}}}_{l\,m}+\bar{a}\left(Q_{l\,m}\tilde{\mathcal{P}}_{l-1\,m}+Q_{l+1\,m}\tilde{\mathcal{P}}_{l+1\,m}\right)\\
&+\bar{a}^2\left(Q_{l-1\,m}Q_{l\,m}\breve{\mathcal{A}}_{l-2\,m}+Q_{l+1\,m}Q_{l+2\,m}\breve{\mathcal{A}}_{l+2\,m}\right)\\
&+m\,\bar{a}^2\left(Q_{l\,m}\breve{\mathcal{P}}_{l-1\,m}+Q_{l+1\,m}\breve{\mathcal{P}}_{l+1\,m}\right)\,,
\end{aligned}
\tag{6.32}
$$

where $\mathcal{P}_{lm}$, $\bar{\mathcal{P}}_{lm}$, $\hat{\mathcal{P}}_{lm}$, $\bar{\bar{\mathcal{P}}}_{l\,m}$, $\tilde{\mathcal{P}}_{l\,m}$, $\breve{\mathcal{P}}_{l\,m}$, $\check{\mathcal{P}}_{l\,m}$, ($\mathcal{A}_{lm}$, $\bar{\mathcal{A}}_{lm}$, $\hat{\mathcal{A}}_{lm}$, $\bar{\bar{\mathcal{A}}}_{l\,m}$, $\tilde{\mathcal{A}}_{l\,m}$, $\breve{\mathcal{A}}_{l\,m}$, $\check{\mathcal{A}}_{l\,m}$) are, as in the previous case, combinations of the polar perturbation functions H_0^{lm}, H_1^{lm}, H_2^{lm}, K^{lm}, Φ^{lm} (of the axial perturbation functions h_0^{lm}, h_1^{lm}). We remark again that the expressions $\mathcal{P}_{lm}, \mathcal{A}_{lm}$, etc. do not depend explicitly on the harmonic index m.

We see that at the second order in the spin, perturbations with harmonic index l are coupled to perturbations with the same parity and harmonic indices $l \pm 2$, and (when $m \neq 0$) to perturbations with opposite parity and harmonic indices $l \pm 1$ [159, 278, 285].

6.2 Quasinormal Mode Spectrum

The QNMs, i.e. the characteristic oscillation modes of BHs or other compact objects when excited by non-radial perturbations, can be found, as explored in the previous chapters, by solving the perturbation equations with outgoing waves boundary conditions at infinity and ingoing waves at the horizon (see e.g. Sec. 2.5). At the horizon and at infinity, the scalar ($\Phi^{lm}(r)$) and gravitational ($H_1^{lm}(r)/r$, $K^{lm}(r)$, etc.) perturbation functions behave as

$$\begin{aligned} &A^{lm}_{\rm in} e^{-ik_H r_*} + A^{lm}_{\rm out} e^{ik_H r_*} \qquad (r \to r_H) \\ &A^{lm}_{\rm in} e^{-i\omega r_*} + A^{lm}_{\rm out} e^{i\omega r_*} \qquad (r \to \infty)\,, \end{aligned} \tag{6.33}$$

where r_* is a properly defined tortoise coordinate for the background spacetime $g^{(0)}_{\mu\nu}$ (see App. E), and

$$k_H = \omega - m\Omega_H \quad \text{with} \quad \Omega_H = -\lim_{r\to r_H} \frac{g_{t\varphi}}{g_{\varphi\varphi}}\,. \tag{6.34}$$

Explicitly,

$$\begin{aligned} k_H =& \omega - \bar{a}\frac{m}{r_H}\left[\frac{1}{2} + \zeta^2\frac{7}{512} + \zeta^3\frac{1664323}{212889600} + \zeta^4\frac{9739215491}{1549836288000} + \zeta^5\frac{12749793916691}{2293076459529000}\right. \\ &\left. + \zeta^6\frac{1223834433730571723849}{230905828521227059200000}\right] + \mathcal{O}\left(\zeta^7\right)\,. \end{aligned} \tag{6.35}$$

At the horizon and at infinity the perturbation equations can be written as two second-order differential equations with the following asymptotic structure (with Z^{lm} being either Φ^{lm} or K^{lm}, for example)

$$\begin{aligned} &Z^{lm}_{,r_*r_*} + k_H^2 Z^{lm} = \mathcal{O}(r - r_H) \qquad (r \to r_H) \\ &Z^{lm}_{,r_*r_*} + \omega^2 Z^{lm} = \mathcal{O}\left(\frac{1}{r^2}\right) \qquad (r \to \infty)\,, \end{aligned} \tag{6.36}$$

with the Sommerfeld boundary conditions

$$\begin{aligned} &Z^{lm} \sim e^{-ik_H r_*} \qquad \text{at} \quad (r \to r_H) \\ &Z^{lm} \sim e^{i\omega r_*} \qquad \text{at} \quad (r \to \infty)\,. \end{aligned} \tag{6.37}$$

that are satisfied by the discrete and infinite set of QNMs.

As already described in Sec. 2.6.3, both the equations (6.31)-(6.32), which include the first order case of Eqs. (6.24)-(6.25), and the boundary conditions for QNMs (6.37) are invariant under the transformation $(\bar{a}, m) \to (-\bar{a}, -m)$ (note that $\Omega_{\rm H} \propto \bar{a}$), as long as axial perturbations change sign and polar perturbations remain the same. Therefore, the solution and the frequencies of the quasi-normal modes are invariant under this transformation as well. This implies that the $\mathcal{O}(\bar{a})$

corrections in the spin are odd in m, while the second-order corrections are even. Since the equations are at most quadratic in m, we shall make the following ansatz, verified a posteriori, for the QNM spectrum in the slow rotation limit

$$\omega(\bar{a},\zeta) = \omega_0(\zeta) + \bar{a}\, m\omega_1(\zeta) + \bar{a}^2 \left[\omega_{2a}(\zeta) + m^2\omega_{2b}(\zeta)\right] + \mathcal{O}(\bar{a}^3)\,, \tag{6.38}$$

where ω_r ($r = 0, 1, 2a, 2b$) do not depend on m. The nonrotating part of the spectrum, corresponding to ω_0 has already been discussed in Chapter 5.

6.2.1 First-order Corrections: ω_1

The only rotating terms in the perturbation Eqs. (6.25)-(6.24) that can contribute to the spectrum at first order $\omega = \omega_0 + \bar{a}\, m\omega_1$ are the ones proportional to m, namely $\bar{\mathcal{A}}, \bar{\mathcal{P}}$, since the remaining terms do not have the same dependence on the azimuthal number and would contribute to higher orders. This means that, in order to compute the QNM spectrum at first order in the rotation, we can simply consider the reduced set of equations given by

$$\mathcal{A}_{lm} + \bar{a}\, m\, \bar{\mathcal{A}}_{lm} = 0 \tag{6.39}$$

$$\mathcal{P}_{lm} + \bar{a}\, m\, \bar{\mathcal{P}}_{lm} = 0\,. \tag{6.40}$$

Applying these considerations, equations (6.18)-(6.22) become

$$0 = A^{(I)}_{lm} + im\,\bar{a}\, C^{(I)}_{lm} \tag{6.41}$$

$$0 = l(l+1)\alpha^{(J)}_l - im\,\bar{a}\left[\tilde{\beta}^{(J)}_l + \zeta^{(J)}_l - (l-1)(l+2)\xi^{(J)}_l\right] \tag{6.42}$$

$$0 = l(l+1)\beta^{(J)}_l + im\,\bar{a}\left[\tilde{\alpha}^{(J)}_l + \eta^{(J)}_l + (l-1)(l+2)\gamma^{(J)}_l\right] \tag{6.43}$$

$$0 = l(l-1)(l+1)(l+2)s_l - im\,\bar{a}(l-1)(l+2)f_l \tag{6.44}$$

$$0 = l(l-1)(l+1)(l+2)t_l + im\,\bar{a}(l-1)(l+2)g_l \quad , \tag{6.45}$$

with $I = 0, 1, 2, 3, 4$ and $J = 0, 1$. This set of equations can be separated according to the parity of the perturbation functions involved, so we shall have a *polar set*, corresponding to Eq. (6.40), given by Eqs. (6.41),(6.42),(6.44), and an *axial set*, corresponding to (6.39), given by Eqs. (6.43), (6.45). Being the two sets completely separated, we can focus on the polar sector (as we did for the static case), which includes the coupling of the dilaton field with the curvature and is described by the perturbation functions K, H_0, H_1, H_2, Φ.

Manipulating the perturbation equations, we can find H_0 and H_2 as algebraic expressions in terms of H_1 and K, thus reducing the number of degrees of freedom involved. Defining the vector quantity

$$\mathbf{\Psi}_{lm} \equiv \begin{pmatrix} H_{1\,lm} \\ K_{lm} \\ \Phi_{lm} \\ \Phi'_{lm} \end{pmatrix} \tag{6.46}$$

we can cast our equations as a set of first-order ODEs in the form

$$\frac{d}{dr}\mathbf{\Psi}_{lm} + \hat{V}_{lm}\mathbf{\Psi}_{lm} + \bar{a}\ m\ \hat{U}_{lm}\mathbf{\Psi}_{lm} = \mathbf{0}\,. \tag{6.47}$$

with $\hat{V}, \hat{U}$ two four-dimensional matrices. Using an appropriate definition of the tortoise coordinate r_* (see Appendix E), the perturbation functions behave at the horizon and an infinity as in Eq. (6.33); however, if ω is a QNM, then it will satisfy purely ingoing boundary conditions at the horizon ($\sim e^{-ik_H r_*}$) with k_H given in Eq. (6.34), and purely outgoing boundary conditions at infinity ($\sim e^{i\omega r_*}$).

We define a square matrix $\hat{X}$ with the same dimension as $\hat{V}, \hat{U}$ and whose columns are two independent solutions satisfying the QNM boundary conditions at the horizon (superscript $^{(H)}$), and two independent solutions satisfying the boundary conditions at infinity (superscript $^{(\infty)}$):

$$\hat{X} = \begin{pmatrix} H_{1a}^{(H)} & H_{1b}^{(H)} & H_{1a}^{(\infty)} & H_{1b}^{(\infty)} \\ K_{a}^{(H)} & K_{b}^{(H)} & K_{a}^{(\infty)} & K_{b}^{(\infty)} \\ \Phi_{a}^{(H)} & \Phi_{b}^{(H)} & \Phi_{a}^{(\infty)} & \Phi_{b}^{(\infty)} \\ \Phi'^{(H)}_{a} & \Phi'^{(H)}_{b} & \Phi'^{(\infty)}_{a} & \Phi'^{(\infty)}_{b} \end{pmatrix} \tag{6.48}$$

in which we omitted the indices lm. The QNMs ω^{nlm} are found by imposing the condition

$$\det\hat{X}(\omega^{nlm}) = 0 \tag{6.49}$$

at a matching point $r = r_m$. Our first goal in to determine the rotational corrections $\omega_1^{nl}(\zeta) = \omega_{1\,R}^{nl}(\zeta) + i\,\omega_{1\,I}^{nl}(\zeta)$ in the spectrum

$$\omega^{nlm}(\bar{a}, \zeta) = \omega_0^{nl}(\zeta) + \bar{a}\,m\,\omega_1^{nl}(\zeta) + \mathcal{O}(\bar{a}^2) \tag{6.50}$$

by studying the $\bar{a} \to 0$ limit of the QNMs. Explicitly, we look at

$$m\,\omega_{1\,R,I}^{nl}(\zeta) = \lim_{\bar{a}\to 0} \frac{\omega_{R,I}^{nlm}(\bar{a}, \zeta) - \omega_{0\,R,I}^{nl}(\zeta)}{\bar{a}}\,. \tag{6.51}$$

In practice, from the condition (6.49) we find the modes $\omega(0, \zeta)$ and$\omega(\bar{a}, \zeta)$ for small values of $\bar{a}$ and for different values of $\zeta \lesssim 0.4$, so that we can extrapolate the limit of the ratio in (6.51) and find analytical fits in ζ.

As discussed Sec. 5.3.2, in modified gravity theories with a scalar field coupled to the metric perturbations two classes of gravitational QNMs exist [3, 330]: the *gravitational-led* modes and the *scalar-led* modes, whose frequencies tend, in the $\zeta \to 0$ limit, to those of gravitational and scalar QNMs in GR, respectively. In a realistic physical scenario, only the gravitational-led modes are expected to be excited significantly and thus be relevant for gravitational spectroscopy (see e.g. Refs. [3, 109], where this was demonstrated by studying the excitation of both the gravitational-led and scalar-led modes following a radial plunge of point particles). Therefore, we shall only study this class of modes.

For gravitational-led modes we recover, for $\zeta \to 0$, the values of ω_1^{nl} corresponding to the rotational corrections of QNMs in Kerr spacetime, e.g. $\omega_{1\,R}^{02}(\zeta = 0) = 0.0629$, $\omega_{1\,I}^{02}(\zeta = 0) = 0.00099$

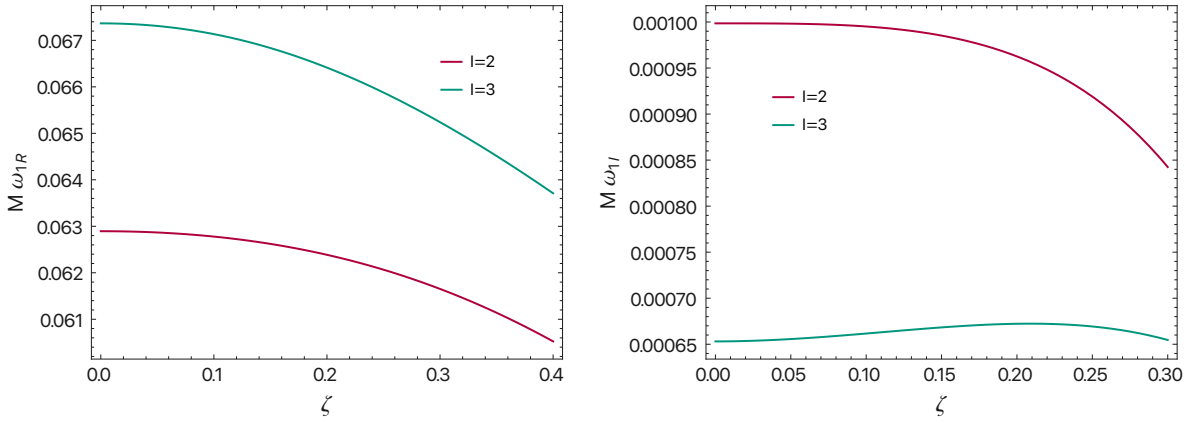

Figure 6.1: *Real (left panel) and imaginary (right panel) parts of the first-order correction $\omega_1(\zeta)$ to the QNM spectrum for $l = 2, l = 3$*

[279, 289].

In Fig. 6.1 we show the real and imaginary parts of ω_1 for the fundamental ($n = 0$) modes with $l = 2, 3$, as functions of the dimensionless coupling parameter [1] ζ.

The analytical fits for $\omega_1^{02}, \omega_1^{03}$, together with the second-order results, are presented in the results section 6.2.5. We provide further details on the numerical integration in Sec. 6.2.4.

6.2.2 Second-order Corrections: ω_{2a}, ω_{2b}

Now we proceed to the computation of QNMs at second order in the spin and apply the same considerations of Sec. 2.6.3 to the EdGB case. We have found that the field equations (3.7), (3.8), linearized in the perturbations and to second order in the spin, yield the system of ordinary differential equations (6.26)-(6.30), with the general structure (6.31), (6.32). We have seen that the equations couple perturbations with different parity, and with different values of the harmonic index l.

As discussed in the previous section, the couplings of the perturbations with index l to those with index $l \pm 1$ can be neglected in the computation of the QNM spectrum to first order in the spin. Similarly, we will show that we can neglect the couplings between perturbations with index l and with index $l \pm 2$ in the computation of the QNMs to second order in the spin.

Expanding any generic polar perturbation P_{lm} ($= H_0^{lm}$, H_1^{lm}, ...) and any generic axial perturbation A_{lm} ($= h_0^{lm}$, h_1^{lm}) to second order in the spin as

$$P_{lm} = P_{lm}^{(0)} + \bar{a}\, P_{lm}^{(1)} + \bar{a}^2\, P_{lm}^{(2)} \tag{6.52}$$

$$A_{lm} = A_{lm}^{(0)} + \bar{a}\, A_{lm}^{(1)} + \bar{a}^2\, A_{lm}^{(2)}\,, \tag{6.53}$$

and assuming that the source of the perturbations excites only a given *polar* l mode, we shall have,

[1] Our numerical integration has convergence issues for $\omega_{1\,R}$ at $\zeta \gtrsim 0.4$ (where the sixth order expansion ζ is no longer enough [3]), and for $\omega_{1\,I}$ at $\zeta \gtrsim 0.3$, due to the smaller values of $\omega_{1\,I}$ (which can be two orders of magnitude smaller than the real part). Therefore, in Fig. 6.1 we show the real part of the rotational correction for $\zeta \in [0, 0.4]$, and the imaginary part for $\zeta \in [0, 0.3]$.

using the arguments of Sec. 2.6.3,

$$A^{(0)}_{lm} = A^{(0)}_{l'm} = P^{(0)}_{l'm} = 0\,, \tag{6.54}$$

where $l' \neq l$, so that the only perturbations present at this order are $P^{(0)}_{lm}$. Axial parity perturbations with index $l \pm 1$ are excited at first order in the spin

$$A_{l\pm1m} = \bar{a} A^{(1)}_{l\pm1m} + \bar{a}^2 A^{(2)}_{l\pm1m}\,, \tag{6.55}$$

while polar parity perturbations with index $l \pm 2$ are excited only at second order in the spin

$$P_{l\pm2m} = \bar{a}^2 P^{(2)}_{l\pm2m}\,. \tag{6.56}$$

Putting all the information together and focusing on the *polar-led* sector, i.e. the one in which only polar perturbations are non-vanishing in the nonrotating limit, neglecting $\mathcal{O}(\bar{a}^3)$ terms, Eqs. (6.31), (6.32) reduce to

$$\begin{aligned}
&\mathcal{P}_{l\,m} + \bar{a}\,m\,\bar{\mathcal{P}}_{l\,m} + \bar{a}^2\hat{\mathcal{P}}_{l\,m} + \, m^2\,\bar{a}^2\bar{\bar{\mathcal{P}}}_{l\,m} + \bar{a}\left(Q_{l\,m}\tilde{\mathcal{A}}_{l-1\,m} + Q_{l+1\,m}\tilde{\mathcal{A}}_{l+1\,m}\right) = 0\\
&\mathcal{A}_{l+1\,m} + \bar{a}\,m\,\bar{\mathcal{A}}_{l+1\,m} + \bar{a}\,Q_{l+1\,m}\tilde{\mathcal{P}}_{l\,m} + m\,\bar{a}^2\,Q_{l+1\,m}\check{\mathcal{P}}_{l\,m} = 0\\
&\mathcal{A}_{l-1\,m} + \bar{a}\,m\,\bar{\mathcal{A}}_{l-1\,m} + \bar{a}\,Q_{l\,m}\tilde{\mathcal{P}}_{l\,m} + m\,\bar{a}^2\,Q_{l\,m}\check{\mathcal{P}}_{l\,m} = 0\,.
\end{aligned} \tag{6.57}$$

Analogously, one can find a set of equations belonging to the *axial-led sector*, which are sourced by an axial perturbation with a given l (see Sec.2.6.3 for the explicit expression). As in Chapter 5, we shall not consider axial-led perturbations, since in the nonrotating case axial QNMs are closer to GR than the polar ones [3], and we expect this general trend to remain in presence of rotation.

While not all of the solutions of the full Eqs. (6.31), (6.32) might be included in the polar- and axial-led classes of QNMs, any solution of the system (6.57) that satisfies the QNMs boundary conditions is also a solution to the original set of equations and belongs to the eigenspectrum up to second order in the spin [278].

Applying the structure of Eq. (6.57) to the equations (6.26)-(6.30), we can write the polar-led sector of perturbation equations as

$$\begin{aligned}
&A^{(I)}_{lm} + \bar{a}^2 A^{(I)}_{2,lm} + \bar{a}^2\hat{A}^{(I)}_{lm}\left[Q^2_{lm} + Q^2_{l+1\,m}\right] + \bar{a}^2\tilde{B}^{(I)}_{lm}\left[lQ^2_{l+1\,m} - (l+1)Q^2_{lm}\right] + i\;\bar{a}\;mC^{(I)}_{lm} + \bar{a}^2m^2E^{(I)}_{lm}\\
&\quad + Q_{lm}\bar{a}\left[\tilde{A}^{(I)}_{l-1\,m} + (l-1)B^{(I)}_{l-1\,m}\right] + Q_{l+1\,m}\bar{a}\left[\tilde{A}^{(I)}_{l+1\,m} - (l+2)B^{(I)}_{l+1\,m}\right] = 0\,,
\end{aligned} \tag{6.58}$$

$$\begin{aligned}
&l(l+1)\alpha^{(J)}_{lm} + l(l+1)\bar{a}^2\alpha^{(J)}_{2,lm} - im\;\bar{a}\left[\tilde{\beta}^{(J)}_{lm} + \zeta^{(J)}_{lm} - (l-1)(l+2)\xi^{(J)}_{lm}\right]\\
&\quad + \bar{a}^2\left[(l+1)(l-2)Q^2_{lm} + l(l+3)Q^2_{l+1\,m}\right]\hat{\alpha}^{(J)}_{lm}\\
&\quad + m^2\bar{a}^2\Delta^{(J)}_{lm} + \bar{a}^2\left[lQ^2_{l+1\,m} - (l+1)Q^2_{lm}\right]\tilde{\eta}^{(J)}_{lm}\\
&\quad + \bar{a}^2\left[2m^2 + Q^2_{lm}(l+1)(l^2-l+4) - Q^2_{l+1\,m}l(l^2+3l+6)\right]\tilde{\gamma}^{(J)}_{l}\\
&\quad + \bar{a}Q_{lm}(l+1)\Big\{(l-1)\tilde{\alpha}^{(J)}_{l-1\,m} - \eta^{(J)}_{l-1\,m} + (l-2)(l-1)\gamma^{(J)}_{l-1\,m}\Big\}\\
&\quad + \bar{a}Q_{l+1\,m}l\Big\{(l+2)\tilde{\alpha}^{(J)}_{l+1\,m} + \eta^{(J)}_{l+1\,m} - (l+2)(l+3)\gamma^{(J)}_{l+1\,m}\Big\} = 0\,,
\end{aligned} \tag{6.59}$$

$$
\begin{aligned}
&(l+1)(l+2)\beta^{(J)}_{l+1\,m} + im\ \bar{a}\left[\tilde{\alpha}^{(J)}_{l+1\,m} + \eta^{(J)}_{l+1\,m} + l(l+3)\gamma^{(J)}_{l+1\,m}\right] \\
&\quad + \bar{a}Q_{l+1\,m}(l+2)\Big\{l\tilde{\beta}^{(J)}_{lm} - \zeta^{(J)}_{lm} - (l-1)l\xi^{(J)}_{lm}\Big\} \\
&\quad + im\ \bar{a}^2 Q_{l+1\,m}\left[2\hat{\alpha}^{(J)}_{lm} - (l+2)\Delta^{(J)}_{lm} + \tilde{\eta}^{(J)}_{lm} + (l-1)(l+4)\tilde{\gamma}^{(J)}_{lm}\right] = 0\,,
\end{aligned}
\tag{6.60}
$$

$$
\begin{aligned}
&l(l-1)\beta^{(J)}_{l-1\,m} + im\ \bar{a}\left[\tilde{\alpha}^{(J)}_{l-1\,m} + \eta^{(J)}_{l-1\,m} + (l-2)(l+1)\gamma^{(J)}_{l-1\,m}\right] \\
&\quad + \bar{a}Q_{lm}(l-1)\Big\{(l+1)\tilde{\beta}^{(J)}_{lm} + \zeta^{(J)}_{lm} + (l+1)(l+2)\xi^{(J)}_{lm}\Big\} \\
&\quad + im\ \bar{a}^2 Q_{lm}\left[2\hat{\alpha}^{(J)}_{lm} + (l-1)\Delta^{(J)}_{lm} + \tilde{\eta}^{(J)}_{lm} + (l-3)(l+2)\tilde{\gamma}^{(J)}_{lm}\right] = 0\,,
\end{aligned}
\tag{6.61}
$$

$$
\begin{aligned}
&l(l-1)(l+1)(l+2)(s_{lm} + \bar{a}^2 s_{2,lm}) - im\ \bar{a}(l-1)(l+2)f_{lm} + \bar{a}^2\Big[2m^2 + Q^2_{lm}(l+1)(l^2-l+4) \\
&\quad - Q^2_{l+1\,m}l(l^2+3l+6)\Big]\tilde{g}_{lm} + \bar{a}^2\left[2m^2 - l(l+1) + (l+1)(l+2)Q^2_{lm} + l(l-1)Q^2_{l+1\,m}\right]\hat{k}_{lm} \\
&\quad + \bar{a}^2\Big\{8m^2 - 2l(l+1) - Q_{lm}l^2(l+1)\left[4(l-2) - l(l+1)(l+4)\right] - Q^2_{l+1\,m}l\left[4(l+3) - l(l+1)(l-3)\right]\Big\}\hat{s}_{lm} \\
&\quad - Q_{lm}\Big\{\bar{a}(l-1)(l+1)(l+2)g_{l-1\,m}\Big\} + Q_{l+1\,m}\Big\{\bar{a}l(l-1)(l+2)g_{l+1\,m}\Big\} = 0\,,
\end{aligned}
\tag{6.62}
$$

$$
\begin{aligned}
&l(l+1)(l+2)(l+3)t_{l+1\,m} + im\ \bar{a}\ l(l+3)g_{l+1\,m} - \bar{a}\ Q_{l+1\,m}\Big\{l(l+2)(l+3)f_{lm}\Big\} \\
&\quad + im\ \bar{a}^2 Q_{l+1\,m}\left[(l-2)(l+3)\tilde{g}_{lm} - 2(l+3)\hat{k}_{lm} + 4(l-1)(l+3)\hat{s}_{lm}\right] = 0\,,
\end{aligned}
\tag{6.63}
$$

$$
\begin{aligned}
&(l-1)(l-2)l(l+1)t_{l-1\,m} + im\ \bar{a}(l-2)(l+1)g_{l-1\,m} + \bar{a}\ Q_{lm}\Big\{(l-1)(l-2)(l+1)f_{lm}\Big\} \\
&\quad + im\ \bar{a}^2 Q_{lm}\left[(l-2)(l+3)\tilde{g}_{lm} + 2(l-2)\hat{k}_{lm} + 4(l-2)(l+2)\hat{s}_{lm}\right] = 0\,.
\end{aligned}
\tag{6.64}
$$

We remark that since some of the tensor spherical harmonics identically vanish for $l = 0, 1$, it is possible to exploit the residual gauge freedom to set to zero the axial perturbations (see e.g. [3]). Therefore, Eqs. (6.58)-(6.64) are valid for $l \geq 2$ and, in the case $l = 2$ (in which polar perturbations with index l are coupled with axial perturbations with index $l \pm 1$), the axial perturbations with index $l - 1$ can be set to zero [2] .

As in the $\mathcal{O}(\bar{a})$ and $\mathcal{O}(\bar{a}^2)$ cases, with appropriate combinations of the perturbation equations, we can find H_0^{lm} and H_2^{lm} as algebraic expressions in terms of H_1^{lm} and K^{lm}. The difference in the second order in the spin is that we now have to keep the axial perturbation functions, even when

[2] We stress that this is the case when $l = 1$ is excited by a polar $l = 2$ mode, it does not mean that the axial-led $l = 1$ mode is zero in general.

considering the polar-led sector. Defining

$$\mathbf{\Psi}_{lm} \equiv \begin{pmatrix} H_{1,lm} \\ K_{lm} \\ \Phi_{lm} \\ \Phi'_{lm} \\ h_{0,l+1\,m} \\ h_{1,l+1\,m} \\ h_{0,l-1\,m} \\ h_{1,l-1\,m} \end{pmatrix} \tag{6.65}$$

we can cast our equations (for given values of l, m) in the form

$$\frac{d}{dr}\mathbf{\Psi}_{lm} + \hat{P}_{lm}\mathbf{\Psi}_{lm} = 0\,, \tag{6.66}$$

where $\hat{P}_{lm} = \hat{P}^{(0)}_{lm} + \bar{a}\hat{P}^{(1)}_{lm} + \bar{a}^2\hat{P}^{(2)}_{lm}$ is now an eight-dimensional square matrix. In the $l = 2$ case, since axial perturbations with $l = 1$ can be set to zero, we shall have a different dimensionality of the problem, as $\mathbf{\Psi}_{2m} \equiv \{H_{1,2m}, K_{2m}, \Phi_{2m}, \Phi'_{2m}, h_{0,3\,m}, h_{1,3\,m}\}$ and the matrix $\hat{P}_{lm}$ is six-dimensional.

To find the complex QNM frequencies, we define the eight-dimensional (six-dimensional for $l = 2$) square matrix $\hat{X}$ whose columns are four (three) independent solutions satisfying the QNM boundary conditions at the horizon (superscript $^{(H)}$), and four (three) independent solutions satisfying the boundary conditions at infinity (superscript $^{(\infty)}$), evaluated at a matching point r_m. For $l = 2$, we can write

$$\hat{X} = \begin{pmatrix} \mathbf{\Psi}^{(H)}_{1a} & \mathbf{\Psi}^{(H)}_{1b} & \mathbf{\Psi}^{(H)}_{1c} & \mathbf{\Psi}^{(\infty)}_{1a} & \mathbf{\Psi}^{(\infty)}_{1b} & \mathbf{\Psi}^{(\infty)}_{1c} \end{pmatrix}. \tag{6.67}$$

When ω is a QNM, we have

$$\det\hat{X}(\omega^{nlm}) = 0\,. \tag{6.68}$$

Similarly to the definition given in Sec.5.3.2 for the nonrotating case, also the polar-led QNMs of rotating dilatonic black holes will be divided in *gravitational-led* modes (which reduce to the QNMs of a slowly rotating Kerr BH when $\zeta = 0$) and *scalar-led* modes (which reduce to the QNMs of a scalar field in a slowly rotating Kerr BH when $\zeta = 0$); as usual, we will only focus on the former class.

Once the perturbation equations have been integrated to build $\hat{X}$ and the QNM ω^{nlm} up to the second order in the spin has been found from the root of Eq.(6.68) for different values of $(\zeta, \bar{a})$, we can isolate the contributions at each order $\omega_1, \omega_{2a}, \omega_{2b}$ in Eq. (6.38). In particular, computing ω_1 from Eq. (6.51), we can compute the total contribution at second order $\omega_2^{nlm} \equiv \left[\omega^{nl}_{2a}(\zeta) + m^2\omega^{nl}_{2b}(\zeta)\right]$ from

$$\omega_2^{nlm}(\zeta) = \lim_{\bar{a}\to 0} \frac{\omega^{nlm}(\zeta,\bar{a}) - \omega^{nl}_0(\zeta) - \bar{a}m\,\omega^{nl}_1(\zeta)}{\bar{a}^2}\,. \tag{6.69}$$

The numerical implementation of this limit would consist in calculating this ratio for smaller and smaller values of $\bar{a}$, until the result does not depend on the spin (within the accuracy). However, we have found this estimation method not to be the most robust for two main reasons: firstly, it relies on a previous estimation of ω_1 (which is inevitably affected by some error), thus ω_2 cannot be

computed directly from the data in a single operation; secondly, when the values of $\bar{a}$ are extremely small, i.e. the region we are most interested in, the ratio in Eq. (6.69) might diverge since we are considering discrete points and we are limited in the numerical precision. For these reasons, to compute ω_2, it was easier to work with continuous functions, obtained by interpolating the discrete differences between the data points of ω^{nlm} and then taking the first derivative with respect to the spin (corresponding to taking the second derivative of the original data).

After having computed the second-order term ω_2^{nlm} in the quasinormal mode spectrum, we can find the m-independent quantities $\omega_{2a}^{nl}, \omega_{2b}^{nl}$ considering the QNMs for different values of m. Namely, if we use for example the modes with $m \geq 0$, we find, for $l = 2$,

$$\omega_{2a}^{n2} = \omega_2^{n20} = \frac{4\omega_2^{n21} - \omega_2^{n22}}{3} \tag{6.70}$$

$$\omega_{2b}^{n2} = \omega_2^{n21} - \omega_2^{n20} = \frac{\omega_2^{n22} - \omega_2^{n20}}{4} = \frac{\omega_2^{n22} - \omega_2^{n21}}{3}\,, \tag{6.71}$$

while for $l = 3$,

$$\omega_{2a}^{n3} = \omega_2^{n30} = \frac{4\omega_2^{n31} - \omega_2^{n32}}{3} = \frac{9\omega_2^{n31} - \omega_2^{n33}}{8} = \frac{9\omega_2^{n32} - 4\omega_2^{n33}}{5} \tag{6.72}$$

$$\omega_{2b}^{n3} = \omega_2^{n31} - \omega_2^{n30} = \frac{\omega_2^{n32} - \omega_2^{n30}}{4} = \frac{\omega_2^{n32} - \omega_2^{n31}}{3} = \frac{\omega_2^{n33} - \omega_2^{n31}}{8} = \frac{\omega_2^{n33} - \omega_2^{n32}}{5} = \frac{\omega_2^{n33} - \omega_2^{n30}}{9}\,. \tag{6.73}$$

Padé Resummation

As already explained in the previous sections, the QNM frequencies at second order in the spin (see Eq. (6.38)) can be written as the Taylor expansion

$$\omega^{nlm}(\bar{a}, \zeta) = \omega_0^{nl}(\zeta) + \bar{a}\, m\omega_1^{nl}(\zeta) + \bar{a}^2 \left[\omega_{2a}^{nl}(\zeta) + m^2\omega_{2b}^{nl}(\zeta)\right] + \mathcal{O}(\bar{a}^3)\,, \tag{6.74}$$

where $\omega_0^{nl}(\zeta)$ is the QNM frequency in the static case. Resumming this expression using *Padé approximants*, we can improve the convergence of the QNM spin expansion, as we verified in GR (see Sec. 2.6.3).

We apply the resummation procedure discussed for GR to the second-order expansion of the EdGB QNM spectrum (6.38). Up to this order, the two choices of Padé approximants are

$$P[1,1](\bar{a}, \zeta) = \frac{m\,\omega_0^{nl}(\zeta)\omega_1^{nl}(\zeta) + \left[m^2\,{\omega_1^{nl}}^2(\zeta) - \omega_0^{nl}(\zeta)\omega_2^{nlm}(\zeta)\right]\bar{a}}{m\,\omega_1^{nl}(\zeta) - \omega_2^{nlm}(\zeta)\bar{a}} \tag{6.75}$$

and

$$P[0,2](\bar{a}, \zeta) = \frac{{\omega_0^{nl}}^3(\zeta)}{{\omega_0^{nl}}^2(\zeta) + \bar{a}^2 m^2 {\omega_1^{nl}}^2(\zeta) - \bar{a}\omega_0^{nl}(\zeta)\left[m\omega_1^{nl}(\zeta) + \bar{a}\omega_2^{nlm}(\zeta)\right]}\,, \tag{6.76}$$

where $\omega_2^{nlm} = \omega_{2a}^{nl} + m^2\omega_{2b}^{nl}$. For the QNMs with $n = 0$, $l = 2, 3$ we shall use $P[1,1]$; for $m = 0$, for which Eq. (6.75) reduces to a constant, and for the imaginary parts of the modes with $m = \pm 1$, for which $P[1,1]$ has a pole close to the considered spin interval, we shall use $P[0,2]$.

As we discuss below, our analysis in GR (see Sec. 2.6.3) provides an indication that, by employing

the Padé resummation, the error due to truncating the spin expansion at second order is limited, leading to an accurate estimate of the QNMs for BH spins as large as $\bar{a} \sim 0.7$.

6.2.3 Boundary Conditions

The numerical implementation of the boundary conditions is analogous to the one for the static case discussed in Chapter 5, except for the introduction of the spin and of the axial perturbation functions, which now may contribute to the polar-led class of QNNs.

Calling $N_{\bar{a}}$ the order of the spin considered (either 1 ord 2 in this chapter), when $N_{\bar{a}} = 2$, we have to include the axial perturbation functions h_0, h_1, which is not needed when $N_{\bar{a}} = 1$, as the couplings with these functions do not contribute to the QNM spectrum at this order (see Sec. 6.2.1). Furthermore, we will have an additional set of expansion coefficients at the boundaries for each order in the spin considered.

Explicitly, at the numerical horizon $r = R_H \sim r_H$ we will have

$$K_{lm}(\omega, r \sim r_H, \zeta) = e^{-ik_H r_*} \sum_{j=0}^{N_{\bar{a}}} \sum_{i=0}^{N_H} \bar{a}^j k^H_{l,ij}(\omega, \zeta)(r - r_H)^i \tag{6.77}$$

$$H_{1l}(\omega, r \sim r_H, \zeta) = e^{-ik_H r_*} \sum_{j=0}^{N_{\bar{a}}} \sum_{i=0}^{N_H} \bar{a}^j h^H_{1l,ij}(\omega, \zeta)(r - r_H)^{i-1} \tag{6.78}$$

$$\Phi_l(\omega, r \sim r_H, \zeta) = e^{-ik_H r_*} \sum_{j=0}^{N_{\bar{a}}} \sum_{i=0}^{N_H} \bar{a}^j \phi^H_{l,ij}(\omega, \zeta)(r - r_H)^i \tag{6.79}$$

$$\Phi_{lm}{}'(\omega, r \sim r_H, \zeta) = e^{-ik_H r_*} \sum_{j=0}^{N_{\bar{a}}} \sum_{i=0}^{N_H} \bar{a}^j \xi^H_{l,ij}(\omega, \zeta)(r - r_H)^{i-1} \tag{6.80}$$

$$h_{0l}(\omega, r \sim r_H, \zeta) = e^{-ik_H r_*} \sum_{j=0}^{N_{\bar{a}}} \sum_{i=0}^{N_H} \bar{a}^j \eta^H_{0l,ij}(\omega, \zeta)(r - r_H)^i \quad (if\ N_{\bar{a}} > 1) \tag{6.81}$$

$$h_{1l}(\omega, r \sim r_H, \zeta) = e^{-ik_H r_*} \sum_{j=0}^{N_{\bar{a}}} \sum_{i=0}^{N_H} \bar{a}^j \eta^H_{1l,ij}(\omega, \zeta)(r - r_H)^{i-1} \quad (if\ N_{\bar{a}} > 1)\,, \tag{6.82}$$

while at the numerical infinity $r = R_\infty$,

$$K_{lm}(\omega, r \to \infty, \zeta) = e^{i\omega r_*} \sum_{j=0}^{N_{\bar{a}}} \sum_{i=0}^{N_\infty} \bar{a}^j \frac{k^\infty_{l,ij}(\omega, \zeta)}{r^i} \tag{6.83}$$

$$H_{1l}(\omega, r \to \infty, \zeta) = e^{i\omega r_*} \sum_{j=0}^{N_{\bar{a}}} \sum_{i=0}^{N_\infty} \bar{a}^j \frac{h^\infty_{1l,ij}(\omega, \zeta)}{r^{i-1}} \tag{6.84}$$

$$\Phi_{lm}(\omega, r \to \infty, \zeta) = e^{i\omega r_*} \sum_{j=0}^{N_{\bar{a}}} \sum_{i=0}^{N_\infty} \bar{a}^j \frac{\phi^\infty_{l,ij}(\omega, \zeta)}{r^i} \tag{6.85}$$

$$\Phi_{lm}{}'(\omega, r \to \infty, \zeta) = e^{i\omega r_*} \sum_{j=0}^{N_{\bar{a}}} \sum_{i=0}^{N_\infty} \bar{a}^j \frac{\xi^\infty_{l,ij}(\omega, \zeta)}{r^i} \tag{6.86}$$

$$h_{0l}(\omega, r\to\infty,\zeta) = e^{i\omega r_*}\sum_{j=0}^{N_{\bar{a}}}\sum_{i=0}^{N_\infty}\bar{a}^j\frac{\eta^{\infty}_{0l,ij}(\omega,\zeta)}{r^{i-1}} \quad (if\ N_{\bar{a}}>1) \tag{6.87}$$

$$h_{1l}(\omega, r\to\infty,\zeta) = e^{i\omega r_*}\sum_{j=0}^{N_{\bar{a}}}\sum_{i=0}^{N_\infty}\bar{a}^j\frac{\eta^{\infty}_{1l,ij}(\omega,\zeta)}{r^{i-1}} \quad (if\ N_{\bar{a}}>1)\,, \tag{6.88}$$

where, as usual, the asymptotic behavior can be verified a-posteriori from the perturbation equations, once these expansions have been substituted. At the second order in the spin, since we are focusing on the polar-led sector, some of these coefficients, such as $\eta^{H,\infty}_{0l\pm1,i0}, \eta^{H,\infty}_{1l\pm1,i0}$, are zero, as these perturbations are not excited. In the end, when solving the equations order by order in $\bar{a}$, $r-r_H$ and $1/r$, we find that the solutions will be identified only by four constants [3].

6.2.4 Stability and Truncation Error

By performing the numerical integration explained in Sections 6.2.1-6.2.2, with the boundary conditions of Sec. 6.2.3, we find the functions $\omega_r^{nl}(\zeta)$, where $r = 0, 1, 2a, 2b$ (see Eq. (6.74)) for the gravitational-led modes in the polar-led sector. We have computed the fundamental (i.e., $n = 0$) QNMs with $l = 2, 3$. Furthermore, we have verified that computing ω_1 both in the first-order and the second-order frameworks produces the same results, as expected. As already mentioned when discussing the limitation of the direct integration method (see Sec. 2.5), it was not possible to consider $n > 0$ QNMs because, due to the larger values of the imaginary parts, our integration approach is not suited to capture with enough accuracy the overtones [97], and thus extracting the EdGB correction.

Numerical Stability

We now investigate the numerical stability of our results with respect to the integration parameters, as done for the static case in Sec. 5.3.2. We find that, also for the rotating case, the choice of the matching point r_m where $\hat{X}$ is evaluated is less relevant than the other parameters, as the results are completely stable when $R_H < r_m < R_\infty$. For the choice of the expansion orders at the boundaries N_H, N_∞ in Eqs.(6.77)-(6.87), we find, after testing smaller and larger values, that $N_H = 11, N_\infty = 13$ lie in a stable range of values, as greater orders do not affect significantly the results for the fundamental modes.

Finally, the most important parameters to be cautious about are the choice of the numerical horizon $R_H = r_H(1+\epsilon)$, where r_H is the physical horizon in Eq. (3.39) and ϵ is a small deviation parameter, and of the numerical infinity R_∞, with the latter being the most relevant, due to the intrinsic divergence of the integration method at infinity (see Sec. 2.5).

We define the relative difference with respect to a specific choice of numerical infinity $\bar{R}_\infty$ as

$$\delta\omega_{i\,R,I}(R_\infty,\epsilon,\zeta,\bar{R}_\infty) \equiv \frac{|\omega_{i\,R,I}(R_\infty,\epsilon,\zeta)-\omega_{i\,R,I}(\bar{R}_\infty,\epsilon,\zeta)|}{|\omega_{i\,R,I}(\bar{R}_\infty,\epsilon,\zeta)|} \quad (i=1,2)\,. \tag{6.89}$$

In Fig. 6.2 we plot the first-order case $\delta_{1\,R,I}$ for $(nl) = (02)$ and a range of $R_\infty \in [20, 80]M$ and $\epsilon \in$

[3] All the other free constants remaining can be reabsorbed in these four. For example, the leading order constant terms in the $r - r_H$ and $1/r$ expansions at first and second order in the spin ($j = 1, 2$) can be reabsorbed in the non-spinning constant term ($j = 0$).

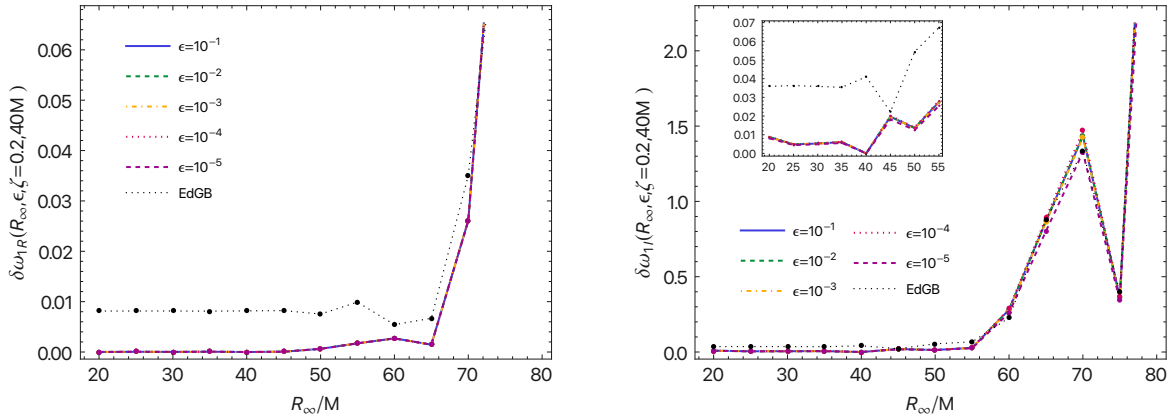

Figure 6.2: *Real (left panel) and imaginary (right panel) parts of the relative difference of* ω_1 *for* $n=0, l=2$*, for different values of* R_∞ *and* ϵ *with respect to* $\bar{R}_\infty = 40M$ *and for a fixed value of* $\zeta = 0.2$

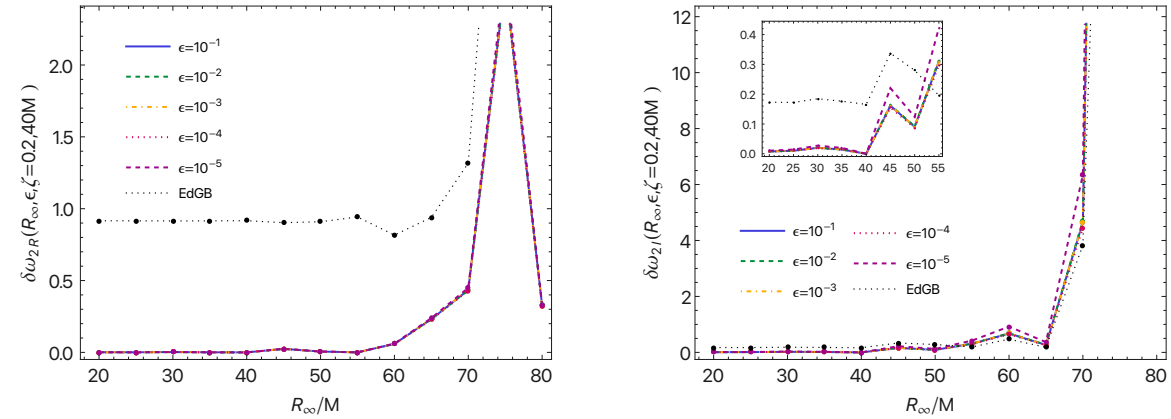

Figure 6.3: *Real (left panel) and imaginary (right panel) parts of the relative difference of* $\omega_2 = \omega_{2a} + m^2\omega_{2b}$ *for* $l = m = 2$*, for different values of* R_∞ *and* ϵ *with respect to* $\bar{R}_\infty = 40M$ *and for a fixed value of* $\zeta = 0.2$

$[10^{-5}, 10^{-1}]$, while in Fig. 6.3 we show the stability of the second-order coefficient $\omega_2 = \omega_{2a} + m^2\omega_{2b}$ for $(nlm) = (022)$. We see that, while the results do not vary much for different values of ϵ, R_∞ plays a crucial role, especially for the imaginary part, since the EdGB correction (represented as a dotted black line in the plots) is smaller in this case. In our code, we fixed $\epsilon = 10^{-2}$ and $R_\infty = 35M$, since the results with these values lie in a stable range – any difference with other options is smaller than the EdGB correction to the QNM.

Expansion in the Spin

Since we do not have the exact QNM spectrum in EdGB gravity to compare our results to, in order to assess the accuracy of the expansion in the spin, we take as a reference the slow-rotation expansion for rotating BHs with $\zeta = 0$ studied in Sec. 2.6.3 (a similar approach has been followed in Ref. [66]). In particular (see Fig. 2.5), for the modes $(nlm) = (022), (033)$, we found that the discrepancy of the first-order Taylor expansion (6.50) with respect to the Kerr QNM is smaller than 1% as long as $\bar{a} \lesssim 0.22$; when we include the second-order correction in Eq. (6.74), the discrepancy is smaller than 1% for $\bar{a} \lesssim 0.4$. Applying the Padé resummation improved the agreement with the Kerr values of the QNMs, which become accurate to $\sim 1\%$ for $\bar{a} \lesssim 0.6$ and to $\sim 2\%$ for $\bar{a} \lesssim 0.7$.

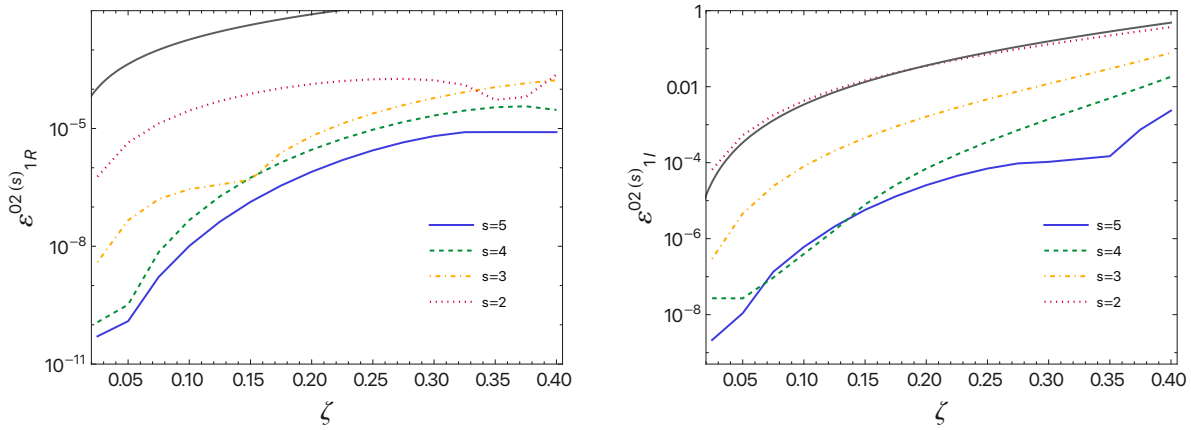

Figure 6.4: *Truncation errors at order $s \leq 5$ for $\omega_1(\zeta)$ for the $(nl) = (02)$ QNM. The real and imaginary parts are shown in the left panels and right panels, respectively. The truncation error is always smaller than the relative correction due to EdGB modifications (solid curves) for $s > 2$.*

These considerations provide an indication that a second-order computation of QNMs may be accurate for $\bar{a} \lesssim 0.4$ ($\bar{a} \lesssim 0.7$ with Padé resummation) for EdGB gravity as well. In the following, then, we shall mostly consider values of the spin in the range $\bar{a} \in [0, 0.7]$.

Expansion in the Coupling Constant

To estimate the accuracy of the expansion in the dimensionless coupling ζ, we have computed the functions $\omega_r^{nl(s)}(\zeta)$ that appear in (6.74), by expanding the background and the perturbation equations up to order s in ζ and up to second order in $\bar{a}$; we have repeated the computation for $s = 2, \ldots, 5$, denoting the functions computed in this way as $\omega_r^{nl(s)}(\zeta)$. We then define the *truncation error* at order s of $\omega_r^{nl}(\zeta)$ as

$$\varepsilon^{nl(s)}_{r\,R,I}(\zeta) = \frac{\left|\omega^{nl(s+1)}_{r\,R,I}(\zeta) - \omega^{(s)}_{r\,R,I}(\zeta)\right|}{\left|\omega^{nl(s)}_{r\,R,I}(\zeta)\right|}\,, \tag{6.90}$$

where $r = 0, 1, 2a, 2b$ and the subscripts R, I refer to the real and imaginary parts of the complex frequencies. The truncation error gives an estimate of the error committed when stopping at order s instead of going to order $s + 1$. Since we considered only up to order $\mathcal{O}(\zeta^6)$, we can compute the truncation error between $s = 5$ and 6, but assessing the error due to stopping the expansion at $s = 6$ would require the computation at $\mathcal{O}(\zeta^7)$. Nevertheless, the truncation error at $s = 5$ provides an upper limit estimate, since we expect $\varepsilon_r^{nl(6)} \lesssim \varepsilon_r^{nl(5)}$. The $r = 0$ case has been discussed in Sec. 5.3.2, here we shall focus on $r = 1, 2a, 2b$. The truncation error of $(nl) = (02)$ for $r = 1$ is plotted in Fig. 6.4, while the $r = 2a, 2b$ cases are presented in Figs. 6.5-6.6.

We see that, for any r, the expansion in ζ is accurate at least within 1% as long as $\zeta \lesssim 0.4$ for the real parts of the modes, and $\zeta \lesssim 0.3$ for the imaginary parts. Thus, to be sure to limit the effect of the truncation in the coupling constant expansion, we shall consider these ranges of ζ. In Figures 6.4-6.6 the relative shift between the functions ω_r^{nl} in GR and in EdGB gravity is also shown as a reference, plotted as a black curve; we can see that the truncation error $\varepsilon_r^{nl(s)}$ at $s = 5$ is always significantly smaller than the EdGB contribution [4].

[4] As seen in the right panel of Fig. 6.4, if we only considered an expansion up to $\mathcal{O}(\zeta^2)$, we would not be able to

We note that, especially for $r = 2a, 2b$, for $\zeta \lesssim 0.1$ the expansion in ζ is in some cases poorly convergent. We think that this is due to the truncation error becoming subleading with respect to the numerical precision of the integration, which becomes significant for small values of the coupling. However, the truncation error is still smaller than the EdGB relative correction to the modes, therefore we think that our approach is reliable even for small values of the coupling constant.

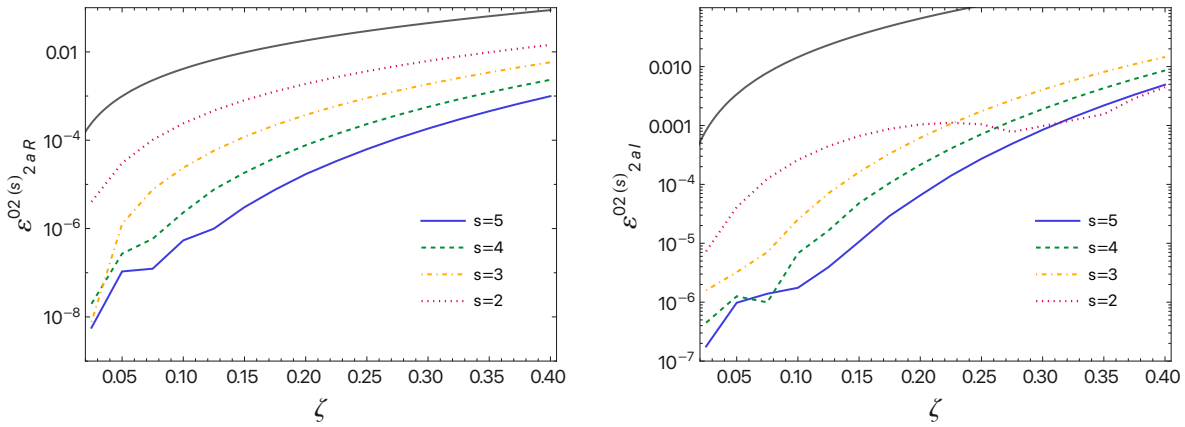

Figure 6.5: *Truncation errors at order $s \leq 5$ for $\omega_{2a}(\zeta)$, for the $(nl) = (02)$ QNM. The real and imaginary parts are shown in the left panels and right panels, respectively. The truncation error is always smaller than the relative correction due to EdGB modifications (solid curves).*

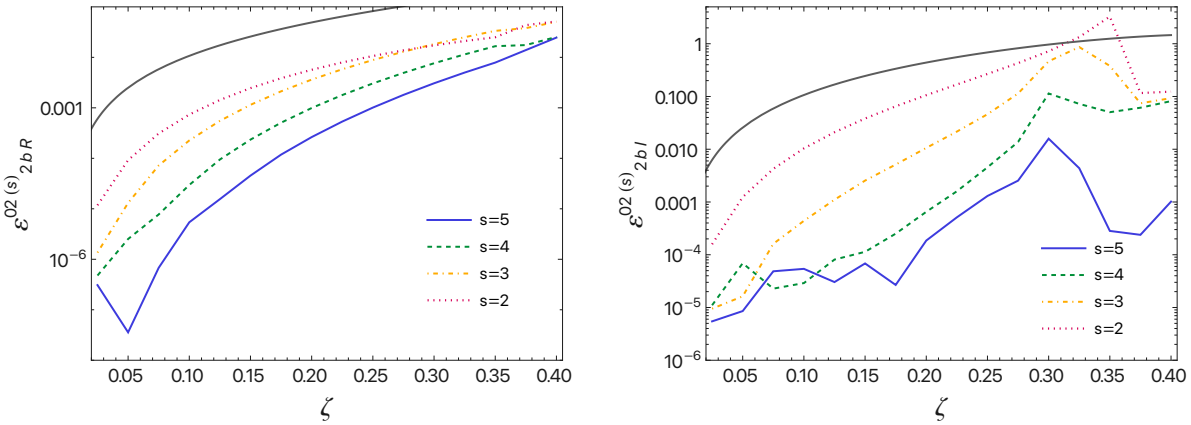

Figure 6.6: *Truncation errors at order $s \leq 5$ for $\omega_{2b}(\zeta)$, for the $(nl) = (02)$ QNM. The real and imaginary parts are shown in the left panels and right panels, respectively. The truncation error is always smaller than the relative correction due to EdGB modifications (solid curves).*

6.2.5 Discussion of the Results

After performing the integration for both the first-order and second-order case, we have fitted the functions $\omega_r^{nl}(\zeta)$ defined in Eq. (6.74) with sixth-order polynomials in ζ (considering $\zeta \in [0.0.4]$ for the real parts, $\zeta \in [0, 0.3]$ for the imaginary parts, as explained in the previous section). The

identify properly the EdGB correction to $\omega_{1,I}$, which is a quite small value to begin with (it goes to zero for larger values of l, as seen using the geometric correspondence in GR).

functional form of the fits is then

$$M\,\omega_r^{nl}(\zeta) = \sum_{i=0}^{6} \zeta^i C_{r\,i}^{nl}\,, \tag{6.91}$$

where the coefficients for the (gravitational-led, polar-led) fundamental modes with $l = 2, 3$ are shown in Tables 6.1-6.4 (for further details on the computation of ω_0^{nl} see Chapter 5). Since for gravitational-led modes the EdGB correction is of $\mathcal{O}(\zeta^2)$, we have set $C_{r\,1}^{nl} = 0$ [3]. As in the other chapters, we have estimated the relative error of the fit (6.91), $\delta_{\rm f}$, as the mean over 100 attempts of the relative difference between the fit, computed from randomly selected 80% of the data points, and the remaining 20% of the data. For $l = 3$ and $r = 2a, 2b$, the functions have been fitted with fourth-order polynomials, because the error $\delta_{\rm f}$ is smaller. The Padé-resummed QNMs with $(nlm) = (022)$, (033) obtained from the second-order spectrum, are shown in Fig. 6.7, as functions of the spin, for different values of ζ. We can see that, while at low values of the spin the EdGB corrections induce an increase (in modulus) in both the real and imaginary parts of the QNMs, when the spin is larger the EdGB effect is to increase the real parts of the modes, while decreasing the imaginary parts.

In order to isolate the modifications to the spectrum induced by the EdGB corrections, it is useful to define the relative differences between the QNMs in EdGB gravity and in GR

$$\Delta\omega_{R,I}^{nlm}(\bar{a},\zeta) = \frac{\omega_{R,I}^{nlm}(\bar{a},\zeta) - \omega_{R,I}^{nlm}(\bar{a},0)}{\omega_{R,I}^{nlm}(\bar{a},0)}\,, \tag{6.92}$$

where R, I refer to the real and imaginary parts, respectively. These quantities are plotted in Fig. 6.8, for different values of ζ, as functions of $\bar{a}$, and in Fig. 6.9 for different values of $\bar{a}$, as functions of ζ. We show the spin expansions at the first and second order (dashed and continuous line respectively), and resummed using Padé approximants (dotted line); in Fig. 6.9 only Padé approximants are presented for clarity.

We can clearly see that the $\mathcal{O}(\bar{a}^2)$ terms enhance the EdGB corrections to the QNMs [5]; moreover, the modifications are further enhanced by the Padé resummation: for $\bar{a} = 0.7$, the (real) frequency of the $l = m = 2$ fundamental mode is shifted of $\sim 0.5\%$ for $\zeta = 0.2$, and of $\sim 2.5\%$ for $\zeta = 0.4$. We also note that the EdGB relative corrections to the imaginary parts change sign for large values of the spins; this explain the overall trend of the EdGB modification discussed above.

From Fig. 6.9 we note that when $\bar{a} \sim 0.7$ and $\zeta \lesssim 0.3$, the contribution of the GR deviations to the QNMs is typically smaller than 2%, which is the error we expect from the slow-rotation expansion (see Fig. 2.5). However, since in Eq. (6.92) we are taking the difference of modes both affected by the slow rotation error, we expect the GR part of the error to cancel away and leave terms of order $\mathcal{O}(\bar{a}\zeta^2)$, which should be smaller than the ones shown in Fig. 2.5. In other words, to minimize the error due to the slow rotation expansion, we can take the (non-perturbed) Kerr modes to compute the GR part of the spectrum ($\mathcal{O}(\zeta^0)$), and add the EdGB corrections ($\mathcal{O}(\zeta^2)$) found here in this work. In this way, the error due to the truncation at the second order in the spin

[5] We remark that this is expected due to symmetry reasons because, by comparison with GR, the first order corrections in the spin only change the $g_{t\phi}$ component of the metric, affecting only the frame-dragging effect, while all the other relevant observational effects (such as in the horizon radius and quadrupole moment) emerge at the second order. However, as it happens in GR, we expect the higher order terms, such as the cubic order, to not be dominant over the quadratic effects.

would only affect the EdGB part of the modes.

Finally, in Fig. 6.10 we show the EdGB relative corrections for the fundamental modes with $l = 2, 3$, for different values of m.

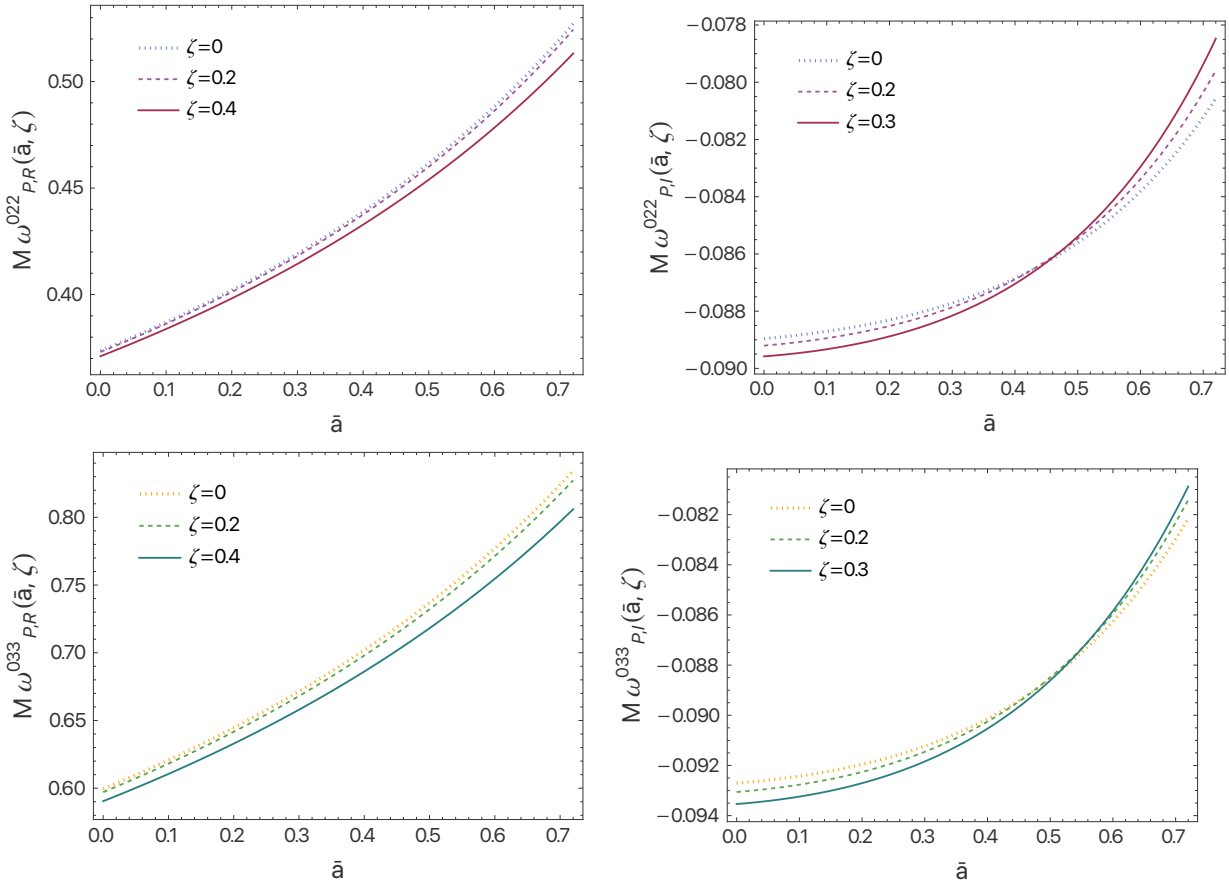

Figure 6.7: *Real (upper panels) and imaginary (lower panels) parts of the* $(nlm) = (022)$ *(left panels) and* $(nlm) = (033)$ *(right panels) QNMs, evaluated using Padé approximants, as functions of the spin, for different values of* ζ.

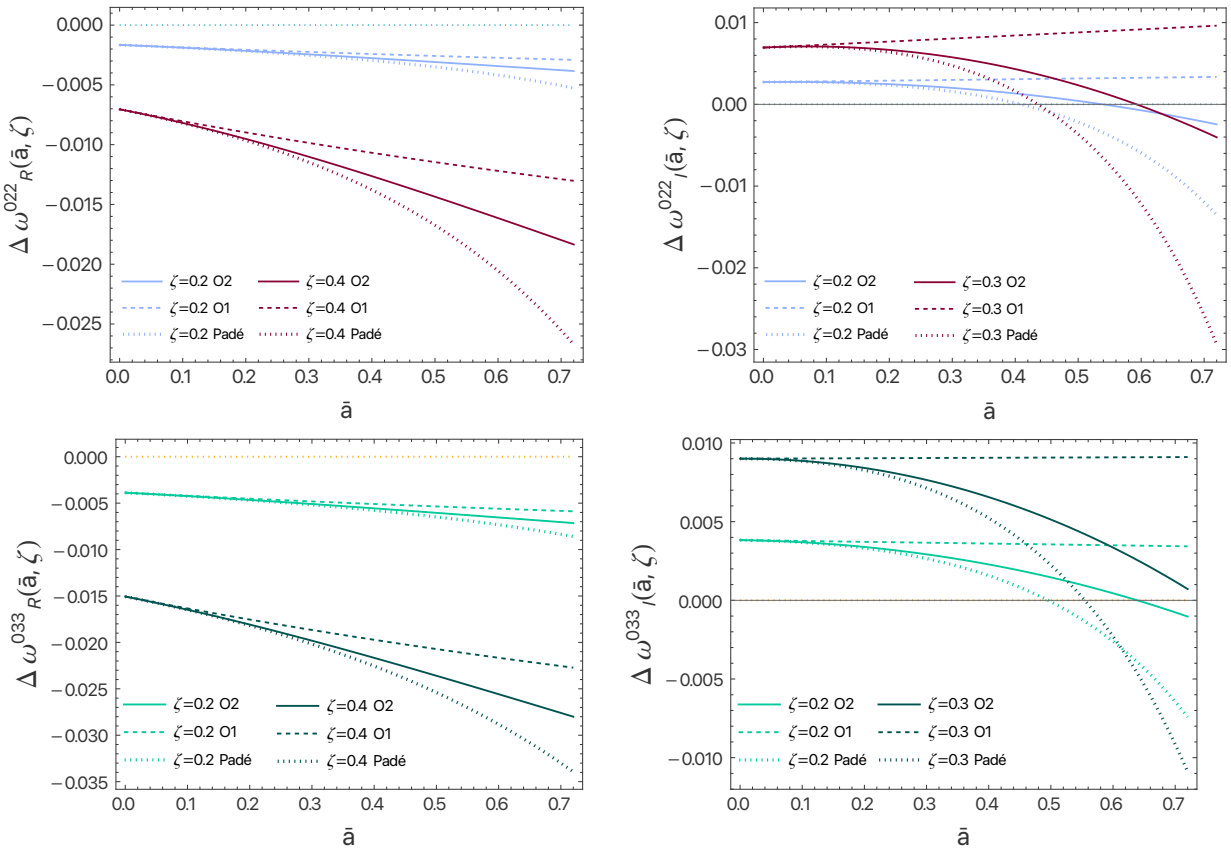

Figure 6.8: *Real (left panels) and imaginary (right panels) parts of the relative difference of EdGB QNMs with respect to GR, as a function of $\bar{a}$. We consider the $(nlm) = (022)$ (upper panels) and $(nlm) = (033)$ (lower panels) QNMs computed up to the first order in the spin, up to second order, and with Padé resummation.*

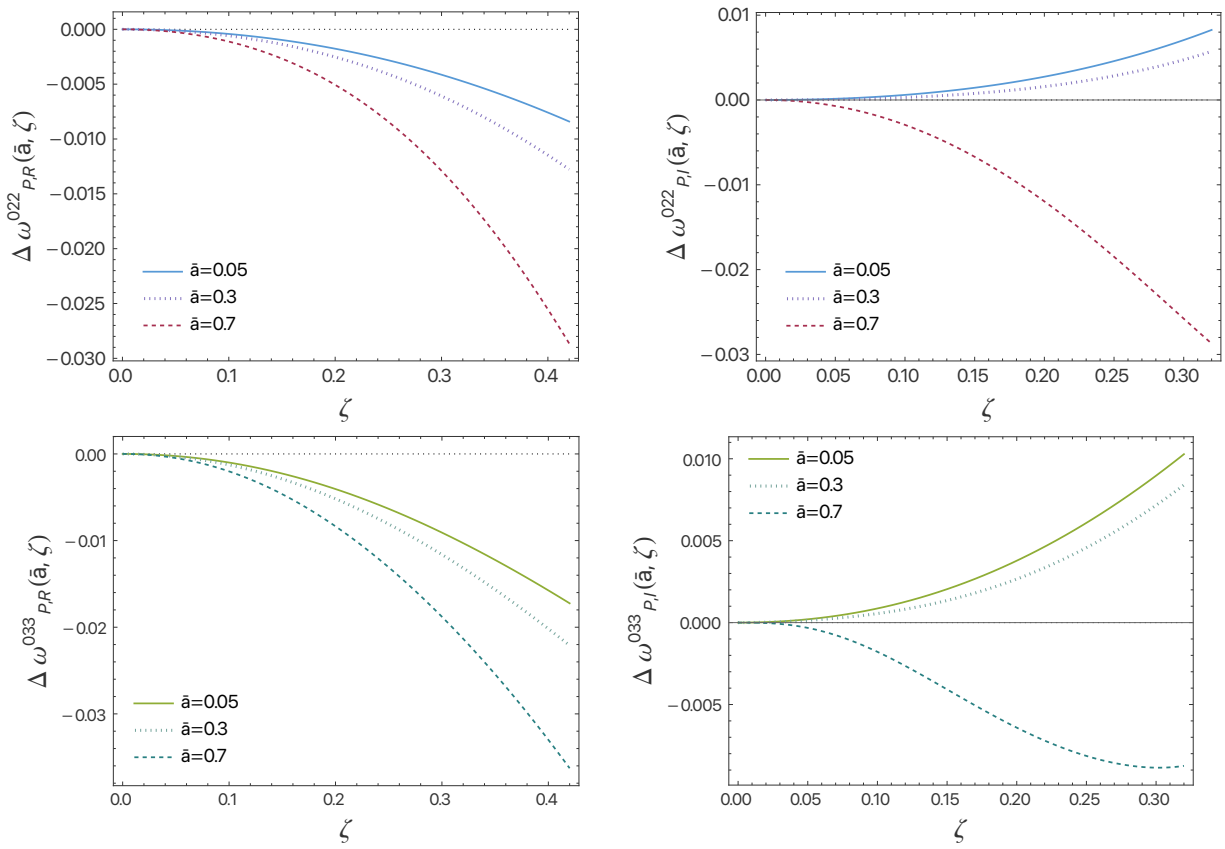

Figure 6.9: *Same as Fig. 6.8, as a function of ζ, with QNMs computed with Padé resummation.*

Table 6.1: *Coefficients of the fit 6.91 of ω_r^{0l} for gravitational-led, polar-led modes, with $r = 0$, $l = 2, 3$, up to $i = 6$. In the last line we show the relative error of the fit, $\delta_{\rm f}$.*

	Re $(l=2)$	Im $(l=2)$	Re $(l=3)$	Im $(l=3)$
C_0	0.37367	-0.08896	0.59944	-0.09270
C_2	$-1.406 \cdot 10^{-2}$	$-4.70 \cdot 10^{-3}$	$-5.453 \cdot 10^{-2}$	$-7.19 \cdot 10^{-3}$
C_3	$-7.53 \cdot 10^{-3}$	$-6.10 \cdot 10^{-3}$	$-3.093 \cdot 10^{-2}$	$-1.098 \cdot 10^{-2}$
C_4	$1.35 \cdot 10^{-3}$	$-3.22 \cdot 10^{-3}$	$6.419 \cdot 10^{-2}$	$1.001 \cdot 10^{-2}$
C_5	$7.09 \cdot 10^{-3}$	$-1.61 \cdot 10^{-3}$	$2.417 \cdot 10^{-2}$	$2.158 \cdot 10^{-2}$
C_6	$-2.03 \cdot 10^{-3}$	$-2.8 \cdot 10^{-4}$	$-5.215 \cdot 10^{-2}$	$-3.345 \cdot 10^{-2}$
$\delta_{\rm f}$	$2 \cdot 10^{-9}$	$3 \cdot 10^{-8}$	10^{-7}	$2 \cdot 10^{-7}$

Table 6.2: *As in Table 6.1, with $r = 1$.*

	Re $(l=2)$	Im $(l=2)$	Re $(l=3)$	Im $(l=3)$
C_0	0.06289	0.00100	0.06737	0.00065
C_2	$-1.048 \cdot 10^{-2}$	$2 \cdot 10^{-5}$	$-2.156 \cdot 10^{-2}$	$1.18 \cdot 10^{-3}$
C_3	$-1.074 \cdot 10^{-2}$	$-2.69 \cdot 10^{-3}$	$-2.056 \cdot 10^{-2}$	$-3.19 \cdot 10^{-3}$
C_4	$-1.53 \cdot 10^{-3}$	$-9.86 \cdot 10^{-3}$	$4.465 \cdot 10^{-2}$	$3.9 \cdot 10^{-4}$
C_5	$-2.40 \cdot 10^{-3}$	$8.90 \cdot 10^{-3}$	$2.341 \cdot 10^{-2}$	$-1.224 \cdot 10^{-2}$
C_6	$1.433 \cdot 10^{-2}$	$-3.773 \cdot 10^{-2}$	$-6.800 \cdot 10^{-2}$	$1.056 \cdot 10^{-2}$
$\delta_{\rm f}$	$5 \cdot 10^{-8}$	$2 \cdot 10^{-5}$	10^{-6}	10^{-4}

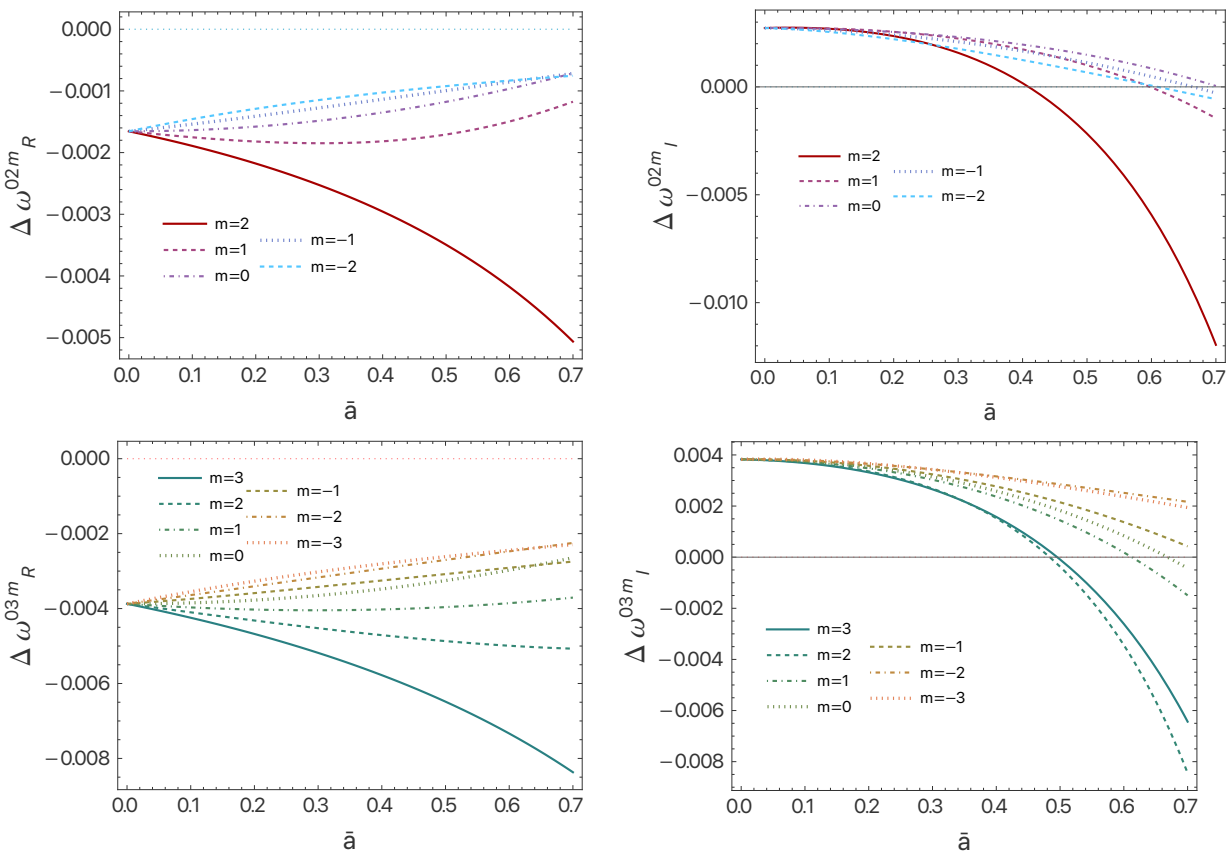

Figure 6.10: *Real (left panels) and imaginary (right panels) of the relative difference of EdGB QNMs with respect to GR as a function of $\bar{a}$, for $\bar{\zeta} = 0.2$ and different values of m. We consider $(nl) = (02)$ (upper panels) and $(nl) = (03)$ (lower panels) QNMs.*

Table 6.3: *As in Table 6.1, with $r = 2a$. The fit for $l = 3$ stops at fourth order in ζ.*

	Re $(l=2)$	Im $(l=2)$	Re $(l=3)$	Im $(l=3)$
C_0	0.03591	0.00638	0.04755	0.00659
C_2	$1.348 \cdot 10^{-2}$	$6.50 \cdot 10^{-3}$	$2.941 \cdot 10^{-2}$	$1.857 \cdot 10^{-2}$
C_3	$1.051 \cdot 10^{-2}$	$8.48 \cdot 10^{-3}$	$2.354 \cdot 10^{-2}$	$8.93 \cdot 10^{-3}$
C_4	$1.051 \cdot 10^{-2}$	$5.06 \cdot 10^{-3}$	$-2.391 \cdot 10^{-2}$	$-2.78 \cdot 10^{-3}$
C_5	$4.85 \cdot 10^{-3}$	$1.402 \cdot 10^{-2}$	–	–
C_6	$1.037 \cdot 10^{-2}$	$-2.24 \cdot 10^{-3}$	–	–
δ_f	$7 \cdot 10^{-7}$	$2 \cdot 10^{-6}$	10^{-4}	10^{-3}

Table 6.4: *As in Table 6.3, with $r = 2b$.*

	Re $(l=2)$	Im $(l=2)$	Re $(l=3)$	Im $(l=3)$
C_0	0.00896	−0.00031	0.00661	0.00006
C_2	$-8.37 \cdot 10^{-3}$	$3.13 \cdot 10^{-3}$	$-9.95 \cdot 10^{-3}$	$7.0 \cdot 10^{-4}$
C_3	$-1.201 \cdot 10^{-2}$	$2.95 \cdot 10^{-3}$	$-4.90 \cdot 10^{-3}$	$-2.27 \cdot 10^{-3}$
C_4	$2.67 \cdot 10^{-3}$	$-1.046 \cdot 10^{-2}$	$4.78 \cdot 10^{-3}$	$-1.57 \cdot 10^{-3}$
C_5	$-5.926 \cdot 10^{-2}$	$3.088 \cdot 10^{-2}$	–	–
C_6	$8.254 \cdot 10^{-2}$	$-6.819 \cdot 10^{-2}$	–	–
δ_f	$5 \cdot 10^{-6}$	$5 \cdot 10^{-4}$	$2 \cdot 10^{-4}$	$4 \cdot 10^{-2}$

Chapter 7

Tests of General Relativity with ParSpec

In this Chapter, we are going to outline two simple examples of possible tests of GR, one theory-agnostic and one theory-specific that uses our computation of the EdGB QNMs, posing as the first steps towards a more detailed spectroscopic analysis [194, 195]. Both methods rely on the ParSpec (Parametrized Ringdown Spin Expansion Coefficients) framework [175], an observable-based parametrization of the ringdown of spinning black holes beyond General Relativity.

Its features can be summarized as the following:

- The QNM spectrum is expanded in a bivariate series in terms of the fundamental parameters (mass and spin) characterizing BH dynamics in GR;
- The expansion parameters take into account the fact that modifications of GR are controlled by coupling constants, which can either have specific dimensions or be dimensionless;
- By combining several observations, it is in principle possible to map the deviation parameters to specific modified theories of gravity for which QNM may be available, like dynamical Chern-Simons (dCS) and EdGB. As soon as large enough values of SNR will be achievable in the ringdown (especially with future detectors), this approach holds the promise of allowing us to constrain several parameters or identify deviations.
- Differently from other parametrizations of the ringdown used by LIGO and Virgo, where the deviation parameters depend on the mass and spin of the BH and thus are specific for each astrophysical source, the ParSpec formalism is inherently a source-independent parametrization [132];
- The ParSpec framework, even if perturbative in the spin, can be made arbitrarily precise through high-order spin expansions.

We shall follow the notation of Refs. [132, 175] and denote with M the mass of the remnant BH resulting from the coalescence of a binary compact object system and with $\chi = J/M^2$ its spin.

7.1 ParSpec Framework

As seen in Chapter 2, we can model the ringdown waveform as a superposition of damped sinusoids. Calling the complex QNMs $\tilde{\omega}_{lmn} = \omega_{lmn} + i/\tau_{lmn}$, with ω_{nlm} the (real) frequencies, τ_{lmn} the damping

times, and introducing the mode amplitudes $\mathcal{A}^{+,-}_{lmn}$ and their phases $\phi^{+,-}_{lmn}$, we can write the waveform as

$$h_+(t) + ih_\times(t) = \frac{M}{D_L}\sum_{l=2}^{\infty}\sum_{m=-l}^{+l}\sum_{n=0}^{\infty}(h^+_{lmn} + h^-_{lmn})\,, \tag{7.1}$$

with

$$\begin{aligned} h^+_{lmn} &= \mathcal{A}^+_{lmn} S_{lmn}(\iota,\varphi) e^{i[(t-t_{lmn})\tilde{\omega}_{lmn}+\phi^+_{lmn}]} \\ h^-_{lmn} &= \mathcal{A}^-_{lmn} S_{l-mn}(\iota,\varphi) e^{-i[(t-t_{lmn})\tilde{\omega}_{lmn}+\phi^-_{lmn}]}\,, \end{aligned} \tag{7.2}$$

where S_{nlm} are the spin-weighted spheroidal harmonics [331], $t_{lmn} = t_0$ is a reference start time, ι is the inclination of the final spin with respect to the observer's line of sight, and φ corresponds to the azimuthal angle of the line of sight in the BH frame. When the progenitors in the binary system have spins aligned with the orbital angular momentum, the two (complex) amplitudes $+/-$ are related by reflection symmetry through a factor $(-1)^l$, effectively halving the degrees of freedom per mode. In our analysis, since we are not interested in inferring the physical value of the amplitude $\mathcal{A}_{lmn}$ – we just check that it is not zero when the mode is excited – we shall use the spherical harmonics Y_{lm} instead of the spheroidal harmonics S_{lmn} and reabsorb any factors inside the amplitude.

If one wanted to parametrize GR deviations in the QNM spectrum, a straightforward option would be

$$\begin{aligned} \omega_{lmn} &= \omega^{Kerr}_{lmn}(1 + \delta\omega_{lmn}) \\ \tau_{lmn} &= \tau^{Kerr}_{lmn}(1 + \delta\tau_{lmn})\,, \end{aligned} \tag{7.3}$$

where the "$Kerr$" superscript denotes the Kerr values computed in GR.

As already mentioned, although completely general, this parametrization has the drawback that the deviations $\delta\omega_{lmn}, \delta\tau_{lmn}$ will depend on the specific mass and spin of the BH. One could still repeat the analysis for multiple sources and study the distribution of the GR deviations across a population; but undoubtedly a source-independent approach, as the one of ParSpec, would be more straightforward to combine constraints from multiple observations. Furthermore, considering an explicit dependence of the spectrum on the mass and spin, such as a perturbative expansion, would improve the parametrization efficiency.

A model that encapsulates these requirements is the bivariate expansion

$$\begin{aligned} \omega^{(J)}_i &= \frac{1}{M_i}\sum_{k=0}^{D}\chi_i^n\omega^{(k)}_J\left(1 + \gamma_i\delta\omega^{(k)}_J\right) \\ \tau^{(J)}_i &= M_i\sum_{k=0}^{D}\chi_i^n\tau^{(k)}_J\left(1 + \gamma_i\delta\tau^{(k)}_J\right)\,, \end{aligned} \tag{7.4}$$

where $J = 1, 2, ..., q$ labels the mode (nlm) considered, i the source; M_i and $\chi_i \ll 1$ are the detector-frame mass and spin of the i-th source; D is the order of the spin expansion, γ_i is the dimensionless coupling constant that might depend on the source but not on the QNM [1]. $\omega^{(k)}_J$ and $\tau^{(k)}_J$ are the

[1] We note that γ_i might not directly correspond to fundamental coupling constants in an underlying Quantum

dimensionless coefficients of the spin expansion for a Kerr black hole in GR, while $\delta\omega_J^{(k)}$ and $\delta\tau_J^{(k)}$ are the beyond-Kerr corrections. Since all the source dependence is inside γ_i, these corrections are now universal dimensionless numbers, unlike the ones in Eq. (7.3). We are assuming perturbative corrections, so we must have $\gamma_i\delta\omega_J^{(k)} \ll 1$ and $\gamma_i\delta\tau_J^{(k)} \ll 1$.

If we consider the deviations as free parameters to be constrained, we can extract M_i and χ_i assuming GR, i.e. either from the full inspiral-merger-ringdown GR waveform or from a measurement of the fundamental $\ell = m = 2$ mode with a standard GR ringdown template. Therefore, in this case, the corrections $\gamma_i\delta\omega_J^{(k)}$ and $\gamma_i\delta\tau_J^{(k)}$ also include the shift between M_i, χ_i and the physical mass and spin (see the Appendix of Ref. [175]). However, if one chooses to fix the beyond-GR parameters to the specific prediction of a modified theory of gravity, then M_i and χ_i would be the physical mass and spin found assuming that theory, which in general would differ from the values found assuming GR.

The corrections induced by a general modified theory of gravity to the QNM spectrum can be broadly divided into three cases:

- Scale-free corrections. It corresponds to the case in which the theory is described by a dimensionless constant, which can be absorbed in the $\delta\omega^{(k)}, \delta\tau^{(k)}$ if we are performing inference on them. The spectrum will be described by $\mathcal{P} = 2(D+1)q$ parameters, with q the number of modes considered, and D the spin truncation order. Theories that belong to this category are for example Einstein-Aether and Horava gravity (to leading order) [18];

- Single dimensionful coupling. In this case, the theory is described by a dimensionful coupling constant α (equal for all the sources) that will have dimensions $[\alpha] = \mathcal{M}^p$, with p fixed by the theory and $\mathcal{M}$ the typical length mass/scale of the system (we are working in geometric units). For BHs the characteristic length scale is fixed by the source frame mass M^s (as measured within GR), which is related to the mass in the detector frame M_i through the redshift z_i. At leading order ($\gamma_i \ll 1$), we can identify

$$\gamma_i = \frac{\alpha}{(M_i^s)^p} = \frac{\alpha(1+z_i)^p}{M_i^p}\,, \tag{7.5}$$

  where z_i is the redshift of the i-th source, which can be estimated from the amplitude of the inspiral waveform (assuming that the modified theory does not change significantly the standard cosmological model). In the case in which the deviation parameters are not fixed, we can reabsorb α inside $\delta\omega^{(k)}, \delta\tau^{(k)}$, making them dimensionful. However, all the source-dependent information is still inside γ_i, while the deformation parameters remain source-independent. Since p is fixed, also in this case the number of parameters will be $\mathcal{P} = 2(D+1)$. In this category, we find, with $p = 4$, Einstein-scalar Gauss-Bonnet, which includes EdGB studied in this Thesis ($\alpha = \alpha_{GB}^2$), and dynamical Chern-Simons [18].

- Individual Charges. This is the case when the GR-deviations are due to an extra charge Q_i that is a primary hair, i.e. not depending on the mass and spin of the BH. We shall have

$$\gamma_i = \frac{Q_i^2}{(M_i^s)^2}\,, \tag{7.6}$$

Field Theory, but, in general, will be non-trivial functions of them.

with N additional parameters, due to the charges of each source. Hence the QNM spectrum would be described by $\mathcal{P}' = \mathcal{P}+N = 2(D+1)q+N$ parameters. Kerr-Newman BHs, which can be used to describe modified theories of gravity with additional charges due to fundamental fields, belong to this category.

In Section 7.3, we shall consider the first case ($p = 0$) and perform a null test of GR by inferring the posterior probabilities for the deviation parameters $\delta\omega_J^{(k)}, \delta\tau_J^{(k)}$ using multiple sources and next generation detectors.

In Section 7.4, instead, we shall fix the deviation parameters to the values predicted by EdGB (see Tab. 7.1), corresponding to the $p = 4$ case, and perform inference on the coupling constant of the theory through the beyond-GR parameter $\ell = \sqrt{\alpha_{GB}}$. Focusing on a single GW event detected by LV, we adopt a time-domain analysis of GW150914 implementing the ParSpec parametrization in the pyRing package.

In the rest of the Chapter, we will not consider the third case discussed above, corresponding to N individual charges.

Table 7.1: *Values of the coefficients for the ParSpec spin expansion for fundamental modes with $\ell = m = 2$, $\ell = m = 3$ and $\ell = 2, m = 1$. In the upper section, the coefficients $\omega_J^{(k)}$ $\omega_J^{(k)}$ are computed up to order $D_{GR} = 6$ by performing a slow rotation expansion of the Kerr QNMs. In the lower section, there are deviation coefficients at the leading order EdGB correction found from the analysis of Ch. 6.*

spin order k	$\omega_{022}^{(k)}$	$\tau_{022}^{(k)}$	$\omega_{033}^{(k)}$	$\tau_{033}^{(k)}$	$\omega_{021}^{(k)}$	$\tau_{021}^{(k)}$
0	0.37367	11.2407	0.59944	10.7871	0.37367	11.2407
1	0.12578	0.2522	0.20206	0.2276	0.06288	0.1261
2	0.07178	0.6650	0.10717	0.8238	0.04487	0.7701
3	0.04800	0.5840	0.06890	0.7345	0.02183	0.4026
4	0.03601	0.6420	0.04841	0.6744	0.01642	0.3563
5	0.01389	0.0733	0.05295	0.5408	0.00590	1.2600
6	0.13021	3.9385	−0.11339	1.3153	0.05859	0
spin order k	$\delta\omega_{022}^{(k)}$	$\delta\tau_{022}^{(k)}$	$\delta\omega_{033}^{(k)}$	$\delta\tau_{033}^{(k)}$	$\delta\omega_{021}^{(k)}$	$\delta\tau_{021}^{(k)}$
0	−0.03773	−0.0528	−0.09112	−0.0778	−0.03773	−0.0528
1	−0.16679	−0.0802	−0.32149	2.4495	−0.16679	−0.0176
2	−0.27788	3.9141	−0.56101	2.6150	0.11256	1.4773

7.2 Statistical Tools

We now illustrate and recap briefly some of the fundamental quantities used for the statistical analysis in the following sections [332].

7.2.1 Bayesian Parameter Estimation

Considering a ringdown model described by some parameters $\boldsymbol{\theta}$, which possibly contains the beyond-GR deviations, the *posterior* probability distribution of the parameters $\boldsymbol{\theta}$ conditioned on the avail-

able data d is, according to Bayes' theorem,

$$P(\boldsymbol{\theta}|d,\mathcal{H},I) = \frac{P(\boldsymbol{\theta}|\mathcal{H},I)\mathcal{L}(d|\boldsymbol{\theta},\mathcal{H},I)}{P(d|\mathcal{H},I)}\,, \tag{7.7}$$

where $\mathcal{H}$ represents the specific parametric template describing the data and I represents all the available background information (in the following sections we shall omit it). $P(\boldsymbol{\theta}|\mathcal{H},I)$ is the *prior* probability distribution, which quantifies our information about the parameters before analyzing the data and is modified by the observations through the *likelihood* $\mathcal{L}(d|\lambda,\mathcal{H},I)$, describing the probability of observing the data assuming that the hypothesis $\mathcal{H}$, identified by the parameters $\boldsymbol{\theta}$, is true; finally $P(d|\mathcal{H},I)$ is the *evidence* of the model $\mathcal{H}$, acting as a normalization factor and representing the probability that the data d can be explained by the considered model.

The evidence plays an important role when comparing the agreement with the data of two competing models $\mathcal{H}_1,\mathcal{H}_2$:

$$\frac{P(\mathcal{H}_1|d,I)}{P(\mathcal{H}_2|d,I)} = \frac{P(\mathcal{H}_1|I)P(d|\mathcal{H}_1,I)}{P(\mathcal{H}_2|I)P(d|\mathcal{H}_2,I)} \equiv \frac{P(\mathcal{H}_1|I)}{P(\mathcal{H}_2|I)}\,\mathcal{B}^1_2\,, \tag{7.8}$$

where we have defined the *Bayes Factor* $\mathcal{B}^1_2$ in terms of the evidences ratio, while $P(\mathcal{H}_1|I)/P(\mathcal{H}_2|I)$ represents the ratio of prior probabilities of the models.

7.2.2 Markov Chain Monte Carlo

We use a Markov Chain Monte Carlo (MCMC) method [333] to infer the posterior distributions on the beyond-Kerr parameters $\boldsymbol{\theta}_{nGR}$. If we call $\bar{\boldsymbol{\theta}}$ the set of free parameters we want to infer, and $\bar{d}$ the set of ringdown observations considered, the MCMC algorithm allows us to obtain a sequence of random samples from the unknown posterior probability distribution by exploiting the proportionality with the likelihood, assumed known,

$$P(\bar{\boldsymbol{\theta}}|\bar{d},\mathcal{H}) \propto \mathcal{L}(\bar{\boldsymbol{\theta}}|\bar{d},\mathcal{H})P(\bar{\boldsymbol{\theta}}|\mathcal{H})\,, \tag{7.9}$$

which follows from Bayes' theorem (7.7).

An example of MCMC is the Metropolis-Hastings algorithm, which consists of the following main steps:

1. An arbitrary point $\bar{\boldsymbol{\theta}}_t$ is selected as a first sample;
2. The proposal density $Q(\bar{\boldsymbol{\theta}}_x|\bar{\boldsymbol{\theta}}_y)$, which controls whether to choose the next sample value $\bar{\boldsymbol{\theta}}_x$ given the previous one $\bar{\boldsymbol{\theta}}_y$, is chosen;
3. For each iteration t:
   - Generate a candidate $\bar{\boldsymbol{\theta}}_{x'}$ from the distribution $Q(\bar{\boldsymbol{\theta}}_{x'}|\bar{\boldsymbol{\theta}}_t)$
   - Compute the acceptance ratio $A = \mathcal{L}(\bar{\boldsymbol{\theta}}_{x'}|\bar{d},\mathcal{H})/\mathcal{L}(\bar{\boldsymbol{\theta}}_t|\bar{d},\mathcal{H})$, which, given the proportionaly in Eq. (7.9), can also be expressed in terms of the posteriors $A = P(\bar{\boldsymbol{\theta}}_{x'}|\bar{d},\mathcal{H})/P(\bar{\boldsymbol{\theta}}_t|\bar{d},\mathcal{H})$.
   - After picking a uniform random number $r \in [0,1]$, accept the candidate $\boldsymbol{\theta}_{t+1} = \boldsymbol{\theta}_{x'}$ if $r \leq A$, or reject the candidate $\boldsymbol{\theta}_{t+1} = \boldsymbol{\theta}_t$ if $r > A$.

The acceptance ratio describes how probable the new proposed sample is with respect to the current sample, taking into account the information of the posterior distribution $P(\bar{\boldsymbol{\theta}}|\bar{d},\mathcal{H})$. The more this probability decreases, the more we will reject the new sample; in this way, we will tend to have a larger number of samples in the high-density regions of the posterior, while only occasionally visiting the low-density regions. Thus, we expect the algorithm to return samples that follow the desired unknown posterior distribution.

7.2.3 Fisher Matrix

The uncertainties on the template parameters can be computed using a *Fisher Matrix* approach [334], which is able to provide accurate estimates of the statistical errors in the high-SNR limit with Gaussian noise (and without systematic errors in the waveform) [335].

Given a waveform $h(t)$ such as the one in Eq. (7.1), described by some parameters $\boldsymbol{\theta}$ the Fisher matrix is defined as

$$F_{ij} = \left(\frac{\partial h}{\partial \theta_i}\middle|\frac{\partial h}{\partial \theta_j}\right)_{\boldsymbol{\theta}=\hat{\boldsymbol{\theta}}}, \tag{7.10}$$

where $\hat{\boldsymbol{\theta}}$ are the theoretical (injected) values, and the scalar product is defined as

$$\left(h_1\middle|h_2\right) = 4Re\int_{f_{min}}^{f_{max}} \frac{\tilde{h}_1^*(f)\tilde{h}_2(f)}{S_n(f)}df\,, \tag{7.11}$$

with $S_n(f)$ the detector spectral density and $\tilde{h}$ the Fourier transform of the waveform.

The statistical error on the i-th parameter can be found from the diagonal elements of the Fisher matrix as

$$\sigma_{\theta_i} = \sqrt{\Sigma_{ii}}\,, \tag{7.12}$$

where $\Sigma = F^{-1}$ is the covariance matrix.

7.2.4 Time Domain Analysis

When we perform a theory-specific test of GR, fixing the beyond-GR parameters in the waveform model to the EdGB values in Tab. 7.1, our goal is to constrain the characteristic length $\ell = \sqrt{\alpha_{GB}}$.

In order to do that, we use pyRing [129, 131, 269, 336], a publicly available Bayesian parameter estimation python [337] package, which focuses on the ringdown part of the GW signal formulating the problem in a fully time-domain framework, both in the likelihood and in the waveform.

A time domain analysis framework, in our case restricted to the post-merger part of the signal, solves several technical issues of a frequency domain approach and avoids contamination from earlier stages of the coalescence (see [129, 132]). For an observed strain $d(t)$, given a GW signal $h(t)$, the log-likelihood function is

$$\log\mathcal{L}(d|\hat{\boldsymbol{\theta}},\mathcal{H}) = -\frac{1}{2}\int\int dtdT\left[d(t)-h(t;\hat{\boldsymbol{\theta}})\right]C^{-1}\left[d(t+T)-h(t+T;\hat{\boldsymbol{\theta}})\right], \tag{7.13}$$

where $C(T) = \int dtdT\, n(t)n(t+T)$ is the two-point autocovariance function, estimated from $4096s$

of data surrounding the event, $n(t)$ is the noise. The likelihood function is determined assuming that the error on the numerical data is distributed as a zero-mean gaussian with a conservative standard deviation estimate of 10^{-5}.

The pyRing package uses a nested sampler algorithm called CPNest [338] to infer the parameters' posterior distributions and uses the LALInference library [339] to compute projections onto detectors. The Nested-Sampling algorithm [332] is able to reconstruct multi-dimensional, strongly correlated posterior distributions, and is now part of the routine merger-ringdown analysis of LIGO-Virgo collaborations [15, 33]. pyRing implements state-of-the-art merger-ringdown-only analytical waveform templates [265, 268, 340, 341] and utilizes other standard IMR waveforms through the LALSimulation library [342]. All the internal waveform and likelihood computations are carried out in cython [343].

7.3 Theory-Independent Null Test of General Relativity

In this section, we perform a theory-agnostic test of GR, working under the hypothesis that GR is the correct description of gravity, and using Bayesian parameter estimation to infer the posterior probability distributions of the deviation parameters $\delta\omega_J^{(k)}, \delta\tau_J^{(k)}$.

Our goal is to understand, considering future detectors such as Cosmic Explorer (CE) and Einstein Telescope (ET), how many sources are needed to put meaningful bounds, which beyond-GR parameter would be constrainable in the future, and to which level.

This next-generation of ground-based interferometers, CE (in the United States) and ET (in Europe), will improve by one order of magnitude the sensitivity of currently available detectors and will extend the bandwidth towards both low and high frequencies [36, 344, 345].

While in Ref. [175] the authors used uniform distributions for masses and spins of the BHs, we repeat their analysis focusing on a realistic distribution of sources, using a population of BBHs with mass and spin distributed according to *Power Law + Peak* and *Default* models, respectively, which are currently favored in the latest LIGO-Virgo-KAGRA (LVK) catalog [13]. The redshifts follow the distribution of the model in Ref. [346]. We shall consider two catalogs of 10^5 binary sources: "Model I" has only positive values of spins between $[0, 1]$, while "Model II" allows for negative values in the range $[-1, 1]$.

Given N sources, we shall have $\mathcal{O}$ observables that we can use to fix $\mathcal{P}$ parameters. The minimum number of sources needed to infer these parameters depends on the way we extract the mass and spin of the BH, whether from the full IMR waveform or only from the ringdown part.

In the former case, using the information about the binary progenitors' masses and spins, we can evaluate the remnant BH's mass and spin using NR semianalytical fits. Thus, for N sources we shall have $\mathcal{O} = 2N\,q$ observables: q frequencies and q damping times for each source. To constrain $\mathcal{P} = 2(D+1)q$ parameters, we must have $N \geq D+1$, with D the maximum spin order considered in the ParSpec expansion (7.4).

Instead, if we examine only the ringdown signal, we must use two parameters for each source (e.g. one frequency and one damping time) to extract the mass and spin of the remnant BH. Thus, we are left with $\mathcal{O} = 2N\,q - 2N = 2N(q-1)$ observables. The minimum number of sources, in this case, is then $N \geq q(1+D)/(q-1)$. We note that we must have at least two modes to constrain the GR modifications, meaning $q > 1$, since the first mode is used to determine the mass and the spin.

Setup

In our analysis, we consider the masses and spins determined from the whole IMR waveform and assume that the $(nlm) = (022), (033), (021)$ modes are detectable – we leave more realistic investigations, considering which modes are more excited depending on the characteristics of the binary sources, to future works.

In order to sample the posterior probability distributions of each beyond-GR deviation parameter using Bayesian analysis, we need to choose the likelihood in Eq. (7.9). For each event we fix it to a Gaussian distribution and, given the "quasi-orthonormality" of the QNMs [170], the combined function can be written as the product of Gaussian distributions

$$\mathcal{L}(d|\boldsymbol{\theta}, \mathcal{H}) = \prod_{i=1}^{N} \mathcal{L}_i(d|\boldsymbol{\theta}, \mathcal{H}) = \prod_{i=1}^{N} \prod_{J=1}^{q} \mathcal{N}\left(\boldsymbol{\mu}_i^{(J)}, \Sigma_i^{(J)}\right) , \tag{7.14}$$

where $\boldsymbol{\mu}_i^{(J)}$ is a two-components vector related to the difference between the observed $J = 1, ..., q$ modes and the parametrized mode templates in Eq. (7.4),

$$\vec{\mu}_i^{(J)} = \begin{pmatrix} \omega_i^{(J)} - \omega_{i,obs}^{(J)} \\ \tau_i^{(J)} - \tau_{i,obs}^{(J)} \end{pmatrix} , \tag{7.15}$$

and Σ_i is the covariance matrix that includes errors and correlations between the frequencies and damping times of the i-th source. Given the properties of QNMs, in this case it is a block-diagonal matrix with each block corresponding to the J-th mode.

The values of $(\omega_i^{(J)}, \tau_i^{(J)})$ in Eq. (7.15) are assumed to be the QNMs of a Kerr BH, while the measured values $(\omega_{i,obs}^{(J)}, \tau_{i,obs}^{(J)})$ that we inject in our analysis are evaluated in the following way.

We extract N sources from the original catalog by requiring that the SNR ρ for the (022) mode is greater than a certain threshold, namely $\rho > 12$, considering the detectors CE and ET [2]. There are currently different design options being considered, as shown in Fig. 7.1, among which we select a length of the interferometer arms of $20\,km$ for CE and $15\,km$ for ET, assuming for the latter two identical L configurations built in the Netherlands and in Sardinia, Italy (the final project is still in the works [347]). The range of frequency in Eq. (7.11) is set to $[3, 5000]Hz$.

The SNR ρ is computed as

$$\rho^2 = (h|h) = 4Re \int_{f_{min}}^{f_{max}} \frac{\tilde{h}^*(f)\tilde{h}(f)}{S_h(f)} df \, , \tag{7.16}$$

where $\tilde{h}(f)$ is the Fourier transform of the waveform, and $S_h(f)$ is the noise spectral density of the detector.

[2] We focus on these detectors, instead of LISA or LVK, because the next step of this analysis will be to constrain EdGB, whose dimensionful coupling constant introduces a scale and inevitably makes certain sources (and consequently certain detectors) more relevant than others. The EdGB deviation is controlled by $\alpha_{GB}^2/M^4 \ll 1$, this is why lower mass compact objects, such as stellar-origin BHs, are more important to constrain the theory; these sources are among the main targets of ET and CE [136].

The SNR can be expressed in terms of the GW energy spectrum dE/df,

$$\rho^2 = \frac{2}{5\pi^2 r^2}\int_{f_{min}}^{f_{max}} \frac{1}{f^2 S_n(f)}\frac{dE}{df}df \ , \tag{7.17}$$

related in turn to the radiation efficiency ϵ_{RD},

$$\epsilon_{RD} = \frac{1}{M}\int_{f_{min}}^{f_{max}} \frac{dE}{df}df \ , \tag{7.18}$$

which controls the amount of energy released by the (n, l, m) mode.

Here we use the semi-analytic formula determined in [348] to compute ϵ_{RD} for a given (n, l, m) combination:

$$\epsilon_{RD} = \left[a_{lm} + b_{lm}\chi_+ + c_{lm}\chi_-\right]^2 \ , \tag{7.19}$$

where a_{lm}, b_{lm} and c_{lm} are functions of the binary mass ratio $q = m_1/m_2 \geq 1$, and of the spin parameters:

$$\chi_\pm = \frac{m_1\chi_1 \pm m_2\chi_2}{m_1 + m_2} \ , \tag{7.20}$$

which in turn depend on the masses $m_{1,2}$ and on the dimensionless spins $\chi_{1,2}$ of the progenitors. We plot in Fig. 7.2 the radiation efficiency for the three modes $(0, 2, 2), (0, 3, 3), (0, 2, 1)$ for the two catalogs considered.

We find a maximum $N = 13401$ of sources with SNR above 12 using ET with the first catalog, and $N = 12280$ in the second catalog. These numbers are compatible with the estimated detections expected with ET in a year [347]. Instead, with CE we find $N = 5104$ within the first catalog of sources and $N = 2844$ in the second one.

Once the N sources have been extracted, we compute the mass and spin of the remnant BH following the BBH coalescence by using semianalytical relations based on NR in GR [349] that relate the progenitors' parameters to the ones of the outcome of the mergers.
In Fig. 7.3 we show the final masses and spins of the sources considered, while in Fig. 7.4 the relative SNR values are plotted.

Given the final masses M_i and spin χ_i $(i = 1, ..., N)$, we determine the measured frequencies and damping times from the GR values in Tab. 7.1, while the uncertainties and correlations are found with the Fisher matrix approach of Sec. 7.2.3, using the parameter basis $(\mathcal{A}, \phi_i^{(J)}, \omega_{i,obs}^{(J)}, \tau_{i,obs}^{(J)})$. The distributions of the errors on the two measured modes for the two detectors are shown in Figs. 7.9-7.10, showing that the damping time is affected by greater uncertainty, as expected due to the difficulty in measuring it [127].

As a first step of the analysis, we shall consider the deviation parameters only for one mode, namely $J = (nlm) = (022)$, which has higher SNR. We set the prior distributions on the beyond-Kerr parameters to be uniform in the range $[-5, 5]$.

We infer the posterior probability distributions of the non-GR parameters $(\delta\omega_J^{(k)}, \delta\tau_J^{(k)})$, whose true value we assume to be zero, from the measured QNM values of the sources adopting the EMCEE algorithm of Ref. [350], which is an advanced version of the Metropolis-Hastings algorithm described in Sec. 7.2.2. We remark that in this case M_i and χ_i appearing in Eq. (7.4) are evaluated assuming GR and that their possible corrections due to the modified theory are included into $(\delta\omega_J^{(k)}, \delta\tau_J^{(k)})$, as well as the dimensionless coupling constant of the theory.

We separate the order of the maximum spin expansion for the GR and the beyond-GR parameters: for the former, we choose $D_{GR} = 6$, in order to get a better agreement with the Kerr values, while for the latter we consider the cases $D_{nGR} = 0$ and $D_{nGR} = 2$. As shown in Ref. [175], a sixth-order expansion for the GR part agrees with numerical Kerr values within 1% at $\chi \sim 0.7$ for both the frequency and damping time.

We show in Fig. 7.5 the marginal posterior distributions of the beyond-GR parameters for the case $D_{nGR} = 0$ as a function of the catalog and number of sources considered.

From the marginal posterior distributions, which are nearly symmetrical around the peak and centered around zero, we can define their width as half the corresponding η confidence interval:

$$\sigma_j = \frac{1}{2}(\theta_j^{max} - \theta_j^{min})\,, \tag{7.21}$$

where j identifies the parameter (in this case $\delta\omega^0, \delta\tau^{(0)}$) and θ_j^{max}, θ_j^{min} are found from the marginalized posteriors

$$\int_{\theta_j^{min}}^{\theta_j^{max}} P(\theta_j) d\theta_j = \eta\,. \tag{7.22}$$

For the case $D_{nGR} = 2$, the resulting bounds at $\eta = 68\%$ and $\eta = 90\%$ credible levels on the constrainable beyond-GR parameters are shown in Fig. 7.6 for the first catalog (the results for the second one are analogous). In Tab. 7.2 we report the width defined in Eq. (7.22), for $\eta = 90\%$, of the bounds for each deviation coefficient in the case $D_{nGR} = 2$, showing only the cases in which it is possible to impose a meaningful bound.

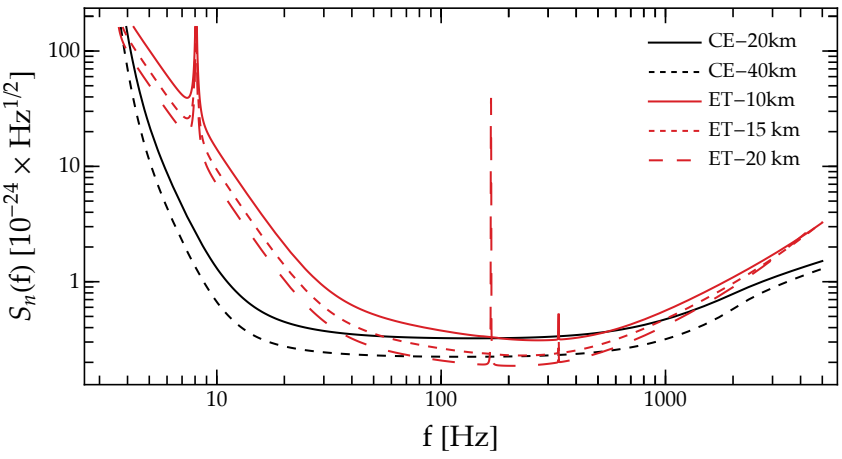

Figure 7.1: *Noise spectral density for the configurations of the Einstein Telescope and the Cosmic Explorer considered in this Chapter.*

7.4 Testing Einstein-dilaton Gauss-Bonnet with PYRING and Gravitational Wave Data

Fixing the deviation coefficients of the expansion (7.4) to a specific theory, it is possible to directly check the agreement of GW data currently available with that specific description of gravity. One

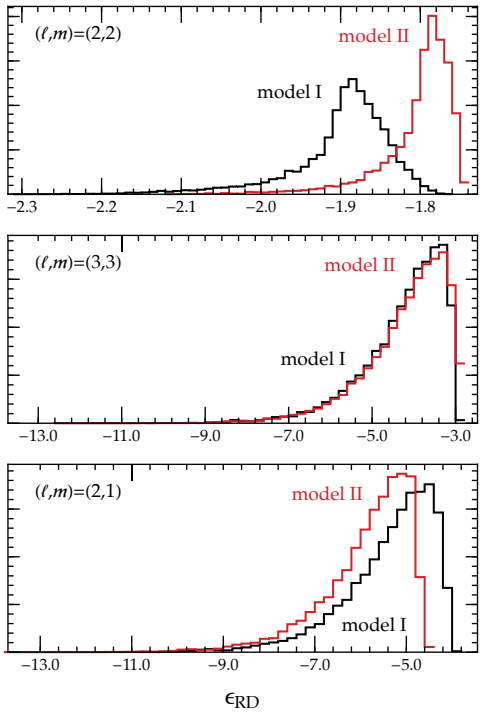

Figure 7.2: *Distribution of the energy released in the $l = m = 2$, $l = m = 3$ and $(l, m) = (2, 1)$ modes for the ringdown events with signal-to-noise ratio of the fundamental QNM larger than 12, as observed by ET, assuming both population models.*

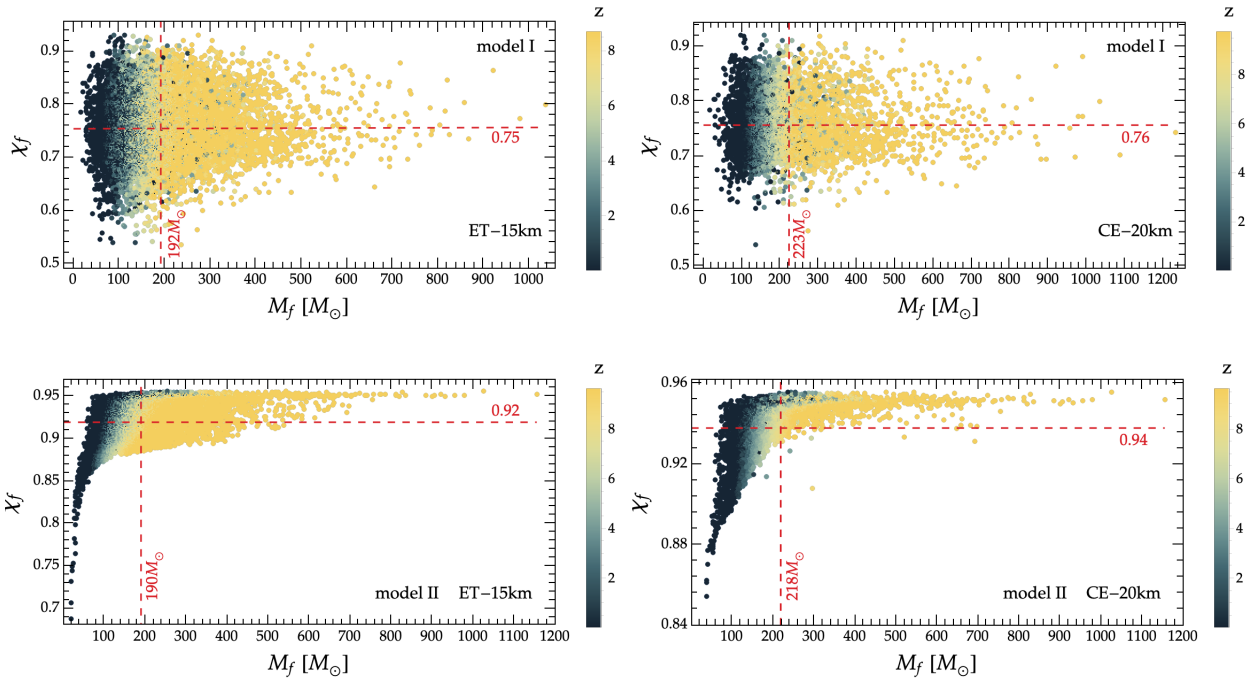

Figure 7.3: *Distribution of the final detector-frame masses and spins obtained from the first (upper panels) and second (lower panels) binary population catalogs, satisfying the requirement that the SNR of the* (022) *mode is larger than $\rho = 12$. The color code identifies the redshift associated to the binary, for a specific detector. Dashed lines lie at the mean values of the distribution.*

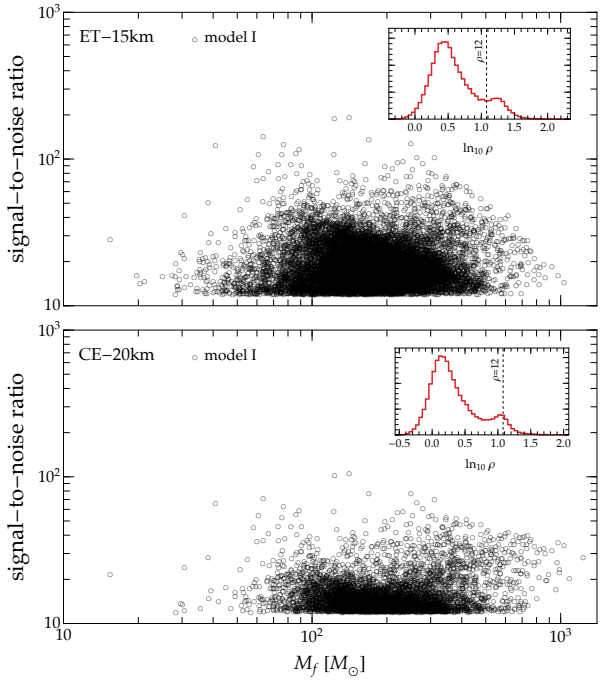

Figure 7.4: *Signal-to-noise ratio as a function of the detector remnant mass for the ringdown events with* $\rho \geq 12$ *for the* (22) *mode, assuming ET (top panel) and CE (bottom panel), and the population* `model I`*. The inset in each panel shows the SNR distribution of the whole catalogue, before applying the threshold cut. After the selection we find* $N = 13401$ *and* $N = 5104$ *events for ET and CE, respectively. The SNR-*M_f *distribution for* `model II` *is similar, although the number of events above the threshold is lower, with* $N = 12280$ *and* $N = 2844$ *binaries for ET and CE.*

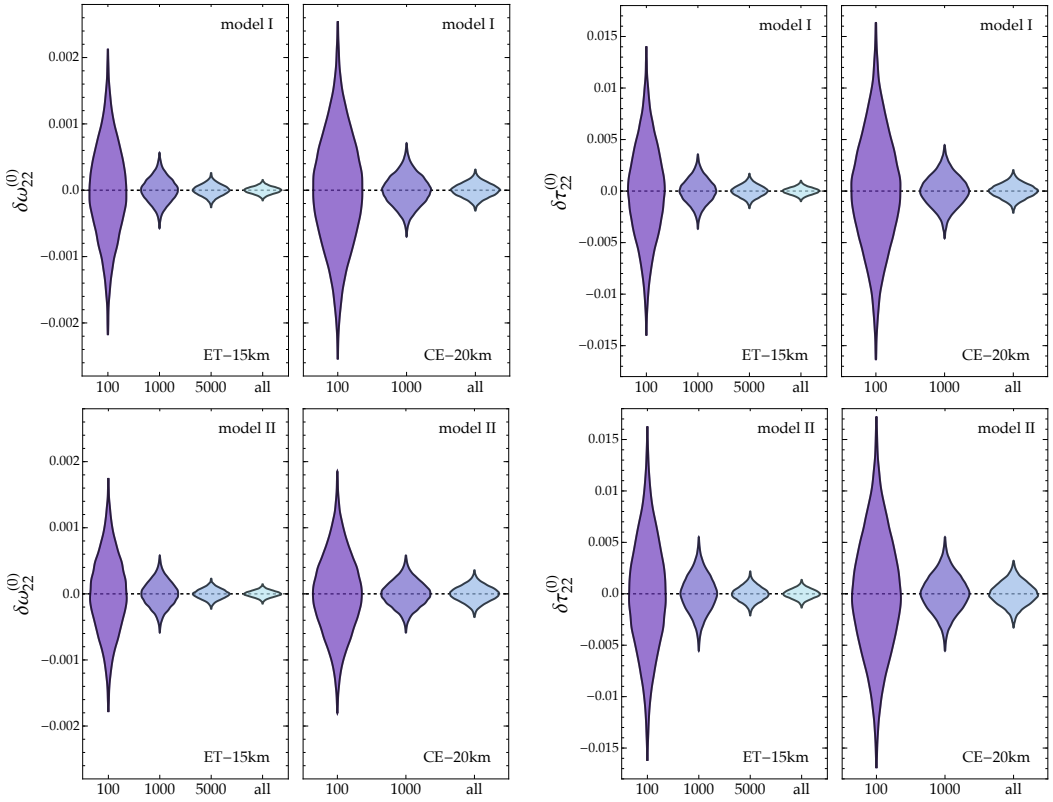

Figure 7.5: *Posterior probability densities for the non-rotating corrections* $(\delta\omega_{22}^{(0)}, \delta\tau_{22}^{(0)})$*, as a function of the number of sources analyzed. Results are derived following a single-mode analysis, in which only the fundamental* $(2, 2)$ *mode is taken into account. The top and bottom panels refer to the two population models.*

	parameters	`model I`	`model II`
CE-20km	$\delta\omega_{22}^{(0)}$	$[-0.0281, 0.0275]$	$[-0.0601, 0.0593]$
	$\delta\omega_{22}^{(1)}$	$[-0.214, 0.217]$	$[-0.391, 0.408]$
	$\delta\omega_{22}^{(2)}$	$[-0.247, 0.242]$	$[-0.401, 0.391]$
	$\delta\tau_{22}^{(0)}$	$[-0.179, 0.189]$	$[-0.335, 0.322]$
ET-15km	$\delta\omega_{22}^{(0)}$	$[-0.0122, 0.0121]$	$[-0.0337, 0.0346]$
	$\delta\omega_{22}^{(1)}$	$[-0.0945, 0.0934]$	$[-0.225, 0.220]$
	$\delta\omega_{22}^{(2)}$	$[-0.106, 0.108]$	$[-0.210, 0.220]$
	$\delta\tau_{22}^{(0)}$	$[-0.079, 0.0779]$	$[-0.0174, 0.0178]$

Table 7.2: 90% *confidence intervals for the marginalized distribution of the ParSpec parameters with quadratic spin corrections, for the* $p = 0$ *scenario. These constraints are obtained by stacking the full set of sources for both models.*

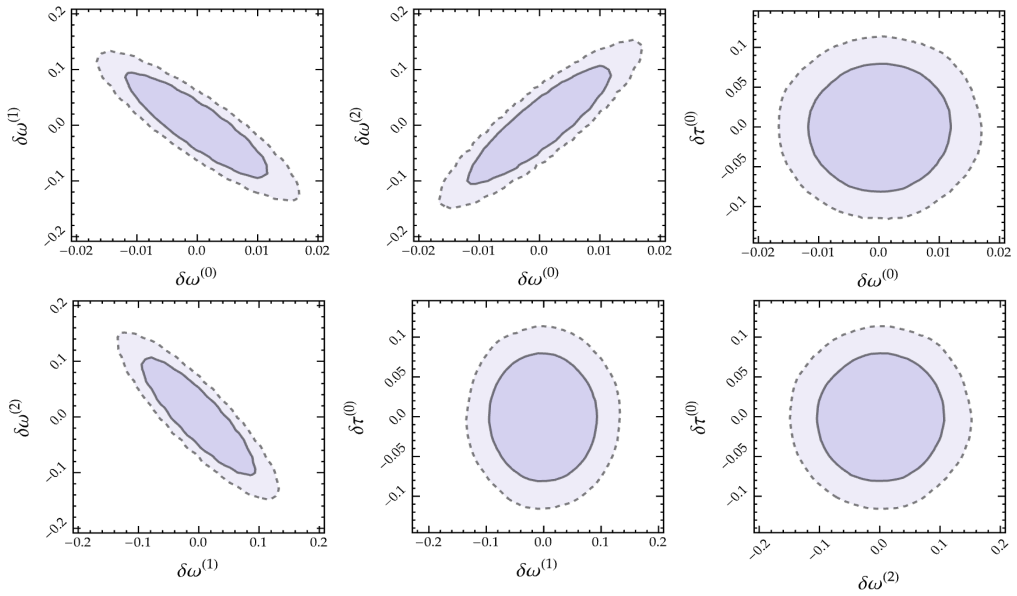

Figure 7.6: *Joint posterior distributions for the ParSpec parameters, with quadratic spin corrections. Solid and dashed contours refer to* 68% *and* 90% *credible regions. Constraints are derived by stacking the full set of* $N = 13401$ *events observed by ET above the threshold, assuming the spin distribution of* `model I`*.*

way to do so is to compare the Bayes factor, introduced in Sec. 7.2.1, computed for a modified theory of gravity with the one of GR to understand which theory better describes the data.

In this section, we apply this strategy to EdGB, including the corrections to the GR QNM spectrum found in Chapter 6 into the ParSpec parametrization. We consider as a test case the first GW observation, GW150914 [5]. This event, being well studied and understood, allows us to use it as a case study, even though, due to the tiny GR modifications introduced by EdGB (especially for such a massive source, since the correction is $\propto \alpha_{GB}/M^2$) and the relatively low SNR in the ringdown, we do not expect to constrain with high accuracy the theory with this single observation, as already investigated in other studies – e.g. [118].

This is just the first step in our ongoing work [195], which will also study simulated signals with arbitrary SNR and an appropriate choice of present or future detectors, to understand, for example, which SNR will be necessary to detect the GR deviation if one assumes EdGB to be the correct

theory of gravity.

At second order in the spin and for a single source, calling $\ell \equiv \sqrt{\alpha_{GB}}$ (which has dimensions of a length in geometric units), Eq. (7.4) becomes:

$$\omega_J = \frac{1}{M}\left[\omega_J^{(0)}\left(1+\frac{\ell^4}{(M^s)^4}\delta\omega_J^{(0)}\right)+\chi\omega_J^{(1)}\left(1+\frac{\ell^4}{(M^s)^4}\delta\omega_J^{(1)}\right)+\chi^2\omega_J^{(2)}\left(1+\frac{\ell^4}{(M^s)^4}\delta\omega_J^{(2)}\right)\right]$$
$$\tau_J = M\left[\tau_J^{(0)}\left(1+\frac{\ell^4}{(M^s)^4}\delta\tau_J^{(0)}\right)+\chi\tau_J^{(1)}\left(1+\frac{\ell^4}{(M^s)^4}\delta\tau_J^{(1)}\right)+\chi^2\tau_J^{(2)}\left(1+\frac{\ell^4}{(M^s)^4}\delta\tau_J^{(2)}\right)\right]. \quad (7.23)$$

We recall that J is the label that identifies the QNM, M, χ are the mass and spin of the remnant BH in the detector frame, while $M^s = M/(1+z)$ is the source-frame mass [3]. The parameters $\delta\omega_J^{(k)}, \delta\tau_J^{(k)}$, $k = 0, 1, 2$, are fixed to the values in Tab. 7.1. These coefficients are obtained from the data used in Ch. 6 by taking the leading order correction of a Taylor expansion around $\zeta = 0$, which is intrinsically different from the fits provided in Tabs. 6.1-6.4. The latter describes accurately the functions $\omega_r^{nl}(\zeta)$, appearing in the spin expansion of the QNM spectrum in Eq. (6.74), in the range $\zeta = \alpha_{GB}/M^2 \in [0, 0.4]$ ($\zeta \in [0, 0.3]$ for the imaginary part).

Since we are fixing the deviation coefficients, we shall infer the posterior probability distribution of the characteristic length of the theory $\ell = \sqrt{\alpha_{GB}}$.

Setup

In this analysis, we use the template in Eqs. (7.1)-(7.2) with the QNMs given by the ParSpec model in Eq. (7.23), under the assumption that the waveform amplitudes satisfy $h_{lm} = h^*_{l-m}$ (which is reasonable for GW150914, since there is no evidence for misaligned spins). We shall include up to two modes, namely $J = (nlm) = \{(022), (122)\}$.

We fix the spin expansion coefficients $\omega_J^{(k)}, \tau_J^{(k)}$ in Eq. (7.23) to the GR values found in Ref. [132] up to order $D_{GR} = 5$ for the frequency ($D_{GR} = 9$ for the damping time), guaranteeing an accuracy of at least 1% (3%) in the whole range of spins $[0, 0.9999]$. The GR modification parameters $\delta\omega_J^{(k)}, \delta\tau_J^{(k)}$ are fixed up to order $D_{nGR} = 2$ to the values in Tab. 7.1, only for $J = (022)$, since the corrections to the first overtone are not available.

We have two options when considering the mass and spin in the expansion (7.23). The first one, adopted in the null test in Sec. 7.3, is to fix their values to the ones measured assuming GR, and include any modification into the deviation parameters $\delta\omega_J^{(k)}, \delta\tau_J^{(k)}$.
In the theory-specific case considered here, since we are no longer keeping the GR modifications to the frequencies and damping times as free parameters, we cannot use them to reabsorb the deviations to the mass and spin. However, one could still assume that, since the deviations are perturbatively small, the values of mass and spin in EdGB are expected to still lie in the proximity of the GR values.

Unlike the previous test, where we have always used the values of mass and spin of the remnant BH from the full IMR waveform, we shall now consider also the case in which we extract the values directly from the ringdown part of the signal. In particular, we will investigate both the option in which we do not make assumptions about their values, namely choosing uniform priors $M \in [10, 100]M_\odot$, $\chi \in [0, 0.99]$, and the one where we assume near-GR values, fixing the priors to

[3] We assume a standard cosmological model, which is not significantly affected by modifications with dimensionful coupling [114, 351].

$M \in [64.95, 70.70] M_\odot$, $\chi \in [0.629, 0.709]$, corresponding to IMR-informed restrictions (assuming GR) for GW150914.

As for the other parameters, we choose a flat prior on the natural logarithm of the luminosity distance, $\log D_L$, to reproduce our lack of knowledge about the parameter and to avoid favoring smaller scales and values of γ (and thus ℓ), since it depends on the redshift (see Eq. (7.5)) and consequently on the luminosity distance, once a certain cosmological model is assumed. Furthermore, since the waveform in Eq. (7.1), once the reflection symmetry of the amplitude is taken into account, is proportional to $\mathcal{A}_J/D_L$, there is a certain degree of degeneracy in specifying $\mathcal{A}_J$ and D_L; we can fix to tighter constraints one between those two parameters, namely D_L and let the other, $\mathcal{A}_J(D_L)$, span a larger (uniform) prior range, namely $[0, 50]$. We set $\log(D_L/Mpc) \in [5.3867, 6.3204]$, which includes the value found assuming GR ($D_L \sim 440 Mpc$). The phase prior for each mode J is $\phi_J \in [0, 2\pi]$, while the angles of the spheroidal harmonics in Eq. (7.2) are set to $\cos\iota = -1$ $\varphi = 0$ rad (which is reasonable for GW150914, with a face-off orientation)[4].

The strain measured by the GW detectors is $h_D(t) = F_+ h_+(t) + F_\times h_\times(t)$, where $F_{+,\times}(\alpha, \delta, \psi)$ are the detector pattern functions (see e.g. [103, 170]), which depend on the right ascension α, declination δ, and polarization ψ angles. We fix $(\alpha, \delta) = (1.16, -1.19)$ rad, while we infer ψ from the data, setting a uniform prior $\psi \in [0, \pi]$ rad.

For the beyond-GR parameter $\ell = \sqrt{\alpha_{GB}}$ we consider two possible prior distributions, $\ell \in [0, 75] km$ and $\ell \in [0, 200] km$, to allow for a broader exploration of the parameter space [5].

We fix the starting time of the analysis with respect to the Hanford detector to be $t^{H1}_{start} = 1126259462\,s$ of GPS time, corresponding to the peak of $h_+^2 + h_\times^2$, and then compute the one for the Livingston interferometer t^{L1}_{start} from the sky position parameters.

When we consider only the fundamental $(nlm) = (022)$ mode we add a time shift $t_0 = 10M$ from the peak, which is put to zero when instead we include the first overtone (122). The first overtone has been shown to improve the fit of a ringdown-only template with the full gravitational waveform of perturbed BHs, enabling the analysis to start at earlier times[238, 246, 267, 352–354], nonetheless its physical interpretation is still up for debate [131, 182]. Even though we do not include any EdGB modification in the overtone, we will consider it in order to start the analysis right from the peak and accumulate more SNR. We did not consider higher angular modes, since for GW150914 they are believed to be less excited with respect to the $l = m = 2$ multipole [129, 130].

The examined cases are summarized in Tab. 7.3, where with "IMR bound" we refer to the prior choice $M \in [64.95, 70.70] M_\odot$, $\chi \in [0.629, 0.709]$, which is based on GR. From the marginal posterior probability distributions of ℓ, which is positively defined and approximately flat around zero, we compute the upper bound at the 90% credible level $\sigma_{90}(\ell)$

$$\sigma_{90}(\ell) = \ell_{90}\,, \tag{7.24}$$

where ℓ_{90} is such that

$$\int_0^{\ell_{90}} P(\ell) d\ell = 0.9\,. \tag{7.25}$$

[4] In any case, the amplitude could be redefined to include any additional factors in the waveform template.

[5] However, one needs to keep in mind that we have to remain within the perturbative framework, $\gamma\delta\omega_J \ll 1, \gamma\delta\tau_J \ll 1$: large values of ℓ must be excluded (either at the prior level or a posteriori)

We write the results in Tab. 7.3.

We repeat the analysis in GR, switching off the EdGB corrections, for the different cases corresponding to the inclusion (or not) of IMR bounds and of the first overtone. Finally, we compute the log-Bayes factor comparing each EdGB model of Tab. 7.3 with its corresponding GR case.

The evidence for each model, evaluated from the nested sampling algorithm CPNest, is affected by a numerical uncertainty $\sqrt{H/\eta}$, with H the *information gain*, or negative entropy, related to the algorithm [332], and η is the number of live points of the MCMC. The sampler settings used correspond to 4096 live points, a maximum number of 10000 MCMC internal steps, and a pool size composed of 100 walkers.

We report these results in the last column of Tab. 7.3, while we show two examples of corner plots in Figures 7.7 and 7.8, corresponding with the cases 1 and 4, respectively.

Table 7.3: *Cases considered for the time-domain analysis of GW150914, corresponding to different prior choices for ℓ, M, χ and different modes included in the waveform. We note that the EdGB deviation is always included only on the fundamental mode* (022).

	ℓ prior	IMR bound	mode (nlm)	$\sigma_{90}(\ell)$ (km)	$\log \mathcal{B}^{EdGB}_{GR}$
1	$[0, 75]km$	✓	(022)	64.2	0.025 ± 0.102
2	$[0, 200]km$	✓	(022)	67.3	0.295 ± 0.101
3	$[0, 75]km$	✗	(022)	68.4	1.158 ± 0.108
4	$[0, 200]km$	✗	(022)	87.5	1.217 ± 0.108
5	$[0, 75]km$	✓	(022), (122)	59.8	0.382 ± 0.130
6	$[0, 200]km$	✓	(022), (122)	60.1	-0.334 ± 0.132
7	$[0, 75]km$	✗	(022), (122)	64.8	0.437 ± 0.138
8	$[0, 200]km$	✗	(022), (122)	79.9	-0.143 ± 0.139

7.5 Results

In this section, we present first a discussion of the null, theory-agnostic test, and then of the theory-specific, time-domain analysis.

Theory-agnostic Test

We have considered as a first case a nonrotating black hole, meaning $D_{nGR} = 0$ in Eq.(7.4), assuming the measurement of only the $n = 0, l = m = 2$ mode – thus we shall drop the index J identifying the mode. The only deviation parameters to constrain are $\delta\omega^{0)}, \delta\tau^{(0)}$, assuming that the masses and spins are the ones measured within GR.

In Fig. 7.5 we show the marginal posterior probability distributions of these parameters, for both CE and ET, for an increasing number of sources N_s considered and for the two catalogs under consideration; we can see how, as expected, the posteriors become narrower as the value of N_s grows.

We find that the general trend of the width of the distribution σ_j is $\sim N_s^{-1/2}$. The second model, with the distribution of sources shown in Fig. 7.3, seems to produce better constraints on the frequency deviations $\delta\omega^{(0)}_{22}$ with respect to the first scenario. The opposite happens for the

damping time corrections $\delta\tau_{22}^{(0)}$. CE, which is able to detect a significantly smaller amount of sources above the $SNR > 12$ threshold, inevitably performs worse than ET.

When considering a spinning BH, with spin corrections up to order $D_{nGR} = 2$, we find that, while we can put meaningful bounds on the frequency deviations $\delta\omega^{(0)}, \delta\omega^{(1)}, \delta\omega^{(2)}$, the same can be done only for the zeroth order damping time coefficient $\delta\tau^{(0)}$, even with a large number of sources. Indeed, with $\delta\tau^{(1)}$ and $\delta\tau^{(2)}$, the perturbative regime $\gamma\delta\tau^{(k)} \ll 1$ is no longer guaranteed.

In Figure 7.6 we show the joint 90% credible regions for the parameters which can be bounded by the data for the full set of $N_s = 13401$ ET sources in the first model. We can see, as expected, that there is a correlation between the frequency coefficients $\delta\omega^{(0)}, \delta\omega^{(1)}, \delta\omega^{(2)}$, while they are not correlated with $\delta\tau^{(0)}$. As written in Tab.7.2, considering only the physically motivated first catalog and the maximum number of sources above the SNR threshold, we find that the width for the zeroth order coefficients is $\sigma(\delta\omega^{(0)}) \sim 3 \cdot 10^{-2}$ for CE and $\sigma(\delta\omega^{(0)}) \sim 10^{-2}$ for ET; for the first order in the spin deviation to the frequency we find $\sigma(\delta\omega^{(1)}) \sim 2.1 \cdot 10^{-1}$ for CE and $\sigma(\delta\omega^{(1)}) \sim 9.4 \cdot 10^{-2}$ for ET; finally, for the second order correction we obtain $\sigma(\delta\omega^{(2)}) \sim 2.5 \cdot 10^{-1}$ for CE and $\sigma(\delta\omega^{(2)}) \sim 1.1 \cdot 10^{-1}$ for ET. As for the zeroth order correction to the damping time, we have $\sigma(\delta\tau^{(0)}) \sim 1.8 \cdot 10^{-1}$ for CE and $\sigma(\delta\tau^{(0)}) \sim 8 \cdot 10^{-2}$ for ET. We have used the second model, which has remnant objects with higher values of the final spin, to assess whether the spin can affect the final results. However, the only case in which the second model yields stronger constraints is for $\delta\tau^{(0)}$ measured from ET observations, for which the width becomes $\sigma(\delta\tau^{(0)}) \sim 2 \cdot 10^{-2}$.

As a general result, ET is expected to perform slightly better than CE.

Due to the additional information needed to resolve a larger number of correlated parameters, the width of the zeroth order beyond-GR parameters is, as expected, larger than the corresponding value for the nonrotating case.

We can conclude that with $\mathcal{O}(10^4)$ ringdown observations with ET of physically motivated BBH populations[6], as the one of the first model shown in Fig. 7.3, we will be able to constrain with good precision up to the second order corrections in the spin to the Kerr QNM frequencies and up to the zeroth order correction to the damping time. The same parameters can be constrained with $\mathcal{O}(10^3)$ ringdown observations with CE, but with larger bounds.

We plan to extend this analysis to the case of dimensionful theories, where $p = 4$, both in a theory-agnostic and theory-specific format. In this way, we will use the computation of the EdGB modifications to the QNM spectrum in Ch.6 to check whether it is possible to put bounds on the coupling constant of the theory using the measurement of the QNM spectrum.

This study will provide a broad overview of the achievable constraining power of future detectors using ringdown observations.

Theory-specific Test

We have performed a time-domain analysis of the ringdown of GW150914, implementing the ParSpec formalism in the pyRing package. We have fixed the beyond-GR parameters for the $(nlm) = (022)$ mode up to the second order in the spin to the values in Tab. 7.1, corresponding to the gravitational polar-led QNMs in EdGB gravity.

A similar analysis has been carried out by Ref. [118] on two LIGO-Virgo detections by consid-

[6] We can expect ET to detect up to $\mathcal{O}(10^5)$ BBH merger events in one year with ET with SNR ~ 10 [347] .

ering the full IMR waveform corrected with ParSpec in the ringdown. The authors show how they are not able to put constraints on EdGB. However, they focus on the axial modes and consider only the leading order corrections in the spin. We believe that including the corrections up to the second order could be crucial, since – as it happens also in GR – they could be dominant with respect to the first-order coefficients for astrophysically relevant values of the spin $\chi \gtrsim 0.5$.

In our study, we have considered both the case in which the mass and spin are free parameters to be inferred from the data and the one where we fix them to be close to the IMR predictions in GR. Furthermore, we have also examined the effect of including the first (GR) overtone to start the analysis earlier and accumulate more SNR. Finally, we allowed the scale parameter of the theory ℓ to span the interval $[0, 200]\,km$, in order to better understand the range covered by its posterior.

When we do not consider the IMR bound and the overtone, a prior $\ell \in [0, 75]km$ is not enough to enclose the posterior distributions and it is necessary to increase its width, as it can be seen from the larger values of $\sigma_{90}(\ell)$ when $\ell \in [0, 200]km$ and from the marginalized posterior for ℓ in Fig. 7.8.

In all cases, given the low SNR (~ 8 for one mode and ~ 12 for two modes) in the ringdown, we were not able to put meaningful constraints of the characteristic length ℓ of EdGB gravity. In fact, as shown by the values in Tab. 7.3 of the upper bound on ℓ at the 90% credible level, the most stringent constraint is $\ell \lesssim 60km$, which is almost near the limit of validity of the perturbative approach and not competitive with currently available bounds (for a quick review see Sec. 1.3). The inclusion of the overtone slightly improves the bounds, as expected by the moderate increase in the SNR, thus we expect these results to improve with better SNR and by stacking multiple events.

Looking at the log Bayes factors in Tab. 7.3, we can see that most of them are slightly positive values, even though when computing the evidence ratio of the two models considered in Eq. (7.8), the one with more parameters, in this case EdGB, should be disfavored by the so-called *Ockham factor* [332]. We believe that one reason behind these results could be the fact that the additional parameter ℓ, spanning a broad range of values, could better accommodate and describe the noise in the data with respect to the GR model.

We are currently further testing the numerical stability of these results – which could be relevant due to the small values of Bayes factors – and investigating their possible causes. One way to do it is by repeating the analysis for simulated signals, which are inherently noiseless, and the computation of the Bayes factors. If in this case, the Bayes factors will not favor EdGB, it could be an indication that our interpretation is correct.

Once we have access to simulated signals with arbitrary values of SNR, we will also be able to understand what is the minimum value, assuming that EdGB is the right model, to detect the deviations from GR. This analysis will be of great importance to determine the ability of future detectors, such as the Einstein Telescope and Cosmic Explorer, naturally preferred to test EdGB, to constrain the theory.

As the main objective of this analysis, which is still in the preliminary stage, we will investigate how much these constraints will improve by stacking multiple observations, and how many of them are necessary to reach high accuracy.

Finally, we will test whether alternative parametrizations, such as a Padé model (see Sec. 6.2.2, could improve the results with respect to the polynomial one of Eq. (7.4), which is known to not be optimal to describe the QNM spectrum (see e.g. [170, 355]).

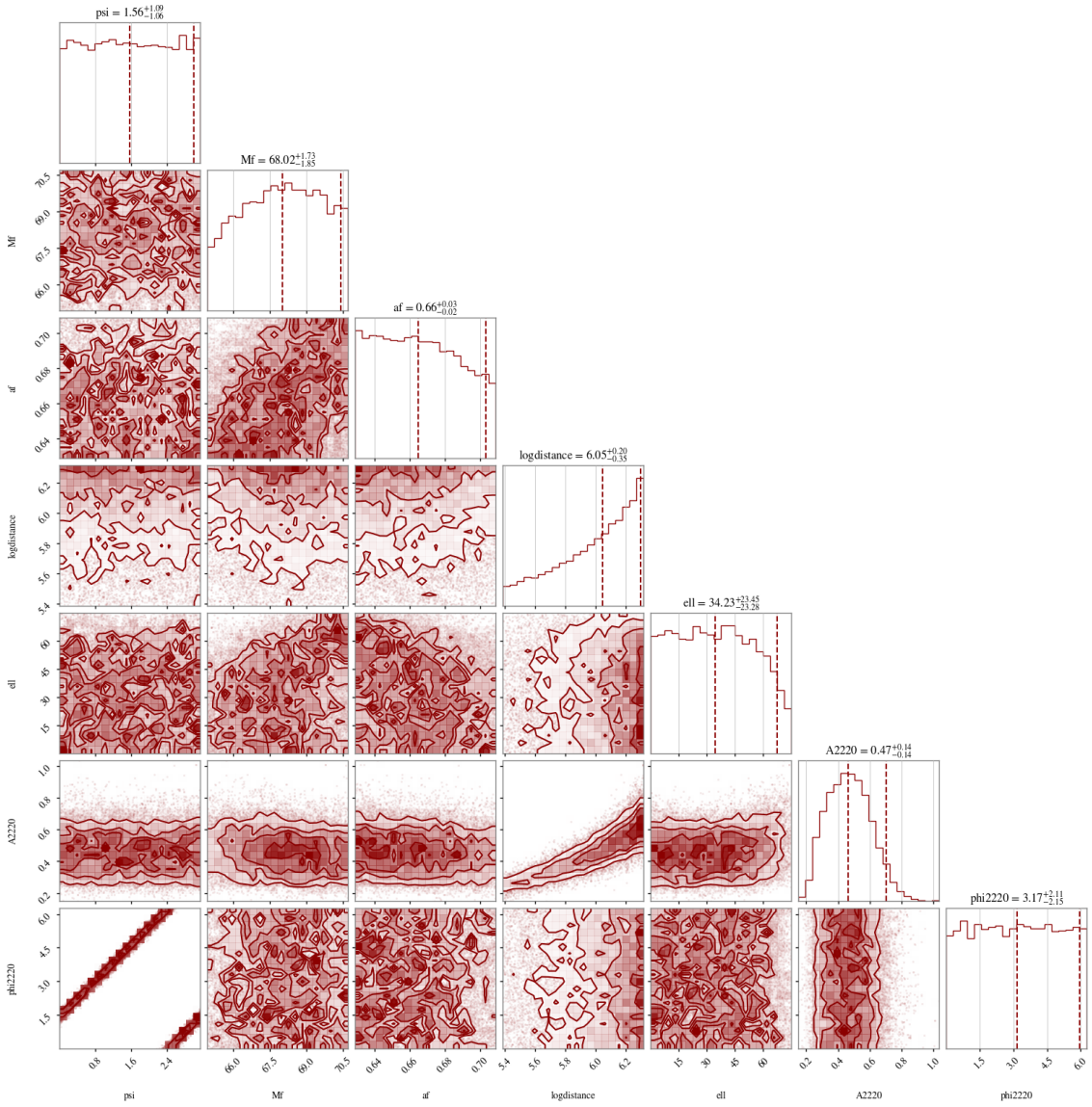

Figure 7.7: *Corner plot containing the marginal posterior distributions of the considered parameters for the case* 1 *in Tab. 7.3. From left to right the parameters are: polarization angle* ψ*, final mass* M*, final spin* χ*,* $\log D_L$*,* ℓ*,* A_{022}*,* ϕ_{022}*.*

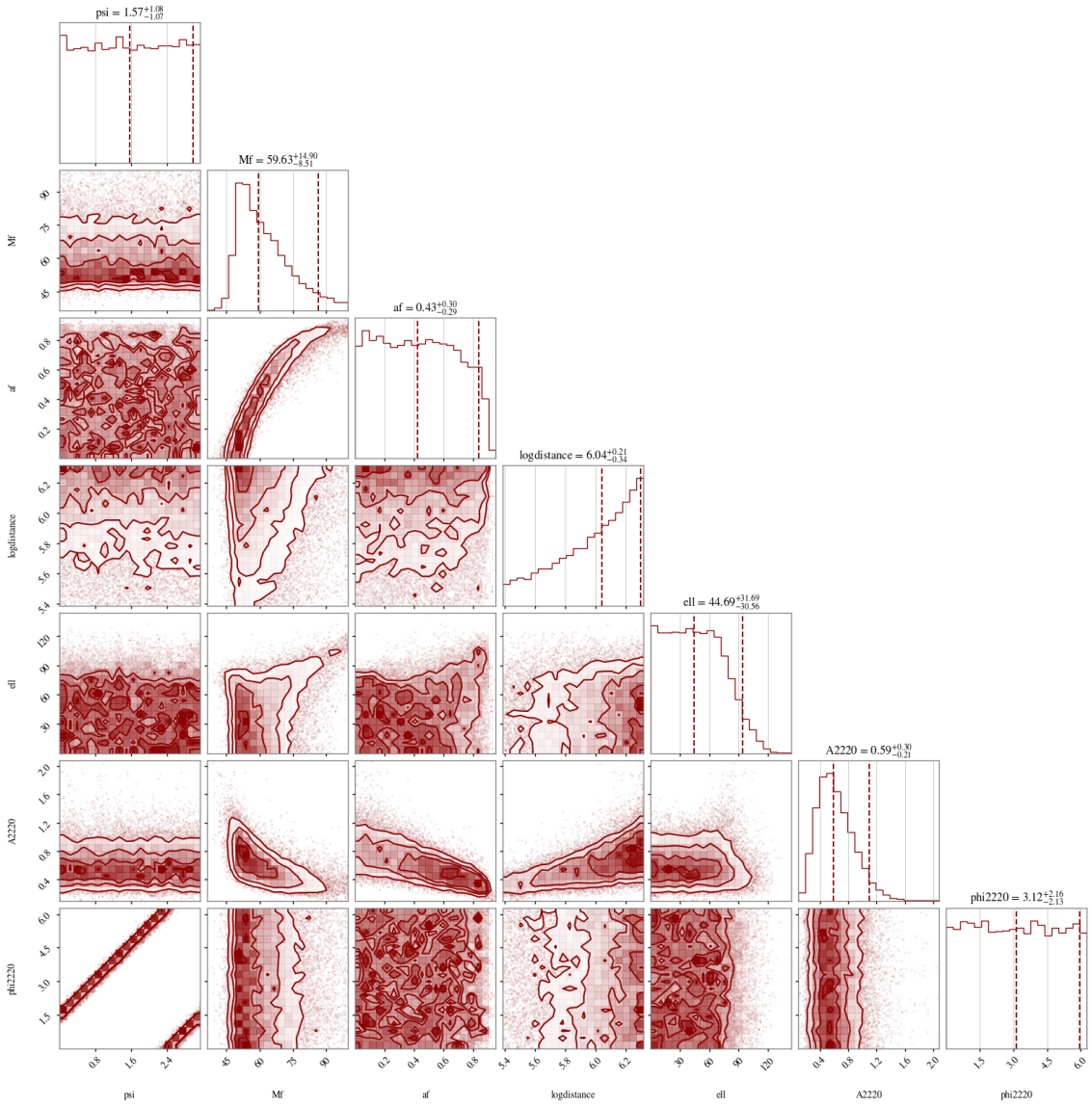

Figure 7.8: *Corner plot containing the marginal posterior distributions of the considered parameters for the case* 4 *in Tab. 7.3. From left to right the parameters are: polarization angle* ψ*, final mass* M*, final spin* χ*,* $\log D_L$*,* ℓ*,* A_{022}*,* ϕ_{022}*.*

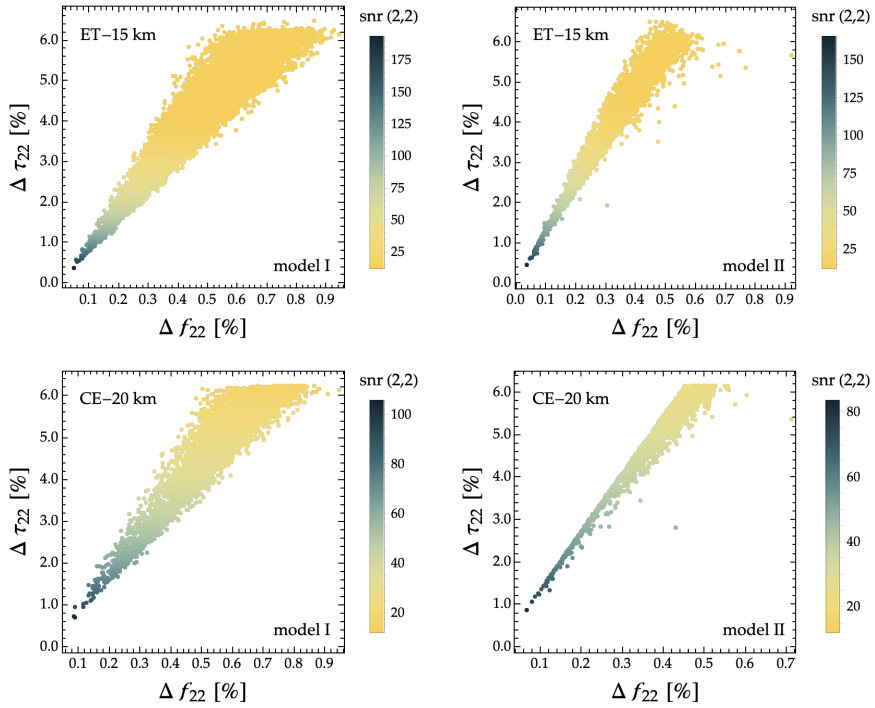

Figure 7.9: *Relative percentage errors on the frequency and the damping time of the fundamental $l = m = 2$ for the binary systems described in Sec. 7.3. The color scheme identifies the SNR of the $(2, 2)$ mode as detected by ET (top row) and CE (bottom row).*

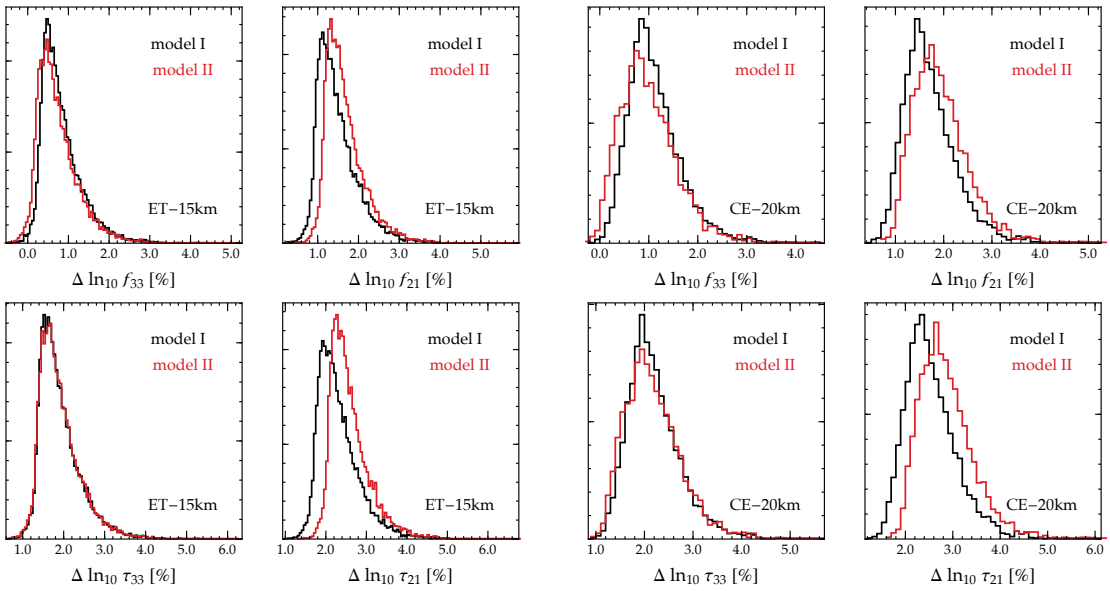

Figure 7.10: *Relative percentage errors on the frequency and the damping time of the secondary modes, $(l, m) = (3, 3)$ and $(\ell, m) = (2, 1)$, for ET and CE. Black and red histograms refer to the two population models we considered.*

Chapter 8

Conclusions

In this Thesis, after introducing the concept of Quasinormal Modes (QNMs) and their connection with the underlying theory of gravity, we have computed the QNM spectrum up to second order in the spin for a quadratic modified theory of gravity, Einstein-dilaton Gauss-Bonnet (EdGB), one of the simplest theories that modify General Relativity (GR) in the large-curvature, strong-field regime.

Starting from the cases of a test scalar field in EdGB gravity and of nonrotating Dilatonic Black Holes, for which we found agreement with results present in the literature, we generalized our direct integration method to compute the EdGB gravitational QNM spectrum in a slow-rotation framework up to the second order in the spin. As suggested by a comparison with the general relativistic case, the use of Padé approximants allows for a broader range of validity of the expansion: the QNMs derived with this approach should be accurate within $\sim 2\%$ up to spins $\bar{a} \lesssim 0.7$.

Our analysis reveals that the second-order contribution yields a significant amplification of the EdGB correction to the quasinormal modes. For instance, assuming a BH spin of $\bar{a} = 0.7$, the real part of the $(nlm) = (022)$ mode – which is typically excited with the largest amplitude in BH ringdowns (see e.g. [178]) – gets a correction, with respect to the GR counterpart, estimated to be of $\simeq 1\%$ at $\mathcal{O}(\bar{a})$, while the same estimate at $\mathcal{O}(\bar{a}^2)$ (with Padé resummation) is of $\simeq 2.5\%$.

Our computation has been performed by expanding the background metric of the dilatonic black hole and the field equations describing its perturbations in the dimensionless coupling constant ζ up to the sixth order and in the spin $\bar{a}$ up to the second order. An analysis of the truncation error indicates that our results are accurate for $\zeta \lesssim 0.4$ for the real parts of the modes, $\zeta \lesssim 0.3$ for the imaginary parts. As a result, we provided analytical fits of the QNMs valid in this range of the coupling constant.

This computation will be useful, once full numerical simulations of BH coalescences in EdGB gravity will be available [72, 73, 75], as a benchmark to test the numerical codes.

The mode corrections in specific extensions of General Relativity are a necessary ingredient for the implementation of gravitational spectroscopy in the context of theory-specific tests of Einstein's theory. Since with the Padé resummation we were able to extend our QNM results up to physically relevant values of the spin, they can be employed to perform such tests.

To this purpose, in the final part of the Thesis, we have explored two possible avenues to construct ringdown tests with a parametrized framework called ParSpec. In the first approach, relying on a Fisher matrix computation of the QNM errors and on an MCMC sampling algorithm

of the posterior distributions, we performed a theory-agnostic null test of GR considering scale-free corrections and inferring the GR-deviation parameters up to the second order in the spin. Focusing on realistic sources detectable by Einstein Telescope and Cosmic Explorer, we have found that all the spin expansion coefficients of the QNM frequency (at least) up to the second order can be bounded with good precision with $\mathcal{O}(10^4)$ observations for the first detector and with $\mathcal{O}(10^3)$ observations for the second, which are within the predicted amount of detections.

We plan on extending this test to theories characterized by a dimensionful coupling constant, such as EdGB and dynamical Chern-Simons, and adapt it to a theory-specific framework by fixing the deviation parameters to the values computed in this Thesis and in Refs. [66, 69].

In the second approach, consisting of a theory-specific test of GR, we have included the ParSpec parametrization and the EdGB deviation parameters into the pyRing package to perform a time-domain analysis of the ringdown signal of GW150914, considered as a first application of the method. As expected, due to the currently available low Signal-to-Noise ratio in the ringdown, we were not able to put meaningful constraints on the coupling constant of the theory. Although a computation of the Bayes factor seems in general to slightly favor EdGB with respect to GR, we are currently testing the numerical stability of the analysis and possible causes of this occurrence. The next steps will be to consider simulated signals to better understand how the noise affects the results and what level of SNR is needed to achieve stringent constraints on the theory.

For both methods, we plan to test an alternative parametrization template of the QNMs, given by the Padé approximant, which might improve the constraining power with respect to the currently used polynomial form.

This is the first computation, in a modified gravity theory, of the QNMs of BHs to second order in rotation. Although EdGB gravity is an interesting theory by itself for several reasons, the analysis carried out in this Thesis can be considered as a case study to understand which kind of deviation we may expect in the ringdown signal and assess its detectability with current and future detectors; the same procedure can be extended to other classes of possible GR deviations.

Bibliography

[1] Emanuele Berti, Vitor Cardoso, and Andrei O. Starinets. Quasinormal modes of black holes and black branes. *Class. Quant. Grav.*, 26:163001, 2009. doi: 10.1088/0264-9381/26/16/163001.

[2] B. P. Abbott et al. Observation of Gravitational Waves from a Binary Black Hole Merger. *Phys. Rev. Lett.*, 116(6):061102, 2016. doi: 10.1103/PhysRevLett.116.061102.

[3] Jose Luis Blázquez-Salcedo, Caio F. B. Macedo, Vitor Cardoso, Valeria Ferrari, Leonardo Gualtieri, Fech Scen Khoo, Jutta Kunz, and Paolo Pani. Perturbed black holes in Einstein-dilaton-Gauss-Bonnet gravity: Stability, ringdown, and gravitational-wave emission. *Phys. Rev. D*, 94(10):104024, 2016. doi: 10.1103/PhysRevD.94.104024.

[4] Pablo A. Cano, Kwinten Fransen, and Thomas Hertog. Ringing of rotating black holes in higher-derivative gravity. *Phys. Rev. D*, 102(4):044047, 2020. doi: 10.1103/PhysRevD.102.044047.

[5] B. P. Abbott et al. Observation of Gravitational Waves from a Binary Black Hole Merger. *Phys. Rev. Lett.*, 116(6):061102, 2016. doi: 10.1103/PhysRevLett.116.061102.

[6] B. P. Abbott et al. GWTC-1: A Gravitational-Wave Transient Catalog of Compact Binary Mergers Observed by LIGO and Virgo during the First and Second Observing Runs. *Phys. Rev. X*, 9(3):031040, 2019. doi: 10.1103/PhysRevX.9.031040.

[7] R. Abbott et al. GWTC-2: Compact Binary Coalescences Observed by LIGO and Virgo During the First Half of the Third Observing Run. *Phys. Rev. X*, 11:021053, 2021. doi: 10.1103/PhysRevX.11.021053.

[8] R. Abbott et al. GWTC-2.1: Deep Extended Catalog of Compact Binary Coalescences Observed by LIGO and Virgo During the First Half of the Third Observing Run. 8 2021.

[9] R. Abbott et al. GWTC-3: Compact Binary Coalescences Observed by LIGO and Virgo During the Second Part of the Third Observing Run. 11 2021.

[10] J. Aasi et al. Advanced LIGO. *Class. Quant. Grav.*, 32:074001, 2015. doi: 10.1088/0264-9381/32/7/074001.

[11] F. Acernese et al. Advanced Virgo: a second-generation interferometric gravitational wave detector. *Class. Quant. Grav.*, 32(2):024001, 2015. doi: 10.1088/0264-9381/32/2/024001.

[12] R. Abbott et al. Constraints on the cosmic expansion history from GWTC-3. 11 2021.

[13] R. Abbott et al. The population of merging compact binaries inferred using gravitational waves through GWTC-3. 11 2021.

[14] Nicolás Yunes, Kent Yagi, and Frans Pretorius. Theoretical physics implications of the binary black-hole mergers gw150914 and gw151226. *Phys. Rev. D*, 94:084002, Oct 2016. doi: 10.1103/PhysRevD.94.084002. URL `https://link.aps.org/doi/10.1103/PhysRevD.94.084002`.

[15] R. Abbott et al. Tests of General Relativity with GWTC-3. 12 2021.

[16] Jonathan R. Gair, Michele Vallisneri, Shane L. Larson, and John G. Baker. Testing General Relativity with Low-Frequency, Space-Based Gravitational-Wave Detectors. *Living Rev. Rel.*, 16:7, 2013. doi: 10.12942/lrr-2013-7.

[17] Nicolás Yunes and Xavier Siemens. Gravitational-Wave Tests of General Relativity with Ground-Based Detectors and Pulsar Timing-Arrays. *Living Rev. Rel.*, 16:9, 2013. doi: 10.12942/lrr-2013-9.

[18] Emanuele Berti et al. Testing General Relativity with Present and Future Astrophysical Observations. *Class. Quant. Grav.*, 32:243001, 2015. doi: 10.1088/0264-9381/32/24/243001.

[19] Kazunori Akiyama et al. First M87 Event Horizon Telescope Results. I. The Shadow of the Supermassive Black Hole. *Astrophys. J. Lett.*, 875:L1, 2019. doi: 10.3847/2041-8213/ab0ec7.

[20] Kazunori Akiyama et al. First Sagittarius A* Event Horizon Telescope Results. I. The Shadow of the Supermassive Black Hole in the Center of the Milky Way. *Astrophys. J. Lett.*, 930(2): L12, 2022. doi: 10.3847/2041-8213/ac6674.

[21] Clifford M. Will. The Confrontation between General Relativity and Experiment. *Living Rev. Rel.*, 17:4, 2014. doi: 10.12942/lrr-2014-4.

[22] Ingrid H. Stairs. Testing general relativity with pulsar timing. *Living Rev. Rel.*, 6:5, 2003. doi: 10.12942/lrr-2003-5.

[23] Norbert Wex. Testing Relativistic Gravity with Radio Pulsars. 2 2014.

[24] M. Kramer et al. Strong-Field Gravity Tests with the Double Pulsar. *Phys. Rev. X*, 11(4): 041050, 2021. doi: 10.1103/PhysRevX.11.041050.

[25] R. Abuter et al. Detection of the gravitational redshift in the orbit of the star S2 near the Galactic centre massive black hole. *Astron. Astrophys.*, 615:L15, 2018. doi: 10.1051/0004-6361/201833718.

[26] Tuan Do et al. Relativistic redshift of the star S0-2 orbiting the Galactic center supermassive black hole. *Science*, 365(6454):664–668, 2019. doi: 10.1126/science.aav8137.

[27] Timothy Clifton, Pedro G. Ferreira, Antonio Padilla, and Constantinos Skordis. Modified Gravity and Cosmology. *Phys. Rept.*, 513:1–189, 2012. doi: 10.1016/j.physrep.2012.01.001.

[28] Austin Joyce, Bhuvnesh Jain, Justin Khoury, and Mark Trodden. Beyond the Cosmological Standard Model. *Phys. Rept.*, 568:1–98, 2015. doi: 10.1016/j.physrep.2014.12.002.

[29] Kazuya Koyama. Cosmological Tests of Modified Gravity. *Rept. Prog. Phys.*, 79(4):046902, 2016. doi: 10.1088/0034-4885/79/4/046902.

[30] Pedro G. Ferreira. Cosmological Tests of Gravity. *Ann. Rev. Astron. Astrophys.*, 57:335–374, 2019. doi: 10.1146/annurev-astro-091918-104423.

[31] B. P. Abbott et al. Tests of general relativity with GW150914. *Phys. Rev. Lett.*, 116(22): 221101, 2016. doi: 10.1103/PhysRevLett.116.221101. [Erratum: Phys.Rev.Lett. 121, 129902 (2018)].

[32] B. P. Abbott et al. Tests of General Relativity with the Binary Black Hole Signals from the LIGO-Virgo Catalog GWTC-1. *Phys. Rev. D*, 100(10):104036, 2019. doi: 10.1103/PhysRevD.100.104036.

[33] Abbott R. *et al.* (LIGO Scientific Collaboration). Tests of general relativity with binary black holes from the second ligo-virgo gravitational-wave transient catalog. *Phys. Rev. D*, 103: 122002, Jun 2021. doi: 10.1103/PhysRevD.103.122002. URL `https://link.aps.org/doi/10.1103/PhysRevD.103.122002`.

[34] Sheila Dwyer, Daniel Sigg, Stefan W. Ballmer, Lisa Barsotti, Nergis Mavalvala, and Matthew Evans. Gravitational wave detector with cosmological reach. *Phys. Rev. D*, 91:082001, Apr 2015. doi: 10.1103/PhysRevD.91.082001. URL `https://link.aps.org/doi/10.1103/PhysRevD.91.082001`.

[35] M. Punturo et al. The Einstein Telescope: A third-generation gravitational wave observatory. *Class. Quant. Grav.*, 27:194002, 2010. doi: 10.1088/0264-9381/27/19/194002.

[36] Michele Maggiore et al. Science Case for the Einstein Telescope. *JCAP*, 03:050, 2020. doi: 10.1088/1475-7516/2020/03/050.

[37] Pau Amaro-Seoane et al. Laser Interferometer Space Antenna. 2 2017.

[38] Emanuele Berti, Alberto Sesana, Enrico Barausse, Vitor Cardoso, and Krzysztof Belczynski. Spectroscopy of kerr black holes with earth- and space-based interferometers. *Phys. Rev. Lett.*, 117:101102, Sep 2016. doi: 10.1103/PhysRevLett.117.101102. URL `https://link.aps.org/doi/10.1103/PhysRevLett.117.101102`.

[39] Benjamin P Abbott et al. Exploring the Sensitivity of Next Generation Gravitational Wave Detectors. *Class. Quant. Grav.*, 34(4):044001, 2017. doi: 10.1088/1361-6382/aa51f4.

[40] Reed Essick, Salvatore Vitale, and Matthew Evans. Frequency-dependent responses in third generation gravitational-wave detectors. *Phys. Rev. D*, 96:084004, Oct 2017. doi: 10.1103/PhysRevD.96.084004. URL `https://link.aps.org/doi/10.1103/PhysRevD.96.084004`.

[41] S. Hild et al. Sensitivity Studies for Third-Generation Gravitational Wave Observatories. *Class. Quant. Grav.*, 28:094013, 2011. doi: 10.1088/0264-9381/28/9/094013.

[42] Leor Barack et al. Black holes, gravitational waves and fundamental physics: a roadmap. *Class. Quant. Grav.*, 36(14):143001, 2019. doi: 10.1088/1361-6382/ab0587.

[43] Valentina Salvatelli, Federico Piazza, and Christian Marinoni. Constraints on modified gravity from Planck 2015: when the health of your theory makes the difference. *JCAP*, 09:027, 2016. doi: 10.1088/1475-7516/2016/09/027.

[44] Mordehai Milgrom. The MOND paradigm. 1 2008.

[45] Benoit Famaey and Stacy McGaugh. Modified Newtonian Dynamics (MOND): Observational Phenomenology and Relativistic Extensions. *Living Rev. Rel.*, 15:10, 2012. doi: 10.12942/lrr-2012-10.

[46] Salvatore Capozziello and Mariafelicia De Laurentis. Extended Theories of Gravity. *Phys. Rept.*, 509:167–321, 2011. doi: 10.1016/j.physrep.2011.09.003.

[47] Christos Charmousis, Edmund J. Copeland, Antonio Padilla, and Paul M. Saffin. Self-tuning and the derivation of a class of scalar-tensor theories. *Phys. Rev. D*, 85:104040, May 2012. doi: 10.1103/PhysRevD.85.104040. URL `https://link.aps.org/doi/10.1103/PhysRevD.85.104040`.

[48] Christos Charmousis, Edmund J. Copeland, Antonio Padilla, and Paul M. Saffin. General second-order scalar-tensor theory and self-tuning. *Phys. Rev. Lett.*, 108:051101, Jan 2012. doi: 10.1103/PhysRevLett.108.051101. URL `https://link.aps.org/doi/10.1103/PhysRevLett.108.051101`.

[49] Claudia de Rham, Gregory Gabadadze, Lavinia Heisenberg, and David Pirtskhalava. Cosmic acceleration and the helicity-0 graviton. *Phys. Rev. D*, 83:103516, May 2011. doi: 10.1103/PhysRevD.83.103516. URL `https://link.aps.org/doi/10.1103/PhysRevD.83.103516`.

[50] Claudia de Rham, Gregory Gabadadze, and Andrew J. Tolley. Resummation of massive gravity. *Phys. Rev. Lett.*, 106:231101, Jun 2011. doi: 10.1103/PhysRevLett.106.231101. URL `https://link.aps.org/doi/10.1103/PhysRevLett.106.231101`.

[51] G. D'Amico, C. de Rham, S. Dubovsky, G. Gabadadze, D. Pirtskhalava, and A. J. Tolley. Massive cosmologies. *Phys. Rev. D*, 84:124046, Dec 2011. doi: 10.1103/PhysRevD.84.124046. URL `https://link.aps.org/doi/10.1103/PhysRevD.84.124046`.

[52] Adam G. Riess, Alexei V. Filippenko, Peter Challis, Alejandro Clocchiatti, Alan Diercks, Peter M. Garnavich, Ron L. Gilliland, Craig J. Hogan, Saurabh Jha, Robert P. Kirshner, B. Leibundgut, M. M. Phillips, David Reiss, Brian P. Schmidt, Robert A. Schommer, R. Chris Smith, J. Spyromilio, Christopher Stubbs, Nicholas B. Suntzeff, and John Tonry. Observational evidence from supernovae for an accelerating universe and a cosmological constant. *The Astronomical Journal*, 116(3):1009, sep 1998. doi: 10.1086/300499. URL `https://dx.doi.org/10.1086/300499`.

[53] S. Perlmutter, G. Aldering, G. Goldhaber, R. A. Knop, P. Nugent, P. G. Castro, S. Deustua, S. Fabbro, A. Goobar, D. E. Groom, I. M. Hook, A. G. Kim, M. Y. Kim, J. C. Lee, N. J. Nunes, R. Pain, C. R. Pennypacker, R. Quimby, C. Lidman, R. S. Ellis, M. Irwin, R. G. McMahon, P. Ruiz-Lapuente, N. Walton, B. Schaefer, B. J. Boyle, A. V. Filippenko, T. Matheson, A. S. Fruchter, N. Panagia, H. J. M. Newberg, W. J. Couch, and The Supernova Cosmology Project.

Measurements of ω and λ from 42 high-redshift supernovae. *The Astrophysical Journal*, 517 (2):565, jun 1999. doi: 10.1086/307221. URL https://dx.doi.org/10.1086/307221.

[54] David J. Gross and John H. Sloan. The quartic effective action for the heterotic string. *Nuclear Physics B*, 291:41–89, 1987. ISSN 0550-3213. doi: https://doi.org/10.1016/0550-3213(87)90465-2. URL https://www.sciencedirect.com/science/article/pii/0550321387904652.

[55] K. S. Stelle. Renormalization of higher-derivative quantum gravity. *Phys. Rev. D*, 16:953–969, Aug 1977. doi: 10.1103/PhysRevD.16.953. URL https://link.aps.org/doi/10.1103/PhysRevD.16.953.

[56] Clifford M. Will. Testing scalar-tensor gravity with gravitational-wave observations of inspiralling compact binaries. *Phys. Rev. D*, 50:6058–6067, Nov 1994. doi: 10.1103/PhysRevD.50.6058. URL https://link.aps.org/doi/10.1103/PhysRevD.50.6058.

[57] Ryan N. Lang. Compact binary systems in scalar-tensor gravity. ii. tensor gravitational waves to second post-newtonian order. *Phys. Rev. D*, 89:084014, Apr 2014. doi: 10.1103/PhysRevD.89.084014. URL https://link.aps.org/doi/10.1103/PhysRevD.89.084014.

[58] Ryan N. Lang. Compact binary systems in scalar-tensor gravity. iii. scalar waves and energy flux. *Phys. Rev. D*, 91:084027, Apr 2015. doi: 10.1103/PhysRevD.91.084027. URL https://link.aps.org/doi/10.1103/PhysRevD.91.084027.

[59] Noah Sennett, Sylvain Marsat, and Alessandra Buonanno. Gravitational waveforms in scalar-tensor gravity at 2pn relative order. *Phys. Rev. D*, 94:084003, Oct 2016. doi: 10.1103/PhysRevD.94.084003. URL https://link.aps.org/doi/10.1103/PhysRevD.94.084003.

[60] Mohammed Khalil, Noah Sennett, Jan Steinhoff, Justin Vines, and Alessandra Buonanno. Hairy binary black holes in einstein-maxwell-dilaton theory and their effective-one-body description. *Phys. Rev. D*, 98:104010, Nov 2018. doi: 10.1103/PhysRevD.98.104010. URL https://link.aps.org/doi/10.1103/PhysRevD.98.104010.

[61] Sharaban Tahura and Kent Yagi. Parametrized post-einsteinian gravitational waveforms in various modified theories of gravity. *Phys. Rev. D*, 98:084042, Oct 2018. doi: 10.1103/PhysRevD.98.084042. URL https://link.aps.org/doi/10.1103/PhysRevD.98.084042.

[62] Laura Bernard. Dynamics of compact binary systems in scalar-tensor theories: Equations of motion to the third post-newtonian order. *Phys. Rev. D*, 98:044004, Aug 2018. doi: 10.1103/PhysRevD.98.044004. URL https://link.aps.org/doi/10.1103/PhysRevD.98.044004.

[63] Laura Bernard. Dynamics of compact binary systems in scalar-tensor theories. ii. center-of-mass and conserved quantities to 3pn order. *Phys. Rev. D*, 99:044047, Feb 2019. doi: 10.1103/PhysRevD.99.044047. URL https://link.aps.org/doi/10.1103/PhysRevD.99.044047.

[64] Thomas Sotiriou and Enrico Barausse. Post-newtonian expansion for gauss-bonnet gravity. *Phys. Rev. D*, 75:084007, Apr 2007. doi: 10.1103/PhysRevD.75.084007. URL https://link.aps.org/doi/10.1103/PhysRevD.75.084007.

[65] Banafsheh Shiralilou, Tanja Hinderer, Samaya M. Nissanke, Néstor Ortiz, and Helvi Witek. Post-Newtonian gravitational and scalar waves in scalar-Gauss–Bonnet gravity. *Class. Quant. Grav.*, 39(3):035002, 2022. doi: 10.1088/1361-6382/ac4196.

[66] Pratik Wagle, Nicolas Yunes, and Hector O. Silva. Quasinormal modes of slowly-rotating black holes in dynamical Chern-Simons gravity. *Phys. Rev. D*, 105(12):124003, 2022. doi: 10.1103/PhysRevD.105.124003.

[67] Lorenzo Pierini and Leonardo Gualtieri. Quasi-normal modes of rotating black holes in Einstein-dilaton Gauss-Bonnet gravity: the first order in rotation. *Phys. Rev. D*, 103:124017, 2021. doi: 10.1103/PhysRevD.103.124017.

[68] Lorenzo Pierini and Leonardo Gualtieri. Quasinormal modes of rotating black holes in Einstein-dilaton Gauss-Bonnet gravity: The second order in rotation. *Phys. Rev. D*, 106 (10):104009, 2022. doi: 10.1103/PhysRevD.106.104009.

[69] Manu Srivastava, Yanbei Chen, and S. Shankaranarayanan. Analytical computation of quasinormal modes of slowly rotating black holes in dynamical Chern-Simons gravity. *Phys. Rev. D*, 104(6):064034, 2021. doi: 10.1103/PhysRevD.104.064034.

[70] Enrico Barausse, Carlos Palenzuela, Marcelo Ponce, and Luis Lehner. Neutron-star mergers in scalar-tensor theories of gravity. *Phys. Rev. D*, 87:081506, Apr 2013. doi: 10.1103/PhysRevD.87.081506. URL `https://link.aps.org/doi/10.1103/PhysRevD.87.081506`.

[71] Masaru Shibata, Keisuke Taniguchi, Hirotada Okawa, and Alessandra Buonanno. Coalescence of binary neutron stars in a scalar-tensor theory of gravity. *Phys. Rev. D*, 89:084005, Apr 2014. doi: 10.1103/PhysRevD.89.084005. URL `https://link.aps.org/doi/10.1103/PhysRevD.89.084005`.

[72] Maria Okounkova. Numerical relativity simulation of GW150914 in Einstein dilaton Gauss-Bonnet gravity. *Phys. Rev. D*, 102(8):084046, 2020. doi: 10.1103/PhysRevD.102.084046.

[73] Helvi Witek, Leonardo Gualtieri, Paolo Pani, and Thomas P. Sotiriou. Black holes and binary mergers in scalar Gauss-Bonnet gravity: scalar field dynamics. *Phys. Rev. D*, 99(6):064035, 2019. doi: 10.1103/PhysRevD.99.064035.

[74] Maria Okounkova, Leo C. Stein, Jordan Moxon, Mark A. Scheel, and Saul A. Teukolsky. Numerical relativity simulation of GW150914 beyond general relativity. *Phys. Rev. D*, 101 (10):104016, 2020. doi: 10.1103/PhysRevD.101.104016.

[75] William E. East and Justin L. Ripley. Evolution of einstein-scalar-gauss-bonnet gravity using a modified harmonic formulation. *Phys. Rev. D*, 103:044040, Feb 2021. doi: 10.1103/PhysRevD.103.044040. URL `https://link.aps.org/doi/10.1103/PhysRevD.103.044040`.

[76] Juan Cayuso, Néstor Ortiz, and Luis Lehner. Fixing extensions to general relativity in the nonlinear regime. *Phys. Rev. D*, 96:084043, Oct 2017. doi: 10.1103/PhysRevD.96.084043. URL `https://link.aps.org/doi/10.1103/PhysRevD.96.084043`.

[77] Ramiro Cayuso and Luis Lehner. Nonlinear, noniterative treatment of eft-motivated gravity. *Phys. Rev. D*, 102:084008, Oct 2020. doi: 10.1103/PhysRevD.102.084008. URL `https://link.aps.org/doi/10.1103/PhysRevD.102.084008`.

[78] Gwyneth Allwright and Luis Lehner. Towards the nonlinear regime in extensions to GR: assessing possible options. *Class. Quant. Grav.*, 36(8):084001, 2019. doi: 10.1088/1361-6382/ab0ee1.

[79] Tyson B. Littenberg and Neil J. Cornish. Bayesian inference for spectral estimation of gravitational wave detector noise. *Phys. Rev. D*, 91:084034, Apr 2015. doi: 10.1103/PhysRevD.91.084034. URL `https://link.aps.org/doi/10.1103/PhysRevD.91.084034`.

[80] Neil J. Cornish, Tyson B. Littenberg, Bence Bécsy, Katerina Chatziioannou, James A. Clark, Sudarshan Ghonge, and Margaret Millhouse. Bayeswave analysis pipeline in the era of gravitational wave observations. *Phys. Rev. D*, 103:044006, Feb 2021. doi: 10.1103/PhysRevD.103.044006. URL `https://link.aps.org/doi/10.1103/PhysRevD.103.044006`.

[81] Gregory Ashton et al. BILBY: A user-friendly Bayesian inference library for gravitational-wave astronomy. *Astrophys. J. Suppl.*, 241(2):27, 2019. doi: 10.3847/1538-4365/ab06fc.

[82] I. M. Romero-Shaw et al. Bayesian inference for compact binary coalescences with bilby: validation and application to the first LIGO–Virgo gravitational-wave transient catalogue. *Mon. Not. Roy. Astron. Soc.*, 499(3):3295–3319, 2020. doi: 10.1093/mnras/staa2850.

[83] Katerina Chatziioannou, Maximiliano Isi, Carl-Johan Haster, and Tyson B. Littenberg. Morphology-independent test of the mixed polarization content of transient gravitational wave signals. *Phys. Rev. D*, 104:044005, Aug 2021. doi: 10.1103/PhysRevD.104.044005. URL `https://link.aps.org/doi/10.1103/PhysRevD.104.044005`.

[84] Maria Okounkova, Maximiliano Isi, Katerina Chatziioannou, and Will M. Farr. Gravitational wave inference on a numerical-relativity simulation of a black hole merger beyond general relativity. *Phys. Rev. D*, 107(2):024046, 2023. doi: 10.1103/PhysRevD.107.024046.

[85] William E. East and Justin L. Ripley. Dynamics of spontaneous black hole scalarization and mergers in einstein-scalar-gauss-bonnet gravity. *Phys. Rev. Lett.*, 127:101102, Sep 2021. doi: 10.1103/PhysRevLett.127.101102. URL `https://link.aps.org/doi/10.1103/PhysRevLett.127.101102`.

[86] Helvi Witek, Leonardo Gualtieri, and Paolo Pani. Towards numerical relativity in scalar gauss-bonnet gravity: $3+1$ decomposition beyond the small-coupling limit. *Phys. Rev. D*, 101:124055, Jun 2020. doi: 10.1103/PhysRevD.101.124055. URL `https://link.aps.org/doi/10.1103/PhysRevD.101.124055`.

[87] Nicolás Yunes and Frans Pretorius. Fundamental theoretical bias in gravitational wave astrophysics and the parametrized post-einsteinian framework. *Phys. Rev. D*, 80:122003, Dec 2009. doi: 10.1103/PhysRevD.80.122003. URL `https://link.aps.org/doi/10.1103/PhysRevD.80.122003`.

[88] M. Agathos, W. Del Pozzo, T. G. F. Li, C. Van Den Broeck, J. Veitch, and S. Vitale. Tiger: A data analysis pipeline for testing the strong-field dynamics of general relativity with gravitational wave signals from coalescing compact binaries. *Phys. Rev. D*, 89:082001, Apr 2014. doi: 10.1103/PhysRevD.89.082001. URL https://link.aps.org/doi/10.1103/PhysRevD.89.082001.

[89] Alvin J. K. Chua and Michele Vallisneri. On parametric tests of relativity with false degrees of freedom. 6 2020.

[90] Luc Blanchet. Gravitational Radiation from Post-Newtonian Sources and Inspiralling Compact Binaries. *Living Rev. Rel.*, 17:2, 2014. doi: 10.12942/lrr-2014-2.

[91] Frans Pretorius. Evolution of binary black-hole spacetimes. *Phys. Rev. Lett.*, 95:121101, Sep 2005. doi: 10.1103/PhysRevLett.95.121101. URL https://link.aps.org/doi/10.1103/PhysRevLett.95.121101.

[92] M. Campanelli, C. O. Lousto, P. Marronetti, and Y. Zlochower. Accurate evolutions of orbiting black-hole binaries without excision. *Phys. Rev. Lett.*, 96:111101, Mar 2006. doi: 10.1103/PhysRevLett.96.111101. URL https://link.aps.org/doi/10.1103/PhysRevLett.96.111101.

[93] John G. Baker, Joan Centrella, Dae-Il Choi, Michael Koppitz, and James van Meter. Gravitational-wave extraction from an inspiraling configuration of merging black holes. *Phys. Rev. Lett.*, 96:111102, Mar 2006. doi: 10.1103/PhysRevLett.96.111102. URL https://link.aps.org/doi/10.1103/PhysRevLett.96.111102.

[94] C. V. Vishveshwara. Stability of the schwarzschild metric. *Phys. Rev. D*, 1:2870–2879, 1970. doi: 10.1103/PhysRevD.1.2870.

[95] C. V. Vishveshwara. Scattering of gravitational radiation by a schwarzschild black-hole. *Nature*, 227(5261):936–938, 1970. doi: 10.1038/227936a0. URL https://doi.org/10.1038/227936a0.

[96] William H. Press. Long Wave Trains of Gravitational Waves from a Vibrating Black Hole. *Astrophysical Journal, Letters*, 170:L105, December 1971. doi: 10.1086/180849.

[97] S. Chandrasekhar and Steven L. Detweiler. The quasi-normal modes of the Schwarzschild black hole. *Proc. Roy. Soc. Lond. A*, 344:441–452, 1975. doi: 10.1098/rspa.1975.0112.

[98] S. Detweiler. Black holes and gravitational waves. III - The resonant frequencies of rotating holes. *Astrophysical Journal*, 239:292–295, July 1980. doi: 10.1086/158109.

[99] Saeed Mirshekari, Nicolás Yunes, and Clifford M. Will. Constraining lorentz-violating, modified dispersion relations with gravitational waves. *Phys. Rev. D*, 85:024041, Jan 2012. doi: 10.1103/PhysRevD.85.024041. URL https://link.aps.org/doi/10.1103/PhysRevD.85.024041.

[100] Maria Okounkova, Will M. Farr, Maximiliano Isi, and Leo C. Stein. Constraining gravitational wave amplitude birefringence and Chern-Simons gravity with GWTC-2. *Phys. Rev. D*, 106 (4):044067, 2022. doi: 10.1103/PhysRevD.106.044067.

[101] Atsushi Nishizawa. Generalized framework for testing gravity with gravitational-wave propagation. i. formulation. *Phys. Rev. D*, 97:104037, May 2018. doi: 10.1103/PhysRevD.97.104037. URL `https://link.aps.org/doi/10.1103/PhysRevD.97.104037`.

[102] Enis Belgacem, Yves Dirian, Stefano Foffa, and Michele Maggiore. Gravitational-wave luminosity distance in modified gravity theories. *Phys. Rev. D*, 97:104066, May 2018. doi: 10.1103/PhysRevD.97.104066. URL `https://link.aps.org/doi/10.1103/PhysRevD.97.104066`.

[103] Michele Maggiore. *Gravitational Waves. Vol. 1: Theory and Experiments*. Oxford Master Series in Physics. Oxford University Press, 2007. ISBN 978-0-19-857074-5, 978-0-19-852074-0.

[104] Douglas M. Eardley, David L. Lee, and Alan P. Lightman. Gravitational-wave observations as a tool for testing relativistic gravity. *Phys. Rev. D*, 8:3308–3321, Nov 1973. doi: 10.1103/PhysRevD.8.3308. URL `https://link.aps.org/doi/10.1103/PhysRevD.8.3308`.

[105] Katerina Chatziioannou, Nicolás Yunes, and Neil Cornish. Model-independent test of general relativity: An extended post-einsteinian framework with complete polarization content. *Phys. Rev. D*, 86:022004, Jul 2012. doi: 10.1103/PhysRevD.86.022004. URL `https://link.aps.org/doi/10.1103/PhysRevD.86.022004`.

[106] Abhirup Ghosh et al. Testing general relativity using golden black-hole binaries. *Phys. Rev. D*, 94(2):021101, 2016. doi: 10.1103/PhysRevD.94.021101.

[107] Abhirup Ghosh, Nathan K. Johnson-Mcdaniel, Archisman Ghosh, Chandra Kant Mishra, Parameswaran Ajith, Walter Del Pozzo, Christopher P. L. Berry, Alex B. Nielsen, and Lionel London. Testing general relativity using gravitational wave signals from the inspiral, merger and ringdown of binary black holes. *Class. Quant. Grav.*, 35(1):014002, 2018. doi: 10.1088/1361-6382/aa972e.

[108] Sudarshan Ghonge, Katerina Chatziioannou, James A. Clark, Tyson Littenberg, Margaret Millhouse, Laura Cadonati, and Neil Cornish. Reconstructing gravitational wave signals from binary black hole mergers with minimal assumptions. *Phys. Rev. D*, 102(6):064056, 2020. doi: 10.1103/PhysRevD.102.064056.

[109] Jose Luis Blázquez-Salcedo, Fech Scen Khoo, and Jutta Kunz. Quasinormal modes of Einstein-Gauss-Bonnet-dilaton black holes. *Phys. Rev. D*, 96(6):064008, 2017. doi: 10.1103/PhysRevD.96.064008.

[110] Valeria Ferrari, Massimo Pauri, and Federico Piazza. Quasinormal modes of charged, dilaton black holes. *Phys. Rev. D*, 63:064009, Feb 2001. doi: 10.1103/PhysRevD.63.064009. URL `https://link.aps.org/doi/10.1103/PhysRevD.63.064009`.

[111] C. Molina, Paolo Pani, Vitor Cardoso, and Leonardo Gualtieri. Gravitational signature of schwarzschild black holes in dynamical chern-simons gravity. *Phys. Rev. D*, 81:124021, Jun 2010. doi: 10.1103/PhysRevD.81.124021. URL `https://link.aps.org/doi/10.1103/PhysRevD.81.124021`.

[112] Nicolás Yunes and Carlos F. Sopuerta. Perturbations of schwarzschild black holes in chern-simons modified gravity. *Phys. Rev. D*, 77:064007, Mar 2008. doi: 10.1103/PhysRevD.77.064007. URL https://link.aps.org/doi/10.1103/PhysRevD.77.064007.

[113] Costantino Pacilio and Richard Brito. Quasinormal modes of weakly charged einstein-maxwell-dilaton black holes. *Phys. Rev. D*, 98:104042, Nov 2018. doi: 10.1103/PhysRevD.98.104042. URL https://link.aps.org/doi/10.1103/PhysRevD.98.104042.

[114] Oliver J. Tattersall, Pedro G. Ferreira, and Macarena Lagos. Speed of gravitational waves and black hole hair. *Phys. Rev. D*, 97:084005, Apr 2018. doi: 10.1103/PhysRevD.97.084005. URL https://link.aps.org/doi/10.1103/PhysRevD.97.084005.

[115] Flora Moulin, Aurélien Barrau, and Killian Martineau. An overview of quasinormal modes in modified and extended gravity. *Universe*, 5(9), 2019. ISSN 2218-1997. doi: 10.3390/universe5090202. URL https://www.mdpi.com/2218-1997/5/9/202.

[116] Jose Luis Blázquez-Salcedo, Daniela D. Doneva, Sarah Kahlen, Jutta Kunz, Petya Nedkova, and Stoytcho S. Yazadjiev. Axial perturbations of the scalarized einstein-gauss-bonnet black holes. *Phys. Rev. D*, 101:104006, May 2020. doi: 10.1103/PhysRevD.101.104006. URL https://link.aps.org/doi/10.1103/PhysRevD.101.104006.

[117] Jose Luis Blázquez-Salcedo, Daniela D. Doneva, Sarah Kahlen, Jutta Kunz, Petya Nedkova, and Stoytcho S. Yazadjiev. Polar quasinormal modes of the scalarized einstein-gauss-bonnet black holes. *Phys. Rev. D*, 102:024086, Jul 2020. doi: 10.1103/PhysRevD.102.024086. URL https://link.aps.org/doi/10.1103/PhysRevD.102.024086.

[118] Hector O. Silva, Abhirup Ghosh, and Alessandra Buonanno. Black-hole ringdown as a probe of higher-curvature gravity theories. 5 2022.

[119] T. G. F. Li, W. Del Pozzo, S. Vitale, C. Van Den Broeck, M. Agathos, J. Veitch, K. Grover, T. Sidery, R. Sturani, and A. Vecchio. Towards a generic test of the strong field dynamics of general relativity using compact binary coalescence. *Phys. Rev. D*, 85:082003, Apr 2012. doi: 10.1103/PhysRevD.85.082003. URL https://link.aps.org/doi/10.1103/PhysRevD.85.082003.

[120] Ajit Kumar Mehta, Alessandra Buonanno, Roberto Cotesta, Abhirup Ghosh, Noah Sennett, and Jan Steinhoff. Tests of general relativity with gravitational-wave observations using a flexible theory-independent method. *Phys. Rev. D*, 107:044020, Feb 2023. doi: 10.1103/PhysRevD.107.044020. URL https://link.aps.org/doi/10.1103/PhysRevD.107.044020.

[121] K G Arun, B R Iyer, M S S Qusailah, and B S Sathyaprakash. Testing post-newtonian theory with gravitational wave observations. *Classical and Quantum Gravity*, 23(9):L37, mar 2006. doi: 10.1088/0264-9381/23/9/L01. URL https://dx.doi.org/10.1088/0264-9381/23/9/L01.

[122] Clifford M. Will. Bounding the mass of the graviton using gravitational-wave observations of inspiralling compact binaries. *Phys. Rev. D*, 57:2061–2068, Feb 1998. doi: 10.1103/PhysRevD.57.2061. URL https://link.aps.org/doi/10.1103/PhysRevD.57.2061.

[123] B. P. Abbott et al. GW170814: A Three-Detector Observation of Gravitational Waves from a Binary Black Hole Coalescence. *Phys. Rev. Lett.*, 119(14):141101, 2017. doi: 10.1103/PhysRevLett.119.141101.

[124] Maximiliano Isi and Alan J. Weinstein. Probing gravitational wave polarizations with signals from compact binary coalescences. 10 2017.

[125] Enrico Barausse, Nicolás Yunes, and Katie Chamberlain. Theory-agnostic constraints on black-hole dipole radiation with multiband gravitational-wave astrophysics. *Phys. Rev. Lett.*, 116:241104, Jun 2016. doi: 10.1103/PhysRevLett.116.241104. URL `https://link.aps.org/doi/10.1103/PhysRevLett.116.241104`.

[126] Vitor Cardoso, Caio F.B. Macedo, Paolo Pani, and Valeria Ferrari. Black holes and gravitational waves in models of minicharged dark matter. *Journal of Cosmology and Astroparticle Physics*, 2016(05):054, may 2016. doi: 10.1088/1475-7516/2016/05/054. URL `https://dx.doi.org/10.1088/1475-7516/2016/05/054`.

[127] J. Meidam, M. Agathos, C. Van Den Broeck, J. Veitch, and B. S. Sathyaprakash. Testing the no-hair theorem with black hole ringdowns using tiger. *Phys. Rev. D*, 90:064009, Sep 2014. doi: 10.1103/PhysRevD.90.064009. URL `https://link.aps.org/doi/10.1103/PhysRevD.90.064009`.

[128] Gregorio Carullo, Laura van der Schaaf, Lionel London, Peter T. H. Pang, Ka Wa Tsang, Otto A. Hannuksela, Jeroen Meidam, Michalis Agathos, Anuradha Samajdar, Archisman Ghosh, Tjonnie G. F. Li, Walter Del Pozzo, and Chris Van Den Broeck. Empirical tests of the black hole no-hair conjecture using gravitational-wave observations. *Phys. Rev. D*, 98:104020, Nov 2018. doi: 10.1103/PhysRevD.98.104020. URL `https://link.aps.org/doi/10.1103/PhysRevD.98.104020`.

[129] Gregorio Carullo, Walter Del Pozzo, and John Veitch. Observational Black Hole Spectroscopy: A time-domain multimode analysis of GW150914. *Phys. Rev. D*, 99(12):123029, 2019. doi: 10.1103/PhysRevD.99.123029. [Erratum: Phys.Rev.D 100, 089903 (2019)].

[130] Richard Brito, Alessandra Buonanno, and Vivien Raymond. Black-hole spectroscopy by making full use of gravitational-wave modeling. *Phys. Rev. D*, 98:084038, Oct 2018. doi: 10.1103/PhysRevD.98.084038. URL `https://link.aps.org/doi/10.1103/PhysRevD.98.084038`.

[131] Maximiliano Isi, Matthew Giesler, Will M. Farr, Mark A. Scheel, and Saul A. Teukolsky. Testing the no-hair theorem with gw150914. *Phys. Rev. Lett.*, 123:111102, Sep 2019. doi: 10.1103/PhysRevLett.123.111102. URL `https://link.aps.org/doi/10.1103/PhysRevLett.123.111102`.

[132] Gregorio Carullo. Accelerating modified gravity detection from gravitational-wave observations using the Parametrized ringdown spin expansion coefficients formalism. 2 2021.

[133] Miriam Cabero, Julian Westerweck, Collin D. Capano, Sumit Kumar, Alex B. Nielsen, and Badri Krishnan. Black hole spectroscopy in the next decade. *Phys. Rev. D*, 101(6):064044, 2020. doi: 10.1103/PhysRevD.101.064044.

[134] Iara Ota and Cecilia Chirenti. Black hole spectroscopy horizons for current and future gravitational wave detectors. *Phys. Rev. D*, 105:044015, Feb 2022. doi: 10.1103/PhysRevD.105.044015. URL https://link.aps.org/doi/10.1103/PhysRevD.105.044015.

[135] Swetha Bhagwat, Costantino Pacilio, Enrico Barausse, and Paolo Pani. Landscape of massive black-hole spectroscopy with lisa and the einstein telescope. *Phys. Rev. D*, 105:124063, Jun 2022. doi: 10.1103/PhysRevD.105.124063. URL https://link.aps.org/doi/10.1103/PhysRevD.105.124063.

[136] Scott E. Perkins, Nicolás Yunes, and Emanuele Berti. Probing Fundamental Physics with Gravitational Waves: The Next Generation. *Phys. Rev. D*, 103(4):044024, 2021. doi: 10.1103/PhysRevD.103.044024.

[137] Costantino Pacilio and Swetha Bhagwat. Identifying modified theories of gravity using binary black-hole ringdowns. 1 2023.

[138] B. Carter. Axisymmetric black hole has only two degrees of freedom. *Phys. Rev. Lett.*, 26:331–333, Feb 1971. doi: 10.1103/PhysRevLett.26.331. URL https://link.aps.org/doi/10.1103/PhysRevLett.26.331.

[139] S. W. Hawking. Black holes in the brans-dicke. *Communications in Mathematical Physics*, 25 (2):167–171, 1972. doi: 10.1007/BF01877518. URL https://doi.org/10.1007/BF01877518.

[140] D. C. Robinson. Uniqueness of the kerr black hole. *Phys. Rev. Lett.*, 34:905–906, Apr 1975. doi: 10.1103/PhysRevLett.34.905. URL https://link.aps.org/doi/10.1103/PhysRevLett.34.905.

[141] R. Penrose. "golden oldie": Gravitational collapse: The role of general relativity. *General Relativity and Gravitation*, 34(7):1141–1165, 2002. doi: 10.1023/A:1016578408204. URL https://doi.org/10.1023/A:1016578408204.

[142] Piotr T. Chrusciel, Joao Lopes Costa, and Markus Heusler. Stationary Black Holes: Uniqueness and Beyond. *Living Rev. Rel.*, 15:7, 2012. doi: 10.12942/lrr-2012-7.

[143] Enrico Barausse, Vitor Cardoso, and Paolo Pani. Can environmental effects spoil precision gravitational-wave astrophysics? *Phys. Rev. D*, 89(10):104059, 2014. doi: 10.1103/PhysRevD.89.104059.

[144] Vitor Cardoso and Paolo Pani. Testing the nature of dark compact objects: a status report. *Living Rev. Rel.*, 22(1):4, 2019. doi: 10.1007/s41114-019-0020-4.

[145] Vitor Cardoso, Seth Hopper, Caio F. B. Macedo, Carlos Palenzuela, and Paolo Pani. Gravitational-wave signatures of exotic compact objects and of quantum corrections at the horizon scale. *Phys. Rev. D*, 94(8):084031, 2016. doi: 10.1103/PhysRevD.94.084031.

[146] Vitor Cardoso and Leonardo Gualtieri. Testing the black hole 'no-hair' hypothesis. *Classical and Quantum Gravity*, 33(17):174001, aug 2016. doi: 10.1088/0264-9381/33/17/174001. URL https://dx.doi.org/10.1088/0264-9381/33/17/174001.

[147] Vitor Cardoso, Edgardo Franzin, and Paolo Pani. Is the gravitational-wave ringdown a probe of the event horizon? *Phys. Rev. Lett.*, 116:171101, Apr 2016. doi: 10.1103/PhysRevLett.116.171101. URL https://link.aps.org/doi/10.1103/PhysRevLett.116.171101.

[148] Elisa Maggio, Paolo Pani, and Guilherme Raposo. Testing the nature of dark compact objects with gravitational waves. 5 2021. doi: 10.1007/978-981-15-4702-7_29-1.

[149] Elisa Maggio, Luca Buoninfante, Anupam Mazumdar, and Paolo Pani. How does a dark compact object ringdown? *Phys. Rev. D*, 102:064053, Sep 2020. doi: 10.1103/PhysRevD.102.064053. URL https://link.aps.org/doi/10.1103/PhysRevD.102.064053.

[150] Juan Calderón Bustillo, Paul D. Lasky, and Eric Thrane. Black-hole spectroscopy, the no-hair theorem, and gw150914: Kerr versus occam. *Phys. Rev. D*, 103:024041, Jan 2021. doi: 10.1103/PhysRevD.103.024041. URL https://link.aps.org/doi/10.1103/PhysRevD.103.024041.

[151] Valentino F. Foit and Matthew Kleban. Testing Quantum Black Holes with Gravitational Waves. *Class. Quant. Grav.*, 36(3):035006, 2019. doi: 10.1088/1361-6382/aafcba.

[152] Danny Laghi, Gregorio Carullo, John Veitch, and Walter Del Pozzo. Quantum black hole spectroscopy: probing the quantum nature of the black hole area using LIGO–Virgo ringdown detections. *Class. Quant. Grav.*, 38(9):095005, 2021. doi: 10.1088/1361-6382/abde19.

[153] Tullio Regge and John A. Wheeler. Stability of a Schwarzschild singularity. *Phys. Rev.*, 108: 1063–1069, 1957. doi: 10.1103/PhysRev.108.1063.

[154] Frank J. Zerilli. Effective potential for even parity Regge-Wheeler gravitational perturbation equations. *Phys. Rev. Lett.*, 24:737–738, 1970. doi: 10.1103/PhysRevLett.24.737.

[155] Saul A. Teukolsky. Rotating black holes: Separable wave equations for gravitational and electromagnetic perturbations. *Phys. Rev. Lett.*, 29:1114–1118, Oct 1972. doi: 10.1103/PhysRevLett.29.1114. URL https://link.aps.org/doi/10.1103/PhysRevLett.29.1114.

[156] C. J. Goebel. Comments on the "vibrations" of a Black Hole. *Astrophysical Journal, Letters*, 172:L95, March 1972. doi: 10.1086/180898.

[157] Subrahmanyan Chandrasekhar. On the equations governing the perturbations of the Schwarzschild black hole. *Proc. Roy. Soc. Lond. A*, 343(1634):289–298, 1975. doi: 10.1098/rspa.1975.0066.

[158] E. W. Leaver. An Analytic representation for the quasi normal modes of Kerr black holes. *Proc. Roy. Soc. Lond. A*, 402:285–298, 1985. doi: 10.1098/rspa.1985.0119.

[159] Paolo Pani. Advanced Methods in Black-Hole Perturbation Theory. *Int. J. Mod. Phys. A*, 28:1340018, 2013. doi: 10.1142/S0217751X13400186.

[160] Cosimo Bambi. Testing the Kerr black hole hypothesis. *Mod. Phys. Lett. A*, 26:2453–2468, 2011. doi: 10.1142/S0217732311036929.

[161] Saul A. Teukolsky. The Kerr Metric. *Class. Quant. Grav.*, 32(12):124006, 2015. doi: 10.1088/0264-9381/32/12/124006.

[162] Kent Yagi and Leo C. Stein. Black Hole Based Tests of General Relativity. *Class. Quant. Grav.*, 33(5):054001, 2016. doi: 10.1088/0264-9381/33/5/054001.

[163] Enrico Barausse and Thomas P. Sotiriou. Perturbed kerr black holes can probe deviations from general relativity. *Phys. Rev. Lett.*, 101:099001, Aug 2008. doi: 10.1103/PhysRevLett.101.099001. URL `https://link.aps.org/doi/10.1103/PhysRevLett.101.099001`.

[164] Olaf Dreyer, Bernard J. Kelly, Badri Krishnan, Lee Samuel Finn, David Garrison, and Ramon Lopez-Aleman. Black hole spectroscopy: Testing general relativity through gravitational wave observations. *Class. Quant. Grav.*, 21:787–804, 2004. doi: 10.1088/0264-9381/21/4/003.

[165] Piotr T. Chruściel, Erwann Delay, Gregory J. Galloway, and Ralph Howard. Regularity of horizons and the area theorem. *Annales Henri Poincaré*, 2(1):109–178, 2001. doi: 10.1007/PL00001029. URL `https://doi.org/10.1007/PL00001029`.

[166] Robert M. Wald. The thermodynamics of black holes. *Living Reviews in Relativity*, 4(1):6, 2001. doi: 10.12942/lrr-2001-6. URL `https://doi.org/10.12942/lrr-2001-6`.

[167] Miriam Cabero, Collin D. Capano, Ofek Fischer-Birnholtz, Badri Krishnan, Alex B. Nielsen, Alexander H. Nitz, and Christopher M. Biwer. Observational tests of the black hole area increase law. *Phys. Rev. D*, 97:124069, Jun 2018. doi: 10.1103/PhysRevD.97.124069. URL `https://link.aps.org/doi/10.1103/PhysRevD.97.124069`.

[168] Maximiliano Isi, Will M. Farr, Matthew Giesler, Mark A. Scheel, and Saul A. Teukolsky. Testing the black-hole area law with gw150914. *Phys. Rev. Lett.*, 127:011103, Jul 2021. doi: 10.1103/PhysRevLett.127.011103. URL `https://link.aps.org/doi/10.1103/PhysRevLett.127.011103`.

[169] Gregorio Carullo, Danny Laghi, John Veitch, and Walter Del Pozzo. Bekenstein-hod universal bound on information emission rate is obeyed by ligo-virgo binary black hole remnants. *Phys. Rev. Lett.*, 126:161102, Apr 2021. doi: 10.1103/PhysRevLett.126.161102. URL `https://link.aps.org/doi/10.1103/PhysRevLett.126.161102`.

[170] Emanuele Berti, Vitor Cardoso, and Clifford M. Will. On gravitational-wave spectroscopy of massive black holes with the space interferometer LISA. *Phys. Rev. D*, 73:064030, 2006. doi: 10.1103/PhysRevD.73.064030.

[171] Emanuele Berti, Jaime Cardoso, Vitor Cardoso, and Marco Cavaglià. Matched filtering and parameter estimation of ringdown waveforms. *Phys. Rev. D*, 76:104044, Nov 2007. doi: 10.1103/PhysRevD.76.104044. URL `https://link.aps.org/doi/10.1103/PhysRevD.76.104044`.

[172] S. Gossan, J. Veitch, and B. S. Sathyaprakash. Bayesian model selection for testing the no-hair theorem with black hole ringdowns. *Phys. Rev. D*, 85:124056, Jun 2012. doi: 10.1103/PhysRevD.85.124056. URL `https://link.aps.org/doi/10.1103/PhysRevD.85.124056`.

[173] Fernando Echeverria. Gravitational-wave measurements of the mass and angular momentum of a black hole. *Phys. Rev. D*, 40:3194–3203, Nov 1989. doi: 10.1103/PhysRevD.40.3194. URL `https://link.aps.org/doi/10.1103/PhysRevD.40.3194`.

[174] Swetha Bhagwat, Miriam Cabero, Collin D. Capano, Badri Krishnan, and Duncan A. Brown. Detectability of the subdominant mode in a binary black hole ringdown. *Phys. Rev. D*, 102 (2):024023, 2020. doi: 10.1103/PhysRevD.102.024023.

[175] Andrea Maselli, Paolo Pani, Leonardo Gualtieri, and Emanuele Berti. Parametrized ringdown spin expansion coefficients: A data-analysis framework for black-hole spectroscopy with multiple events. *Phys. Rev. D*, 101:024043, Jan 2020. doi: 10.1103/PhysRevD.101.024043. URL `https://link.aps.org/doi/10.1103/PhysRevD.101.024043`.

[176] Kostas Glampedakis, George Pappas, Hector O. Silva, and Emanuele Berti. Post-kerr black hole spectroscopy. *Phys. Rev. D*, 96:064054, Sep 2017. doi: 10.1103/PhysRevD.96.064054. URL `https://link.aps.org/doi/10.1103/PhysRevD.96.064054`.

[177] B. P. Abbott et al. Tests of General Relativity with GW170817. *Phys. Rev. Lett.*, 123(1): 011102, 2019. doi: 10.1103/PhysRevLett.123.011102.

[178] Abhirup Ghosh, Richard Brito, and Alessandra Buonanno. Constraints on quasinormal-mode frequencies with LIGO-Virgo binary–black-hole observations. *Phys. Rev. D*, 103(12):124041, 2021. doi: 10.1103/PhysRevD.103.124041.

[179] Zack Carson and Kent Yagi. Testing General Relativity with Gravitational Waves. 11 2020. doi: 10.1007/978-981-15-4702-7_41-1.

[180] Zack Carson and Kent Yagi. Probing Einstein-dilaton Gauss-Bonnet Gravity with the inspiral and ringdown of gravitational waves. *Phys. Rev. D*, 101(10):104030, 2020. doi: 10.1103/PhysRevD.101.104030.

[181] Zack Carson and Kent Yagi. Probing string-inspired gravity with the inspiral–merger–ringdown consistency tests of gravitational waves. *Class. Quant. Grav.*, 37(21): 215007, 2020. doi: 10.1088/1361-6382/aba221.

[182] Roberto Cotesta, Gregorio Carullo, Emanuele Berti, and Vitor Cardoso. Analysis of ringdown overtones in gw150914. *Phys. Rev. Lett.*, 129:111102, Sep 2022. doi: 10.1103/PhysRevLett.129.111102. URL `https://link.aps.org/doi/10.1103/PhysRevLett.129.111102`.

[183] Maximiliano Isi and Will M. Farr. Revisiting the ringdown of GW150914. 2 2022.

[184] Eliot Finch and Christopher J. Moore. Searching for a ringdown overtone in gw150914. *Phys. Rev. D*, 106:043005, Aug 2022. doi: 10.1103/PhysRevD.106.043005. URL `https://link.aps.org/doi/10.1103/PhysRevD.106.043005`.

[185] Vishal Baibhav and Emanuele Berti. Multimode black hole spectroscopy. *Phys. Rev. D*, 99: 024005, Jan 2019. doi: 10.1103/PhysRevD.99.024005. URL `https://link.aps.org/doi/10.1103/PhysRevD.99.024005`.

[186] R. Abbott et al. GW190521: A Binary Black Hole Merger with a Total Mass of $150M_{\odot}$. *Phys. Rev. Lett.*, 125(10):101102, 2020. doi: 10.1103/PhysRevLett.125.101102.

[187] Jiahui Bao, Changfu Shi, Haitian Wang, Jian-dong Zhang, Yiming Hu, Jianwei Mei, and Jun Luo. Constraining modified gravity with ringdown signals: An explicit example. *Phys. Rev. D*, 100:084024, Oct 2019. doi: 10.1103/PhysRevD.100.084024. URL `https://link.aps.org/doi/10.1103/PhysRevD.100.084024`.

[188] Oliver J. Tattersall and Pedro G. Ferreira. Forecasts for low spin black hole spectroscopy in horndeski gravity. *Phys. Rev. D*, 99:104082, May 2019. doi: 10.1103/PhysRevD.99.104082. URL `https://link.aps.org/doi/10.1103/PhysRevD.99.104082`.

[189] Roy P. Kerr. Gravitational field of a spinning mass as an example of algebraically special metrics. *Phys. Rev. Lett.*, 11:237–238, Sep 1963. doi: 10.1103/PhysRevLett.11.237. URL `https://link.aps.org/doi/10.1103/PhysRevLett.11.237`.

[190] Saul A. Teukolsky. Perturbations of a Rotating Black Hole. I. Fundamental Equations for Gravitational, Electromagnetic, and Neutrino-Field Perturbations. *Astrophysical Journal*, 185:635–648, October 1973. doi: 10.1086/152444.

[191] James B. Hartle. Slowly Rotating Relativistic Stars. I. Equations of Structure. *Astrophys. J.*, 150:1005, December 1967. doi: 10.1086/149400.

[192] James B. Hartle and Kip S. Thorne. Slowly Rotating Relativistic Stars. II. Models for Neutron Stars and Supermassive Stars. *Astrophys. J.*, 153:807, 1968. doi: 10.1086/149707.

[193] Y. Kojima. Equations governing the nonradial oscillations of a slowly rotating relativistic star. *Phys. Rev.*, D46:4289–4303, 1992. doi: 10.1103/PhysRevD.46.4289.

[194] Vania Vellucci, Lorenzo Pierini, Luca Reali, Andrea Maselli, and Emanuele Berti. in preparation.

[195] Lorenzo Pierini, Gregorio Carullo, and Emanuele Berti. in preparation.

[196] J. E. Chase. Event horizons in static scalar-vacuum space-times. *Communications in Mathematical Physics*, 19(4):276–288, 1970. doi: 10.1007/BF01646635. URL `https://doi.org/10.1007/BF01646635`.

[197] Jacob D. Bekenstein. Novel "no-scalar-hair" theorem for black holes. *Phys. Rev. D*, 51:R6608–R6611, Jun 1995. doi: 10.1103/PhysRevD.51.R6608. URL `https://link.aps.org/doi/10.1103/PhysRevD.51.R6608`.

[198] Thomas P. Sotiriou and Valerio Faraoni. Black holes in scalar-tensor gravity. *Phys. Rev. Lett.*, 108:081103, 2012. doi: 10.1103/PhysRevLett.108.081103.

[199] Lam Hui and Alberto Nicolis. No-hair theorem for the galileon. *Phys. Rev. Lett.*, 110:241104, Jun 2013. doi: 10.1103/PhysRevLett.110.241104. URL `https://link.aps.org/doi/10.1103/PhysRevLett.110.241104`.

[200] Thomas P. Sotiriou and Shuang-Yong Zhou. Black hole hair in generalized scalar-tensor gravity. *Phys. Rev. Lett.*, 112:251102, Jun 2014. doi: 10.1103/PhysRevLett.112.251102. URL `https://link.aps.org/doi/10.1103/PhysRevLett.112.251102`.

[201] P. Kanti, N. E. Mavromatos, J. Rizos, K. Tamvakis, and E. Winstanley. Dilatonic black holes in higher curvature string gravity. *Phys. Rev.*, D54:5049–5058, 1996. doi: 10.1103/PhysRevD.54.5049.

[202] S. Mignemi and N. R. Stewart. Charged black holes in effective string theory. *Phys. Rev. D*, 47:5259–5269, Jun 1993. doi: 10.1103/PhysRevD.47.5259. URL `https://link.aps.org/doi/10.1103/PhysRevD.47.5259`.

[203] Kent Yagi, Leo C. Stein, Nicolás Yunes, and Takahiro Tanaka. Post-Newtonian, Quasi-Circular Binary Inspirals in Quadratic Modified Gravity. *Phys. Rev. D*, 85:064022, 2012. doi: 10.1103/PhysRevD.85.064022. [Erratum: Phys.Rev.D 93, 029902 (2016)].

[204] Kent Yagi. A New constraint on scalar Gauss-Bonnet gravity and a possible explanation for the excess of the orbital decay rate in a low-mass X-ray binary. *Phys. Rev. D*, 86:081504, 2012. doi: 10.1103/PhysRevD.86.081504.

[205] Paolo Pani, Caio F. B. Macedo, Luís C. B. Crispino, and Vitor Cardoso. Slowly rotating black holes in alternative theories of gravity. *Phys. Rev. D*, 84:087501, Oct 2011. doi: 10.1103/PhysRevD.84.087501. URL `https://link.aps.org/doi/10.1103/PhysRevD.84.087501`.

[206] Leo C. Stein and Kent Yagi. Parametrizing and constraining scalar corrections to general relativity. *Phys. Rev. D*, 89:044026, Feb 2014. doi: 10.1103/PhysRevD.89.044026. URL `https://link.aps.org/doi/10.1103/PhysRevD.89.044026`.

[207] Dimitry Ayzenberg and Nicolas Yunes. Slowly-Rotating Black Holes in Einstein-Dilaton-Gauss-Bonnet Gravity: Quadratic Order in Spin Solutions. *Phys. Rev.*, D90:044066, 2014. doi: 10.1103/PhysRevD.91.069905,10.1103/PhysRevD.90.044066. [Erratum: Phys. Rev.D91,no.6,069905(2015)].

[208] Andrea Maselli, Paolo Pani, Leonardo Gualtieri, and Valeria Ferrari. Rotating black holes in einstein-dilaton-gauss-bonnet gravity with finite coupling. *Phys. Rev. D*, 92:083014, Oct 2015. doi: 10.1103/PhysRevD.92.083014. URL `https://link.aps.org/doi/10.1103/PhysRevD.92.083014`.

[209] Burkhard Kleihaus, Jutta Kunz, Sindy Mojica, and Eugen Radu. Spinning black holes in Einstein–Gauss-Bonnet–dilaton theory: Nonperturbative solutions. *Phys. Rev. D*, 93(4): 044047, 2016. doi: 10.1103/PhysRevD.93.044047.

[210] Bruce A. Campbell, Nemanja Kaloper, and Keith A. Olive. Classical hair for kerr-newman black holes in string gravity. *Physics Letters B*, 285(3):199–205, 1992. ISSN 0370-2693. doi: https://doi.org/10.1016/0370-2693(92)91452-F. URL `https://www.sciencedirect.com/science/article/pii/037026939291452F`.

[211] Emanuele Berti, Kent Yagi, and Nicolás Yunes. Extreme Gravity Tests with Gravitational Waves from Compact Binary Coalescences: (I) Inspiral-Merger. *Gen. Rel. Grav.*, 50(4):46, 2018. doi: 10.1007/s10714-018-2362-8.

[212] Nicolas Yunes and Leo C. Stein. Non-Spinning Black Holes in Alternative Theories of Gravity. *Phys. Rev. D*, 83:104002, 2011. doi: 10.1103/PhysRevD.83.104002.

[213] Thomas P. Sotiriou and Shuang-Yong Zhou. Black hole hair in generalized scalar-tensor gravity: An explicit example. *Phys. Rev. D*, 90:124063, 2014. doi: 10.1103/PhysRevD.90.124063.

[214] A. Bakopoulos, G. Antoniou, and P. Kanti. Novel black-hole solutions in einstein-scalar-gauss-bonnet theories with a cosmological constant. *Phys. Rev. D*, 99:064003, Mar 2019. doi: 10.1103/PhysRevD.99.064003. URL `https://link.aps.org/doi/10.1103/PhysRevD.99.064003`.

[215] Kartik Prabhu and Leo C. Stein. Black hole scalar charge from a topological horizon integral in Einstein-dilaton-Gauss-Bonnet gravity. *Phys. Rev. D*, 98(2):021503, 2018. doi: 10.1103/PhysRevD.98.021503.

[216] G. Antoniou, A. Bakopoulos, and P. Kanti. Evasion of No-Hair Theorems and Novel Black-Hole Solutions in Gauss-Bonnet Theories. *Phys. Rev. Lett.*, 120(13):131102, 2018. doi: 10.1103/PhysRevLett.120.131102.

[217] G. Antoniou, A. Bakopoulos, and P. Kanti. Black-Hole Solutions with Scalar Hair in Einstein-Scalar-Gauss-Bonnet Theories. *Phys. Rev. D*, 97(8):084037, 2018. doi: 10.1103/PhysRevD.97.084037.

[218] Félix-Louis Julié and Emanuele Berti. Post-Newtonian dynamics and black hole thermodynamics in Einstein-scalar-Gauss-Bonnet gravity. *Phys. Rev. D*, 100(10):104061, 2019. doi: 10.1103/PhysRevD.100.104061.

[219] Félix-Louis Julié, Hector O. Silva, Emanuele Berti, and Nicolás Yunes. Black hole sensitivities in Einstein-scalar-Gauss-Bonnet gravity. *Phys. Rev. D*, 105(12):124031, 2022. doi: 10.1103/PhysRevD.105.124031.

[220] S. Chandrasekhar. *The mathematical theory of black holes*. 1983.

[221] Kostas Glampedakis, Aaron D. Johnson, and Daniel Kennefick. Darboux transformation in black hole perturbation theory. *Phys. Rev. D*, 96:024036, Jul 2017. doi: 10.1103/PhysRevD.96.024036. URL `https://link.aps.org/doi/10.1103/PhysRevD.96.024036`.

[222] Michele Lenzi and Carlos F. Sopuerta. Darboux covariance: A hidden symmetry of perturbed schwarzschild black holes. *Phys. Rev. D*, 104:124068, Dec 2021. doi: 10.1103/PhysRevD.104.124068. URL `https://link.aps.org/doi/10.1103/PhysRevD.104.124068`.

[223] Paolo Pani, Emanuele Berti, and Leonardo Gualtieri. Scalar, electromagnetic, and gravitational perturbations of kerr-newman black holes in the slow-rotation limit. *Phys. Rev. D*, 88:064048, Sep 2013. doi: 10.1103/PhysRevD.88.064048. URL `https://link.aps.org/doi/10.1103/PhysRevD.88.064048`.

[224] Paolo Pani, Emanuele Berti, and Leonardo Gualtieri. Gravitoelectromagnetic perturbations of kerr-newman black holes: Stability and isospectrality in the slow-rotation limit. *Phys. Rev. Lett.*, 110:241103, Jun 2013. doi: 10.1103/PhysRevLett.110.241103. URL `https://link.aps.org/doi/10.1103/PhysRevLett.110.241103`.

[225] Maria Okounkova. Stability of Rotating Black Holes in Einstein Dilaton Gauss-Bonnet Gravity. *Phys. Rev. D*, 100(12):124054, 2019. doi: 10.1103/PhysRevD.100.124054.

[226] Abhishek Hegade K. R., Justin L. Ripley, and Nicolás Yunes. Where and why does Einstein-Scalar-Gauss-Bonnet theory break down? 11 2022.

[227] Giuseppe Papallo and Harvey S. Reall. On the local well-posedness of lovelock and horndeski theories. *Phys. Rev. D*, 96:044019, Aug 2017. doi: 10.1103/PhysRevD.96.044019. URL `https://link.aps.org/doi/10.1103/PhysRevD.96.044019`.

[228] Giuseppe Papallo. On the hyperbolicity of the most general horndeski theory. *Phys. Rev. D*, 96:124036, Dec 2017. doi: 10.1103/PhysRevD.96.124036. URL `https://link.aps.org/doi/10.1103/PhysRevD.96.124036`.

[229] Paolo Pani and Vitor Cardoso. Are black holes in alternative theories serious astrophysical candidates? The Case for Einstein-Dilaton-Gauss-Bonnet black holes. *Phys. Rev.*, D79: 084031, 2009. doi: 10.1103/PhysRevD.79.084031.

[230] P. Kanti, N. E. Mavromatos, J. Rizos, K. Tamvakis, and E. Winstanley. Dilatonic black holes in higher curvature string gravity. 2: Linear stability. *Phys. Rev.*, D57:6255–6264, 1998. doi: 10.1103/PhysRevD.57.6255.

[231] Swetha Bhagwat, Xisco Jiménez Forteza, Paolo Pani, and Valeria Ferrari. Ringdown overtones, black hole spectroscopy, and no-hair theorem tests. *Phys. Rev. D*, 101:044033, Feb 2020. doi: 10.1103/PhysRevD.101.044033. URL `https://link.aps.org/doi/10.1103/PhysRevD.101.044033`.

[232] Remya Nair, Scott Perkins, Hector O. Silva, and Nicolás Yunes. Fundamental physics implications for higher-curvature theories from binary black hole signals in the ligo-virgo catalog gwtc-1. *Phys. Rev. Lett.*, 123:191101, Nov 2019. doi: 10.1103/PhysRevLett.123.191101. URL `https://link.aps.org/doi/10.1103/PhysRevLett.123.191101`.

[233] Scott E. Perkins, Remya Nair, Hector O. Silva, and Nicolás Yunes. Improved gravitational-wave constraints on higher-order curvature theories of gravity. *Phys. Rev. D*, 104:024060, Jul 2021. doi: 10.1103/PhysRevD.104.024060. URL `https://link.aps.org/doi/10.1103/PhysRevD.104.024060`.

[234] R. Abbott et al. Observation of Gravitational Waves from Two Neutron Star–Black Hole Coalescences. *Astrophys. J. Lett.*, 915(1):L5, 2021. doi: 10.3847/2041-8213/ac082e.

[235] Zhenwei Lyu, Nan Jiang, and Kent Yagi. Constraints on einstein-dilation-gauss-bonnet gravity from black hole-neutron star gravitational wave events. *Phys. Rev. D*, 105:064001, Mar 2022. doi: 10.1103/PhysRevD.105.064001. URL `https://link.aps.org/doi/10.1103/PhysRevD.105.064001`.

[236] Hans-Peter Nollert and Richard H. Price. Quantifying excitations of quasinormal mode systems. *J. Math. Phys.*, 40:980–1010, 1999. doi: 10.1063/1.532698.

[237] Hans-Peter Nollert. Quasinormal modes: the characteristic 'sound' of black holes and neutron stars. *Classical and Quantum Gravity*, 16(12):R159, dec 1999. doi: 10.1088/0264-9381/16/12/201. URL https://dx.doi.org/10.1088/0264-9381/16/12/201.

[238] Edward W. Leaver. Spectral decomposition of the perturbation response of the schwarzschild geometry. *Phys. Rev. D*, 34:384–408, Jul 1986. doi: 10.1103/PhysRevD.34.384. URL https://link.aps.org/doi/10.1103/PhysRevD.34.384.

[239] Kostas D. Kokkotas and Bernd G. Schmidt. Quasinormal modes of stars and black holes. *Living Rev. Rel.*, 2:2, 1999. doi: 10.12942/lrr-1999-2.

[240] Horst R. Beyer. On the completeness of the quasinormal modes of the Poschl-Teller potential. *Commun. Math. Phys.*, 204:397–423, 1999. doi: 10.1007/s002200050651.

[241] Horst R. Beyer. On the stability of the Kerr metric. *Commun. Math. Phys.*, 221:659–676, 2001. doi: 10.1007/s002200100494.

[242] E. S. C. Ching, P. T. Leung, A. Maassen van den Brink, W. M. Suen, S. S. Tong, and K. Young. Quasinormal-mode expansion for waves in open systems. *Rev. Mod. Phys.*, 70:1545–1554, Oct 1998. doi: 10.1103/RevModPhys.70.1545. URL https://link.aps.org/doi/10.1103/RevModPhys.70.1545.

[243] Hans-Peter Nollert and Bernd G. Schmidt. Quasinormal modes of schwarzschild black holes: Defined and calculated via laplace transformation. *Phys. Rev. D*, 45:2617–2627, Apr 1992. doi: 10.1103/PhysRevD.45.2617. URL https://link.aps.org/doi/10.1103/PhysRevD.45.2617.

[244] Nils Andersson. Excitation of schwarzschild black-hole quasinormal modes. *Phys. Rev. D*, 51:353–363, Jan 1995. doi: 10.1103/PhysRevD.51.353. URL https://link.aps.org/doi/10.1103/PhysRevD.51.353.

[245] Nils Andersson. Evolving test fields in a black-hole geometry. *Phys. Rev. D*, 55:468–479, Jan 1997. doi: 10.1103/PhysRevD.55.468. URL https://link.aps.org/doi/10.1103/PhysRevD.55.468.

[246] Emanuele Berti and Vitor Cardoso. Quasinormal ringing of kerr black holes: The excitation factors. *Phys. Rev. D*, 74:104020, Nov 2006. doi: 10.1103/PhysRevD.74.104020. URL https://link.aps.org/doi/10.1103/PhysRevD.74.104020.

[247] Karl Schwarzschild. On the gravitational field of a mass point according to Einstein's theory. *Sitzungsber. Preuss. Akad. Wiss. Berlin (Math. Phys.)*, 1916:189–196, 1916.

[248] Charles W. Misner, K. S. Thorne, and J. A. Wheeler. *Gravitation*. W. H. Freeman, San Francisco, 1973. ISBN 978-0-7167-0344-0, 978-0-691-17779-3.

[249] E. Berti. Black hole perturbation theory. *Summer School on Gravitational-Wave Astronomy*, August 2016. URL https://www.dropbox.com/sh/9th1um175m8gco9/AACCIkvNa3h-zdHBMZkQ31Baa?dl=0.

[250] Mark Ho-Yeuk Cheung, Vishal Baibhav, Emanuele Berti, Vitor Cardoso, Gregorio Carullo, Roberto Cotesta, Walter Del Pozzo, Francisco Duque, Thomas Helfer, Estuti Shukla, and Kaze W. K. Wong. Nonlinear effects in black hole ringdown. *arXiv e-prints*, art. arXiv:2208.07374, August 2022.

[251] Keefe Mitman, Macarena Lagos, Leo C. Stein, Sizheng Ma, Lam Hui, Yanbei Chen, Nils Deppe, François Hébert, Lawrence E. Kidder, Jordan Moxon, Mark A. Scheel, Saul A. Teukolsky, William Throwe, and Nils L. Vu. Nonlinearities in black hole ringdowns, 2022. URL `https://arxiv.org/abs/2208.07380`.

[252] Hiroyuki Nakano and Kunihito Ioka. Second Order Quasi-Normal Mode of the Schwarzschild Black Hole. *Phys. Rev. D*, 76:084007, 2007. doi: 10.1103/PhysRevD.76.084007.

[253] Nicholas Loutrel, Justin L. Ripley, Elena Giorgi, and Frans Pretorius. Second Order Perturbations of Kerr Black Holes: Reconstruction of the Metric. *Phys. Rev. D*, 103(10):104017, 2021. doi: 10.1103/PhysRevD.103.104017.

[254] F. J. Zerilli. Gravitational field of a particle falling in a schwarzschild geometry analyzed in tensor harmonics. *Phys. Rev. D*, 2:2141–2160, 1970. doi: 10.1103/PhysRevD.2.2141.

[255] Karl Martel. Gravitational wave forms from a point particle orbiting a Schwarzschild black hole. *Phys. Rev. D*, 69:044025, 2004. doi: 10.1103/PhysRevD.69.044025.

[256] Dieter R. Brill, Paul L. Chrzanowski, C. Martin Pereira, Edward D. Fackerell, and James R. Ipser. Solution of the scalar wave equation in a kerr background by separation of variables. *Phys. Rev. D*, 5:1913–1915, Apr 1972. doi: 10.1103/PhysRevD.5.1913. URL `https://link.aps.org/doi/10.1103/PhysRevD.5.1913`.

[257] Dongjun Li, Pratik Wagle, Yanbei Chen, and Nicolás Yunes. Perturbations of spinning black holes beyond General Relativity: Modified Teukolsky equation. *arXiv e-prints*, art. arXiv:2206.10652, June 2022.

[258] Asad Hussain and Aaron Zimmerman. Approach to computing spectral shifts for black holes beyond Kerr. *Physical Review D*, 106(10):104018, November 2022. doi: 10.1103/PhysRevD.106.104018.

[259] Lester A. Edelstein and C. V. Vishveshwara. Differential equations for perturbations on the schwarzschild metric. *Phys. Rev. D*, 1:3514–3517, Jun 1970. doi: 10.1103/PhysRevD.1.3514. URL `https://link.aps.org/doi/10.1103/PhysRevD.1.3514`.

[260] E. S. C. Ching, P. T. Leung, W. M. Suen, and K. Young. Late-time tail of wave propagation on curved spacetime. *Phys. Rev. Lett.*, 74:2414–2417, Mar 1995. doi: 10.1103/PhysRevLett.74.2414. URL `https://link.aps.org/doi/10.1103/PhysRevLett.74.2414`.

[261] E. S. C. Ching, P. T. Leung, W. M. Suen, and K. Young. Wave propagation in gravitational systems: Late time behavior. *Phys. Rev. D*, 52:2118–2132, 1995. doi: 10.1103/PhysRevD.52.2118.

[262] Richard H. Price. Nonspherical perturbations of relativistic gravitational collapse. i. scalar and gravitational perturbations. *Phys. Rev. D*, 5:2419–2438, May 1972. doi: 10.1103/PhysRevD.5.2419. URL https://link.aps.org/doi/10.1103/PhysRevD.5.2419.

[263] B. P. Jensen and P. Candelas. Schwarzschild radial functions. *Phys. Rev. D*, 33:1590–1595, Mar 1986. doi: 10.1103/PhysRevD.33.1590. URL https://link.aps.org/doi/10.1103/PhysRevD.33.1590.

[264] Yonghe Sun and Richard H. Price. Excitation of quasinormal ringing of a schwarzschild black hole. *Phys. Rev. D*, 38:1040–1052, Aug 1988. doi: 10.1103/PhysRevD.38.1040. URL https://link.aps.org/doi/10.1103/PhysRevD.38.1040.

[265] Ioannis Kamaretsos, Mark Hannam, and B. Sathyaprakash. Is black-hole ringdown a memory of its progenitor? *Phys. Rev. Lett.*, 109:141102, 2012. doi: 10.1103/PhysRevLett.109.141102.

[266] Emanuele Berti, Vitor Cardoso, José A. Gonzalez, Ulrich Sperhake, Mark Hannam, Sascha Husa, and Bernd Brügmann. Inspiral, merger, and ringdown of unequal mass black hole binaries: A multipolar analysis. *Phys. Rev. D*, 76:064034, Sep 2007. doi: 10.1103/PhysRevD.76.064034. URL https://link.aps.org/doi/10.1103/PhysRevD.76.064034.

[267] Alessandra Buonanno, Gregory B. Cook, and Frans Pretorius. Inspiral, merger, and ringdown of equal-mass black-hole binaries. *Phys. Rev. D*, 75:124018, Jun 2007. doi: 10.1103/PhysRevD.75.124018. URL https://link.aps.org/doi/10.1103/PhysRevD.75.124018.

[268] Lionel London, Deirdre Shoemaker, and James Healy. Modeling ringdown: Beyond the fundamental quasinormal modes. *Phys. Rev. D*, 90(12):124032, 2014. doi: 10.1103/PhysRevD.90.124032. [Erratum: Phys.Rev.D 94, 069902 (2016)].

[269] Maximiliano Isi and Will M. Farr. Analyzing black-hole ringdowns. 7 2021.

[270] Lorena Magaña Zertuche et al. High precision ringdown modeling: Multimode fits and BMS frames. *Phys. Rev. D*, 105(10):104015, 2022. doi: 10.1103/PhysRevD.105.104015.

[271] Ssohrab Borhanian, K. G. Arun, Harald P. Pfeiffer, and B. S. Sathyaprakash. Comparison of post-Newtonian mode amplitudes with numerical relativity simulations of binary black holes. *Class. Quant. Grav.*, 37(6):065006, 2020. doi: 10.1088/1361-6382/ab6a21.

[272] Sizheng Ma, Keefe Mitman, Ling Sun, Nils Deppe, François Hébert, Lawrence E. Kidder, Jordan Moxon, William Throwe, Nils L. Vu, and Yanbei Chen. Quasinormal-mode filters: A new approach to analyze the gravitational-wave ringdown of binary black-hole mergers. *Phys. Rev. D*, 106(8):084036, 2022. doi: 10.1103/PhysRevD.106.084036.

[273] Arnab Dhani. Importance of mirror modes in binary black hole ringdown waveform. *Phys. Rev. D*, 103(10):104048, 2021. doi: 10.1103/PhysRevD.103.104048.

[274] Arnab Dhani and B. S. Sathyaprakash. Overtones, mirror modes, and mode-mixing in binary black hole mergers. 7 2021.

[275] Eliot Finch and Christopher J. Moore. Modeling the ringdown from precessing black hole binaries. *Phys. Rev. D*, 103(8):084048, 2021. doi: 10.1103/PhysRevD.103.084048.

[276] Xisco Jiménez Forteza, Swetha Bhagwat, Paolo Pani, and Valeria Ferrari. Spectroscopy of binary black hole ringdown using overtones and angular modes. *Phys. Rev. D*, 102(4):044053, 2020. doi: 10.1103/PhysRevD.102.044053.

[277] Valeria. Ferrari, Leonardo Gualtieri, and Stefania Marassi. A New approach to the study of quasi-normal modes of rotating stars. *Phys. Rev. D*, 76:104033, 2007. doi: 10.1103/PhysRevD.76.104033.

[278] Paolo Pani, Vitor Cardoso, Leonardo Gualtieri, Emanuele Berti, and Akihiro Ishibashi. Perturbations of slowly rotating black holes: massive vector fields in the Kerr metric. *Phys. Rev. D*, 86:104017, 2012. doi: 10.1103/PhysRevD.86.104017.

[279] `https://pages.jh.edu/eberti2/ringdown/`.

[280] Edward W. Leaver. Quasinormal modes of Reissner-Nordstrom black holes. *Phys. Rev. D*, 41:2986–2997, 1990. doi: 10.1103/PhysRevD.41.2986.

[281] Hans-Peter Nollert. Quasinormal modes of schwarzschild black holes: The determination of quasinormal frequencies with very large imaginary parts. *Phys. Rev. D*, 47:5253–5258, Jun 1993. doi: 10.1103/PhysRevD.47.5253. URL `https://link.aps.org/doi/10.1103/PhysRevD.47.5253`.

[282] Yasufumi Kojima. Normal Modes of Relativistic Stars in Slow Rotation Limit. *Astrophys. J.*, 414:247, September 1993. doi: 10.1086/173073.

[283] Y. Kojima. Coupled Pulsations between Polar and Axial Modes in a Slowly Rotating Relativistic Star. *Progress of Theoretical Physics*, 90(5):977–990, November 1993. doi: 10.1143/ptp/90.5.977.

[284] Paolo Pani, Vitor Cardoso, Leonardo Gualtieri, Emanuele Berti, and Akihiro Ishibashi. Black hole bombs and photon mass bounds. *Phys. Rev. Lett.*, 109:131102, 2012. doi: 10.1103/PhysRevLett.109.131102.

[285] Paolo Pani, Leonardo Gualtieri, Andrea Maselli, and Valeria Ferrari. Tidal deformations of a spinning compact object. *Phys. Rev. D*, 92(2):024010, 2015. doi: 10.1103/PhysRevD.92.024010.

[286] Subrahmanyan Chandrasekhar and Valeria Ferrari. On the non-radial oscillations of slowly rotating stars induced by the Lense-Thirring effect. *Proc. R. Soc. Lond. A*, 433:423–440, 1991. doi: 10.1098/rspa.1991.0056.

[287] S. W. Hawking. Black holes in general relativity. *Comm. Math. Phys.*, 25(2):152–166, 1972. URL `https://projecteuclid.org:443/euclid.cmp/1103857884`.

[288] Keith H. Lockitch and John L. Friedman. Where are the r modes of isentropic stars? *Astrophys. J.*, 521:764, 1999. doi: 10.1086/307580.

[289] Yasuyuki Hatsuda and Masashi Kimura. Semi-analytic expressions for quasinormal modes of slowly rotating Kerr black holes. *Phys. Rev. D*, 102(4):044032, 2020. doi: 10.1103/PhysRevD.102.044032.

[290] Thibault Damour, Bala R. Iyer, and B. S. Sathyaprakash. Improved filters for gravitational waves from inspiralling compact binaries. *Phys. Rev. D*, 57:885–907, 1998. doi: 10.1103/PhysRevD.57.885.

[291] William H Press, Saul A Teukolsky, William T Vetterling, and Brian P Flannery. *Numerical recipes 3rd edition: The art of scientific computing*. Cambridge university press, 2007.

[292] Swetha Bhagwat, Duncan A. Brown, and Stefan W. Ballmer. Spectroscopic analysis of stellar mass black-hole mergers in our local universe with ground-based gravitational wave detectors. *Phys. Rev. D*, 94(8):084024, 2016. doi: 10.1103/PhysRevD.94.084024. [Erratum: Phys.Rev.D 95, 069906 (2017)].

[293] Huan Yang, Kent Yagi, Jonathan Blackman, Luis Lehner, Vasileios Paschalidis, Frans Pretorius, and Nicolás Yunes. Black hole spectroscopy with coherent mode stacking. *Phys. Rev. Lett.*, 118(16):161101, 2017. doi: 10.1103/PhysRevLett.118.161101.

[294] Sebastian H. Völkel, Nicola Franchini, and Enrico Barausse. Theory-agnostic reconstruction of potential and couplings from quasinormal modes. *Phys. Rev. D*, 105(8):084046, 2022. doi: 10.1103/PhysRevD.105.084046.

[295] Lam Hui, Alessandro Podo, Luca Santoni, and Enrico Trincherini. An analytic approach to quasinormal modes for coupled linear systems. *JHEP*, 03:060, 2023. doi: 10.1007/JHEP03(2023)060.

[296] Valeria Ferrari and Bahram Mashhoon. New approach to the quasinormal modes of a black hole. *Phys. Rev. D*, 30:295–304, Jul 1984. doi: 10.1103/PhysRevD.30.295. URL `https://link.aps.org/doi/10.1103/PhysRevD.30.295`.

[297] Vitor Cardoso, Alex S. Miranda, Emanuele Berti, Helvi Witek, and Vilson T. Zanchin. Geodesic stability, Lyapunov exponents and quasinormal modes. *Phys. Rev. D*, 79(6):064016, 2009. doi: 10.1103/PhysRevD.79.064016.

[298] Huan Yang, David A. Nichols, Fan Zhang, Aaron Zimmerman, Zhongyang Zhang, and Yanbei Chen. Quasinormal-mode spectrum of Kerr black holes and its geometric interpretation. *Phys. Rev. D*, 86:104006, 2012. doi: 10.1103/PhysRevD.86.104006.

[299] D. Lovelock. The Einstein tensor and its generalizations. *J. Math. Phys.*, 12:498–501, 1971. doi: 10.1063/1.1665613.

[300] D. Lovelock. The Four-Dimensionality of Space and the Einstein Tensor. *Journal of Mathematical Physics*, 13:874–876, June 1972. doi: 10.1063/1.1666069.

[301] Thomas P Sotiriou, Valerio Faraoni, and Stefano Liberati. Theory of gravitation theories: A No-progress report. *Int. J. Mod. Phys.*, D17:399–423, 2008. doi: 10.1142/S0218271808012097.

[302] Richard P. Woodard. Avoiding dark energy with 1/r modifications of gravity. *Lect. Notes Phys.*, 720:403–433, 2007. doi: 10.1007/978-3-540-71013-4_14.

[303] J. Polchinski. String theory. *Cambridge Monographs on Mathematical Physics*, 1998. doi: 10.1017/CBO9780511816079.

[304] Filipe Moura and Ricardo Schiappa. Higher-derivative corrected black holes: Perturbative stability and absorption cross-section in heterotic string theory. *Class. Quant. Grav.*, 24: 361–386, 2007. doi: 10.1088/0264-9381/24/2/006.

[305] Markus Heusler. *Black Hole Uniqueness Theorems*. Cambridge Lecture Notes in Physics. Cambridge University Press, 1996. doi: 10.1017/CBO9780511661396.

[306] Eugeny Babichev and Christos Charmousis. Dressing a black hole with a time-dependent Galileon. *JHEP*, 08:106, 2014. doi: 10.1007/JHEP08(2014)106.

[307] Carlos A. R. Herdeiro and Eugen Radu. Kerr black holes with scalar hair. *Phys. Rev. Lett.*, 112:221101, 2014. doi: 10.1103/PhysRevLett.112.221101.

[308] Óscar J. C. Dias, Jorge E. Santos, and Benson Way. Black holes with a single Killing vector field: black resonators. *JHEP*, 12:171, 2015. doi: 10.1007/JHEP12(2015)171.

[309] Thomas P. Sotiriou and Enrico Barausse. Post-Newtonian expansion for Gauss-Bonnet gravity. *Phys. Rev.*, D75:084007, 2007. doi: 10.1103/PhysRevD.75.084007.

[310] Daniela D. Doneva, Fethi M. Ramazanoğlu, Hector O. Silva, Thomas P. Sotiriou, and Stoytcho S. Yazadjiev. Scalarization. 11 2022.

[311] Emanuele Berti, Kent Yagi, Huan Yang, and Nicolás Yunes. Extreme Gravity Tests with Gravitational Waves from Compact Binary Coalescences: (II) Ringdown. *Gen. Rel. Grav.*, 50 (5):49, 2018. doi: 10.1007/s10714-018-2372-6.

[312] Dimitry Ayzenberg, Kent Yagi, and Nicolas Yunes. Linear Stability Analysis of Dynamical Quadratic Gravity. *Phys. Rev.*, D89(4):044023, 2014. doi: 10.1103/PhysRevD.89.044023.

[313] Fabrizio Corelli. Instability of Schwarzschild Black Holes in Einstein-scalar-Gauss-Bonnet Gravity: Perturbative Approach and Time-Domain Analysis. Master's thesis, Rome U., 2020.

[314] Nicola Franchini, Miguel Bezares, Enrico Barausse, and Luis Lehner. Fixing the dynamical evolution in scalar-Gauss-Bonnet gravity. *Phys. Rev. D*, 106(6):064061, 2022. doi: 10.1103/PhysRevD.106.064061.

[315] Hector O. Silva, Jeremy Sakstein, Leonardo Gualtieri, Thomas P. Sotiriou, and Emanuele Berti. Spontaneous scalarization of black holes and compact stars from a Gauss-Bonnet coupling. *Phys. Rev. Lett.*, 120(13):131104, 2018. doi: 10.1103/PhysRevLett.120.131104.

[316] Daniela D. Doneva and Stoytcho S. Yazadjiev. New Gauss-Bonnet Black Holes with Curvature-Induced Scalarization in Extended Scalar-Tensor Theories. *Phys. Rev. Lett.*, 120 (13):131103, 2018. doi: 10.1103/PhysRevLett.120.131103.

[317] Caio F. B. Macedo, Jeremy Sakstein, Emanuele Berti, Leonardo Gualtieri, Hector O. Silva, and Thomas P. Sotiriou. Self-interactions and Spontaneous Black Hole Scalarization. *Phys. Rev. D*, 99(10):104041, 2019. doi: 10.1103/PhysRevD.99.104041.

[318] Alexandru Dima, Enrico Barausse, Nicola Franchini, and Thomas P. Sotiriou. Spin-induced black hole spontaneous scalarization. *Phys. Rev. Lett.*, 125(23):231101, 2020. doi: 10.1103/PhysRevLett.125.231101.

[319] Emanuele Berti, Lucas G. Collodel, Burkhard Kleihaus, and Jutta Kunz. Spin-induced black-hole scalarization in Einstein-scalar-Gauss-Bonnet theory. *Phys. Rev. Lett.*, 126(1):011104, 2021. doi: 10.1103/PhysRevLett.126.011104.

[320] David Garfinkle, Gary T. Horowitz, and Andrew Strominger. Charged black holes in string theory. *Phys. Rev. D*, 43:3140–3143, May 1991. doi: 10.1103/PhysRevD.43.3140. URL `https://link.aps.org/doi/10.1103/PhysRevD.43.3140`.

[321] Brian C. Seymour and Kent Yagi. Testing General Relativity with Black Hole-Pulsar Binaries. *Phys. Rev. D*, 98(12):124007, 2018. doi: 10.1103/PhysRevD.98.124007.

[322] MATHEMATICA notebook `supplemental material.nb` in the repository `https://bitbucket.org/paolopani_uniroma1/repository_gmunu/src/master/QNMs-EdGB/Pierini-Thesis/`.

[323] Burkhard Kleihaus, Jutta Kunz, and Eugen Radu. Rotating Black Holes in Dilatonic Einstein-Gauss-Bonnet Theory. *Phys. Rev. Lett.*, 106:151104, 2011. doi: 10.1103/PhysRevLett.106.151104.

[324] Eric Poisson. *A Relativist's Toolkit: The Mathematics of Black-Hole Mechanics*. Cambridge University Press, 2004. doi: 10.1017/CBO9780511606601.

[325] Richard Brito, Vitor Cardoso, and Paolo Pani. Superradiance: New Frontiers in Black Hole Physics. *Lect. Notes Phys.*, 906:pp.1–237, 2015. doi: 10.1007/978-3-319-19000-6.

[326] S. A. Teukolsky and W. H. Press. Perturbations of a rotating black hole. III. Interaction of the hole with gravitational and electromagnetic radiation. *Astrophysical Journal*, 193:443–461, October 1974. doi: 10.1086/153180.

[327] Tamara Evstafyeva, Michalis Agathos, and Justin L. Ripley. Measuring the ringdown scalar polarization of gravitational waves in Einstein scalar Gauss-Bonnet gravity. 12 2022.

[328] R. A. Konoplya, A. F. Zinhailo, and Z. Stuchlík. Quasinormal modes, scattering, and Hawking radiation in the vicinity of an Einstein-dilaton-Gauss-Bonnet black hole. *Phys. Rev. D*, 99 (12):124042, 2019. doi: 10.1103/PhysRevD.99.124042.

[329] Norichika Sago, Hiroyuki Nakano, and Misao Sasaki. Gauge problem in the gravitational selfforce. 1. Harmonic gauge approach in the Schwarzschild background. *Phys. Rev. D*, 67: 104017, 2003. doi: 10.1103/PhysRevD.67.104017.

[330] Vitor Cardoso and Leonardo Gualtieri. Perturbations of Schwarzschild black holes in Dynamical Chern-Simons modified gravity. *Phys. Rev. D*, 80:064008, 2009. doi: 10.1103/PhysRevD.81.089903. [Erratum: Phys.Rev.D 81, 089903 (2010)].

[331] Emanuele Berti and Antoine Klein. Mixing of spherical and spheroidal modes in perturbed kerr black holes. *Phys. Rev. D*, 90:064012, Sep 2014. doi: 10.1103/PhysRevD.90.064012. URL `https://link.aps.org/doi/10.1103/PhysRevD.90.064012`.

[332] D. Sivia and J. Skilling. *Data Analysis: A Bayesian Tutorial*. Oxford science publications. OUP Oxford, 2006. ISBN 9780198568315. URL `https://books.google.it/books?id=lYMSDAAAQBAJ`.

[333] Robert E. Kass, Bradley P. Carlin, Andrew Gelman, and Radford M. Neal. Markov chain monte carlo in practice: A roundtable discussion. *The American Statistician*, 52(2):93–100, 1998. ISSN 00031305. URL http://www.jstor.org/stable/2685466.

[334] R. A. Fisher. On the Mathematical Foundations of Theoretical Statistics. *Philosophical Transactions of the Royal Society of London Series A*, 222:309–368, January 1922. doi: 10.1098/rsta.1922.0009.

[335] Michele Vallisneri. Use and abuse of the fisher information matrix in the assessment of gravitational-wave parameter-estimation prospects. *Phys. Rev. D*, 77:042001, Feb 2008. doi: 10.1103/PhysRevD.77.042001. URL https://link.aps.org/doi/10.1103/PhysRevD.77.042001.

[336] pyRing package https://lscsoft.docs.ligo.org/pyring/.

[337] Guido Van Rossum and Fred L. Drake. *Python 3 Reference Manual*. CreateSpace, Scotts Valley, CA, 2009. ISBN 1441412697.

[338] John Veitch, Walter Del Pozzo, Michael Williams, Colm Talbot, Matt Pitkin, Gregory Ashton, Cody, Moritz Hübner, Alex Nitz, Duncan Macleod, Gregorio Carullo, Guy Davies, and Tony. johnveitch/cpnest: Version 0.11, January 2021. URL https://doi.org/10.5281/zenodo.4428902.

[339] J. Veitch, V. Raymond, B. Farr, W. Farr, P. Graff, S. Vitale, B. Aylott, K. Blackburn, N. Christensen, M. Coughlin, W. Del Pozzo, F. Feroz, J. Gair, C.-J. Haster, V. Kalogera, T. Littenberg, I. Mandel, R. O'Shaughnessy, M. Pitkin, C. Rodriguez, C. Röver, T. Sidery, R. Smith, M. Van Der Sluys, A. Vecchio, W. Vousden, and L. Wade. Parameter estimation for compact binaries with ground-based gravitational-wave observations using the lalinference software library. *Phys. Rev. D*, 91:042003, Feb 2015. doi: 10.1103/PhysRevD.91.042003. URL https://link.aps.org/doi/10.1103/PhysRevD.91.042003.

[340] L. London. Modeling ringdown. ii. aligned-spin binary black holes, implications for data analysis and fundamental theory. *Phys. Rev. D*, 102:084052, Oct 2020. doi: 10.1103/PhysRevD.102.084052. URL https://link.aps.org/doi/10.1103/PhysRevD.102.084052.

[341] Thibault Damour and Alessandro Nagar. New analytic representation of the ringdown waveform of coalescing spinning black hole binaries. *Phys. Rev. D*, 90:024054, Jul 2014. doi: 10.1103/PhysRevD.90.024054. URL https://link.aps.org/doi/10.1103/PhysRevD.90.024054.

[342] LIGO Scientific Collaboration. LIGO Algorithm Library - LALSuite. free software (GPL), 2018. URL https://git.ligo.org/lscsoft/lalsuite.

[343] Stefan Behnel, Robert Bradshaw, Craig Citro, Lisandro Dalcin, Dag Sverre Seljebotn, and Kurt Smith. Cython: The best of both worlds. *Computing in Science & Engineering*, 13(2):31–39, 2011. doi: 10.1109/MCSE.2010.118.

[344] Vicky Kalogera et al. The Next Generation Global Gravitational Wave Observatory: The Science Book. 11 2021.

[345] Matthew Evans et al. A Horizon Study for Cosmic Explorer: Science, Observatories, and Community. 9 2021.

[346] Ken K. Y. Ng, Salvatore Vitale, Will M. Farr, and Carl L. Rodriguez. Probing multiple populations of compact binaries with third-generation gravitational-wave detectors. *Astrophys. J. Lett.*, 913(1):L5, 2021. doi: 10.3847/2041-8213/abf8be.

[347] Marica Branchesi et al. Science with the Einstein Telescope: a comparison of different designs. 3 2023. URL `https://arxiv.org/abs/2303.15923`.

[348] Vishal Baibhav, Emanuele Berti, Vitor Cardoso, and Gaurav Khanna. Black hole spectroscopy: Systematic errors and ringdown energy estimates. *Phys. Rev. D*, 97:044048, Feb 2018. doi: 10.1103/PhysRevD.97.044048. URL `https://link.aps.org/doi/10.1103/PhysRevD.97.044048`.

[349] James Healy, Carlos O. Lousto, and Yosef Zlochower. Remnant mass, spin, and recoil from spin aligned black-hole binaries. *Phys. Rev. D*, 90:104004, Nov 2014. doi: 10.1103/PhysRevD.90.104004. URL `https://link.aps.org/doi/10.1103/PhysRevD.90.104004`.

[350] Daniel Foreman-Mackey, David W. Hogg, Dustin Lang, and Jonathan Goodman. emcee: The MCMC Hammer. *Publ. Astron. Soc. Pac.*, 125:306–312, 2013. doi: 10.1086/670067.

[351] Gilles Esposito-Farese. Scalar tensor theories and cosmology and tests of a quintessence Gauss-Bonnet coupling. In *38th Rencontres de Moriond on Gravitational Waves and Experimental Gravity*, 6 2003.

[352] Zhongyang Zhang, Emanuele Berti, and Vitor Cardoso. Quasinormal ringing of kerr black holes. ii. excitation by particles falling radially with arbitrary energy. *Phys. Rev. D*, 88:044018, Aug 2013. doi: 10.1103/PhysRevD.88.044018. URL `https://link.aps.org/doi/10.1103/PhysRevD.88.044018`.

[353] Naritaka Oshita. Ease of excitation of black hole ringing: Quantifying the importance of overtones by the excitation factors. *Phys. Rev. D*, 104(12):124032, 2021. doi: 10.1103/PhysRevD.104.124032.

[354] Matthew Giesler, Maximiliano Isi, Mark A. Scheel, and Saul A. Teukolsky. Black hole ringdown: The importance of overtones. *Phys. Rev. X*, 9:041060, Dec 2019. doi: 10.1103/PhysRevX.9.041060. URL `https://link.aps.org/doi/10.1103/PhysRevX.9.041060`.

[355] Alessandro Nagar, Sebastiano Bernuzzi, Walter Del Pozzo, Gunnar Riemenschneider, Sarp Akcay, Gregorio Carullo, Philipp Fleig, Stanislav Babak, Ka Wa Tsang, Marta Colleoni, Francesco Messina, Geraint Pratten, David Radice, Piero Rettegno, Michalis Agathos, Edward Fauchon-Jones, Mark Hannam, Sascha Husa, Tim Dietrich, Pablo Cerdá-Duran, José A. Font, Francesco Pannarale, Patricia Schmidt, and Thibault Damour. Time-domain effective-one-body gravitational waveforms for coalescing compact binaries with nonprecessing spins, tides, and self-spin effects. *Phys. Rev. D*, 98:104052, Nov 2018. doi: 10.1103/PhysRevD.98.104052. URL `https://link.aps.org/doi/10.1103/PhysRevD.98.104052`.

Appendix A

Spherical Harmonics Decomposition

We define the metric of a 2-sphere as

$$\gamma_{AB} = \begin{pmatrix} 1 & 0 \\ 0 & \sin^2\theta \end{pmatrix}, \tag{A.1}$$

where the capital Latin indices refer to the angular coordinates (θ, ϕ).

The spherical harmonics are eigenvectors of the Laplacian operator on the sphere. Denoting with ∇_A the covariant derivative with respect to the metric γ_{AB}, the Legendre equation can be written as:

$$\gamma^{AB}\nabla_A\nabla_B Y^{lm} = -l\,(l+1)\,Y^{lm}\,. \tag{A.2}$$

The perturbation tensor $h_{\mu\nu}$ in Eq. (2.11) is symmetric and has 10 components which transform differently under rotation of the frame around the origin:

- 3 SO(2) scalars $\rightarrow h_{00},\ \ h_{01},\ \ h_{11} \rightarrow h_{ab}$
- 2 SO(2) vectors $\rightarrow (h_{02}, h_{03});\ (h_{12}, h_{13}) \rightarrow h_{aA}$
- 1 SO(2) second-order symmetrical tensor $\rightarrow \begin{pmatrix} h_{22} & h_{23} \\ h_{32} & h_{33} \end{pmatrix} \rightarrow h_{AB}$

in which the lower case indeces a, b run over (t, r) and the capital indeces A, B run over (θ, ϕ). Scalar spherical harmonics have parity $(-1)^l$ since:

$$\hat{P}Y^{lm}(\theta,\phi) = Y^{lm}(\pi-\theta, \pi+\phi) = (-1)^l Y^{lm}(\theta,\phi)\,. \tag{A.3}$$

It is possible to expand the perturbation in a complete basis using suitably defined scalar, vector, and tensor spherical harmonics either with the same parity of the spherical harmonics $(-1)^l$, i.e. *even* or *polar* quantities, or with the opposite parity $(-1)^{l+1}$, i.e. *odd* or *axial* quantities [153, 249, 254]. We construct vector and tensor harmonics of a given parity in the following way:

- **EVEN - POLAR**

$$\begin{aligned} Y^{lm}_{A} &\equiv \nabla_A Y^{lm} \\ U^{lm}_{AB} &\equiv \gamma_{AB} Y^{lm} \\ Y^{lm}_{AB} &\equiv \left[\nabla_A \nabla_B + \frac{1}{2} l(l+1)\gamma_{AB}\right] Y^{lm} \end{aligned} \tag{A.4}$$

- **ODD - AXIAL**

$$\begin{aligned} X^{lm}_{A} &\equiv \epsilon_{AC}\gamma^{BC}\nabla_B Y^{lm} = \epsilon_A{}^B \nabla_B Y^{lm} \\ X^{lm}_{AB} &\equiv \frac{1}{2}(\epsilon_A{}^C \nabla_B + \epsilon_B{}^C \nabla_A)\nabla_C Y^{lm} \end{aligned} \tag{A.5}$$

where we have used the Levi-Civita tensor in spherical coordinates

$$\epsilon_{AB} = \begin{pmatrix} 0 & \sin\theta \\ -\sin\theta & 0 \end{pmatrix}. \tag{A.6}$$

Any quantity can therefore be expanded in a function of t and r (that does not change the property of transformation under rotation) multiplied by a suitable spherical harmonic (scalar, vector, tensor) of a given parity. The same rule holds true for the perturbation components, which are written as a multipole expansion as:

$$\begin{aligned} h_{tt} &= A(r)\sum_{l=0}^{\infty}\sum_{m=-l}^{l} H_{0,lm}(t,r)Y^{lm} \\ h_{tr} &= \sum_{l=0}^{\infty}\sum_{m=-l}^{l} H_{1,lm}(t,r)Y^{lm} \\ h_{rr} &= \frac{1}{B(r)}\sum_{l=0}^{\infty}\sum_{m=-l}^{l} H_{2,lm}(t,r)Y^{lm} \\ h_{tA} &= \sum_{l=0}^{\infty}\sum_{m=-l}^{l}\left[q_{0,lm}(t,r)Y^{lm}_{A} + h_{0,lm}(t,r)X^{lm}_{A}\right] \\ h_{rA} &= \sum_{l=0}^{\infty}\sum_{m=-l}^{l}\left[q_{1,lm}(t,r)Y^{lm}_{A} + h_{1,lm}(t,r)X^{lm}_{A}\right] \\ h_{AB} &= r^2\sum_{l=0}^{\infty}\sum_{m=-l}^{l}\left[K_{lm}(t,r)U^{lm}_{AB} + G_{lm}(t,r)Y^{lm}_{AB} + h_{2,lm}(t,r)X^{lm}_{AB}\right] \end{aligned} \tag{A.7}$$

.

For easier calculations, we factored out the metric functions A and B in the radial part of the decomposition. We have defined functions of t and r such that H_0, H_1, H_2, q_0, q_1, K and G characterize *even parity modes*, while h_0, h_1 and h_2 identifiy the *odd parity modes*.

Due to the diffeomorphism invariance of Einstein equations, it is always possible to perform a

gauge transformation to set four coefficients to zero. In the *Regge-Wheeler gauge*, this freedom is used to set $q_0 = q_1 = G = 0$ and $h_2 = 0$ [153]. When $l = 0, l = 1$ some spherical harmonics vanish, thus it is not necessary to fix to zero the corresponding radial functions; it is then possible to use this residual gauge freedom to put different functions to zero.

Appendix B

Schwarzschild Background Perturbation Equations

In this Appendix, we review the steps that lead, from Einstein equations for a perturbed Schwarzschild BH, to the Zerilli master equation for *polar* perturbations. From the tr component of Einstein equations at linear order in perturbation theory, δG_{tr}, leaving the l index implicit, we find

$$\frac{(3M-r)}{2Mr-r^2}K(r) - \frac{il(l+1)}{2r^2\omega}H_1(r) - \frac{H_2(r)}{r} + K'(r) = 0\,. \tag{B.1}$$

From δG_{tt}

$$\begin{aligned}&\frac{\left(l^2+l-2\right)(2M-r)}{2r^3}K(r) + \frac{\left(l^2+l+2\right)(2M-r)}{2r^3}H_2(r) - \frac{(r-2M)^2}{r^3}H_2{}'(r)\\ &+ \frac{(5M-3r)(2M-r)}{r^3}K'(r) + \frac{(r-2M)^2}{r^2}K''(r) = 0\,.\end{aligned} \tag{B.2}$$

From $\delta G_{t\phi}$

$$-\frac{ir\omega}{2M-r}\left[K(r)+H_2(r)\right] + \frac{2MH_1(r)}{r(r-2M)} + H_1{}'(r) = 0\,. \tag{B.3}$$

From δG_{rr}

$$\begin{aligned}&\frac{(l-1)(l+2)(r-2M)-2r^3\omega^2}{2r(r-2M)^2}K(r) + \frac{l^2+l}{4Mr-2r^2}H_0(r) - \frac{2i\omega}{2M-r}H_1(r)\\ &+ \frac{H_2(r)}{r(r-2M)} + \frac{(M-r)}{r(r-2M)}K'(r) + \frac{H_0{}'(r)}{r} = 0\,.\end{aligned} \tag{B.4}$$

From $\delta G_{r\theta}$

$$\left(1-\frac{2M}{r}\right)H_0{}'(r) + \frac{(3M-r)}{r^2}H_0(r) + i\omega H_1(r) + \frac{(r-M)}{r^2}H_2(r) + \left(\frac{2M}{r}-1\right)K'(r) = 0\,. \tag{B.5}$$

From $\delta G_{\theta\theta} - \delta G_{\phi\phi}/\sin^2\theta$

$$\frac{1}{2}\left[H_0(r) - H_2(r)\right] = 0\,. \tag{B.6}$$

Finally, from $\delta G_{\theta\theta} + \delta G_{\phi\phi}/\sin^2\theta$

$$\frac{r\omega^2}{2M-r}K(r) - \frac{2i\omega(M-r)}{r(r-2M)}H_1(r) + \left(\frac{r\omega^2}{2M-r} + \frac{l(l+1)}{2r^2}\right)H_2(r) - \frac{l(l+1)}{2r^2}H_0(r)$$
$$+ \frac{(M+r)}{r^2}H_0{}'(r) + 2i\omega H_1{}'(r) + \frac{(r-M)}{r^2}H_2{}'(r) + \frac{2(M-r)}{r^2}K'(r)$$
$$+ \left(1 - \frac{2M}{r}\right)H_0{}''(r) + \left(\frac{2M}{r} - 1\right)K''(r) = 0\,. \tag{B.7}$$

Having simplified the time dependence $e^{-i\omega t}$, all of our equations are in the frequency domain – the time derivatives have introduced the factors $-i\omega$.

From Eq. (B.6), which gives $H_0(r) = H_2(r)$, it is already possible to see that not all the degrees of freedom we have introduced in the perturbation tensor $h_{\mu\nu}$ are necessary to describe the dynamics of the perturbation. Indeed, we already know that in GR the gravitational wave is described only by two degrees of freedom.

We now manipulate these equations in order to obtain a set that only contains the relevant degrees of freedom. The choice of the functions to describe the perturbation has some degree of arbitrariness, and in our case, we will express all the quantities in terms of H_1 and K. After some substitutions, we get

$$K'(r) - \frac{4Ml(l+1) + r\left(4r^2\omega^2 + l^4 + 2l^3 - l^2 - 2l\right)}{2r^2\omega\left(6M + r\left(l^2+l-2\right)\right)}iH_1(r)$$
$$+ \frac{12M^2 + Mr\left(l^2+l-6\right) - 2r^4\omega^2}{r(2M-r)\left(6M + r\left(l^2+l-2\right)\right)}K(r) = 0 \tag{B.8}$$
$$H_1{}'(r) + \frac{\left(12M^2 + Mr(3l(l+1)-4) - 2r^4\omega^2\right)}{r(r-2M)\left(6M + r\left(l^2+l-2\right)\right)}H_1(r)$$
$$- \frac{2ir\omega\left(9M^2 + 2Mr\left(l^2+l-4\right) + r^4\omega^2 - r^2\left(l^2+l-2\right)\right)}{(r-2M)^2\left(6M + r\left(l^2+l-2\right)\right)}K(r) = 0\,. \tag{B.9}$$

This set of coupled differential equations can be already solved in this form, as explained in Section 2.5.1, but it is generally simpler to cast it in a single second-order differential equation. This can be achieved introducing the *Zerilli function* $Z(r)$

$$Z(r) \equiv \frac{r^2}{\Lambda r + 3M}K(r) + \frac{r-2M}{i\omega(\Lambda r + 3M)}\,, \tag{B.10}$$

where we have defined

$$\Lambda \equiv \frac{1}{2}(l-1)(l+2)\,. \tag{B.11}$$

From the definition of $Z(r)$ and its derivative $Z'(r)$ we can find the inverse relations

$$K = \frac{\Lambda(\Lambda+1)r^2 + 3\Lambda Mr + 6M^2}{r^2(\Lambda r + 3M)}Z(r) + \left(1 - \frac{2M}{r}\right)Z'(r) \tag{B.12}$$
$$H_1 = -i\omega\left[\frac{\Lambda r^2 - 3\Lambda Mr - 3M^2}{(r-2M)(\Lambda r + 3M)}Z(r) + rZ'(r)\right]\,. \tag{B.13}$$

Using the tortoise coordinate r_* such that $dr/dr_* = 1 - 2M/r$, we evaluate

$$\frac{d^2Z}{dr_*^2} = \left(1 - \frac{2M}{r}\right) \frac{d}{dr}\left[\left(1 - \frac{2M}{r}\right) Z'(r)\right] \tag{B.14}$$

and, substituting Eqs. (B.12)-(B.13), we finally find the *Zerilli master equation*

$$\frac{d^2Z}{dr_*^2} + \left(\omega^2 - V_{polar}\right) Z = 0\,, \tag{B.15}$$

with

$$V_{polar} = \left(1 - \frac{2M}{r}\right) \frac{2\Lambda^2(\Lambda+1)r^3 + 6\Lambda^2 M r^2 + 18\Lambda M^2 r + 18M^3}{r^3(\Lambda r + 3M)^2} \tag{B.16}$$

Starting from the other components of Einstein equations containing the axial perturbations, a completely analogous result can be found for the axial sector, described by the Regge-Wheeler function $\Psi(r)$. In this case one finds the *Regge-Wheeler master equation* [153, 249]

$$\frac{d^2\Psi}{dr_*^2} + \left(\omega^2 - V_{axial}\right) \Psi = 0 \tag{B.17}$$

$$V_{axial} = -\left(1 - \frac{2M}{r}\right) \frac{2}{r^3} \left[3M - (\Lambda+1)r\right]\,. \tag{B.18}$$

Appendix C

Physical Quantities

When using Hartle formalism [191] to find the spacetime of a slowly rotating black hole in GR, one starts from the spherically symmetric case, described by a mass M_0, and then adds the rotation-induced deformations described by the radial functions in Eqs.(2.86)-(2.89). The final slowly rotating object has a physical mass M and angular momentum J, while the "bare" mass M_0 has no longer a physical meaning.

Similarly, when computing the spacetime of a slowly rotating BH in EdGB gravity, as described in Section 3.2.2, we work in a two-parameter perturbation theory framework:

1. We start from a nonrotating BH in GR, described by the mass M_0;
2. We apply the slow rotation; the BH will have an angular momentum $\tilde{J}_0$, while the bare mass M_0 will acquire spin corrections, which are then absorbed in the physical mass $\tilde{M}_0$;
3. We apply the small coupling expansion in ζ; the mass and angular momentum $\tilde{M}_0, \tilde{J}_0$ will both acquire EdGB corrections at each order in the spin, then reabsorbed in the physical mass and angular momentum M, J, which describe the slowly rotating DBH.

The physical quantities are defined as the mass and angular momentum (and any additional charge) measured by an observer at spatial infinity. Therefore, for a given metric, the physical mass and the physical angular momentum can be found from the asymptotic behavior of

$$g_{tt} \to -1 + \frac{2M}{r} + ... \tag{C.1}$$

$$\omega(r) \to \frac{2J}{r^3} + ... \tag{C.2}$$

where $\omega(r)$ is the gravitomagnetic function present in $g_{t\phi}$. When there is a scalar charge D, it can be found from

$$\varphi(r) \to \varphi_\infty + \frac{D}{r} + ... \tag{C.3}$$

as we have seen in Sec. 3.2.

C.1 Nonrotating Case

In this section, we shall see explicitly the corrections acquired by the bare mass M_0, describing a Schwarzschild BH in GR, when considering the EdGB corrections.

The ADM mass M of the nonrotating DBH found from the asymptotic behavior in Eq. (C.1) is connected to M_0 through the relation

$$\begin{aligned} M =& M_0 + \frac{49\alpha_{GB}^2}{1280M_0^3} + \frac{66319\alpha_{GB}^3}{2419200M_0^5} + \frac{846414013\alpha_{GB}^4}{39739392000M_0^7} + \frac{110088297441377\alpha_{GB}^5}{6137351700480000M_0^9} \\ &+ \frac{2919829004957865881 29\alpha_{GB}^6}{18229407514833715200000M_0^{11}} + \mathcal{O}(\alpha_{GB}^7) \end{aligned} \tag{C.4}$$

which, when inverted, gives

$$\begin{aligned} M_0 =& M - \frac{49}{1280M^3}\alpha_{GB}^2 - \frac{66319}{2419200M^5}\alpha_{GB}^3 - \frac{510561389}{19869696000M^7}\alpha_{GB}^4 - \frac{161613926636417\alpha_{GB}^5}{6137351700480000M^9} \\ &- \frac{17481835000660977214 3\alpha_{GB}^6}{607646917161123840000 0M^{11}} + \mathcal{O}(\alpha_{GB}^7) \end{aligned} \tag{C.5}$$

We can find the dilaton charge D from the coefficient of the $1/r$ term in the asymptotic expansion (C.3)

$$\begin{aligned} D =& \frac{\alpha_{GB}}{2M_0} + \frac{73\alpha_{GB}^2}{480M_0^3} + \frac{1249\alpha_{GB}^3}{16128M_0^5} + \frac{13469327\alpha_{GB}^4}{266112000M_0^7} + \frac{23528854133\alpha_{GB}^5}{619934515200M_0^9} \\ &+ \frac{6038334697710077 09\alpha_{GB}^6}{19475862729523200000M_0^{11}} + \mathcal{O}(\alpha_{GB}^7) \end{aligned} \tag{C.6}$$

or, alternatively, using Eq. (C.5), in terms of the physical mass M and $\zeta = \alpha_{GB}/M^2$

$$\frac{D}{M} = \frac{\zeta}{2} + \frac{73\zeta^2}{480} + \frac{15577\zeta^3}{161280} + \frac{58039297\zeta^4}{709632000} + \frac{17461067857\zeta^5}{221405184000} + \frac{11230503805065163\zeta^6}{136194844262400000} + \mathcal{O}(\zeta^7) \tag{C.7}$$

We can now see clearly that, as mentioned in Sec. 3.2, the scalar charge D is dependent on the BH mass M and $D/M \sim \zeta/2$ for $\zeta \to 0$. Since this additional hair is dependent on the mass, it is called a *secondary hair*.

The horizon of the dilatonic black hole in the small coupling limit, found from the largest root r_H of the equation $g_{\phi\phi}g_{tt} - g_{t\phi}^2 = 0$ [324] is

$$\begin{aligned} \frac{r_H}{M} =& 2 - \frac{49}{640}\zeta^2 - \frac{66319}{1209600}\zeta^3 - \frac{510561389}{9934848000}\zeta^4 - \frac{161613926636417}{3068675850240000}\zeta^5 \\ &- \frac{1748183500066097721 43}{30382345858056192000 00}\zeta^6 + \mathcal{O}(\zeta^7) \end{aligned} \tag{C.8}$$

C.2 Slowly Rotating Case

In the slow-rotating GR BH we described in Sec. 2.6.1, we found that the "bare" mass M_0 of a nonrotating case acquires corrections due to the angular momentum

$$\tilde{M_0} = M_0 - \frac{\tilde{J}_0^2\delta m}{M_0^2} + \mathcal{O}(\tilde{J}_0^3) \tag{C.9}$$

When including the EdGB corrections, the asymptotic behavior (C.1) gives the definition of the ADM mass M

$$\begin{aligned} M =& M_0 + \frac{49\alpha_{GB}^2}{1280 M_0^3} + \frac{66319\alpha_{GB}^3}{2419200 M_0^5} + \frac{846414013\alpha_{GB}^4}{39739392000 M_0^7} + \frac{110088297441377\alpha_{GB}^5}{6137351700480000 M_0^9} \\ &+ \frac{2919829004957865881 29\alpha_{GB}^6}{18229407514833715200000 M_0^{11}} - \frac{\tilde{J}_0^2}{M_0^2}\Big(\delta m + \tilde{A}_2\alpha_{GB}^2 + \tilde{A}_3\alpha_{GB}^3 + \tilde{A}_4\alpha_{GB}^4 \\ &+ \tilde{A}_5\alpha_{GB}^5 + \tilde{A}_6\alpha_{GB}^6\Big) + \mathcal{O}(\alpha_{GB}^7) + \mathcal{O}(\tilde{J}_0^3) \end{aligned} \tag{C.10}$$

with $\tilde{A}_j$ $(j = 2, ..., 6)$ integration constants. The angular momentum, found from Eq. (C.2), gets corrections at each order in α_{GB} starting from the second

$$J = \tilde{J}_0\left[1 + \tilde{C}_2\alpha_{GB}^2 + \tilde{C}_3\alpha_{GB}^3 + \tilde{C}_4\alpha_{GB}^4 + \tilde{C}_5\alpha_{GB}^5 + \tilde{C}_6\alpha_{GB}^6 + \mathcal{O}(\alpha_{GB}^7)\right] \tag{C.11}$$

with $\tilde{C}_j$ $(j = 2, ..., 6)$ integration constants.

The expressions for the horizon and the scalar charge in the slowly rotating case are given in the main text in Eqs. (3.39)-(3.40) and Tab. 3.1. They are plotted in Fig. 3.1 as a function of ζ and for different values of spin $\bar{a}$.

Appendix D

Static Equations

We write here the expression of the $\hat{V}_l$ matrix in Eq. (5.9) up to order $\mathcal{O}(\zeta^2)$ for the nonrotating case; we redirect to the Supplemental material [322] for the full lengthy expressions up to $\mathcal{O}(\zeta^6)$. In the following we define

$$\lambda \equiv \frac{1}{2}(l^2+l+2)\,, \tag{D.1}$$

so that the matrix elements read

$$\begin{aligned}
V_{11} =& \frac{-6M^2+(5-3\lambda)Mr+r^4\omega^2}{r(2M-r)(3M+(\lambda-2)r)} + \frac{\zeta^2}{480r^7(r-2M)^2(3M+\lambda r-2r)^2}\Big[172800M^{10} \\
&- 461760M^9r + 479424M^8r^2 - 242888M^7r^3 + 71280M^6r^4 - 26880M^5r^5 + 13420M^4r^6 \\
&- 2670M^3r^7 - 120M^2r^8 + 85920M^9r\lambda - 190368M^8r^2\lambda + 155644M^7r^3\lambda - 52512M^6r^4\lambda \\
&+ 11760M^5r^5\lambda - 8690M^4r^6\lambda + 2865M^3r^7\lambda + 120M^2r^8\lambda + 6720M^8r^2\lambda^2 - 19440M^7r^3\lambda^2 \\
&+ 11376M^6r^4\lambda^2 - 1050M^5r^5\lambda^2 + 900M^4r^6\lambda^2 - 765M^3r^7\lambda^2 - 30M^2r^8\lambda^2 + 29760M^8r^4\omega^2 \\
&- 47696M^7r^5\omega^2 + 19248M^6r^6\omega^2 + 546M^5r^7\omega^2 + 740M^4r^8\omega^2 - 935M^3r^9\omega^2 \\
&+ 12640M^7r^5\lambda\omega^2 - 9408M^6r^6\lambda\omega^2 + 132M^5r^7\lambda\omega^2 + 20M^4r^8\lambda\omega^2 + 490M^3r^9\lambda\omega^2\Big]\,,
\end{aligned} \tag{D.2}$$

$$\begin{aligned}
V_{12} =& -\frac{ir\omega\left(9M^2+4Mr(-3+\lambda)+r^2\left(4-2\lambda+r^2\omega^2\right)\right)}{(-2M+r)^2(3M+r(-2+\lambda))} + \frac{i\omega M^2\zeta^2}{480r^5(-2M+r)^3(3M-2r+r\lambda)^2} \\
&\Big\{-4r^2(-2M+r)\left(8720M^5-5712M^4r+30M^3r^2-340M^2r^3+375Mr^4+15r^5\right)\lambda^2 \\
&+2r\lambda\Big[M\big(169920M^6-193808M^5r+53936M^4r^2-5862M^3r^3+9730M^2r^4-2935Mr^5 \\
&-165r^6\big)+r^4\left(5440M^5-4656M^4r+96M^3r^2+150M^2r^3+260Mr^4+15r^5\right)\omega^2\Big]+3M \\
&\Big[M\left(138720M^6-157136M^5r+42444M^4r^2-3930M^3r^3+7570M^2r^4-2235Mr^5-120r^6\right) \\
&+r^4\left(8160M^5-7376M^4r+204M^3r^2+550M^2r^3+290Mr^4+45r^5\right)\omega^2\Big]\Big\}\,,
\end{aligned} \tag{D.3}$$

$$V_{13} = -\frac{iM\zeta\omega\left(-160M^4 - Mr^3 + r^4 + 16M^3r(5-4\lambda) + 8M^2\left(4r^2\lambda + r^4\omega^2\right)\right)}{4r^3(-2M+r)^2(3M+r\lambda)} - \frac{iM\zeta^2\omega}{960r^6(-2M+r)^2(3M+r\lambda)}\Big[-26240M^7 - 73Mr^6 + 73r^7 - 2048M^6r(3+5\lambda) + 240M^4r^3\left(41 - 16\lambda + 4r^2\omega^2\right) + 16M^5r^2\left(-591 - 160\lambda + 80r^2\omega^2\right) + 960M^3\left(4r^4\lambda + r^6\omega^2\right)\Big], \tag{D.4}$$

$$V_{14} = -\frac{iM\left(4M^2 + 2Mr + r^2\right)\zeta\omega}{4r^2(3M+r\lambda)} - \frac{iM\zeta^2\omega\left(320M^5 + 448M^4r + 584M^3r^2 + 292M^2r^3 + 146Mr^4 + 73r^5\right)}{960r^5(3M+r\lambda)}, \tag{D.5}$$

$$V_{21} = -\frac{i\left((1+\lambda)(2M+r\lambda) + r^3\omega^2\right)}{r^2(3M+r\lambda)\omega} + \frac{iM^2\zeta^2}{480r^8(3M+r\lambda)^2\omega}\Big\{M(1+\lambda)\Big[17280M^5 - 440Mr^4\lambda + 15r^5\lambda - 90M^2r^3(8+7\lambda) - 96M^3r^2(15+13\lambda) + 80M^4r(-36+89\lambda)\Big] + r^3\Big[-17520M^5 + 288M^4r(9-25\lambda) - 30r^5\lambda + 60M^2r^3(10+9\lambda) + 18M^3r^2(65+64\lambda) + 5Mr^4(-9+80\lambda)\Big]\omega^2\Big\}, \tag{D.6}$$

$$V_{22} = \frac{-M(6M + r(-2+\lambda)) + r^4\omega^2}{r(-2M+r)(3M+r\lambda)} + \frac{M^3\zeta^2}{480r^7(-2M+r)^2(3M+r\lambda)^2}\Big[6M^2\big(-12480M^5 + 13520M^4r - 3792M^3r^2 - 450M^2r^3 + 140Mr^4 + 135r^5\big) + r^2\big(-33600M^5 + 38480M^4r - 11472M^3r^2 + 1470M^2r^3 - 1900Mr^4 + 735r^5\big)\lambda^2 - 3r^4\big(9920M^5 - 7472M^4r + 144M^3r^2 + 270M^2r^3 + 260Mr^4 + 15r^5\big)\omega^2 + 2r\lambda\big(-58800M^6 + 65616M^5r - 19082M^4r^2 + 1392M^3r^3 - 2115M^2r^4 + 985Mr^5 + 15r^6 - r^4\big(6320M^4 - 4704M^3r + 66M^2r^2 + 10Mr^3 + 245r^4\big)\omega^2\big)\Big], \tag{D.7}$$

$$V_{23} = -\frac{M\zeta\left(64M^4 + 4Mr^3 + 32M^3r(-1+\lambda) - 16M^2r^2\lambda + r^4\left(-1+\lambda-8M^2\omega^2\right)\right)}{4r^5(-2M+r)(3M+r\lambda)} + \frac{M\zeta^2}{960r^8(-2M+r)(3M+r\lambda)}\Big[10240M^7 - 292Mr^6 - 73r^7(-1+\lambda) + 384M^6r(-9+5\lambda) + 960M^3r^4\left(\lambda + r^2\omega^2\right) + 240M^4r^3\left(5 - 9\lambda + 4r^2\omega^2\right) + 64M^5r^2\left(-69 - 26\lambda + 20r^2\omega^2\right)\Big], \tag{D.8}$$

$$V_{24} = \frac{M\zeta\left(16M^3 + r^3 + 8M^2r\lambda\right)}{4r^4(3M+r\lambda)} + \frac{M\zeta^2\left(3200M^6 + 73r^6 + 960M^3r^3\lambda + 240M^4r^2(9+4\lambda) + 256M^5r(9+5\lambda)\right)}{960r^7(3M+r\lambda)}, \tag{D.9}$$

$$V_{31} = V_{32} = V_{33} = 0\,, \tag{D.10}$$

$$V_{34} = -1\,, \tag{D.11}$$

$$\begin{aligned} V_{41} =& -\frac{iM^2\zeta\left(M(1+\lambda)(32M+r(-1+12\lambda))+r^3(4M+r)\omega^2\right)}{r^5(3M+r\lambda)\omega} - \frac{iM^2\zeta^2}{240r^8(3M+r\lambda)\omega}\Big[M(1+\lambda) \\ &\left(4960M^4-73r^4+32M^3r(107+60\lambda)+12M^2r^2(287+120\lambda)+4Mr^3(-73+360\lambda)\right) \\ &+r^3\left(800M^4+896M^3r+876M^2r^2+292Mr^3+73r^4\right)\omega^2\Big]\,, \end{aligned} \tag{D.12}$$

$$\begin{aligned} V_{42} =& \frac{M^2\zeta\left(-96M^3-r^3\lambda+M^2r(35+8\lambda)+r^5\omega^2+Mr^2\left(-1+2\lambda(5+6\lambda)+4r^2\omega^2\right)\right)}{r^4(-2M+r)(3M+r\lambda)} \\ &+\frac{M^2\zeta^2}{240r^7(-2M+r)(3M+r\lambda)}\Big[-14880M^6+64M^5r(-83+25\lambda) \\ &+73r^6\left(-\lambda+r^2\omega^2\right)+73Mr^5\left(-1-2\lambda+4r^2\omega^2\right)+8M^3r^3\left(540+\lambda(287+180\lambda)+112r^2\omega^2\right) \\ &+4M^4r^2\left(-1727+8\lambda(91+60\lambda)+200r^2\omega^2\right)+M^2r^4\left(-73+4\lambda(287+360\lambda)+876r^2\omega^2\right)\Big]\,, \end{aligned} \tag{D.13}$$

$$\begin{aligned} V_{43} =& \frac{-2(-2M+r)(M+r+r\lambda)+r^4\omega^2}{r^2(-2M+r)^2}+\frac{12M^4\zeta}{r^5(-2M+r)}+\frac{M^2\zeta^2}{240r^8(-2M+r)^3(3M+r\lambda)} \\ &\Big\{-3r(-2M+r)\big(-18720M^6-3376M^5r+9972M^4r^2-390M^3r^3-930M^2r^4-45Mr^5 \\ &+5r^6\big)\lambda+2r^2(-2M+r)\left(9680M^5-5712M^4r+30M^3r^2+260M^2r^3+15Mr^4+15r^5\right)\lambda^2 \\ &-r^5\left(-2240M^5+144M^4r+96M^3r^2+390M^2r^3+20Mr^4+15r^5\right)\lambda\omega^2+3M\Big[14080M^7 \\ &-103520M^6r+108432M^5r^2-28996M^4r^3-5550M^3r^4+2370M^2r^5+55Mr^6+5r^7 \\ &-r^4\left(-4800M^5+2064M^4r+96M^3r^2+230M^2r^3+20Mr^4+15r^5\right)\omega^2\Big]\Big\}\,, \end{aligned} \tag{D.14}$$

$$\begin{aligned} V_{44} =& \frac{2M}{-2Mr+r^2}+\frac{M\zeta^2}{1920}\Bigg\{-\frac{147}{(-2M+r)^2}+\frac{1}{r^7(3M+r\lambda)}\Big[249600M^6+4M^3r^3(1353-2224\lambda) \\ &+147r^6\lambda+9Mr^5(49+52\lambda)+12M^2r^4(157+97\lambda)+480M^5r(-141+184\lambda) \\ &-32M^4r^2(834+665\lambda)\Big]\Bigg\}\,. \end{aligned} \tag{D.15}$$

Appendix E

Tortoise Coordinate for Stationary Black Holes in Einstein-dilaton Gauss-Bonnet Gravity

The tortoise coordinate r_* is a redefinition of the radial coordinate r used to map the region outside the BH horizon $r \in [r_H, +\infty]$ into $r_* \in [-\infty, +\infty]$. Since the intrinsic geometry of a slowly rotating BH in Hartle coordinates is nonspherical [208], a definition of the tortoise coordinate in terms of mapping principal null geodesics to straight lines can become impractical and ambiguous. However, we can proceed in another way by noting that, when using this coordinate, the vacuum equations describing a perturbation $Z(r)$ can be reduced to a second-order differential equation of the form

$$\frac{d^2}{dr_*^2} Z + (\omega^2 - V) Z = 0 \tag{E.1}$$

where the first derivative of Z is not present (see e.g. Sec. 2.3) and V possibly contains the spin corrections. The asymptotic behavior is

$$\begin{aligned} Z^{lm}_{,r_*r_*} + k_H^2 Z^{lm} &= \mathcal{O}(r - r_H) \qquad (r \to r_H) \\ Z^{lm}_{,r_*r_*} + \omega^2 Z^{lm} &= \mathcal{O}\left(\frac{1}{r^2}\right) \qquad (r \to \infty)\,, \end{aligned} \tag{E.2}$$

where $k_H = \omega - m\Omega_H \to \omega$ (for $\bar{\mathrm{a}} \to 0$). By defining

$$\frac{dr}{dr_*} = F(r) \tag{E.3}$$

the function $F(r)$, satisfying $F(r) \sim r - r_H$ for $r \to r_H$ and $F(r) \to 1$ for $r \to \infty$, can be found by requiring that the perturbation equations reduce, at the horizon and at infinity, to Eq. (E.2).

In general relativity, $F(r) = 1 - 2M/r = (r - r_H)/r$ for Schwarzschild BHs ($r_H = 2M$), and $F(r) = (r^2 + a^2 - 2Mr)/(r^2 + a^2) \sim (r - r_H)$ for Kerr BHs ($r_H = 2M - a^2/(2M) + O(a^4)$), where $a = J/M$.

We find the tortoise coordinate in EdGB gravity, by requiring the equation for a test scalar field to have the form (E.2). This coordinate will define the boundary conditions for the gravitational perturbations as well, since the null ingoing coordinate $v = t + r_*$ (with a similar redefinition of

the azimuthal coordinate ϕ) regularizes the coordinate singularity at the horizon, regardless of the nature of the perturbation.

Nonrotating Black Holes

The metric of a static BH in EdGB gravity is given by Eq. (3.11),

$$ds^2 = -A(r)dt^2 + \frac{dr^2}{B(r)} + r^2 d\Omega^2 \,. \tag{E.4}$$

The Klein-Gordon equation for a test scalar field, $\nabla_\mu \nabla^\mu \Phi = 0$, after an expansion in spherical harmonics, $\Phi = \sum_{lm} \frac{1}{r}\Phi^{lm}(r) Y^{lm}(\theta,\phi) e^{-i\omega t}$, reads

$$AB\Phi^{lm\prime\prime} + \frac{1}{2}(A'B + B'A)\Phi^{lm\prime} + \left(\omega^2 - \frac{A'B + B'A}{2r} - A\frac{l(l+1)}{r^2}\right)\Phi^{lm} = 0 \tag{E.5}$$

where a prime denotes differentiation with respect to r. By defining the tortoise coordinate, in analogy with Schwarzschild, as $F(r) = \sqrt{A(r)B(r)}$ [3], Eq. (E.5) can be written as

$$\Phi^{lm}_{,r_* r_*} + (\omega^2 - V^l)\Phi^{lm} = 0 \tag{E.6}$$

where $V^l = FF' - Al(l+1)/r^2$, vanishing both at the horizon and at infinity (since $F' \sim r^{-2}$). Since, for a nonrotating BH, $k_H = \omega$, Eq. (E.6) coincides with Eq. (E.2).

First Order in the Spin

At $\mathcal{O}(\bar{a})$, the metric (E.4) acquires the extra term $g_{t\phi} = -r^2 \sin^2\theta \varpi(r)$, where

$$\varpi(r) = \frac{2J}{r^3}\left[1 - \frac{147}{960}\zeta^2\left(1 + \mathcal{O}\left(\frac{M}{r}\right)\right) + O(\zeta^3)\right] \,. \tag{E.7}$$

Since $g_{\phi\phi} = r^2 \sin^2\theta$,

$$\Omega_H = -\lim_{r\to r_H} \frac{g_{t\phi}}{g_{\phi\phi}} = \varpi(r_H) \,. \tag{E.8}$$

The equation for a test scalar field in this spacetime acquires the extra term $-2m\omega\varpi(r)$

$$AB\Phi^{lm\prime\prime} + \frac{1}{2}(A'B + B'A)\Phi^{lm\prime} + \left[\omega^2 - \frac{A'B + B'A}{2r} - A\frac{l(l+1)}{r^2} - 2m\omega\varpi(r)\right]\Phi^{lm} = 0 \,. \tag{E.9}$$

Then, by defining the tortoise coordinate as in the nonrotating case $F(r) = \sqrt{A(r)B(r)}$, the scalar field equation near the horizon (neglecting $\mathcal{O}(\bar{a}^2)$ terms) reads

$$\Phi^{lm}_{,r_* r_*} + (\omega^2 - 2m\Omega_H\omega)\Phi^{lm} = \phi^{lm}_{,r_* r_*} + k_H^2 \Phi^{lm} = 0 \,, \tag{E.10}$$

which is in agreement with Eq. (E.2).

Second Order in the Spin

To define the tortoise coordinate we write $F(r)$ as a generic expansion in powers of ζ, $\bar{a}$ and $1/r$, such that $F \sim r - r_H$ near the horizon and $F(r) \to 1$ as $r \to \infty$. There is some arbitrariness in the exact final expression, but we have found that the coefficients of the expansion are uniquely determined by requiring that the equation for a test scalar field at $r \to \infty$ behaves as

$$Z^{lm}_{,r_*r_*} + \omega^2 Z^{lm} = \frac{l(l+1)}{r^2} Z^{lm} + \mathcal{O}\left(\frac{1}{r^3}\right)$$

which is slightly stronger than Eq. (E.2). The expression we find, available up to order $\mathcal{O}(\zeta^6)$ in the Supplemental Material [322], is

$$\begin{aligned} F(r) = \left(1 - \frac{r_H}{r}\right) \Bigg\{ 1 - \bar{a}^2 \frac{r_H(r^2 + r r_H + r_H^2)}{8r^3} - \zeta^2 \Bigg[\frac{r_H}{3840 r^4}(147 r^3 + 117 r^2 r_H - 526 r r_H^2 + 263 r_H^3) \\ + \bar{a}^2 \frac{r_H}{30720 r^3}(375 r^2 + 435 r r_H + 343 r_H^2) \Bigg] \Bigg\} + \mathcal{O}(\zeta^3) + \mathcal{O}(\bar{a}^3)\,. \end{aligned} \tag{E.11}$$

We have verified that other options of $F(r)$, still satisfying Eq. (E.2), yield QNMs that differ only in a negligible way.

Appendix F

Angular Integration

Once the perturbation functions have been expanded in spherical harmonics, in order to remove the angular dependence from the perturbation equations and obtain radial equations, we perform an integration over the solid angle and exploit the orthogonality rules for the spherical harmonics

$$\int d\Omega Y^*_{l'm'} Y_{lm} = \delta_{l'l}\delta_{m'm} \tag{F.1}$$

and the results of the integrals

$$\int d\Omega \left(\frac{dY^*_{l'm'}}{d\theta}\frac{dY_{lm}}{d\theta} + \frac{m\ m'}{\sin^2\theta} Y^*_{l'm'} Y_{lm} \right) = l(l+1)\delta_{l'l}\delta_{m'm} \tag{F.2}$$

$$\int d\Omega \left(Y^*_{l'm'}\frac{dY_{lm}}{d\theta} + \frac{dY^*_{l'm'}}{d\theta} Y_{lm} \right) \frac{\cos\theta}{\sin\theta} = \delta_{ll'}\,. \tag{F.3}$$

Using these relations we also find

$$\int d\Omega \left(W^*_{l'm'} W_{lm} + \frac{X^*_{l'm'} X_{lm}}{\sin^2\theta} \right) = l(l-1)(l+1)(l+2)\delta_{l'l}\delta_{m'm} \tag{F.4}$$

$$\begin{aligned} \int d\Omega \left[imW^*_{l'm'} Y_{lm} - X^*_{l'm'}\partial_\theta Y_{lm} \right] &= \int d\Omega \left[imY^*_{lm} W_{l'm'} + X_{l'm'}\partial_\theta Y^*_{l'm'} \right] \\ &= im(l-1)(l+2)\delta_{ll'}\delta_{m'm} \end{aligned} \tag{F.5}$$

$$\int d\Omega \left[W^*_{l'm'}\frac{X_{lm}}{\sin\theta} - \frac{X^*_{l'm'}}{\sin\theta} W_{lm} \right] = 0\,. \tag{F.6}$$

Furthermore, from the definition of spherical harmonics, one finds the useful relations

$$\cos\theta Y_{lm} = Q_{l+1m} Y_{l+1m} + Q_{lm} Y_{l-1m} \tag{F.7}$$

$$\sin\theta\partial_\theta Y_{lm} = lQ_{l+1m} Y_{l+1m} - Q_{lm}(l+1) Y_{l-1m} \tag{F.8}$$

where we have defined

$$Q_{lm} \equiv \sqrt{\frac{(l-m)(l+m)}{(2l-1)(2l+1)}}\,. \tag{F.9}$$

When substituting these formulas, possibly multiple times, inside the field equations at second order in the spin, we get couplings with the harmonic indices $l \pm 1, l \pm 2$, while m remains unchanged. In fact, since the ϕ dependence of the spherical harmonics is $\sim e^{im\phi}$, we always get $\int d\phi e^{i(m-m')\phi} \sim$

$\delta_{m'm}$.

We define the operators that couple terms l with terms $l \pm 1$ as $\mathcal{L}_j^{\pm 1}$. They will act on a generic coefficient A, i.e. one of the coefficients appearing in the field equations, in the following way

$$\mathcal{L}_0^{\pm 1} A \equiv \sum_{l'm'} A_{l'm'} \int d\Omega Y_{lm}^* \cos\theta Y_{l'm'} = Q_{lm} A_{l-1m} + Q_{l+1m} A_{l+1m} \tag{F.10}$$

$$\mathcal{L}_1^{\pm 1} A \equiv \sum_{l'm'} A_{l'm'} \int d\Omega Y_{lm}^* \sin\theta \partial_\theta Y_{l'm'} = (l-1) Q_{lm} A_{l-1m} - (l+2) Q_{l+1m} A_{l+1m} \tag{F.11}$$

$$\mathcal{L}_2^{\pm 1} A \equiv \sum_{l'm'} A_{l'm'} \int d\Omega \partial_\theta Y_{lm}^* \sin\theta Y_{l'm'} = -(l+1) Q_{lm} A_{l-1m} + l Q_{l+1m} A_{l+1m} \tag{F.12}$$

$$\begin{aligned} \mathcal{L}_3^{\pm 1} A &\equiv \sum_{l'm'} A_{l'm'} \int d\Omega \left(\partial_\theta Y_{lm}^* \partial_\theta Y_{l'm'} + \frac{m\ m'}{\sin^2\theta} Y_{lm}^* Y_{l'm'} \right) \cos\theta \\ &= (l-1)(l+1) Q_{lm} A_{l-1m} + l(l+2) Q_{l+1m} A_{l+1m} \end{aligned} \tag{F.13}$$

$$\mathcal{L}_4^{\pm 1} A \equiv \sum_{l'm'} A_{l'm'} \int d\Omega \left(im' \partial_\theta Y_{lm}^* Y_{l'm'} + im Y_{lm}^* \partial_\theta Y_{l'm'} \right) \sin\theta = im(\mathcal{L}_1^{\pm 1} + \mathcal{L}_2^{\pm 1}) \tag{F.14}$$

$$\begin{aligned} \mathcal{L}_5^{\pm 1} A &\equiv \sum_{l'm'} A_{l'm'} \int d\Omega \left(\sin\theta \partial_\theta Y_{lm}^* W_{l'm'} - im Y_{lm}^* \frac{X_{l'm'}}{\sin\theta} \right) \\ &= (l-2)(l-1)(l+1) Q_{lm} A_{l-1m} - l(l+2)(l+3) Q_{l+1m} A_{l+1m} \end{aligned} \tag{F.15}$$

$$\begin{aligned} \mathcal{L}_6^{\pm 1} A &\equiv \sum_{l'm'} A_{l'm'} \int d\Omega \left(\sin\theta \partial_\theta Y_{l'm'} W_{lm}^* + im Y_{l'm'} \frac{X_{lm}^*}{\sin\theta} \right) \\ &= -(l-1)(l+1)(l+2) Q_{lm} A_{l-1m} + l(l-1)(l+2) Q_{l+1m} A_{l+1m} \end{aligned} \tag{F.16}$$

$$\begin{aligned} \mathcal{L}_7^{\pm 1} A &\equiv \sum_{l'm'} A_{l'm'} \int d\Omega \left(\partial_\theta Y_{lm}^* X_{l'm'} + im Y_{lm}^* W_{l'm'} \right) \cos\theta \\ &= im(l-2)(l+3) \left[Q_{lm} A_{l-1m} + Q_{l+1m} A_{l+1m} \right] \end{aligned} \tag{F.17}$$

$$\begin{aligned} \mathcal{L}_8^{\pm 1} A &\equiv \sum_{l'm'} A_{l'm'} \int d\Omega \left(X_{lm}^* W_{l'm'} - W_{lm}^* X_{l'm'} \right) \sin\theta \\ &= 4im \left[(l-2)(l+2) Q_{lm} A_{l-1m} + (l-1)(l+3) Q_{l+1m} A_{l+1m} \right] \end{aligned} \tag{F.18}$$

$$\begin{aligned} \mathcal{L}_9^{\pm 1} A &\equiv \sum_{l'm'} A_{l'm'} \int d\Omega \left(im' W_{lm}^* Y_{l'm'} - X_{lm}^* \partial_\theta Y_{l'm'} \right) \cos\theta \\ &= im(l-3)(l+2) Q_{lm} A_{l-1m} + im(l-1)(l+4) Q_{l+1m} A_{l+1m} \end{aligned} \tag{F.19}$$

$$\mathcal{L}_{10}^{\pm 1} A \equiv \sum_{l'm'} A_{l'm'} \int d\Omega \ \sin\theta \ X_{lm}^* Y_{l'm'} = 2im(l+2) Q_{lm} A_{l-1m} - 2im(l-1) Q_{l+1m} A_{l+1m} \tag{F.20}$$

In a similar way, we define the operators $\mathcal{L}_j^{\pm 2}$ that introduce couplings with indices $l \pm 2$ couplings

$$\mathcal{L}_0^{\pm 2} A \equiv \sum_{l'm'} A_{l'm'} \int d\Omega Y_{lm}^* \cos^2\theta Y_{l'm'} = Q_{l-1m} Q_{lm} A_{l-2m} + (Q_{lm}^2 + Q_{l+1m}^2) A_{lm}$$
$$+ Q_{l+1m} Q_{l+2m} A_{l+2m} \tag{F.21}$$

$$\mathcal{L}_1^{\pm 2} A \equiv \sum_{l'm'} A_{l'm'} \int d\Omega Y_{lm}^* \sin^2\theta Y_{l'm'} = -Q_{l-1m} Q_{lm} A_{l-2m} + (1 - Q_{lm}^2 - Q_{l+1m}^2) A_{lm}$$
$$- Q_{l+1m} Q_{l+2m} A_{l+2m} \tag{F.22}$$

$$\mathcal{L}_2^{\pm 2} A \equiv \sum_{l'm'} A_{l'm'} \int d\Omega \partial_\theta Y_{lm}^* \ \sin\theta\cos\theta \ Y_{l'm'} = -(l+1) Q_{l-1m} Q_{lm} A_{l-2m}$$
$$+ \left[l Q_{l+1m}^2 - (l+1) Q_{lm}^2 \right] A_{lm} + l Q_{l+1m} Q_{l+2m} A_{l+2m} \tag{F.23}$$

$$\mathcal{L}_3^{\pm 2} A \equiv \sum_{l'm'} A_{l'm'} \int d\Omega Y_{lm}^* \ \sin\theta\cos\theta \ \partial_\theta Y_{l'm'} = (l-2) Q_{l-1m} Q_{lm} A_{l-2m}$$
$$+ \left[l Q_{l+1m}^2 - (l+1) Q_{lm}^2 \right] A_{lm} - (l+3) Q_{l+1m} Q_{l+2m} A_{l+2m} \tag{F.24}$$

$$\mathcal{L}_4^{\pm 2} A \equiv \sum_{l'm'} A_{l'm'} \int d\Omega \partial_\theta Y_{lm}^* \ \sin^2\theta \ \partial_\theta Y_{l'm'} = \left[l^2 Q_{l+1m}^2 + (l+1)^2 Q_{lm}^2 \right] A_{lm}$$
$$- l(l+3) Q_{l+1m} Q_{l+2m} A_{l+2} - (l-2)(l+1) Q_{lm} Q_{l-1m} A_{l-2m} \tag{F.25}$$

$$\mathcal{L}_5^{\pm 2} A \equiv \sum_{l'm'} A_{l'm'} \int d\Omega \left(\partial_\theta Y_{lm}^* \partial_\theta Y_{l'm'} + \frac{m \ m'}{\sin^2\theta} Y_{lm}^* Y_{l'm'} \right) \sin^2\theta = -(l-2)(l+1) Q_{l-1m} Q_{lm} A_{l-2m}$$
$$+ \left[l(l+1) - (l+1)(l-2) Q_{lm}^2 - l(l+3) Q_{l+1m}^2 \right] A_{lm} - l(l+3) Q_{l+1m} Q_{l+2m} A_{l+2m} \tag{F.26}$$

$$\mathcal{L}_6^{\pm 2} A \equiv \sum_{l'm'} A_{l'm'} \int d\Omega \cos\theta \left(\sin\theta \partial_\theta Y_{lm}^* W_{l'm'} - i m Y_{lm}^* \frac{X_{l'm'}}{\sin\theta} \right) =$$
$$\left[2m^2 + Q_{lm}^2 (l+1)(l^2 - l + 4) - Q_{l+1m}^2 l(l^2 + 3l + 6) \right] A_{lm}$$
$$+ (l-2)(l+1)(l-3) Q_{l-1m} Q_l A_{l-2m} - l(l+3)(l+4) Q_{l+1m} Q_{l+2m} A_{l+2m} \tag{F.27}$$

$$\mathcal{L}_7^{\pm 2} A \equiv \sum_{l'm'} A_{l'm'} \int d\Omega \left(\sin\theta \partial_\theta Y_{l'm'} W_{lm}^* + i m Y_{l'm'} \frac{X_{lm}^*}{\sin\theta} \right) \cos\theta =$$
$$\left[2m^2 + Q_{lm}^2 (l+1)(l^2 - l + 4) - Q_{l+1m}^2 l(l^2 + 3l + 6) \right] A_{lm}$$
$$- (l-2)(l+1)(l+2) Q_{l-1m} Q_l A_{l-2m} + l(l+3)(l-1) Q_{l+1m} Q_{l+2m} A_{l+2m} \tag{F.28}$$

$$\mathcal{L}_8^{\pm 2} A \equiv \sum_{l'm'} A_{l'm'} \int d\Omega \left[W_{lm}^* W_{l'm'} + \frac{1}{\sin^2\theta} X_{lm}^* X_{l'm'} \right] \sin^2\theta =$$
$$\Big\{ Q_{lm}^2 (l+1) \left[4(l-2) - l(l+1)(l+4) \right] + \left[l^2 (l+1)^2 - 8m^2 \right]$$
$$+ Q_{l+1m}^2 l \left[4(l+3) - l(l+1)(l-3) \right] \Big\} A_{lm} - (l-3)(l-2)(l+1)(l+2) Q_{lm} Q_{l-1m} A_{l-2m}$$
$$- (l-1) l (l+3)(l+4) Q_{l+1m} Q_{l+2m} A_{l+2m} \tag{F.29}$$

$$\mathcal{L}_9^{\pm 2} A \equiv \sum_{l'm'} A_{l'm'} \int d\Omega \sin^2\theta W_{lm}^* Y_{l'm'} = \left[2m^2 - l(l+1) + (l+1)(l+2) Q_{lm}^2 + l(l-1) Q_{l+1m}^2 \right] A_{lm}$$
$$+ (l+1)(l+2) Q_{l-1m} Q_{lm} A_{l-2m} + l(l-1) Q_{l+1m} Q_{l+2m} A_{l+2m} \tag{F.30}$$

For example, we obtain the expression of $\mathcal{L}_0^{\pm 2}$ by considering $\cos\theta$ applied once on Y^* and once on Y, then applying the rule (F.8).

Acknowledgements

I would like to express my sincere gratitude to my supervisor, Professor Leonardo Gualtieri, for his guidance and support throughout my Ph.D. journey. His insights and feedback were instrumental in shaping this thesis.

I would also like to thank Andrea Maselli for his support and words of encouragement, not only for this thesis but also for my future trajectory.

Thank you to my colleagues for the fruitful discussions and for giving me crucial advice that made me understand what is really like to be a researcher.

Finally, I am deeply grateful to my family and friends for their constant love and support. Their patience and understanding during this process meant the world to me.

Lorenzo Pierini, Rome, May 2023